

UNIVERSITY OF SOUTHAMPTON



**Synthesis and characterization of new
supramolecular receptors and study of
their anion binding properties**

by

Ismael El Drubi Vega

A thesis submitted for the
degree of Doctor of Philosophy

in the
School of Chemistry
Synthetic Department
Synthesis Group

February 2007

UNIVERSITY OF SOUTHAMPTON

ABSTRACT

SCHOOL OF CHEMISTRY
SYNTHETIC CHEMISTRY DEPARTMENT

Doctor of Philosophy

by *Ismael El Drubi Vega*

This thesis deals with the synthesis and study of the anion complexation properties of new organic and metal-organic receptors. Previously, pyrrole amide cleft receptors had been shown to be efficient anion coordinating agents. We decided to explore the anion binding properties of some related dipyrrolylmethane-bisamides in polar solvent mixtures. These compounds were synthesized and shown to be remarkably selective for dihydrogen phosphate in DMSO water mixtures.

New tetrakis pyrrole-pyridine platinum (II) complexes have also been synthesized and their anion complexation properties studied. One of these compounds showed a solvent switchable binding site using either the pyrrole CH or NH to bind the anionic guest depending upon the nature of the solvent (DMSO or MeNO₂ respectively).

Platinum (II) complexes with hydroxyl groups at 2-position of the nicotinamide ligands were synthesized in collaboration with Dr. Stephen J. Loeb at the University of Windsor. The anion complexation properties of these calixarene-like compounds were studied using proton NMR titration techniques, and selectivity toward oxoanions was observed.

Finally, two novel platinum (II) complexes were prepared containing amidopyrrole moiety and either a pyridine or isoquinoline to bind to the platinum centre. The isoquinoline complex showed a higher degree of selectivity for oxo-anions than the pyridine complex.

Contents

Nomenclature	xiii
Declaration of Authorship	xvi
Acknowledgements	xvii
Agradecimientos	xviii
1 Introduction	1
1.1 Supramolecular chemistry	1
1.2 Anion coordination	7
1.3 Synthetic receptors	12
1.3.1 Metal based	13
1.3.1.1 Receptors containing inert metal ions	14
1.3.1.2 Complexes with labile metal centres	19
1.3.2 Heterocycle containing receptors	25
1.3.2.1 Acyclic pyrrole derivatives	26
1.3.2.2 Cyclic pyrrolic derivatives	27
1.3.2.3 Calix[n]pyrroles	29
1.4 Aim of the project	30
2 Dipyrrolylmethane based receptors	32
2.1 2,2'-Bisamidodipyrrolylmethanes	34
2.1.1 Synthesis and characterization	34
2.1.2 Binding studies results. Selectivity for dihydrogenphosphate	37
2.2 5,5'-Dicarboxamido-dipyrrolylmethanes	41
2.2.1 Synthesis and characterization	42
2.2.2 Binding studies results	45
2.3 (Dipyrrol-2-yl)alkane receptors	54
2.3.1 Synthesis and characterization	54
2.3.2 Binding studies results	55
2.4 Conclusion	58
3 NH vs. CH hydrogen bond formation in metal-organic anion receptors containing pyrrolylpyridine ligands and pyridine metal complexes with locked rotation around the metal	60
3.1 Tetrakis pyrrolylpyridine platinum II receptors	61
3.1.1 Synthesis and characterization	61

3.1.2	Binding studies results	65
3.2	Tetrakis hydroxy-pyridine platinum II receptors	74
3.2.1	Synthesis and characterization	75
3.2.2	Binding studies results	79
3.3	Conclusions	83
4	Hydrogen bond formation in metal-organic anion receptors containing quinolineamidopyrrole and pyridineamidopyrrole ligands	84
4.1	(isoquinoline & pyridinylmethyl) pyrrole carboxamide platinum II receptors	85
4.1.1	Synthesis and characterization	85
4.1.2	Binding studies results	89
4.2	Conclusions	92
5	Experimental	94
5.1	Solvent and reagent pre-treatment	94
5.2	Instrumental methods	94
5.3	Synthesis	95
5.3.1	Syntheses included in chapter 2	95
5.3.2	Syntheses included in chapter 3	101
5.3.3	Syntheses included in chapter 4	108
5.4	General method used for NMR titration	113
A	X-ray Tables	114
A.1	Bis- <i>N</i> -butylamide-5,5'-methylenebis(4-ethyl-3-methyl-2-pyrrolicarboxylate). 2.4(a)	114
A.2	Bis- <i>N</i> -phenylamide-5,5'-methylene bis(4-ethyl-3-methyl-2-pyrrolicarboxylate). 2.4(b)	118
A.3	5-(2-(5-(phenylcarbamoyl)-3,4-dimethyl-1 <i>H</i> -pyrrol-2-yl)propan-2-yl)-3,4-dimethyl- <i>N</i> -phenyl-1 <i>H</i> -pyrrole-2-carboxamide. 2.11(a)	121
A.4	5-(2-(5-(butylcarbamoyl)-3,4-dimethyl-1 <i>H</i> -pyrrol-2-yl)propan-2-yl)-3,4-dimethyl- <i>N</i> -butyl-1 <i>H</i> -pyrrole-2-carboxamide. 2.11(b)	124
A.5	Ethyl 5-(2-(5-(butylcarbamoyl)-3,4-dimethyl-1 <i>H</i> -pyrrol-2-yl)propan-2-yl)-3,4-dimethyl-1 <i>H</i> -pyrrole-2-carboxylate. 2.11(c)	128
A.6	Tetrakis(3-(1 <i>H</i> -pyrrol-2-yl)pyridine)platinum(II) tetrafluoroborate. 3.1(b)	131
A.7	Tetrakis(3-(1 <i>H</i> -pyrrol-2-yl)pyridine)platinum(II) methanesulfonate.	133
A.8	Tetrakis(3-(1 <i>H</i> -pyrrol-2-yl)pyridine)platinum(II) phosphorodifluoridate.	136
A.9	Tetrakis(2-hydroxypyridine)platinum(II) hexafluorophosphate.	138
A.10	Tetrakis(<i>N</i> -butyl-6-methoxynicotinamide)platinum(II) tetrafluoroborate. 3.17(c)	140
A.11	<i>N</i> -butyl-6-hydroxynicotinamide.	142
A.12	7,11a-diaza-1-(1 <i>H</i> -pyrrole-2-carbonyl)-1 <i>H</i> -azuleno[6,5,4- <i>ij</i>]isoquinolin-8(7- <i>H</i> ,11a <i>H</i> ,11b <i>H</i>)-one.	144
A.13	<i>N</i> -(isoquinolin-8-yl)-1 <i>H</i> -pyrrole-2-carboxamide.	146
A.14	3,4-dimethyl- <i>N</i> -((pyridin-3-yl)methyl)-1 <i>H</i> -pyrrole-2-carboxamide.	148
A.15	<i>N</i> -((pyridin-3-yl)methyl)-1 <i>H</i> -pyrrole-2-carboxamide.	150

List of Figures

1.1	Pedersen reported in 1967 the synthesis and coordination chemistry of crown ethers which marked the beginning of modern supramolecular chemistry.	1
1.2	The NaCl ionic lattice.	2
1.3	The chloride templated capsule $[(\text{Pt}(\text{SC}(\text{NH}_2)_2)_4)_2 \cdot (\text{C}_5\text{O}_5)_3 \cdot (\text{C}_5\text{O}_4\text{OH}) \cdot \text{Cl}]^{4-}$ present in the solid-state structure. $\text{C}_5\text{O}_5 =$ croconate.	2
1.4	(a) Na^+ hexahydrate (b) Na^+ crown ether complex and (c) $[\text{Ru}(\text{bipy})_3]^{2+}$ bipy = 2,2'-bipyridyl.	3
1.5	Dipole-dipole interactions in carbonyls.	3
1.6	(a) Sulfate binding protein where hydrogen bonds keep the overall 3D shape of the protein and bind the anion. (b) Base pairing in DNA by hydrogen bonding.	5
1.7	Limiting types of π - π stacking. Note the offset to the face-to-face mode (direct overlap is repulsive).	5
1.8	Hydrophobic binding of organic guests in aqueous solution.	6
1.9	Descriptive terms used to illustrate spatial relationships between host and guest.	7
1.10	Bone disease, cardiovascular problems (heart disease and stroke), calcifications and mineral deposits (kidneys, lungs, joints, eyes, heart and skin) are health disorders related to high levels of phosphate anion in human body.	10
1.11	Crystal structures of (a) sulfate binding protein and (b) phosphate binding protein.	11
1.12	Crystal structures of (a) ATP (b) ADP and (c) AMP.	12
1.13	The 24-membered macrocyclic polyamine that catalyze the hydrolysis of the ATP.	12
1.14	The structure of the Δ -form of 2a with ellipsoids at 20% probability (left). Two chlorides are bound, each <i>via</i> three hydrogen bonds from the amide NH groups as illustrated in the CPK representation of the structure (right).	15
1.15	The X-ray crystal structure of the perrhenate complex of 3 ²⁺	16
1.16	The chloride (c) and sulfate (d) complexes of receptor 4 . ¹ H NMR titrations demonstrate that the anions interact with the urea NH hydrogen atoms and α -CH hydrogens (b)	17
1.17	View of the two crystallographically independent $[\text{ZnCl}(\text{Hpz}^{\text{tBu}})_3]\text{PF}_6$ moieties in the crystal structure of 8e CH_2Cl_2 , showing the atom numbering scheme employed. Only one orientation of the hexafluorophosphate anion is shown.	21
1.18	Partial packing diagram of 9c , showing the association of the $[\text{ZnCl}(\text{Hpz}^{\text{tBu}})_3]^+$ cations into a hydrogen-bonded 1-D polymer.	21

1.19	The silver complex 10 (a) and the discrete $[\mathbf{10}](\text{NO}_3)\cdot\text{MeOH}$ complex (b) showing nitrate binding in an asymmetrical arrangement to the bis-urea metal complex.	22
1.20	Two of the proposed conformations adopted by complex 10 in solution binding either one or two equivalents of added anionic guest.	23
1.21	The X-ray crystal structure of the complex cations.	24
1.22	Crystal structure of the AS diastereomer of the complex cation $[\text{Co}_2(\mathbf{13})_3(\text{NO}_3)]^{3+}$	25
1.23	Crystal structure of the $\text{N}(\text{Me})_4\text{Cl}\cdots$ pyrrole complex.	26
1.24	2,5-diamidopyrroles as simple anion binding agents.	27
1.25	Guanidinium-based carboxylate receptors derived from 5-amino-pyrrole-2-carboxylate	27
1.26	Calculated energy minimized structure for the complex. Hydrogen bonds are shown in green, unfavorable steric interactions in red.	27
1.27	This receptor recognize the salt as an associated ion-pair.	28
1.28	This system acts as an affective redox-based sensor for F^- and H_2PO_4^-	28
1.29	Crystal chloride complex of the calix[4]pyrrole.	29
1.30	<i>N</i> -ethylpyridinium chloride- <i>meso</i> -octamethyl[4]calixpyrrole dichloromethane solvate.	29
1.31	Pentapyrrolic calix[4]pyrrole has three different NH proton resonances the pendant pyrrole NH (a) and two inequivalent NH resonances from the calixpyrrole (b (upfield calixpyrrole NH) and c(downfield calixpyrrole NH)).	30
1.32	Molecular model of the acetate pentapyrrolic complex.	30
2.1	The hydrogen bond donor group of the pyrrole molecule become an excellent anion receptor when is combined with amides.	32
2.2	(a) Red pigment first isolated from <i>Serratia Marcescens</i> and the initial member of a class of naturally-occurring polypyrroles possessing a common characteristic pyrrolylpyrromethane skeleton (b-f).	33
2.3	Crystal structure of the benzoate complex (a) front and (b) side	34
2.4	Compounds (a) and (b) were prepared in a single step reaction from the bisester precursor.	34
2.5	(a) Thermal ellipsoid plot of 2.4(a) . Ellipsoids drawn at the 35% probability level and non NH hydrogens omitted for clarity. (b) Hydrogen bonded sheet of 2.4(a) formed in the solid state <i>via</i> $\text{NH}\cdots\text{OC}$ hydrogen bonds. Side chain ethyl, methyl and butyl groups and non-acidic hydrogen atoms have been omitted for clarity.	35
2.6	(a) Thermal ellipsoid plot of 2.4(b) . Ellipsoids drawn at the 35% probability level and non NH hydrogens omitted for clarity. (b) Hydrogen bonded sheet of 2.4(b) formed in the solid state <i>via</i> $\text{NH}\cdots\text{OC}$ hydrogen bonds. Side chain ethyl, methyl and phenyl groups and non-acidic hydrogen atoms have been omitted for clarity.	36
2.7	^1H NMR titration curves with fluoride, chloride, bromide, and benzoate in dichloromethane- d_2 at 298 K. Anions added as their tetrabutylammonium salts. NH downfield shift is observed to occur up to one equivalent of anion added, appearing afterwards a plateau that indicates saturation of the receptor.	37

2.8	¹ H NMR titration curves with fluoride, chloride, bromide, benzoate, hydrogensulfate and dihydrogenphosphate in DMSO- <i>d</i> ₆ /5% water at 298 K. Anions added as their tetrabutylammonium salts.	38
2.9	¹ H NMR titration curves with fluoride, and dihydrogenphosphate in DMSO- <i>d</i> ₆ /25% water at 298 K. Anions added as their tetrabutylammonium salts.	39
2.10	Previous generation of pyrrole-amide clefts used to compare the anion binding properties of the novel dypyrrolylamides 2.4(a) and 2.4(b)	40
2.11	Compounds containing two alkyl groups attached to the <i>sp</i> ³ hybridized <i>meso</i> carbon which would not be as susceptible to oxidation.	41
2.12	The X-ray crystal structure of 2.11(a) ·MeOH. Non-acidic hydrogen atoms have been omitted for clarity. The pyrrole and amide groups are involved in a three dimensional network of hydrogen bonds.	43
2.13	The X-ray crystal structure of 2.11(b) . Non-acidic hydrogen atoms have been omitted for clarity. The pyrrole and amide groups are involved in a three dimensional network of hydrogen bonds.	44
2.14	The X-ray crystal structure of 2.11(c) . Non-acidic hydrogen atoms have been omitted for clarity. The pyrrole and amide groups are involved in a three dimensional network of hydrogen bonds. (a) Molecular structure, only one orientation of the disordered ethyl acetate is shown. (b) Detail of the hydrogen bonded slabs in the <i>bc</i> plane showing the two types of interaction. (c) View down the <i>a</i> axis.	45
2.15	(a) ¹ H NMR titration curves for compound 2.11(c) with fluoride, chloride, bromide, benzoate, dihydrogen phosphate and hydrogen sulfate in DMSO- <i>d</i> ₆ /5% water at 298 K. Anions added as their tetrabutylammonium salts and (b) Job plot of compound 2.11(c) and tetrabutylammonium dihydrogen phosphate in DMSO- <i>d</i> ₆ indicating 1:1 receptor:anion stoichiometry.	46
2.16	¹ H NMR titration curves for compounds 2.11(d) (a) and 2.11(b) (b) with fluoride, chloride, bromide, benzoate, dihydrogen phosphate and hydrogen sulfate in DMSO- <i>d</i> ₆ /5% water at 298 K. Anions added as their tetrabutylammonium salts.	48
2.17	¹ H NMR titration curves for compound 2.11(c) with fluoride, chloride, bromide, benzoate, dihydrogen phosphate and hydrogen sulfate in DMSO- <i>d</i> ₆ /0.5% water at 298 K. Anions added as their tetrabutylammonium salts.	49
2.18	¹ H NMR stack plot titration of compound 2.11(c) with (a) dihydrogen phosphate (i) 0, (ii) 0.24, (iii) 0.58, (iv) 1.20, (v) 3.90 equivalents, and (b) fluoride (i) 0, (ii) 0.25, (iii) 0.61, (iv) 1.21, (v) 3.00 equivalents in DMSO- <i>d</i> ₆ /0.5% water (amide proton resonance in blue, the adjacent pyrrole NH resonance is in green and the pyrrole-ester NH resonance is in red).	50
2.19	Structure of the dihydrogen phosphate complex of 2.11(c) generated by DFT calculation using Spartan 02.	50
2.20	(a) A portion of the NOESY spectrum of compound 2.11(d) in DMSO- <i>d</i> ₆ and (b) a schematic showing the through space couplings present in this compound.	51
2.21	Three dimensional views of the NOESY spectra of compound 2.11(d) in DMSO- <i>d</i> ₆ solutions.	52
2.22	¹ H NMR stack plot of compound 2.11(d) in the presence of five equivalents of dihydrogen phosphate (black) and ten minutes after the addition of one hundred equivalents of D ₂ O (blue).	52

2.23	Structure of the dihydrogen phosphate complex of 2.11(d) generated by DFT calculation using Spartan 02.	53
2.24	Dialdehyde dipyrrolyl anion based receptors.	54
2.25	X-ray crystal structure of compound 2.24(a) . Hydrogen atoms have been omitted for clarity. In the solid state each molecule ^ζ interacts with another molecule ^ξ through four hydrogen bonds between NH ^ζ . . . CO ^ξ and NH ^ξ . . . CO ^ζ	55
2.26	Titrations performed in CD ₃ CN. Anions added as tetrabutylammonium salts.	56
2.27	When tetrabutylammonium fluoride is added to dichloromethane- <i>d</i> ₂ solutions of compound 2.27(a) , pyrrolate anion 2.27(b) is formed.	57
2.28	Formation of pyrrolate is the process that justifies the sharp upfield NH shift inversion. Once the equilibrium in this process is reached, the concentration of pyrrolate remains constant and we start seeing again a downfield NH pyrrole shift upon addition of more tetrabutylammonium fluoride.	57
2.29	Delocalization of the negative charge in this molecule, leaving it over another electronegative atom will make this anion more stable being the pK _a lower than that reported for pyrrole.	58
3.1	Series of platinum(II) tetrakis(pyrrolylpyridine) salts prepared for anion complexation studies.	61
3.2	Classical syntheses of C-substituted pyrroles.	62
3.3	A ball-and-stick representation of the X-ray crystal structure of 3.1(b) ·(BF ₄) ₂ crystallized from nitromethane. The hydrogen bonding network is shown with BF ₄ ⁻ anions bound above and below the plane of the complex by CH . . . F and NH . . . F hydrogen bonds.	63
3.4	A ball-and-stick representation of the X-ray crystal structure of the methanesulfonate salt of cation 3.1(b) ²⁺ . The hydrogen bonding network is shown with MeSO ₃ ⁻ anions bound above and below the plane of the complex by CH . . . O and NH . . . O hydrogen bonds.	64
3.5	³¹ P{ ¹ H} NMR of the silver hexafluorophosphate used to prepare compound 3.1(b) ·(PF ₂ O ₂) ₂ . The triplet is attributed to the presence of difluorophosphinate anions.	65
3.6	X-ray crystal structure of the unexpected PF ₂ O ₂ ⁻ complex.	66
3.7	¹ H NMR titration curves for compound 3.1(a) with fluoride, chloride, bromide, iodide, methanesulfonate, nitrate, acetate, benzoate, sulfate and hydrogen sulfate in DMSO- <i>d</i> ₆ at 298 K. Anions added as their tetrabutylammonium salts.	67
3.8	Proton NMR stack plot titration of compound 3.1(a) in DMSO- <i>d</i> ₆ with tetrabutylammonium chloride at 298 K showing a downfield shift of the pyridine CH proton in the 2-position (green).	67
3.9	¹ H NMR titration curves for compound 3.1(a) with fluoride, chloride, bromide, iodide, methanesulfonate, nitrate, acetate, benzoate, sulfate and hydrogen sulfate in DMSO- <i>d</i> ₆ at 298 K. Anions added as their tetrabutylammonium salts. CH shift at 2-position of the pyridines.	69

3.10	¹ H NMR stack plots titrations of compound 3.1(b) in DMSO- <i>d</i> ₆ with tetrabutylammonium chloride and methanesulfonate at 298 K showing a downfield shift of the pyridine CH proton in both the 2-position (green) and the 6-position (violet), the pyrrole proton in the 3-position (orange) does shifts downfield too.	70
3.11	¹ H NMR stack plot titration of compound 3.1(b) in DMSO- <i>d</i> ₆ with tetrabutylammonium acetate at 298 K showing a downfield shift of the pyridine CH proton in the 2-position (green), the pyrrole NH proton does shifts downfield (dark yellow).	71
3.12	(a) ¹ H NMR titration curves of the pyridine CH proton in the 2-position for compound 3.1(c) with chloride, bromide, iodide, benzoate, acetate, methanesulfonate, nitrate and hydrogen sulfate in DMSO- <i>d</i> ₆ at 298 K and (b) ¹ H NMR stack plot titration of compound 3.1(c) in DMSO- <i>d</i> ₆ with chloride at 298 K showing a downfield shift of the pyridine CH proton in the 2-position (green). Anions added as their tetrabutylammonium salts.	72
3.13	(a) ¹ H NMR titration curves of the pyrrole NH proton for compound 3.1(c) with benzoate and acetate in DMSO- <i>d</i> ₆ at 298 K and (b) ¹ H NMR stack plot titration of compound 3.1(c) in DMSO- <i>d</i> ₆ with acetate at 298 K showing a downfield shift of the pyrrole NH proton (dark yellow). Anions added as their tetrabutylammonium salts.	73
3.14	A ball-and-stick representation of the X-ray crystal structure of the methanesulfonate salt of cation 3.1(b) . The hydrogen bonding network is shown with MeSO ₃ ⁻ anions bound above and below the plane of the complex by CH···O and NH···O hydrogen bonds.	74
3.15	Binding modes of complex 3.1(b) with anions such as methanesulfonate (A ⁻) in nitromethane- <i>d</i> ₃ and DMSO- <i>d</i> ₆	74
3.16	Hydrogen bond network within the calix[4]arene lower rim.	75
3.17	Platinum (II) complexes prepared to lock the free rotation of the ligands.	75
3.18	Platinum (II) complex of 2-hydroxypyridine. Intramolecular hydrogen bonds among the hydroxyl groups in the complex are observed in the solid state.	76
3.19	X-ray crystal structure of 2-hydroxypyridine.	77
3.20	A ball-and-stick representation of the X-ray crystal structure of 3.17(c) crystallized from acetonitrile.	78
3.21	¹ H NMR stack plot titration curves of compound 3.17(b) and tetrabutylammonium acetate.	79
3.22	¹ H NMR stack plot titration curves of compound 3.17(b) and tetrabutylammonium benzoate.	80
3.23	¹ H NMR stack plot titration curves of compound 3.17(b) and tetrabutylammonium sulfate.	80
3.24	¹ H NMR stack plot titrations of compound 3.17(c)	81
3.25	¹ H NMR stack plot titrations of compound 3.17(c)	82
4.1	Series of platinum(II) pyrrole carboxamides salts prepared for anion complexation studies.	85
4.2	(a) Thermal ellipsoids drawn at the 35% probability level, solvent omitted for clarity. (b) Part of a hydrogen bonded slab.	86

4.3	(a) Thermal ellipsoids drawn at the 35% probability level, solvent omitted for clarity. (b) Part of one of the chains of hydrogen bonded dimmers linked <i>via</i> one of the solvent ethanols.	87
4.4	(a) Thermal ellipsoids drawn at the 35% probability level. (b) Slabs lie in the <i>ab</i> plane.	88
4.5	^1H NMR titration curves for compound 4.1(a) with fluoride, chloride, bromide, iodide, methanesulfonate, acetate, and benzoate in $\text{DMSO-}d_6$ at 298 K. Anions added as their tetrabutylammonium salts.	89
4.6	Proton NMR stack plot titration of compound 4.1(a) in $\text{DMSO-}d_6$ with tetrabutylammonium chloride at 298 K showing a downfield shift of the isoquinoline CH proton in the 1-position (green), NH amide (brown), and NH pyrrole (violet).	89
4.7	^1H NMR titration curves for compound 4.1(b) with fluoride, chloride, bromide, iodide, methanesulfonate, acetate, benzoate, and dihydrogenphosphate in $\text{DMSO-}d_6$ at 298 K. Anions added as their tetrabutylammonium salts.	91
4.8	Proton NMR stack plot titration of compound 4.1(b) in $\text{DMSO-}d_6$ with tetrabutylammonium dihydrogenphosphate at 298 K showing a downfield shift of the pyridine CH proton in the 2-position (green), NH amide (brown), and NH pyrrole (violet).	92

List of Tables

1.1	Properties of hydrogen bond interactions.	4
1.2	Properties of some common anions and cations.	8
1.3	Shapes and geometries of anions.	8
2.1	Stability constants K_a (M^{-1}) of compounds 2.4(a) and 2.4(b) with a variety of putative anionic guests (added as tetrabutylammonium salts) at 298K in DMSO- d_6 /5% water (except where noted).	39
2.2	Stability constants K_a (M^{-1}) of compound 2.11(a) with a variety of putative anionic guests (added as tetrabutylammonium salts) at 298K in DMSO- d_6 /5% water (except where noted).	47
2.3	Stability constants K_a (M^{-1}) of compounds 2.11(b) and 2.11(d) with a variety of putative anionic guests (added as tetrabutylammonium salts) at 298K in DMSO- d_6 /5% water.	47
2.4	Stability constants K_a (M^{-1}) of compound 2.11(c) with a variety of putative anionic guests (added as tetrabutylammonium salts) at 298K in DMSO- d_6 /0.5% water.	49
2.5	pK _a values.	57
3.1	¹ H NMR chemical shifts upon addition of three equivalents of tetrabutylammonium anion salt to solutions of [3.1(a) , 3.1(b) and 3.1(c)] \cdot (BF ₄) ₂ in DMSO- d_6	68
3.2	Stability constants of the tetrafluoroborate salts of 3.1(a) , 3.1(b) and 3.1(c) with anionic guests in DMSO- d_6 at 298 K calculated from the shift of the resonance of the pyridine hydrogen in the 2-position except where noted assuming 1:1 stoichiometry in all cases except where noted.	69
4.1	¹ H NMR chemical shifts upon addition of three equivalents of tetrabutylammonium anion salt to solutions of [4.1(a) and 4.1(b)] \cdot (BF ₄) ₂ in DMSO- d_6	90
4.2	Stability constants of the salts 4.1(a) and 4.1(b) with anionic guests in DMSO- d_6 at 298 K calculated from the shift of the resonance of the isoquinoline and pyridine hydrogen in the 2-position assuming 1:1 stoichiometry in all cases.	91
A.1	Crystal data and structure refinement details.	114
A.2	Atomic coordinates ($\times 10^4$), equivalent isotropic displacement parameters ($\text{\AA}^2 \times 10^3$) and site occupancy factors. U_{eq} is defined as one third of the trace of the orthogonalized U^{ij} tensor.	115
A.3	Crystal data and structure refinement details.	118

A.4	Atomic coordinates ($\times 10^4$), equivalent isotropic displacement parameters ($\text{\AA}^2 \times 10^3$) and site occupancy factors. U_{eq} is defined as one third of the trace of the orthogonalized U^{ij} tensor.	118
A.5	Crystal data and structure refinement details.	121
A.6	Atomic coordinates ($\times 10^4$), equivalent isotropic displacement parameters ($\text{\AA}^2 \times 10^3$) and site occupancy factors. U_{eq} is defined as one third of the trace of the orthogonalized U^{ij} tensor.	121
A.7	Crystal data and structure refinement details.	124
A.8	Atomic coordinates ($\times 10^4$), equivalent isotropic displacement parameters ($\text{\AA}^2 \times 10^3$) and site occupancy factors. U_{eq} is defined as one third of the trace of the orthogonalized U^{ij} tensor.	124
A.9	Crystal data and structure refinement details.	128
A.10	Atomic coordinates ($\times 10^4$), equivalent isotropic displacement parameters ($\text{\AA}^2 \times 10^3$) and site occupancy factors. U_{eq} is defined as one third of the trace of the orthogonalized U^{ij} tensor.	128
A.11	Crystal data and structure refinement details.	131
A.12	Atomic coordinates ($\times 10^4$), equivalent isotropic displacement parameters ($\text{\AA}^2 \times 10^3$) and site occupancy factors. U_{eq} is defined as one third of the trace of the orthogonalized U^{ij} tensor.	131
A.13	Crystal data and structure refinement details.	133
A.14	Atomic coordinates ($\times 10^4$), equivalent isotropic displacement parameters ($\text{\AA}^2 \times 10^3$) and site occupancy factors. U_{eq} is defined as one third of the trace of the orthogonalized U^{ij} tensor.	133
A.15	Crystal data and structure refinement details.	136
A.16	Atomic coordinates ($\times 10^4$), equivalent isotropic displacement parameters ($\text{\AA}^2 \times 10^3$) and site occupancy factors. U_{eq} is defined as one third of the trace of the orthogonalized U^{ij} tensor.	136
A.17	Crystal data and structure refinement details.	138
A.18	Atomic coordinates ($\times 10^4$), equivalent isotropic displacement parameters ($\text{\AA}^2 \times 10^3$) and site occupancy factors. U_{eq} is defined as one third of the trace of the orthogonalized U^{ij} tensor.	138
A.19	Crystal data and structure refinement details.	140
A.20	Atomic coordinates ($\times 10^4$), equivalent isotropic displacement parameters ($\text{\AA}^2 \times 10^3$) and site occupancy factors. U_{eq} is defined as one third of the trace of the orthogonalized U^{ij} tensor.	140
A.21	Crystal data and structure refinement details.	142
A.22	Atomic coordinates ($\times 10^4$), equivalent isotropic displacement parameters ($\text{\AA}^2 \times 10^3$) and site occupancy factors. U_{eq} is defined as one third of the trace of the orthogonalized U^{ij} tensor.	142
A.23	Crystal data and structure refinement details.	144
A.24	Atomic coordinates ($\times 10^4$), equivalent isotropic displacement parameters ($\text{\AA}^2 \times 10^3$) and site occupancy factors. U_{eq} is defined as one third of the trace of the orthogonalized U^{ij} tensor.	144
A.25	Crystal data and structure refinement details.	146
A.26	Atomic coordinates ($\times 10^4$), equivalent isotropic displacement parameters ($\text{\AA}^2 \times 10^3$) and site occupancy factors. U_{eq} is defined as one third of the trace of the orthogonalized U^{ij} tensor.	146
A.27	Crystal data and structure refinement details.	148

A.28 Atomic coordinates ($\times 10^4$), equivalent isotropic displacement parameters ($\text{\AA}^2 \times 10^3$) and site occupancy factors. U_{eq} is defined as one third of the trace of the orthogonalized U^{ij} tensor.	148
A.29 Crystal data and structure refinement details.	150
A.30 Atomic coordinates ($\times 10^4$), equivalent isotropic displacement parameters ($\text{\AA}^2 \times 10^3$) and site occupancy factors. U_{eq} is defined as one third of the trace of the orthogonalized U^{ij} tensor.	150

List of Schemes

1.1	Two ligands bind to a metal forming a convergent hydrogen-bonding array suitable for anion coordination.	13
1.2	The synthesis of a ruthenium containing bis-thiourea dicarboxylate receptor.	14
2.1	Suggested product from the oxidation of compound 2.4(a)	40
2.2	Synthesis of the symmetric receptors 2.11(a) and 2.11(b)	42
2.3	General synthesis of the dialdehydes.	54
3.1	General synthesis for the square planar platinum (II) complexes.	61
3.2	Synthesis of the <i>meta</i> and <i>para</i> pyrrolepyridine ligands.	62
3.3	Path followed in the synthesis of 3.17(b)	77
4.1	Synthesis of the ligand <i>N</i> -(isoquinolin-8-yl)-1 <i>H</i> -pyrrole-2-carboxamide.	86
4.2	Synthesis of the ligand <i>N</i> -(isoquinolin-8-yl)-1 <i>H</i> -pyrrole-2-carboxamide.	88

Nomenclature

<i>atm</i>	Atmosphere
<i>Ac</i>	Acetyl
<i>AcOEt</i>	Ethylacetate
<i>Ala</i>	Alanine
<i>bp</i>	Boiling point in °C at 760 mm pressure, unless otherwise specified
<i>cm</i>	Centimeter
<i>conc.</i>	Concentrated
<i>d</i>	Doublet
<i>DCC</i>	<i>N,N'</i> -methanediylienedicyclohexanamine
<i>dil.</i>	Dilute
<i>DCM</i>	Methylene chloride
<i>DMAP</i>	Dimethylaminopyridine
<i>DMF</i>	Dimethylformamide
<i>DMSO</i>	Dimethyl sulfoxide
<i>eq</i>	Equivalent
<i>ES</i>	Electrospray
<i>g</i>	Gram
<i>h</i>	Hours
<i>IR</i>	Infrared
<i>ⁱPrOH</i>	Isopropanol
<i>J</i>	Coupling constant
<i>K</i>	Equilibrium constant
<i>L</i>	Ligand
<i>M</i>	Molarity of solution
<i>m</i>	Mass
<i>MeOH</i>	Methanol
<i>meq</i>	Milliequivalent
<i>mg</i>	Milligrams
<i>MHz</i>	Megahertz
<i>min.</i>	Minute, also minimum
<i>mm</i>	Millimeter
<i>mmol</i>	Millimole

<i>mp</i>	Melting point in °C
<i>MS</i>	Mass spectrum
<i>N</i>	Normality of solution
<i>NMR</i>	Nuclear magnetic resonance
<i>pH</i>	Value taken to represent the acidity or alkalinity of an aqueous solution
<i>pK_a</i>	Used to express the extent of dissociation of a weak acid or base
<i>ppb</i>	Parts per billion
<i>ppm</i>	Parts per million
<i>pptd.</i>	Precipitated
<i>qr</i>	Quartet
<i>R_f</i>	Reference factor
<i>s</i>	Singlet
<i>soln.</i>	Solution
<i>t</i>	Triplet
<i>temp.</i>	Temperature
<i>titr.</i>	Titration
<i>TLC</i>	Thin-layer chromatography
<i>UV</i>	Ultraviolet
<i>vol.</i>	Volume
<i>v/v</i>	Volume to volume ratio for a solution
<i>ws</i>	Wide singlet
<i>wt</i>	Weight
<i>w/w</i>	Weight to weight ratio
<i>z</i>	Charge
<i>X</i>	Counteranion
Δ	Error
δ	Chemical shift (ppm)
μg	Microgramme
μL	Microliter

Acknowledgements

Three years of hard research are the foundations of this thesis. During this period of my life, I never thought of the future - it came soon enough. I'd like to mention the people who contributed, one way or another, to this project.

I would like to thank Dr. P.A. Gale for his supervision and help during all this time. A professor is one who talks in someone else's sleep. There were several times where his advice reoriented my research to achieve our goals. My thanks also go to the current and past members of the Gale group.

I am also grateful to many people within the Supramolecular Chemistry group of the School of Chemistry at the University of Southampton, and both staff and graduate students of the University, who contributed to an excellent working atmosphere.

I would like to thank the EPSRC and the School of Chemistry for financially supporting me during three years.

I would like to thank the EPSRC Crystallographic Center that has solved the majority of the structures reported in this thesis. Especially my thanks go to Dr. Mark Light and Dr. Simon Coles who supported me over the last years and Prof. Mike Hursthouse. Thanks also to Dr. Stephen Loeb and his group members, for their help on the synthesis of some platinum compounds reported in chapter 3. Thanks to Dr. Malcolm Levitt and members of his group for their help with the NOESY experiments.

Thanks to all the friends who supported me during these years, from Spain, in Southampton or elsewhere. Thanks to my family, in particular my parents Nieves and Mohammad. Finally, thanks to María for her unconditional and endless support, this thesis belong to you too.

Agradecimientos

Tres años de dura investigación son la base que fundamenta esta tesis. Durante este periodo de mi vida no he tenido mucho tiempo para pensar en el futuro porque este llegaba demasiado rápido. Me gustaría agradecer a la gente que de una forma u otra ha contribuido a desarrollar este trabajo.

Me gustaría agradecer al Dr. P.A. Gale por su supervisión y ayuda durante estos tres años. Un profesor es aquel que consigue hablar en tus sueños. Ha habido varias ocasiones donde su consejo me ha servido para reorientar mi trabajo y conseguir nuestros objetivos. Quisiera agradecer también a los miembros presentes y pasados del grupo del Dr. P.A. Gale.

Estoy también agradecido a los miembros del grupo de Química Supramolecular en la Universidad de Southampton, así como tanto al personal como estudiantes de la Universidad que contribuyen a un maravilloso ambiente.

Me gustaría agradecer al EPSRC y la Escuela de Química por su financiación durante los últimos tres años.

Quisiera agradecer al Centro de Cristalografía EPSRC que ha resuelto la mayor parte de las estructuras cristalinas presentes en esta tesis. Agradezco especialmente a los Dres. Mark Light y Simon Coles que me han ayudado en este terreno, así como al Catedrático Mike Hursthouse. Gracias también al Dr. Stephen Loeb y los miembros de su grupo, por su ayuda en la síntesis de algunos de los compuestos que forman el tercer capítulo. Gracias al Dr. Malcolm Levitt y los miembros de su grupo por su ayuda con los experimentos NOESY.

Gracias a todos los amigos que me han apoyado durante estos tres años, desde España, en Southampton o donde sea. Gracias a mi familia, particularmente a mis padres Nieves y Mohammad. Finalmente, gracias a María por su apoyo incondicional e infinito, esta tesis te pertenece también a ti.

"I have not failed. I've just found 10,000 ways that won't work."

– Thomas Alva Edison (1847-1931).

To the memory of my grandfather José.

To María.

Chapter 1

Introduction

Jean-Marie Lehn, who shared the Nobel Prize in 1987 for his work in the area of supramolecular chemistry, described this field as ‘the chemistry of molecular assemblies and the intermolecular bond’.¹ Supramolecular chemistry has also been described as: ‘the chemistry beyond the molecule’, ‘the chemistry of the noncovalent bond’, and ‘non-molecular chemistry’.¹⁻⁴ Each of these definitions is useful as are others, but each has limitations and exceptions when the definitions are pushed to specific examples. Indeed, supramolecular chemistry can be defined to encompass the chemistry of molecular assemblies from a molecule in a molecular solvent cage to the constellation of molecular assemblies (composed of proteins, lipids, DNA, RNA) that constitute the enormous chemical complexity of a living cell.

1.1 Supramolecular chemistry

Although the roots of supramolecular chemistry are with the beginning of modern chemistry itself, as it is now known, is a young discipline dating back to the late 1960s and early 1970s. At that stage, development of macrocyclic ligands for metal cations was especially important.⁵⁻⁹

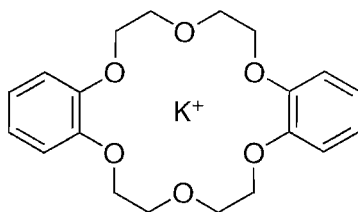


FIGURE 1.1: Pedersen reported in 1967 the synthesis and coordination chemistry of crown ethers which marked the beginning of modern supramolecular chemistry.

As a consequence of the early interest that cation recognition generated during the first

stages of this discipline, this is now a well-developed and mature area of supramolecular chemistry.

The kind of forces we must consider when a supramolecular complex is formed are:

- I) ion-ion interactions ($100\text{--}350\text{ kJ mol}^{-1}$) are in similar strength range to covalent bonding. Sodium chloride, the most typical example of an ionic solid, is a cubic lattice in which each Cl^- anion is surrounded by six Na^+ cations (Figure 1.2). Although NaCl is not considered a supramolecular compound it is a good example of the cation-anion selforganization (i.e. Figure 1.2).

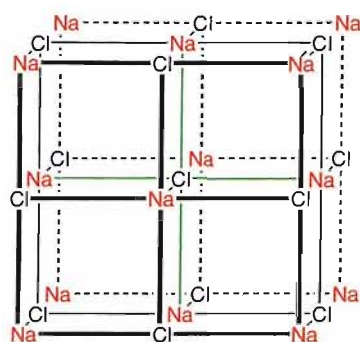


FIGURE 1.2: The NaCl ionic lattice.

A much more classic supramolecular exampleⁱ of ion-ion interaction is the chloride and tetrakis(thiourea)platinum (II) interaction (Figure 1.3), where linear platinum chloride ion-ion interaction geometry is observed.¹⁰

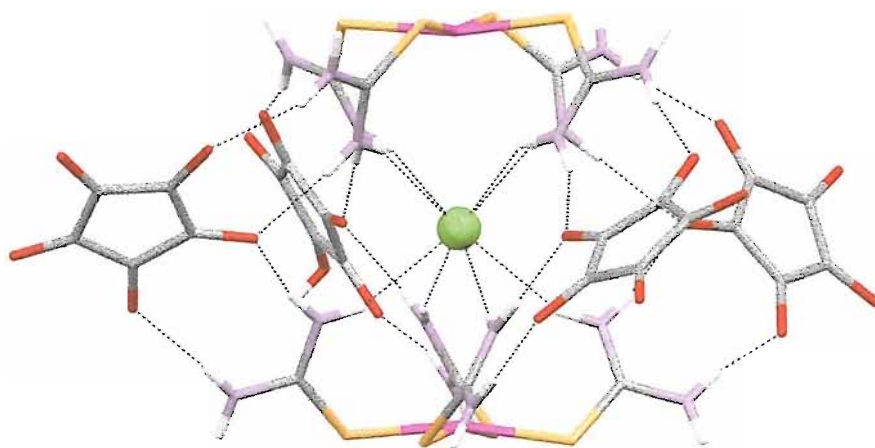


FIGURE 1.3: The chloride templated capsule $[(\text{Pt}(\text{SC}(\text{NH}_2)_2)_4)_2 \cdot (\text{C}_5\text{O}_5)_3 \cdot (\text{C}_5\text{O}_4\text{-OH}) \cdot \text{Cl}]^{4-}$ present in the solid-state structure. C_5O_5 = croconate.

ⁱHydrogen bond forces included.

II) ion-dipole interactions ($50\text{--}200\text{ kJ mol}^{-1}$) consist in the coordination of a polar molecule, such as water, with an ion, such as Na^+ (Figure 1.4(a)). This behavior is apparent in the solid state and in solution. A supramolecular analogue is readily apparent in the structures of alkali metal cations with macrocyclic (large ring) ethers in which the ether oxygen atoms play the same role as the polar water molecules. The oxygen lone pairs are attracted to the cation positive charge (Figure 1.4(b)). Ion-dipole interactions also include coordinative bonds, which are mostly electrostatic in nature in the case of the interactions of nonpolarisable metal cations and hard bases. Coordinative (dative) bonds with a significant covalent component, as in $[\text{Ru}(\text{bipy})_3]^{2+}$ are also used in supramolecular assembly and the distinction between supramolecular species can become rather blurred (Figure 1.4(c)).

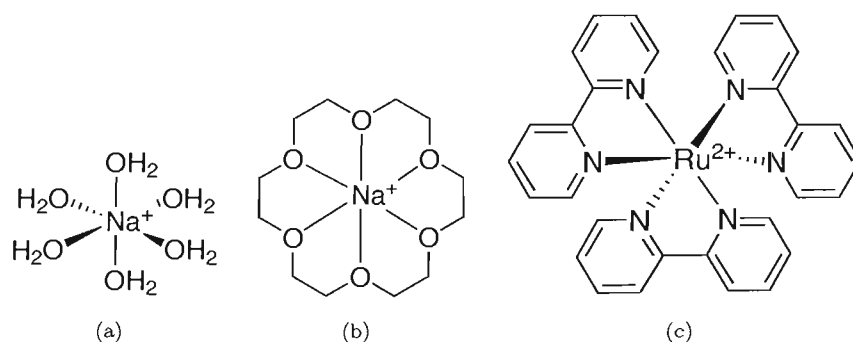


FIGURE 1.4: (a) Na^+ hexahydrate (b) Na^+ crown ether complex and (c) $[\text{Ru}(\text{bipy})_3]^{2+}$ bipy = 2,2'-bipyridyl.

III) dipole-dipole interactions ($5\text{--}50\text{ kJ mol}^{-1}$) occurs when molecules with permanent dipoles (polar molecules), attract each other, this pushes up the boiling points. Organic carbonyl compounds show this behavior well in the solid state and calculations have suggested that opposing alignment of one dipole with the other have an energy of about 20 kJ mol^{-1} comparable to a moderately strong hydrogen bond (Figure 1.5(b)).

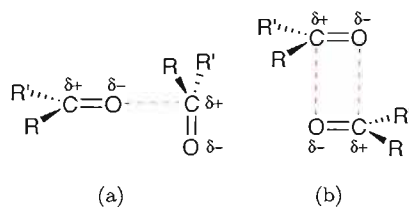
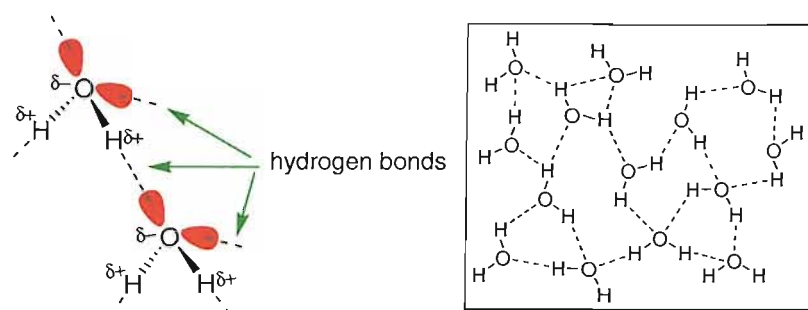


FIGURE 1.5: Dipole-dipole interactions in carbonyls.

IV) hydrogen bonding ($4\text{--}120\text{ kJ mol}^{-1}$) is probably the most important interaction on earth, as water physical properties (ie. boiling point, melting point, superficial

tension, and others) are directly related to this force and water is the molecule of life.



A hydrogen atom covalently bonded to an electronegative atom H-X (X = oxygen, nitrogen, sulfur, fluoride ...) has got a partial positive charge generated by the charge withdraw of its neighbour atom $H^{\delta+} \rightarrow X^{\delta-}$. The interaction of the dipoles $H^{\delta+} \rightarrow X^{\delta-} \cdots H^{\delta+} \rightarrow X^{\delta-}$ constitute a hydrogen bond. Because of its relatively strong and highly directional nature, hydrogen bonding has been described as the ‘*masterkey interaction* in supramolecular chemistry’.¹¹

This interaction is ubiquitous in organisms. Hydrogen bonds stabilize the tertiary structure of proteins, double helix structure of DNA,¹² and are involved in recognition of substrates by numerous enzymes (Figure 1.6).^{13,14}

Hydrogen bonds come in a bewildering range of lengths, strengths and geometries. This force exert a marked influence on substances in the solid state, solution and gas phases. Table 1.1 gives some general parameters.

	Strong	Moderate	Weak
X-H...B interaction	Mainly covalent	Mainly electrostatic	Electrostatic
Bond energy (kJ mol ⁻¹)	60–120	16–60	< 12
Bond lengths (Å) H...B	1.2–1.5	1.5–2.2	2.2–3.2
Bond lengths (Å) X...B	2.2–2.5	2.5–3.2	3.2–4
Bond angles (°)	175–180	130–180	90–150
Relative IR vibration shift (stretching symmetrical mode, cm ⁻¹)	25%	10–25%	< 10%
Examples	Gas phase dimers with strong acid bases, proton sponge, HF complexes	Acids, alcohols, and biological molecules	Minor components of bifurcated bonds, C–H hydrogen bonds, O–H...π hydrogen bonds

TABLE 1.1: Properties of hydrogen bond interactions.

V) π - π stacking (0–50 kJ mol⁻¹) occur between aromatic rings, often in situations where one is relatively electron rich and one is electron poor. There are two

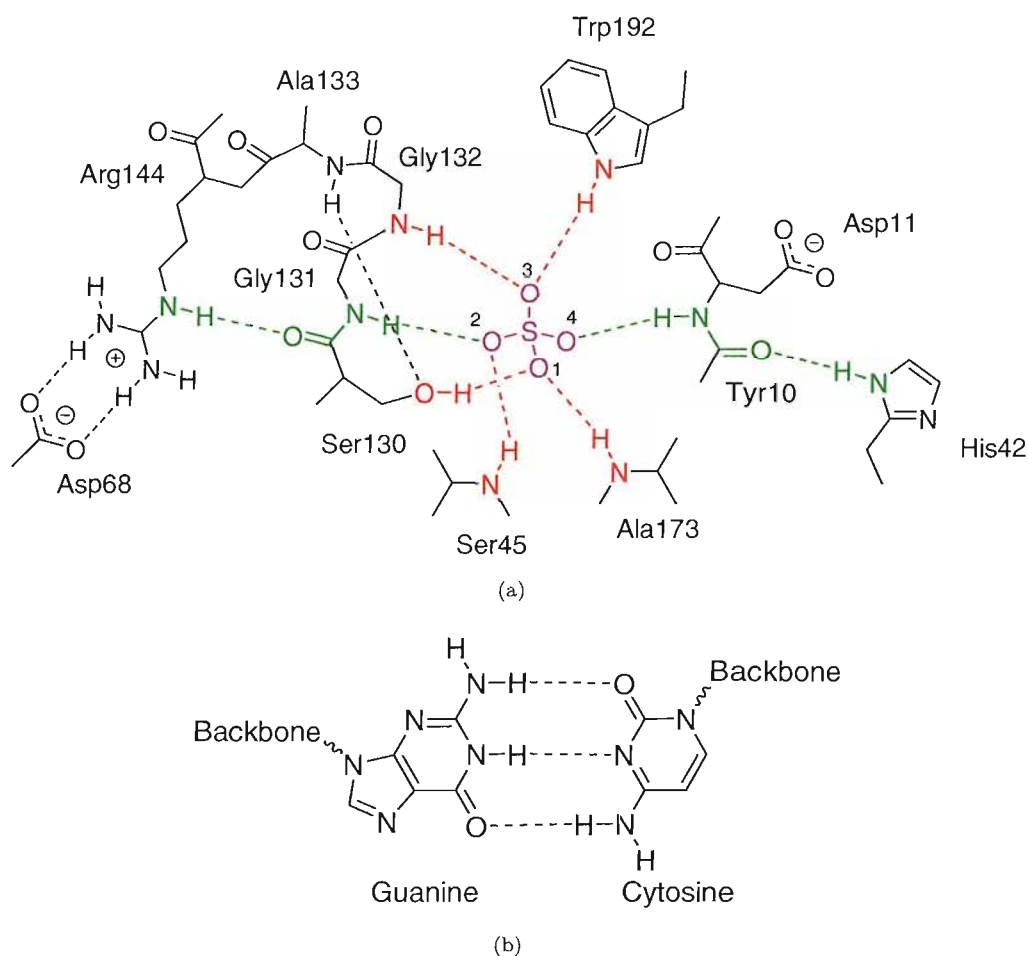


FIGURE 1.6: (a) Sulfate binding protein where hydrogen bonds keep the overall 3D shape of the protein and bind the anion. (b) Base pairing in DNA by hydrogen bonding.

general types of π -stacking: face-to-face and face-to-edge (Figure 1.7), although a wide variety of intermediate geometries are known.¹⁵

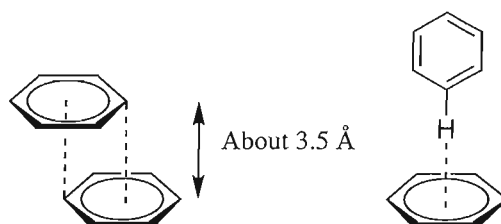


FIGURE 1.7: Limiting types of π - π stacking. Note the offset to the face-to-face mode (direct overlap is repulsive).

VI) van der Waals forces ($< 5 \text{ kJ mol}^{-1}$) also called dispersion and induction forces occur from the polarization of an electron cloud by the proximity of an adjacent nucleus, resulting in a weak electrostatic attraction.

VII) hydrophobic effects are the driving force for the formation of membranes and

micelles from aqueous solution. Hydrophobic effects are commonly believed to play a similar role in the folding of globular proteins, although proteins are very much more complex systems. This force, also called solvatophobic, may be divided into two energetic components:

- *enthalpic hydrophobic effect* involves the stabilization of water molecules that are driven from a host cavity upon guest binding. Because host cavities are often hydrophobic, intercavity-water does not interact strongly with the host walls and is therefore of high energy. Upon release into the bulk solvent, it is stabilized by interactions with other water molecules.
- *entropic hydrophobic effect* arises from the fact that the presence of two (often organic) molecules in solution (host and guest) creates two ‘holes’ in the structure of bulk water. Combining host and guest to form a complex results in less disruption to the solvent structure and hence an entropic gain (resulting in a lowering of overall free energy). The process is presented schematically in Figure 1.8.

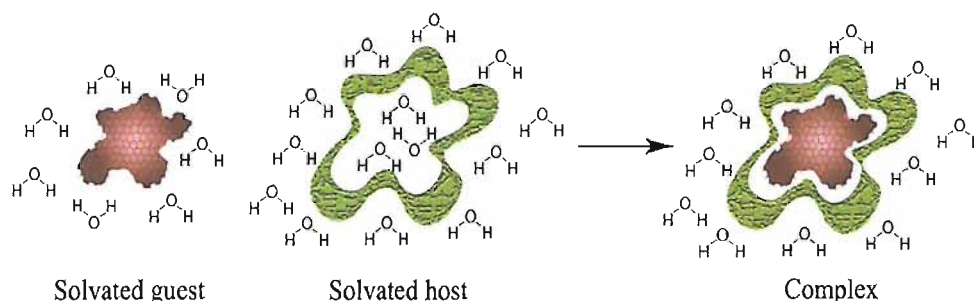


FIGURE 1.8: Hydrophobic binding of organic guests in aqueous solution.

Supramolecular host-guest compounds can be described in terms of the spatial relationships between them (Figure 1.9). By neighbourhood relationships in supramolecular chemistry we mean that two molecules are in the proximity of one another during a certain time period. During this time period the two molecules may be considered to be bonded irrespective of the nature of the bonding and the reason the atoms are close to one another. Thus, the idea of neighborhood relationships allows the acceptance of any type of interactions that keep molecules in each other's neighborhood. For example, a molecule that is contained as a guest inside a host fullerene has a clear neighborhood relationship to the internal cage of the fullerene. Similarly, a molecule that is contained as a guest in the cavity of a host such as a cyclodextrin or a cavitand has a clear neighborhood relationship to the cavity of the host. A molecule that is contained as a guest in a crystal and is surrounded by molecules of a crystalline host has a clear neighborhood relationship to the surrounding molecules of the crystal. Finally, a guest molecule that

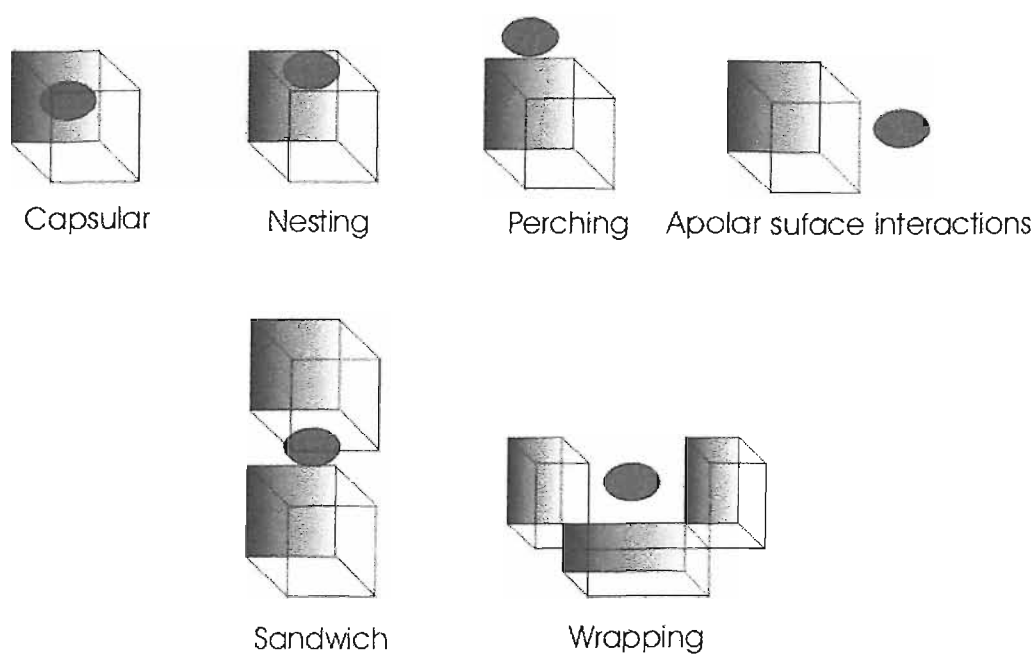


FIGURE 1.9: Descriptive terms used to illustrate spatial relationships between host and guest.

is intercalated in a host DNA double-helix has a chemical relationship to a small set of specific bases that are in its neighborhood.

1.2 Anion coordination

Anion recognition chemistry received little attention, and only over the last three decades has started to receive the recognition it deserves.ⁱⁱ There are a number of reasons for this growth of interest in anion reconnaissance. All biological systems are composed by anion aqueous solutions, being the DNA the more relevant polyanion present in all live organisms. Most enzyme substrates and co-factors are anionic. ATP is the anion that carries energy in biological systems. Phosphate is an anion widely used in soaps and detergents and its presence in lakes and rivers may cause eutrophication.¹⁷

The development of anion receptors requires a higher level of design due to a number of reasons: Anions use to have a lower effective charge versus isoelectronic cations because of its bigger radius (see Table 1.2).¹⁶ Compared to cations of similar size, anions have

ⁱⁱChronology:

- 1968 report by C. H. Park and H. E. Simmons of the du Pont de Nemours Company concerning the halide complexation properties of *katapinands*.¹⁶ This was the second major contribution to the unborn field of supramolecular chemistry.
- 1967 paper by Pedersen regarding the cation binding properties of dibenzo[18]crown-6 marked the beginning of modern supramolecular chemistry.⁹

a high degree of solvation and hence anion host must compete more effectively with the surrounding medium (see Table 1.2).¹⁶ Especially important is the wide range of shapes that exist of anions (see Table 1.3).¹⁷ The state in which anions are in solution depends on the pH value and consequently receptors must be designed to bind the anion within its pH window. If we take into account the lock and key analogy, when a host-guest complex is formed, it is easy to imagine that similar degree of design must be required to make receptors complementary to their anionic guest.

Ion	Radius (Å)	$\Delta G_{hydration}$ (kJ mol ⁻¹)	pK _a (298K)
F ⁻	1.33	-465	3.3
Cl ⁻	1.81	-340	Low
Br ⁻	1.95	-315	Low
I ⁻	2.16	-275	Low
ClO ₄ ⁻	2.50	-430	-
NO ₃ ⁻	1.79	-300	-1.4
CO ₃ ²⁻	1.78	-1315	6.4, 10.3
SO ₄ ²⁻	2.30	-1080	Low, 2.0
PO ₄ ³⁻	2.38	-2765	2.1, 6.2, 12.4
H ₂ PO ₄ ⁻	2.00	-465	2.1, 6.2, 12.4
PdCl ₆ ²⁻	3.19	-695	-
Na ⁻	2.2	n/a	-
Cs ⁻	3.5	n/a	-
Li ⁺	0.69	-475	-
Na ⁺	1.02	-365	-
K ⁺	1.38	-295	-
Cs ⁺	1.70	-250	-
Ca ²⁺	1.00	-505	-
Zn ²⁺	0.75	-1955	-
Al ³⁺	0.53	-4525	-
La ³⁺	1.05	-3145	-
NH ₄ ⁺	1.48	-285	-

TABLE 1.2: Properties of some common anions and cations.

Anion	Shape
Halides	spherical
SCN ⁻ , N ₃ ⁻	linear
NO ₃ ⁻ , PtCl ₄ ²⁻	planar
PO ₄ ³⁻ , SO ₄ ²⁻	tetrahedral
PF ₆ ⁻ , Fe(CN) ₆ ³⁻	octahedral
DNA, ATP	complicated shapes

TABLE 1.3: Shapes and geometries of anions.

Since the last three decades many sustained efforts are being applied to resolve problems inherent to the anion binding chemistry.¹⁸ A widespread armory of selective receptors for anions was developed as a consequence of the increasing interest in anionic species

in areas such as the environment, biology, catalysis and medical applications.^{19–21}

High proportions of anions can be found naturally in the sea, as well as in contaminated lakes and rivers. The anthropogenic enrichment of lakes and rivers with anions is the major cause of changes in ecosystems and jeopardies many of these natural resources. Anthropogenic eutrophication is caused by increasing concentrations of nitrate and phosphate anions in water.²² These anions act as a source of nutrients for phytoplankton, which could multiply at high rate if provided also with enough light. An abnormal population of phytoplankton is a cause of increasing turbidity of water as well as decreasing levels of oxygen. Turbidity causes the death of organisms (such as algae and sea grass) as they shielded from the sun, and deoxygenation causes asphyxiation of many other aerobic species. Pertechnetate is a nuclear waste from the reprocessing of nuclear fuel and can cause severe damage if is shed to oceans.²³ The long half-life of technetium-99 and its ability to form anionic species makes it (along with ¹²⁹I) a major concern when considering long-term disposal of high-level radioactive waste. In addition many of the processes designed to remove fission products from medium active process streams in reprocessing plants are designed to remove cationic species (for example ¹³⁷Cs and ⁹⁰Sr). Hence the pertechnetate is able to escape through these treatment processes. As a result of nuclear fuel reprocessing, technetium has been discharged into the sea in a number of locations, and some seafood contains tiny but measurable quantities. For example, lobster from west Cumbria contains small amounts of technetium.²⁴ Moreover, the abnormal concentration of anions in water may cause infant methemoglobinaemia ('blue baby' syndrome), and have been related with certain cancers.²⁵

Anions also play roles in disease. *Hyperphosphatemia* occurs when the phosphorus load (from gastrointestinal absorption, exogenous administration, or cellular release) exceeds renal excretion and tissue uptake. Hyperphosphatemia causes hypocalcemia by precipitating calcium, decreasing vitamin D production, and interfering with parathyroid hormone-mediated bone resorption.²⁶ Severe life-threatening hypocalcemia may result. Signs and symptoms of acute hyperphosphatemia are due to the effects of hypocalcemia. Prolonged hyperphosphatemia promotes metastatic calcification, an abnormal deposition of calcium phosphate in previously healthy connective tissues such as cardiac valves and in solid organs such as muscles.²⁷ The calcium-phosphate product predicts the risk of metastatic calcification. Excess free serum phosphorus is taken up into vascular smooth muscle *via* a sodium-phosphate co-transporter. The increased cellular phosphate activates a gene, *cbfa-1*, that promotes calcium deposition in the vascular cell, making smooth muscle cells engage in osteogenesis. Vascular walls become calcified and arteriosclerotic, leading to increased systolic blood pressure, widened pulse pressure, and subsequent left ventricular hypertrophy. Hyperphosphatemia is an independent risk factor contributing to the increased incidence of aortic and mitral stenosis and other cardiovascular disease among dialysis-dependent patients. A peripheral form known as calcific uremic arteriolopathy (calciphylaxis) can induce necrotic ulcer-

ation and gangrene in affected extremities. Hyperphosphatemia-induced resistance to parathyroid hormone contributes to secondary hyperparathyroidism and renal osteodystrophy. Hyperphosphatemia occurs most often in patients with renal insufficiency. Most patients with acute or chronic renal failure have hyperphosphatemia in some degree. To avoid hyperphosphatemia, patients with end-stage renal disease and a glomerular filtration rate (GFR) < 30 must restrict their intake of dietary phosphorus.²⁸ If dietary restriction alone does not reduce serum phosphate levels into the normal range, oral phosphate binders should be added to reduce absorption.²⁹ Current therapies include calcium- and aluminium-based agents. Binders containing calcium may cause hypercalcemia and promote vascular calcium deposition by increasing the calcium-phosphate product. Aluminium can cause aluminium intoxication and even dementia after long term use (Figure 1.10).³⁰

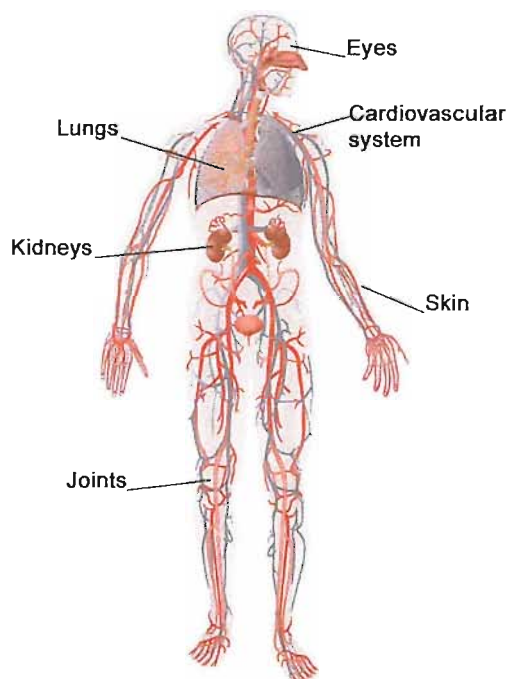


FIGURE 1.10: Bone disease, cardiovascular problems (heart disease and stroke), calcifications and mineral deposits (kidneys, lungs, joints, eyes, heart and skin) are health disorders related to high levels of phosphate anion in human body.

Thus, the existence of a phosphate selective binder could be of prime clinical utility in terms of treating a major public health problem.

In biological systems it was found that proteins interact selectively with anions. During the last years many efforts were dedicated to resolve the crystal structures of this kind of systems, and probably the most known examples are the sulfate binding protein and the phosphate binding protein crystal structures published by Quioco and co-workers (Figure 1.11).^{13,14,31}

Adenosine triphosphate is one of the most important anions in biology (Figure 1.12).

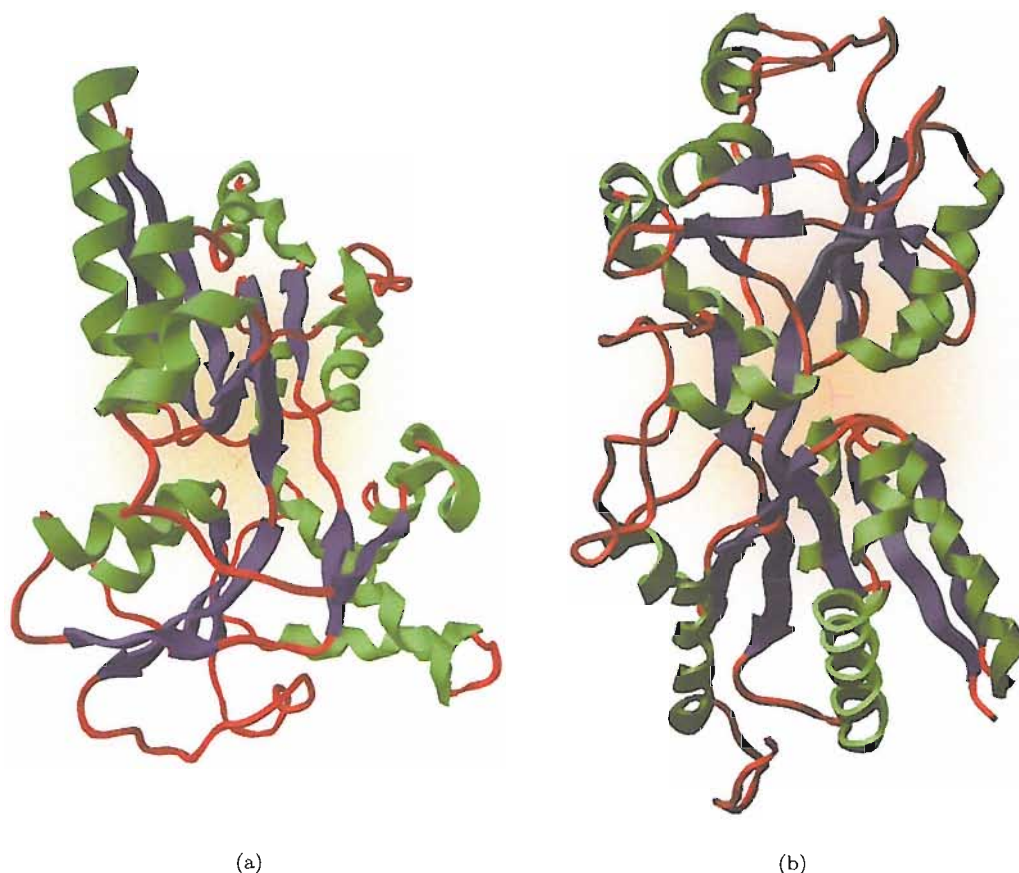


FIGURE 1.11: Crystal structures of (a) sulfate binding protein and (b) phosphate binding protein.

All living things require a continual supply of energy in order to function, and this anion represents the energy the organisms can handle. ATP works by losing the endmost phosphate group when instructed to do so by an enzyme. This reaction releases a lot of energy, which the organism can then use to build proteins, contract muscles, etc. The reaction product is adenosine diphosphate (ADP), and the phosphate group either ends up as orthophosphate (HPO_4^{2-}) or attached to another molecule (e.g. an alcohol). Even more energy can be extracted by removing a second phosphate group to produce adenosine monophosphate (AMP). When the organism is resting and energy is not immediately needed, the reverse reaction takes place and the phosphate group is reattached to the molecule using energy obtained from food or sunlight. Thus the ATP molecule acts as a chemical ‘battery’, storing energy when it is not needed, but able to release it instantly when the organism requires it.

The polyaza macrocycle shown in Figure 1.13 is able to form stable complexes with ATP, ADP, and AMP in acid media. These supramolecular assemblies catalyze the solvolysis of the bound substrates.³²

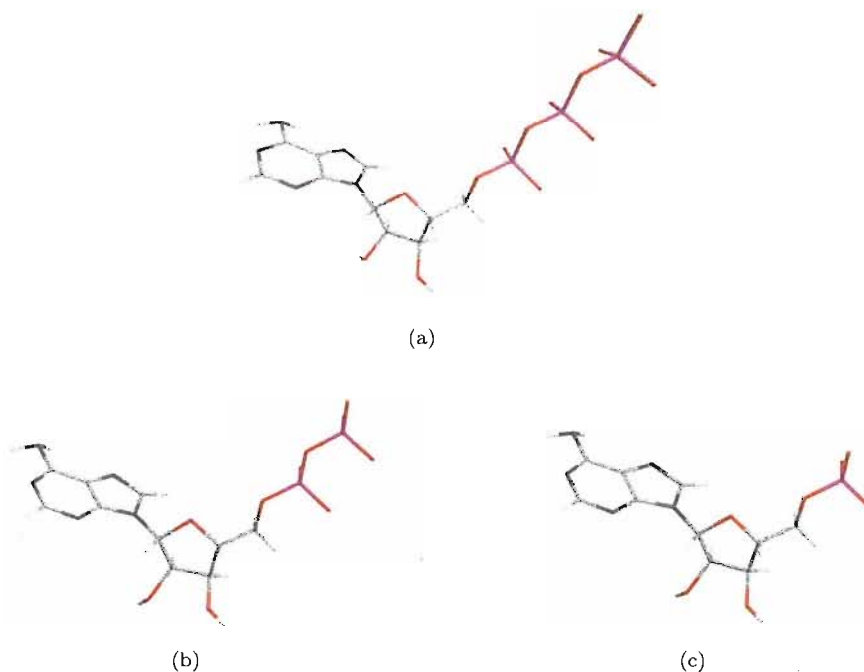


FIGURE 1.12: Crystal structures of (a) ATP (b) ADP and (c) AMP.

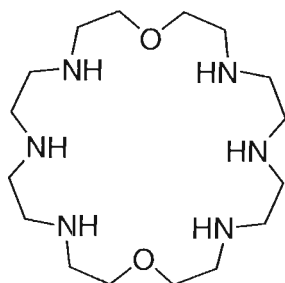


FIGURE 1.13: The 24-membered macrocyclic polyamine that catalyze the hydrolysis of the ATP.

1.3 Synthetic receptors

To design an artificial anion host molecule, there are some fundamental points of host-guest relationships¹⁸ which must be considered:

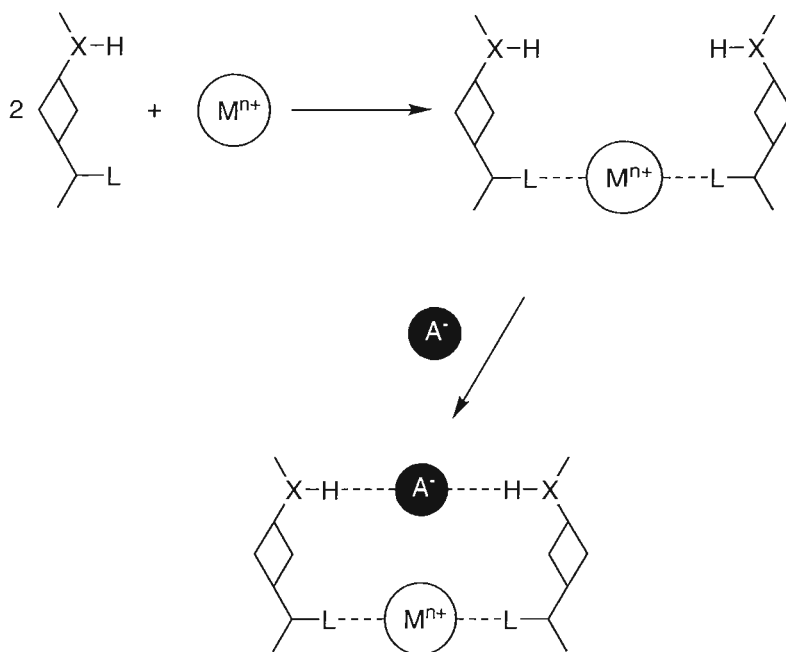
- The nature of the guest selected to be bonded by the molecular host. Discrimination of similar guest species by the host must be maximized.
- The kind of solvent used for the host-guest complexation. Solvent choice is crucial when we study a host-guest interaction as both binding constant values and binding sites may be severely affected by solvent properties.ⁱⁱⁱ

ⁱⁱⁱWe report in Section 3.1.2 an example where the solvent election changes completely the binding behavior of the receptor (see also Figure 3.15).

Supramolecular host design is a very challenging task as the combination of the receptor shapes, functional groups, and nature of forces to consider are huge. In the next subsections we will see how different authors addressed these host design issues.

1.3.1 Metal based

There are many examples of anion receptors containing metal ions. These might be present as an anion coordination site or to increase the acidity of hydrogen bond donor groups on coordinated organic ligands in order to form stronger anion complexes. Alternatively the metal may be present as a reporter group that undergoes a significant change in optical or electrochemical properties upon anion complexation. Our interest covers an important sub-group of metal containing anion receptors and specifically those in which hydrogen bond donor groups on different ligands are organised by space by coordination to a metal (Scheme 1.1). The advantages of this approach to the construction of anion receptor systems are that the ligands themselves can be simple and easy to synthesise. It is the metal complexation step that organises the simple components into an anion receptor system. Secondly electrostatic interactions between the metal and bound anion may play a role in stabilising the anion complex.

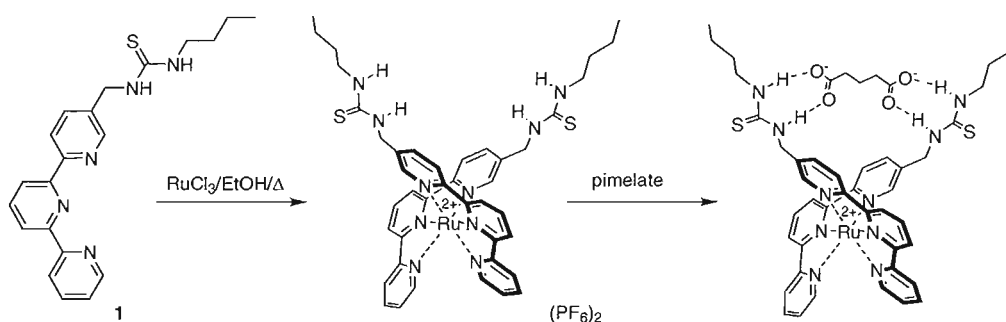


SCHEME 1.1: Two ligands bind to a metal forming a convergent hydrogen-bonding array suitable for anion coordination.

1.3.1.1 Receptors containing inert metal ions

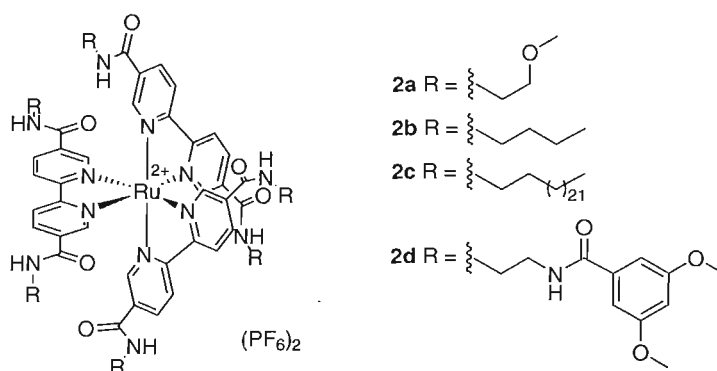
The use of inert metal cations to template such systems allows the metal complex to be treated as a discrete stable entity.

An early report of such a receptor was made in 1995 by Hamilton and co-workers in the context of combinatorial approaches to receptor design. Several ruthenium(II) complexes were prepared containing two terpyridine ligands appended with different guest binding sites. One of the complexes $(1)_2\text{Ru}^{2+}(\text{PF}_6)_2$ (Scheme 1.2) contained two thiourea appended terpyridines and was shown to bind pimelate in DMSO solution with a stability constant $K_a > 10^4 \text{ M}^{-1}$.^{33,34}



SCHEME 1.2: The synthesis of a ruthenium containing bis-thiourea dicarboxylate receptor.

Beer and co-workers used ruthenium (II) tris(5,5'-diamide-2,2'-bipyridine) receptors to bind Cl^- and NO_3^- selectively, and to study the effect of the amide substituent and the ratio of DCM/MeOH solvent mixture medium on anion selectivity.³⁵



The four host molecules **2a-2d** were prepared as their hexafluorophosphate salts by reacting ruthenium (III) trichloride with the respective ligands in EtOH-H₂O or dimethylformamide (DMF) solution. Complexation of the metal arranges the ligands such that there are two potential anion-binding sites each containing three NH hydrogen bond

donor groups. The Δ and Λ forms of **2a** were resolved by cation exchange chromatography. Stability constants were determined by UV-VIS spectroscopy in dichloromethane (DCM) and DCM-MeOH solutions with tetrabutylammonium chloride, acetate and nitrate salts. The results demonstrate that anion binding strength, stoichiometry (the receptors either bound one or two anions) and selectivity are strongly dependent on the type of anion, the solvent system and the receptor amide substituent. The structure of the chloride complex of Δ -**2a** is shown in Figure 1.14. As the amount of polar solvent increases in the solvent mixture DCM/MeOH, the value of the binding constant decreases with all three anions. Binding with acetate was only observed at the lower concentrations of MeOH (1:0 and 9:1). The non-complementarity shape of acetate may explain why the weakest complexes are formed with this anion. Receptors **2a** and **2b** remain chloride selective when the ratio of MeOH increases in the DCM/MeOH solvent mixture, while receptors **2c** and **2d** become selective for nitrate.

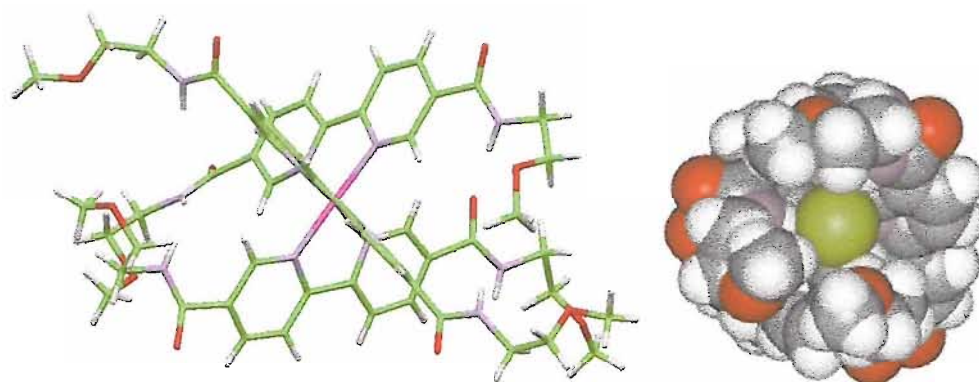


FIGURE 1.14: The structure of the Δ -form of **2a** with ellipsoids at 20% probability (left). Two chlorides are bound, each *via* three hydrogen bonds from the amide NH groups as illustrated in the CPK representation of the structure (right).

Square planar platinum complexes have been used by Bondy, Gale and Loeb as scaffolding upon which to construct an anion receptors.^{36,37} Receptor **3** was synthesised by complexation of *n*-butylnicotinamide with $\text{PtCl}_2(\text{EtCN})_2$ followed by metathesis with AgPF_6 . The receptor provides both hydrogen bond donating groups and an electrostatic contribution to binding from the metal center. The pyridine ligands are free to rotate around the pyridine platinum bond allowing the complex to adopt four different conformations which can be labelled using calixarene type nomenclature. Interestingly, this receptor binds planar anions such as nitrate or acetate in a 2:1 anion:receptor stoichiometry, whilst tetrahedral or pseudo-tetrahedral anions bind in a 1:1 stoichiometry. Unfortunately, the conformation in solution could not be determined, however the crystal structure of the perrhenate complex of **3** (shown in Figure 1.15) shows the anion bound in the 1,2-alternate conformation in the solid state *via* two amide NH-O hydrogen bonds and two pyridine CH-O interactions.

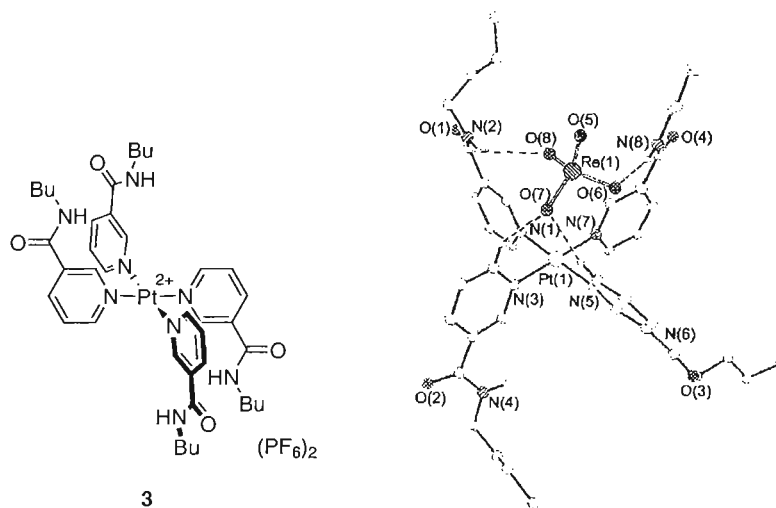


FIGURE 1.15: The X-ray crystal structure of the perrhenate complex of 3^{2+} .

A second generation receptor has recently been reported which contains four urea functionalised iso-quinoline ligands that exhibits remarkably strong binding of sulfate by completely encapsulating the anion in a “cone” conformation in both solution and solid state.³⁸ Receptor $[\text{Pt}(\text{L})_4]^{2+}$ **4**, was synthesised by reaction of $\text{PtCl}_2(\text{EtCN})_2$ with two equivalents of silver tetrafluoroborate and four equivalents of $\text{L} = 8\text{-}(n\text{-butylurea})\text{isoquinoline}$ in acetonitrile. The solubility of 4.2BF_4 limited studies of anion interactions to relatively polar solvents such as a mixture of 35% $\text{MeNO}_2\text{-}d_3$ and 65% $\text{DMF-}d_7$ or $\text{DMSO-}d_6$. Negligible interactions with triflate, perrhenate and nitrate were observed in those solvent mixtures by ^1H NMR titration techniques. Proton NMR titrations in $\text{DMSO-}d_6$ were used to determine the association constants of 4.2BF_4 with halide anions, dihydrogenphosphate and sulfate. Two distinct types of anion-receptor interactions were observed with this set of anions. First, for the halide anions, chloride, bromide, and iodide titration curves using NH resonance were best fitted to 1:2 receptor:anion complex stoichiometry in solution. Crystallization of the chloride complex of the receptor gave X-ray quality crystals suitable for X-ray analysis. This crystal structure (Figure 1.16(c)) shows that the complex adopts a 1,2-alternate conformation in which two pairs of adjacent urea groups hydrogen bond each chloride anion. Among the halides, the receptor has association constants following the trend $\text{Cl}^- > \text{Br}^- > \text{I}^-$. The binding curves appear somewhat sigmoid in nature, inferring allosteric behavior, but all K_1 values are greater than their K_2 counterparts, reflecting the reduction in electrostatic interactions upon the first anion binding. A different binding mode is observed with the oxo-anions dihydrogenphosphate and sulfate. These anions are bound very strongly even in highly competitive solvent $\text{DMSO-}d_6$. In both cases large shifts are observed for resonances of both NH and $\alpha\text{-CH}$ (Figure 1.16(b)). An X-ray crystal structure of the complex $[\text{Pt}(\text{L})_4]\cdot\text{SO}_4$ shows that the metal organic receptor interacts with the anion in a 1:1

anion:receptor ratio adopting a cone conformation with all eight NH groups oriented towards the anion (Figure 3.15(b)).

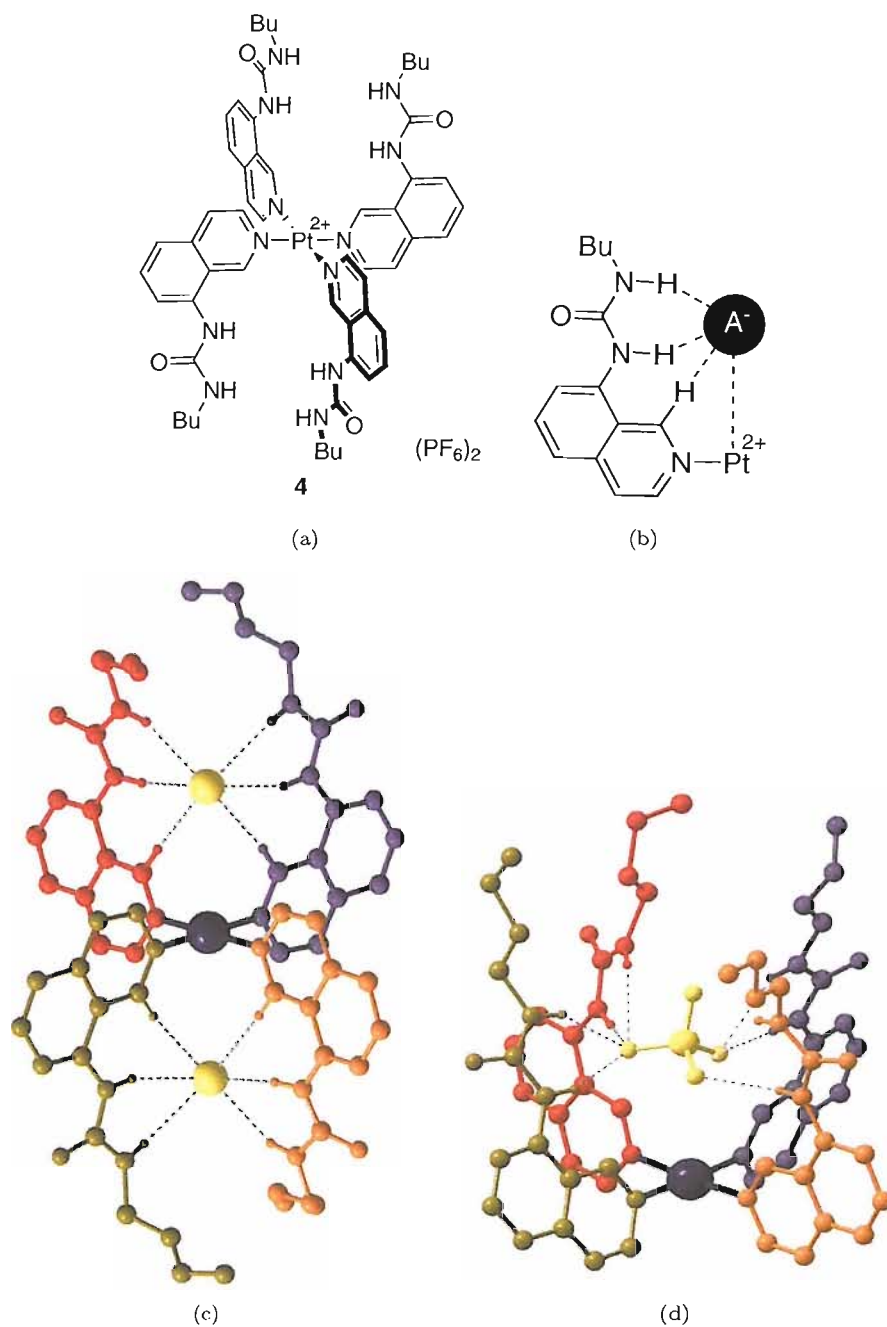
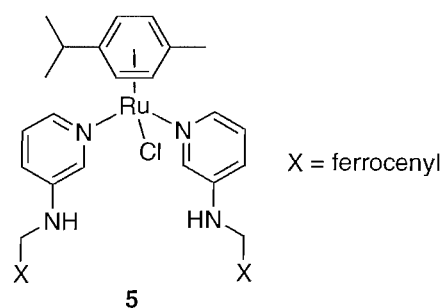


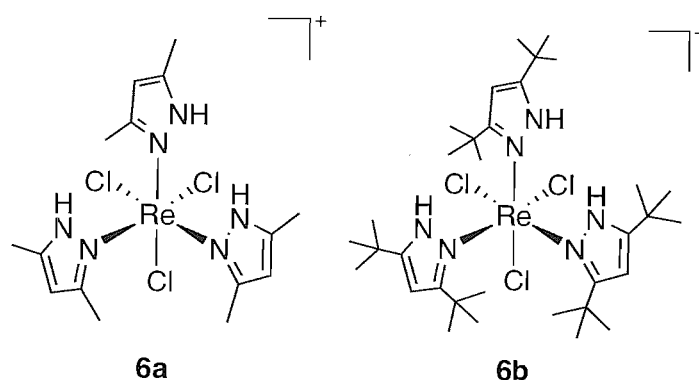
FIGURE 1.16: The chloride (c) and sulfate (d) complexes of receptor 4. 1H NMR titrations demonstrate that the anions interact with the urea NH hydrogen atoms and α -CH hydrogens (b)

Steed and co-workers employed ruthenium metal centres combined with aminopyridine ligands³⁹ to prepare selective receptors for oxoanions such as NO_3^- and HSO_4^- . The

anion binding behaviour of the bis(pyridyl) receptor **5** was studied using ^1H NMR titration with a variety of oxo-anions in CDCl_3 . The strongest interaction was observed with HSO_4^- (K_{11} 5240M^{-1} , K_{21} 136M^{-1}). This high affinity for HSO_4^- may be due to the acidity of the anion resulting in protonation of the host secondary amine sites, leading to the formation of a stable ion pair between protonated host and SO_4^{2-} . Such an effect cannot be responsible for the strong binding of NO_3^- however (K_{11} 1412M^{-1} , K_{21} 52M^{-1}), and stable complex formation in this case is presumably due to a high degree of structural complementarity between the host and guest.

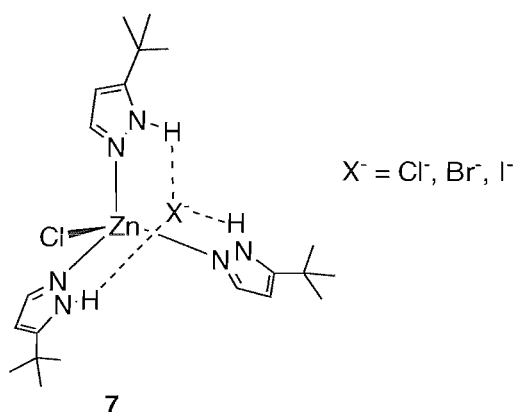


Pérez and co-workers used *fac*-tris(pyrazole) octahedral rhenium complexes **6a** and **6b** as chloride anion receptors.⁴⁰ Compounds **6a** and **6b** were synthesized by reaction of $[\text{Re}(\text{OTf})(\text{CO})_5]$ with the corresponding pyrazole in toluene, followed by anion metathesis with $\text{NaB}(3,5\text{-(CF}_3)_2\text{-C}_6\text{H}_3)_4$. Proton NMR of **6a** indicates the non-equivalence of the two methyl groups in the 3- and 5-positions on the pyrazole rings indicating absence of intramolecular pyrazole exchange. Proton NMR titrations of receptors **6a** and **6b** *vs.* NH_4Cl were carried out in CD_3CN . The large shift to higher frequencies of the NH signals of compounds **6a** and **6b** suggests a strong hydrogen bond interaction. The titration data show that complexes **6a** and **6b** bind chloride with stability constants of 6385 and 4692 M^{-1} respectively.



1.3.1.2 Complexes with labile metal centres

Halcrow and co-workers have shown that monodentate pyrazole that acts as a ditopic receptor for Zn(II) halide salts e.g. **7** in the solid state and in non-polar solvents. The complexes $[\text{ZnX}(\text{Hpz}^{\text{tBu}})]\text{X}$ ($\text{X}^- = \text{Cl}^-, \text{Br}^-, \text{I}^-$) ($\text{Hpz}^{\text{tBu}} = 3\{5\}\text{-tert-butylpyrazole}$) contain a non-coordinated X^- anion hydrogen bonded within a pocket formed by the Hpz^{tBu} *tert*-butyl groups.



Complex **7** was prepared by reaction of ZnX_2 ($\text{X}^- = \text{Cl}^-, \text{Br}^-, \text{I}^-$) with three equivalents of 3{5}-*tert*-butylpyrazole (Hpz^{tBu}) in MeOH affording after work up crystals of $[\text{ZnCl}(\text{Hpz}^{\text{tBu}})_3]\text{Cl} \cdot \frac{1}{2}(\text{C}_5\text{H}_{12})$ (**7a**, $\frac{1}{2}\text{C}_5\text{H}_{12}$), $[\text{ZnBr}(\text{Hpz}^{\text{tBu}})_3]\text{Br} \cdot \frac{1}{2}(\text{C}_5\text{H}_{12})$ (**7b**, $\frac{1}{2}\text{C}_5\text{H}_{12}$), and $[\text{ZnI}(\text{Hpz}^{\text{tBu}})_3]\text{I} \cdot \text{CH}_2\text{Cl}_2$ (**7c**, DCM). All compounds lose their occluded solvent upon drying. The single crystal structures of **7a-7c** show that the anion X^- is hydrogen-bonded to all three Hpz^{tBu} NH groups, and lies within a bowl-shaped pocket formed by the pyrazole *t*Bu substituents. The chemical shift of the NH ^1H NMR resonance (δ_{NH}) for the complexes in a given solvent follows the sequence **7a** > **7b** >> **7c**. This is consistent with the anions' relative polarising power ($\text{Cl}^- > \text{Br}^- > \text{I}^-$), and implies that $\text{NH} \cdots \text{X}$ hydrogen bonding is an important feature of the solution structures of these compounds. In the presence of $\text{NBu}_4^+\text{BF}_4^-$, δ_{NH} is lowered by 0.2-0.7 ppm for **7a** and **7b** and by 1.2-1.5 ppm for **7c**, depending on the solvent, implying that BF_4^- competes with halides for the complex anion-binding site. Addition of *ca.* 1.5 mol equivalents of the relevant NBu_4^+X^- ($\text{X}^- = \text{Cl}^-, \text{Br}^-, \text{I}^-$) salt to **7a-7c** in all four solvents greatly broadens the pyrazole C³ and C⁵ resonances. This shows that the excess halide promotes Hpz^{tBu} exchange, presumably by acting as a nucleophile to Zn.

Replacement of the hydrogen bonded anion was possible by treatment of **7a** with the appropriate Ag(I) or Tl(I) salts to afford $[\text{ZnCl}(\text{Hpz}^{\text{tBu}})_3]\text{X}$ ($\text{X}^- = \text{BF}_4^-$ (**8a**), ClO_4^- (**8b**), NO_3^- (**8c**), CF_3SO_3^- (**8d**), PF_6^- (**8e**)).⁴¹ All the complexes contain Hpz^{tBu} and the appropriate X^- anion by IR spectroscopy, while electrospray mass spectrometry showed in each case a strong peak at $m/z=471$ from $[\text{ZnCl}(\text{Hpz}^{\text{tBu}})_3]$. Importantly, no

mass peaks corresponding to $[\text{ZnX}(\text{Hpz}^{\text{tBu}})_3]$ were detected, suggesting that X^- counter anion does not displace the Cl^- ligand at Zn in the MeOH matrix. Single crystal X-ray structures were obtained for **8a-8d**. For **8a-8d**, all three pyrazole ligands hydrogen bond to the X^- anion in the solid state, although the topology of the hydrogen bonds varies from compound to compound. As for **7a, 8a-8d**, the PF_6^- anion in **8e**, lie within the cavities formed by the Hpz^{tBu} ligands of the complex cations. However, in contrast to **8a-8d** only two of the three NH groups of each receptor form hydrogen bonds to this anion. Proton NMR studies were carried out in CDCl_3 with compounds **8a-8d**. The fact that NH depends on X^- in $[\text{ZnCl}(\text{Hpz}^{\text{tBu}})_3]\text{X}$ suggest that $\text{NH}\cdots\text{X}$ hydrogen bonding is important in the solution structures of **8a-8d**. There is an approximate correlation of NH with the identity of the hydrogen bond acceptor atom in the guest anion halide [Cl^- , Br^- , I^-], O [NO_3^- , ClO_4^- , CF_3SO_3^-] > F [BF_4^- , PF_6^-]. This is reasonable, since a more basic anion should form stronger hydrogen bonds to the receptor complex which would in turn lead to a higher value of NH. For **7b, 7c, 8a, 8d, 8e** NH increases with increasing concentration between 0.036-0.143 mol \times dm $^{-3}$, reaching a plateau at higher concentrations. This demonstrates that these five complexes are in equilibrium in solution, most likely reflecting only partial binding of the guest anion X^- . This dependence is markedly more pronounced for **8a** and **8e** than for other compounds, suggesting that BF_4^- and PF_6^- bind much more weakly to $[\text{ZnCl}(\text{Hpz}^{\text{tBu}})_3]^+$ than the halide or oxo-anions studied. In contrast, the strongest interactions in solution were observed with **7a, 8b**, and **8d** as no detectable equilibrium was observed during the concentration studies. Although no binding constants were reported for these systems, from the concentration dependence of NH for **7a-7c** and **8a-8e** they rank the different anions in order of their relative affinities for the $[\text{ZnY}(\text{Hpz}^{\text{tBu}})_3]^+$ ($\text{Y} = \text{Cl}^-$, Br^- , I^-) receptor: $(\text{Cl}^-, \text{ClO}_4^-, \text{NO}_3^-) > (\text{Br}^-, \text{I}^-, \text{SO}_3^-) \gg (\text{BF}_4^-, \text{PF}_6^-)$. The single crystal structure of $[\text{ZnCl}(\text{Hpz}^{\text{tBu}})_3]\text{PF}_6$ showed some structural distortion of the complex cation, owing to steric interactions between the Hpz^{tBu} ligands and the PF_6^- anion (Figure 1.17). This suggested that anions larger than PF_6^- might not interact with the Zn complex in the same way.

Halcrow and co-workers have also prepared some new salts of $[\text{ZnCl}(\text{Hpz}^{\text{tBu}})_3]^+$ with a series of globular, carborane anions.⁴² The Ag(I) salts of $[\text{Co}(\text{C}_2\text{B}_9\text{H}_{11})_2]^-$, $[\text{1-Ph-}closo\text{-1-CB}_9\text{H}_9]^-$ and $[\text{6, 7, 8, 9, 10-Br}_5\text{-}closo\text{-1-CB}_9\text{H}_5]^-$ were prepared by metathesis of either the sodium or tetraethylammonium salts of these anions with AgNO_3 in water. Treatment of $[\text{ZnCl}(\text{Hpz}^{\text{tBu}})_3]\text{Cl}$ with the generated silver salts afforded $[\text{ZnCl}(\text{Hpz}^{\text{tBu}})_3]\text{Y}$ ($\text{Y}^- = [\text{Co}(\text{C}_2\text{B}_9\text{H}_{11})_2]^-$ (**9a**), $[\text{1-Ph-}closo\text{-1-CB}_9\text{H}_9]^-$ (**9b**) and $[\text{6, 7, 8, 9, 10-Br}_5\text{-}closo\text{-1-CB}_9\text{H}_5]^-$ (**9c**)). X-ray analysis of crystals revealed that as in salts of $[\text{ZnCl}(\text{Hpz}^{\text{tBu}})_3]^+$ with small inorganic anions, the cations in all three compounds have a distorted tetrahedral geometry and interact with the carbaborane anion *via* the Hpz^{tBu} ligands. However in the case of **9a** and **9b**, two of the three pyrazole ligands are rotated away from the carbaborane anions, so that these form hydrogen bonds to the Cl^- ligand of a neighbouring complex cation. As in **9a** and **9b**, two of the three Hpz^{tBu} ligands in **9c** take part in hydrogen-bonding to the chloride ligand of a neighbouring complex anion (Fig-

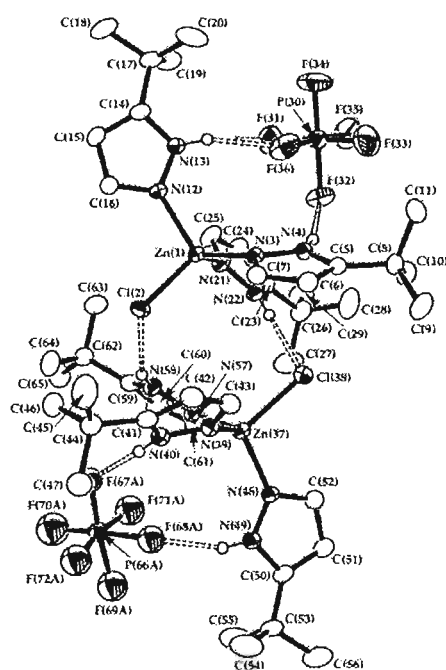


FIGURE 1.17: View of the two crystallographically independent $[\text{ZnCl}-(\text{Hpz}^{\text{tBu}})_3]\text{PF}_6$ moieties in the crystal structure of **8e** CH_2Cl_2 , showing the atom numbering scheme employed. Only one orientation of the hexafluorophosphate anion is shown.

ure 1.18). The third Hpz^{tBu} ligand on each cation hydrogen bonds *via* a water molecule to the anion.

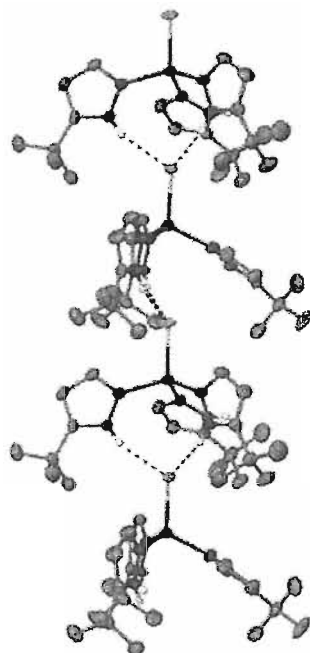


FIGURE 1.18: Partial packing diagram of **9c**, showing the association of the $[\text{ZnCl}-(\text{Hpz}^{\text{tBu}})_3]^+$ cations into a hydrogen-bonded 1-D polymer.

Receptor **10**, containing a kinetically labile silver (I) template reported by Steed and co-workers, shows a particularly high affinity for nitrate.^{43,44} This complex was formed by reaction of 1-(pyridin-3-yl)-3-*p*-tolylurea with silver nitrate. X-ray crystallographic analysis revealed that the nitrate anion is bound by five hydrogen bonds from urea NH and also pyridine CH hydrogen bond donors in the solid state (Figure 1.19(b)).

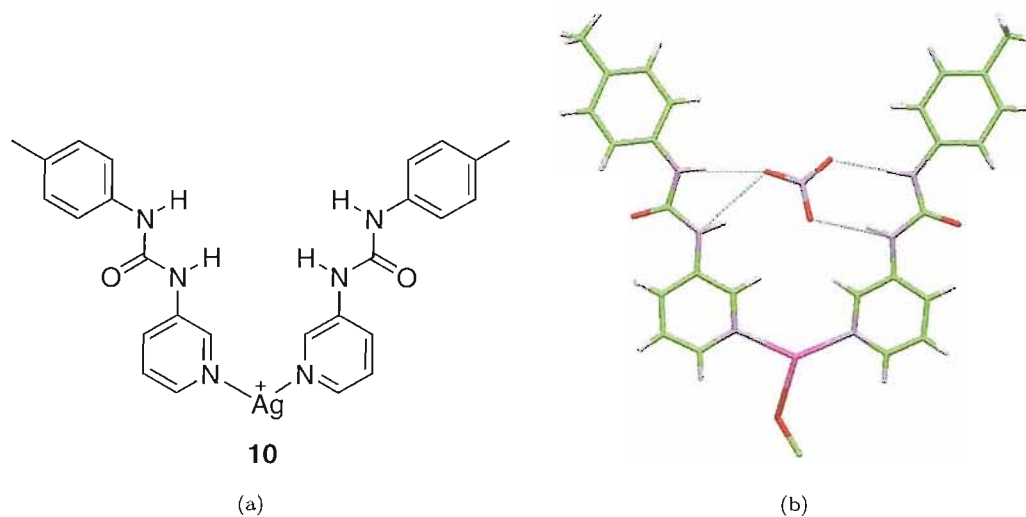


FIGURE 1.19: The silver complex **10** (a) and the discrete [10](NO₃).MeOH complex (b) showing nitrate binding in an asymmetrical arrangement to the bis-urea metal complex.

The tweezer-like conformation of the complex [Ag(1-(pyridin-3-yl)-3-*p*-tolylurea)₂]NO₃ that exists in the solid state, is also observed in solution over particular nitrate concentration ranges. Proton NMR titration experiments with **10**.CF₃SO₃ and NO₃⁻ afford stability constants K₁₁ of 30200 M⁻¹, K₁₂ 2900 M⁻¹, and K₁₃ 550 M⁻¹ in acetone-*d*₆ corresponding to the tweezer conformation binding one equivalent of nitrate, one nitrate binding to each urea independently (Figure 1.20), and a third nitrate binding to the metal respectively. Model experiments with triflate show that there is apparently little or no chelation of this anion within the tweezer-like cavity, whereas nitrate brings about a change in conformation of the silver complex, resulting in the chelated geometry observed in the crystal structure. This structure persists until addition of more than one equivalent of nitrate, at which point the chelated 1:1 structure gradually converts to a situation in which nitrate anions bind separately to the two ligands on the outside of the complex.

In a very interesting communication Rice and co-workers report the self assembly of the ligand **11** with Co²⁺ into a dinuclear triple helicates [Co₂(**11**)₃]⁴⁺ to produce an anion binding pocket which encapsulates perchlorate anions. Furthermore, they demonstrate how this ability to bind anions can control ligand self assembly processes.⁴⁵

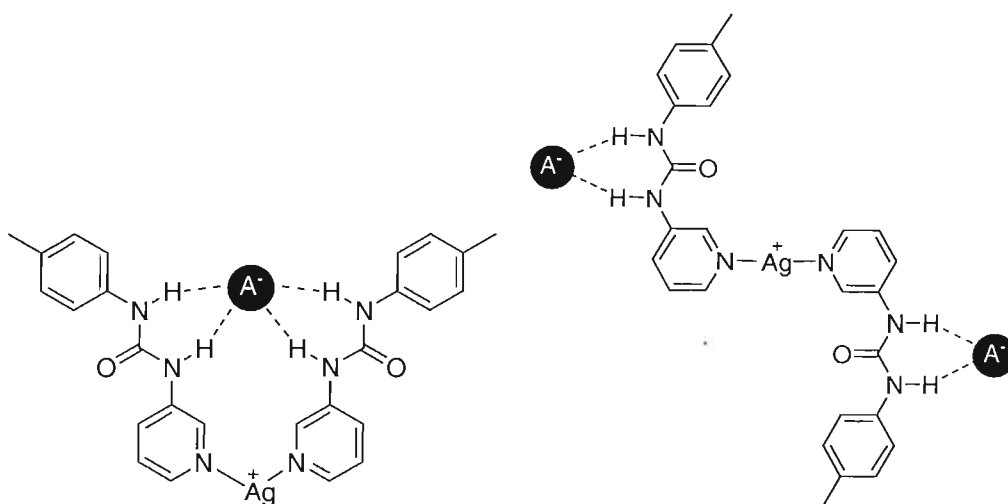
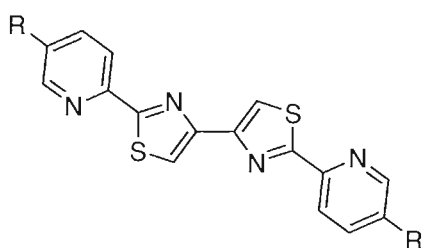


FIGURE 1.20: Two of the proposed conformations adopted by complex **10** in solution binding either one or two equivalents of added anionic guest.



11 R = (S)-CONHCH(CH(CH₃)₂)CO₂Me
12 R = H

This dinuclear complex $[\text{Co}_2(\mathbf{11})_3]^{4+}$ was prepared by reaction of $[\text{Co}(\text{ClO}_4)_2] \cdot 6\text{H}_2\text{O}$ with the respective **11** in acetonitrile. A mixture of diastereomers was observed in solution corresponding to the different helical forms (Δ or Λ) due to the presence of the chiral terminal groups on the ligand. The crystal structure of the complex cation $[\text{Co}_2(\mathbf{11})_3](\text{ClO}_4)_2^{2+}$ shows that upon self-assembly into a dinuclear triple helicate, two cavities are formed, at either end of the helicate that contain amide groups capable of hydrogen bonding to anions. Indeed the structure contains a perchlorate anion encapsulated within each of these self-assembled cavities (Figure 1.21(a)). Both perchlorate anions are bound *via* two of their oxygens to two of the three NH donors at distances between 2.14–2.34 Å. In both cases the third amide NH group is directed away from the perchlorate anion forming an intramolecular NH \cdots O hydrogen bond (2.98 Å). By contrast the crystal structure of $[\text{Co}_2(\mathbf{11})_3](\text{ClO}_4)_2(\text{NO}_3)_2$, shows all three amide groups in the pocket forming hydrogen bonds to the NO_3^- anion with shorter bond lengths (2.06–2.38 Å) (Figure 1.21(b)). Furthermore, the nitrate is bound deeper within the receptor cleft than perchlorate (*av.* $\text{Co}\cdots\text{NO}_3$ 4.42 Å, $\text{Co}\cdots\text{ClO}_4$ 5.00 Å), perhaps illustrating a stronger binding of the nitrate anion than that of perchlorate. Rice performed two experiments in order to show the importance of the anion in the ligand-ligand self-recognition process. First ^1H NMR spectroscopy was used to monitor the reaction of a mixture of **11** and **12** with $[\text{Co}(\text{ClO}_4)_2] \cdot 6\text{H}_2\text{O}$ in CD_3CN . The ^1H NMR spectrum showed that

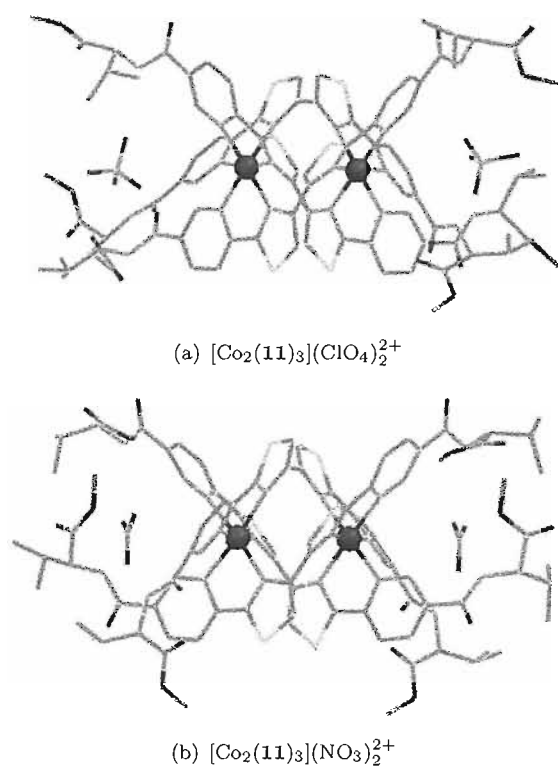
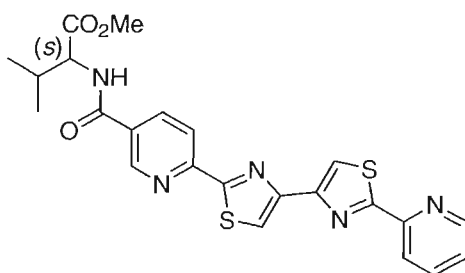


FIGURE 1.21: The X-ray crystal structure of the complex cations.

four helical species were present $[\text{Co}_2(\mathbf{11})_3]^{4+}$, $[\text{Co}_2(\mathbf{11})_2(\mathbf{12})]^{4+}$, $[\text{Co}_2(\mathbf{11})(\mathbf{12})_2]^{4+}$, and $[\text{Co}_2(\mathbf{12})]^{4+}$ in the statistical ratio 1:3:3:1. In the second experiment potassium nitrate was added to the same reaction mixture and the ^1H NMR spectrum was re-recorded. In this case, the major products of the reaction were the homoleptic products $[\text{Co}_2(\mathbf{11})_3]^{4+}$ and $[\text{Co}_2(\mathbf{12})]^{4+}$ and only *ca.* 5% of the heteroleptic complexes were present in the mixture. When nitrate anion is added, ligand-anion interactions trigger effective ligand-ligand ‘recognition’.

In later work Rice has reported the anion control of the formation of a dinuclear triple helicate by coordination of an amide-substituted unsymmetrical ligand **13** with cobalt(II).⁴⁶ This complex exists in solution as both possible C_1 (HHT) (head to head to tail) and C_3 (HHH) (head to head to head) symmetric geometric isomers. Complex $[\text{Co}_2(\mathbf{13})_3](\text{ClO}_4)_4$ was synthesised in a similar way to $[\text{Co}_2(\mathbf{11})_3](\text{ClO}_4)_4$.



13

Proton NMR spectrum of this complex is consistent with a 1:3 ratio of HHH:HHT isomers being present in solution. Addition of two equivalents of NBu_4NO_3 to a CD_3CN solution of $[\text{Co}_2(\mathbf{13})_3](\text{ClO}_4)_4$ affords the C_3 HHH product in 95% yield and the HHT C_1 product in *ca.* 5% yield. In this case the HHH product was detected as *ca.* 1:1 mixture of diastereoisomers which again arise from the chirality of the helicate (Δ or Λ) and the resolved chiral (*S*) amide substituents. The solid state structure of the ΛS diastereoisomer of the complex cation $[\text{Co}_2(\mathbf{13})_3(\text{NO}_3)]^{3+}$ nitrate encapsulated by strong hydrogen bonds to the three amide NH protons at the end of the complex (Figure 1.22).

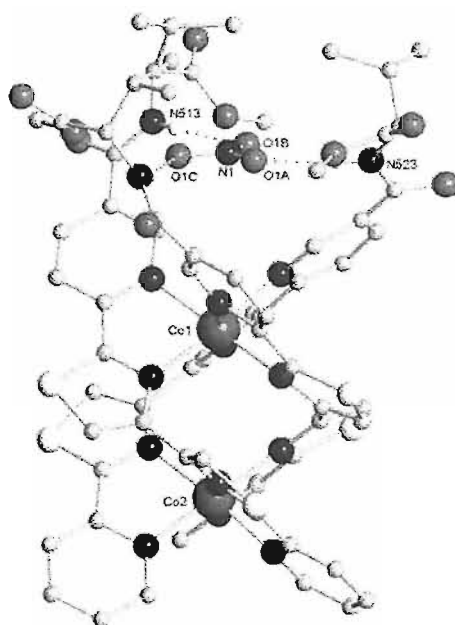


FIGURE 1.22: Crystal structure of the ΛS diastereomer of the complex cation $[\text{Co}_2(\mathbf{13})_3(\text{NO}_3)]^{3+}$.

The use of metal-organic hydrogen bond donors to bind anions is still at a relatively early stage. Inert metals may be used to construct discrete receptors with high affinities for anionic guests, whilst systems containing labile metals can be employed in interesting new self-assembly processes with anions driving the distribution of complexes in solution. There is still much to do in this area and we predict metal-organic receptors will be of increasing importance in the anion recognition arena over the coming years.

1.3.2 Heterocycle containing receptors

The importance of heterocyclic receptors in the anion recognition arena is enormous, specially by the number of annual publications they generate. A special mention into this field must be dedicated to the pyrrole functional group. Since anion binding properties of calixpyrrole were studied, many were the receptors prepared from the pyrrole moiety.

It occurs that pyrrole offers a neutral NH hydrogen bond group that is able to bind anions. Furthermore, this small molecule is a suitable brick from which to build a wide range of receptors of multiple possible geometries that could be combined with a vast number of functional groups that generate additional anion binding properties.

1.3.2.1 Acyclic pyrrole derivatives

In an effort to demonstrate the anion binding capabilities of the pyrrole molecule, Gale and co-workers crystallized tetramethylammonium chloride from pyrrole. The resulting complex (Figure 1.23) in which two pyrrole units hydrogen bond the chloride anion ($\text{NH}\cdots\text{Cl}^- = 2.327 \text{ \AA}$) demonstrate the pyrrole ability to bind anions through its NH group in the solid state.⁴⁷

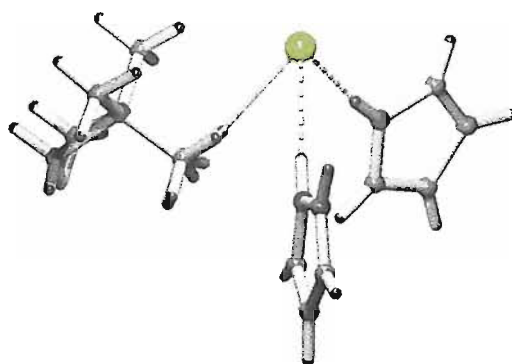


FIGURE 1.23: Crystal structure of the $\text{N}(\text{Me})_4\text{Cl}\cdots\text{pyrrole}$ complex.

Gale and co-workers moved one step forward in the design of new anion receptors by successfully combining a pyrrole with an amide functional group (Figure 1.24(a) and 1.24(b)).⁴⁸ Crystal structures of these compounds show hydrogen bond interaction of the pyrrole-amide moiety, suggesting an efficient combination for anion coordination. The association constants for the complexation of these receptors and various anionic guest species was investigated by using ^1H NMR titration experiments, in acetonitrile and $\text{DMSO}/\text{H}_2\text{O}$ 0.5% solutions respectively. The butylamide receptor showed 1:1 selectivity for the benzoate anion ($K_a = 2.5 \times 10^3 \text{ M}^{-1}$), while the phenylamide receptor was 1:1 selective for the dihydrogenphosphate anion ($K_a = 1.45 \times 10^3 \text{ M}^{-1}$).

Schmuck and co-workers produced a new set of pyrrole based receptors by combining a pyrrole with a guanidinium and an amide group (see Figure 1.25).⁴⁹ The guanidinium functional group introduces a positive charge in these receptors making this molecules even more anion-*philia*. ^1H NMR titrations in $\text{DMSO-}d_6/\text{H}_2\text{O}$ 40% solutions of these receptors were performed *vs.* N-Ac-L-Ala-O^- and N-Ac-L-Ala-O^- ,^{iv} obtaining 1:1 association constants in the range of $(2.7\text{-}4.6) \times 10^2 \text{ M}^{-1}$.

^{iv} Added as tetramethylammonium salts.

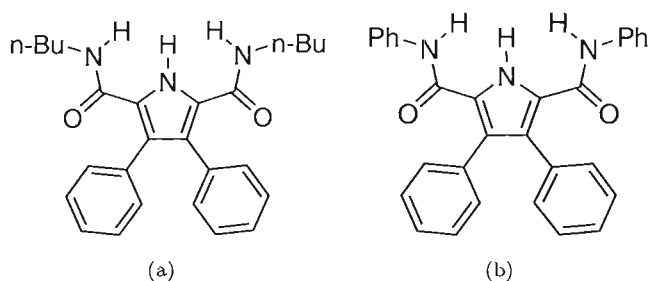


FIGURE 1.24: 2,5-diamidopyrroles as simple anion binding agents.

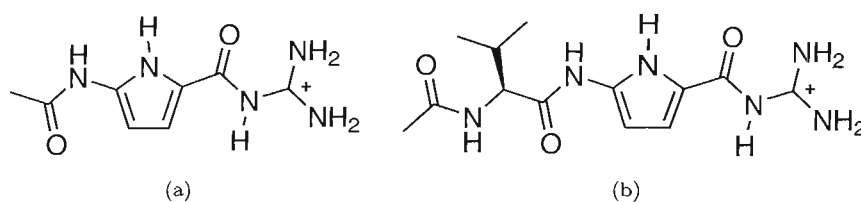


FIGURE 1.25: Guanidinium-based carboxylate receptors derived from 5-amino-pyrrole-2-carboxylate

The energy minimized structure of the complex between the acetyl receptor **1.25(a)** and alanine carboxylate shown in Figure **1.26** offers a possible explanation of the interactions that take place in this complex.

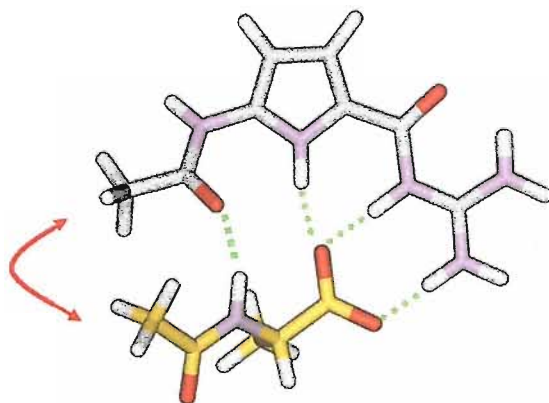


FIGURE 1.26: Calculated energy minimized structure for the complex. Hydrogen bonds are shown in green, unfavorable steric interactions in red.

1.3.2.2 Cyclic pyrrolic derivatives

Gale, Smith and co-workers reported the synthesis of a cyclic 2,5-diamidopyrrole crown macrobicyclic (Figure **1.27**).⁵⁰ Chloride association constants of this receptor in DMSO-*d*₆ solutions were measured by ¹H NMR titrations. It is remarkable the difference in

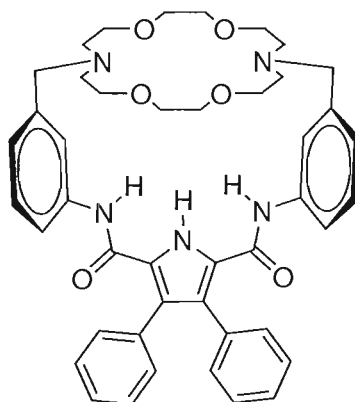


FIGURE 1.27: This receptor recognize the salt as an associated ion-pair.

the association constants obtained depending on the counter-ion present in solution, 109 M^{-1} no ion present,^v 540 M^{-1} potassium, and 128 M^{-1} sodium.^{vi}

Sessler and co-workers have recently reported the synthesis of a bridged dipyrrole *ansa*-ferrocene (Figure 1.28).⁵¹ The complex's stoichiometry was found to be strongly de-

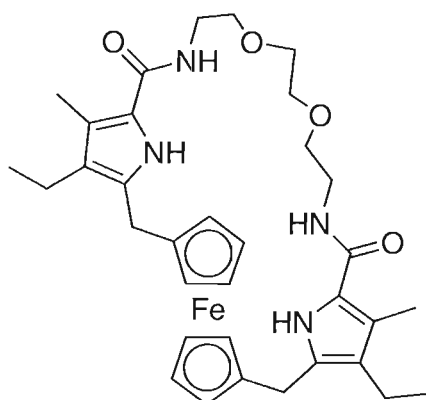


FIGURE 1.28: This system acts as an affective redox-based sensor for F^- and H_2PO_4^- .

pendent upon the nature of the anion. Whilst a 2:1 (anion to host) stoichiometry was observed in the case of fluoride, a 1:1 complex was formed in the presence of other anions such as chloride, bromide, hydrogensulfate and dihydrogenphosphate. ^1H NMR titration experiments revealed that this macrocycle is selective for fluoride, chloride and dihydrogenphosphate over the other putative anions. Different selectivity has been observed by electrochemical measurements. Co-ordination of the different anionic species to the host can be detected through the cathodic shift in the ferrocene-ferrocenium redox couple. Electrochemical data of this compound gave a greater response in the presence of dihydrogenphosphate (136 mV) followed by fluoride and chloride (80 and 24 mV, respectively).

^vChloride added as tetrabutylammonium salt.

^{vi} Na^+ and K^+ added as tetrphenylborate salt (one molar equivalent).

1.3.2.3 Calix[n]pyrroles

In the nineteenth century Baeyer reported the synthesis of the first calixpyrrole macrocycle by condensing pyrrole and acetone in acid media.⁵² After 110 years, Sessler and co-workers reported the anion binding properties of this receptor. ¹H NMR titrations of this calixpyrrole in dichloromethane-*d*₆ vs. a putative anions showed very strong affinity for fluorides ($17 \times 10^3 \text{ M}^{-1}$) and interaction with chloride ($3.5 \times 10^2 \text{ M}^{-1}$). It is

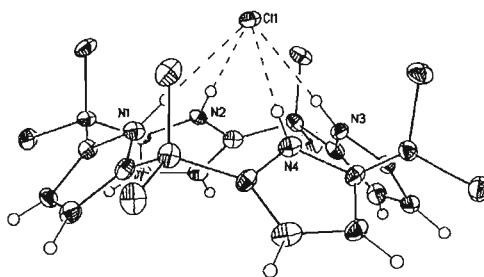


FIGURE 1.29: Crystal chloride complex of the calix[4]pyrrole.

also remarkable the change of conformation observed for this molecule, although in the solid state calixpyrrole adopts a 1,3-alternate conformation, crystallization of calixpyrrole with chloride and bromide yields to a *cone*-calixpyrrole conformation forming four hydrogen bonds with the anion (Figure 1.29).

It was recently reported the ability of the calix[4]pyrrole to bind in the solid state pyridinium based ionic liquids by interacting both with the anion and cation (Figure 1.30).⁵³

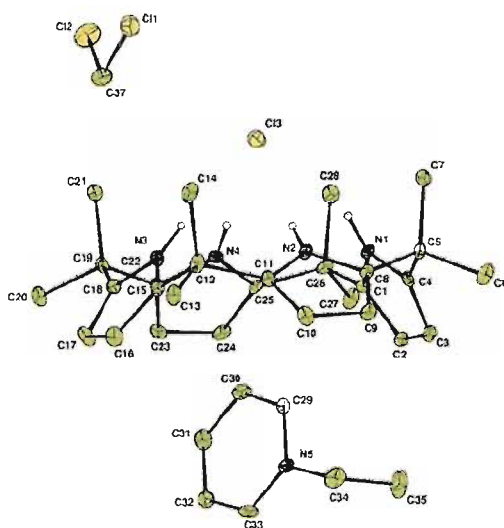


FIGURE 1.30: *N*-ethylpyridinium chloride-*meso*-octamethyl[4]calixpyrrole dichloromethane solvate.

In an effort to expand the lexicon of macrocyclic pyrroles, it was reported a new calix[4]pyrrole that contains a 3, 4, 5-trisubstituted pyrrole appended to a *meso*-position which shows enhanced anion affinity as compared to the parent *meso*-octamethylcalix[4]pyrrole macrocycle (Figure 1.31).⁵⁴ Stability constants of this compound determined

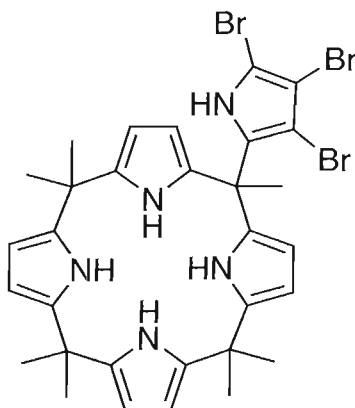


FIGURE 1.31: Pentapyrrolic calix[4]pyrrole has three different NH proton resonances: the pendant pyrrole NH (a) and two inequivalent NH resonances from the calixpyrrole (b (upfield calixpyrrole NH) and c (downfield calixpyrrole NH)).

in dichloromethane- d_6 by ^1H NMR titrations showed selectivity for chloride anion (*c.a.* 1000 M^{-1}). Moderate interaction was observed for dihydrogenphosphate (*c.a.* 100 M^{-1}), and other anions such as hydrogensulfate and bromide were found to bind weakly (*c.a.* 20 M^{-1}). Preliminary molecular modelling studies (using Spartan) indicate the pentapyrrolic calix[4]pyrrole acetate complex to be more stable than the calix[4]pyrrole acetate complex (Figure 1.32).

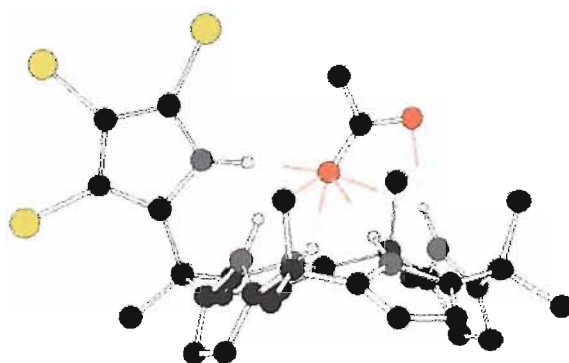


FIGURE 1.32: Molecular model of the acetate-pentapyrrolic complex.

1.4 Aim of the project

The former sections and subsections of this chapter contain information about a wide number of anion receptors that base their anion binding properties on amide, urea, and

thiourea functional groups, pyrrole moieties and other hydrogen bond donor groups as well as electrostatic contributions. One of the biggest challenges the research groups have to face is the innovation in new selective receptors towards an anionic substrate. For this reason, anion coordination chemistry is a field in continuous growth, and many researchers employ considerable effort in designing and synthesising new and more selective anion receptors.

In this thesis, new anion receptors are reported and their complexation properties toward anionic species investigated. We focussed on two topics:

- Functionalization of dipyrrolylmethane derivatives with amide groups in the 5 and 5' positions in order to investigate whether simple pyrrolic clefts can behave as efficient anion receptors designed to bind oxo-anions *via* multiple hydrogen bonds.
- Synthesis of novel square planar platinum (II) complexes of pyridine analogs containing hydrogen bond donors and the study of their anion binding properties.

Chapter 2

Dipyrrolylmethane based receptors

Pyrrole is one of the most commonly employed molecules in the development of new anion receptors.^{55,56} The main reason for its exploitation in this field is the ability of pyrrole to form neutral hydrogen bonds (Figure 2.1(a)). Pyrrole is an ideal molecule from which to construct more complex receptor by attaching another functional group to it. Amide groups can be attached at the 2- and 5- positions of a pyrrole to form a NH array that has been demonstrated to be an effective motif to bind anions (Figure 2.1(b)).^{48,57-61}

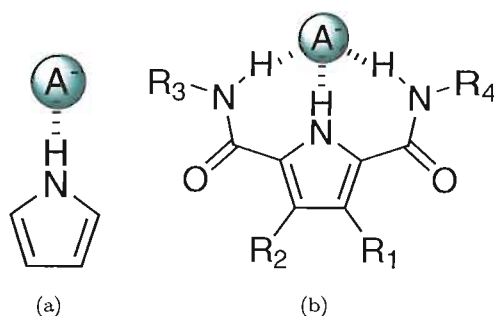


FIGURE 2.1: The hydrogen bond donor group of the pyrrole molecule become an excellent anion receptor when is combined with amides.

Biological examples of anion complexation by pyrrole are quite rare. In 1992, crystallographic studies on porphobilinogen deaminase,⁶² a key enzyme in the biosynthetic pathway of tetrapyrroles, revealed the presence of a dipyrrolylmethane cofactor coordinating a carboxylate group from the protein backbone (Asp 84) *via* NH \cdots OC hydrogen bond interactions.

Other natural examples include the prodigiosins, tripyrrolic molecules that function as

HCl symport agents (Figure 2.2).^{63–65} Compound 2.2(f) have been shown to possess confirmed, potent antimicrobial and cytotoxic properties.⁶⁶

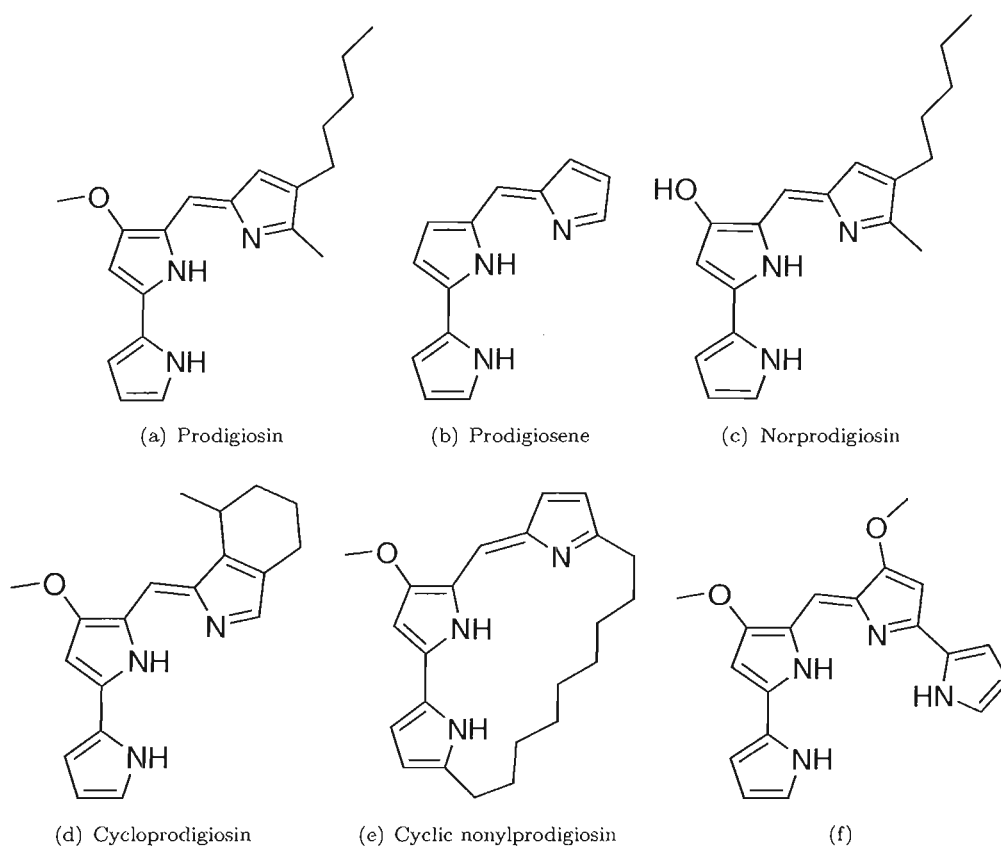


FIGURE 2.2: (a) Red pigment first isolated from *Serratia Marcescens* and the initial member of a class of naturally-occurring polypyrroles possessing a common characteristic pyrrolylpyrromethane skeleton (b-f).

Gale and co-workers have recently shown that in the solid state, a bis-*n*-butyl-2,5-diamidopyrrole forms a complex with benzoate wherein two hydrogen bonds (one pyrrole NH and one amide NH) are formed to one oxygen atom of the anion whilst the other oxygen accepts a third hydrogen bond from the other amide group (Figure 2.3).⁵⁸

Inspired by these examples we decided to extend Gale's recent work on 2,5-bisamidopyrrole anion complexation^{48,57,60,61,67} to dipyrrolylmethane systems by synthesising amide functionalised dipyrrolic molecules and studying their anion complexation ability. The receptors reported here have the potential to form four hydrogen bonds to an oxo-anionic guest and hence we believed that these receptors may show enhanced oxo-anion selectivity.

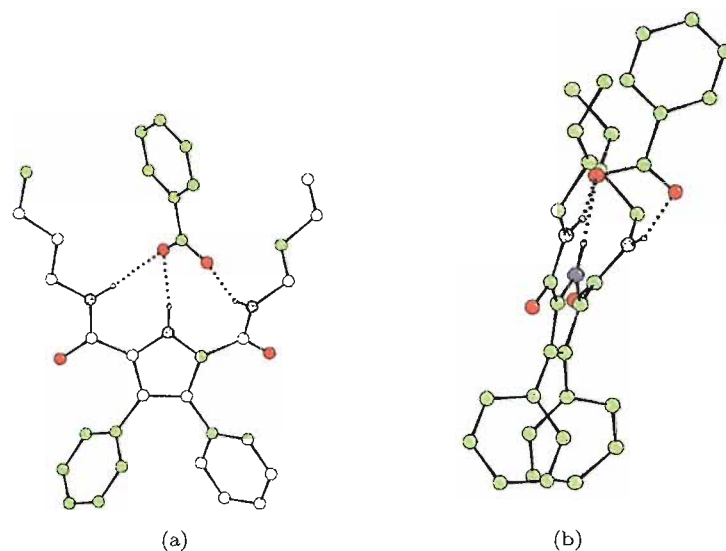


FIGURE 2.3: Crystal structure of the benzoate complex (a) front and (b) side .

2.1 2,2'-Bisamidodipyrrolylmethanes

Two new bis-amido dipyrrolylmethanes [bis-*N*-butylamide-5,5'-methylenebis(4-ethyl-3-methyl-2-pyrrolecarboxylate) and bis-*N*-phenylamide-5,5'-methylenebis(4-ethyl-3-methyl-2-pyrrolecarboxylate)] have been synthesised and shown to exhibit selectivity for oxo-anions from among a variety of putative anionic guest species in DMSO/water solution.

2.1.1 Synthesis and characterization

Compounds 2.4(a) and 2.4(b) were synthesised by reaction of diethyl-5,5'-methylenebis(4-ethyl-3-methyl-2-pyrrole carboxylate) with *n*-butylamine or aniline in the presence of trimethylaluminium in dry dichloromethane at 35°C during three days.⁶⁸ The reac-

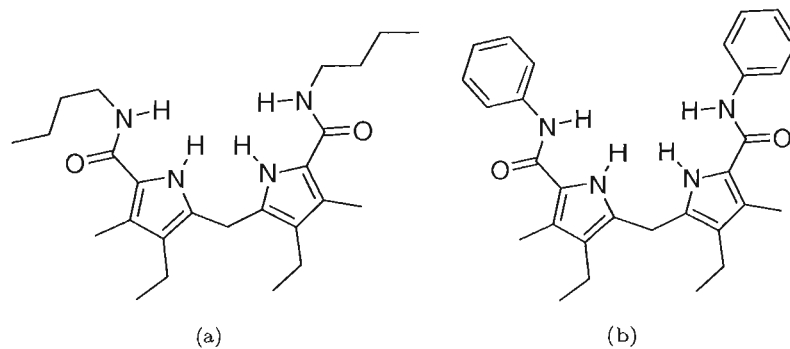


FIGURE 2.4: Compounds (a) and (b) were prepared in a single step reaction from the bisester precursor.

tions were quenched with dilute HCl and were extracted with dichloromethane, dried over MgSO_4 , reduced in *vacuo* and purified by column chromatography on silica gel gradient eluted with dichloromethane and dichloromethane/2% methanol affording the compounds **2.4(a)** and **2.4(b)** in 43 and 40% respective yields.

X-ray quality single crystals of **2.4(a)** have been obtained by slow evaporation of a dichloromethane/methanol solution of this receptor. The crystal structure reveals the formation polymers bridged by intramolecular hydrogen bonds (Figure 2.5). The dihe-

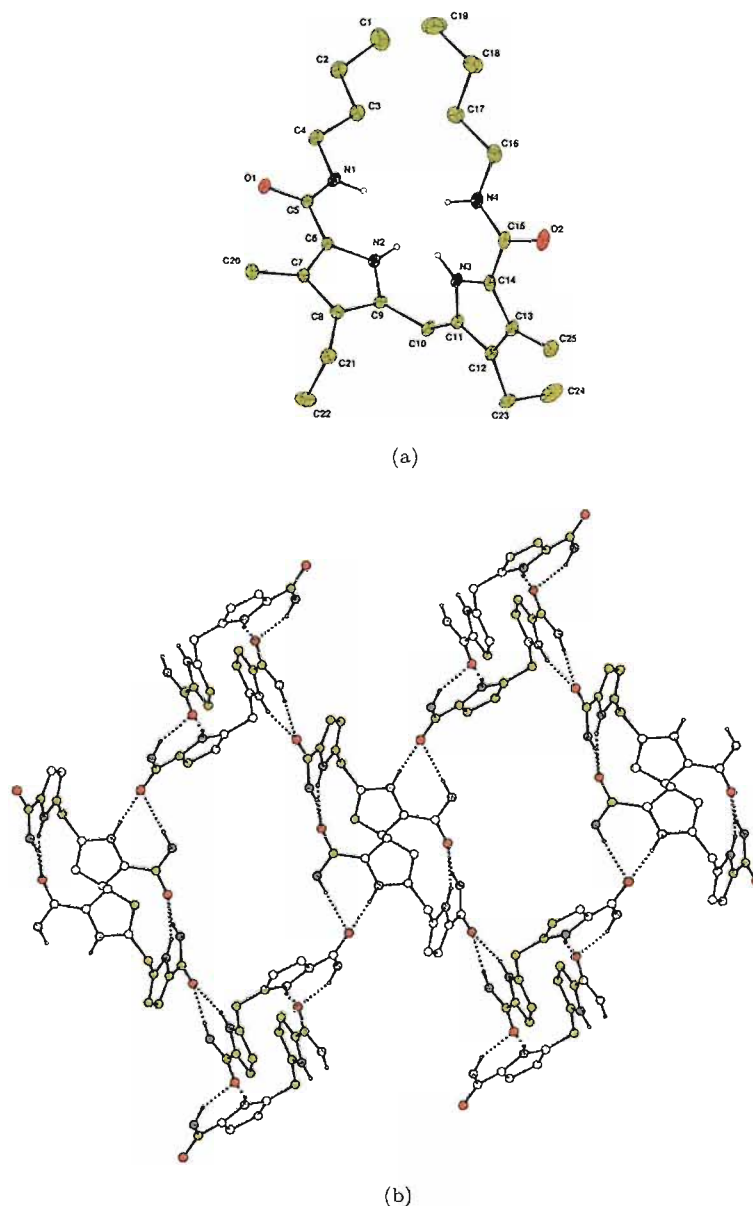


FIGURE 2.5: (a) Thermal ellipsoid plot of **2.4(a)**. Ellipsoids drawn at the 35% probability level and non NH hydrogens omitted for clarity. (b) Hydrogen bonded sheet of **2.4(a)** formed in the solid state *via* $\text{NH}\cdots\text{OC}$ hydrogen bonds. Side chain ethyl, methyl and butyl groups and non-acidic hydrogen atoms have been omitted for clarity.

dral angles formed between the butyl chains and the pyrrolic plane are -0.8° and -167.0° . The amide moieties deviate from the pyrrole plane by -2.3° and 1.0° with the amide NH groups converging with the pyrrole NH (Figure 2.5(a)). Pyrrole NH and amide NH groups form a convergent hydrogen bonding array coordinating a carbonyl group from an adjacent molecule. Each molecule binds two molecules on their carbonyl groups through its amidopyrrole moieties, and its carbonyl groups are bound by another two neighboring molecules from their amidopyrrole moieties. The result is a 3D network sustained by hydrogen bonds (Figure 2.5(b)).

Single crystals of 2.4(b) have been obtained by slow recrystallization from a dichloromethane/methanol solution of this receptor (Figure 2.6). We observe here a similar pyrrole

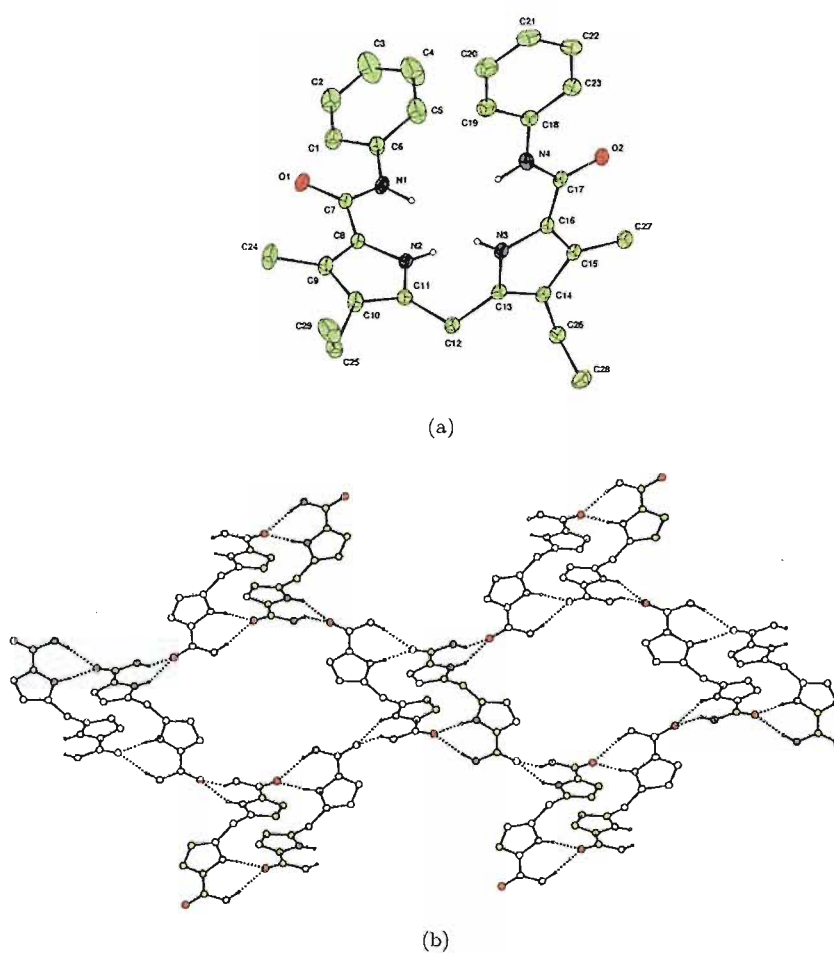


FIGURE 2.6: (a) Thermal ellipsoid plot of 2.4(b). Ellipsoids drawn at the 35% probability level and non NH hydrogens omitted for clarity. (b) Hydrogen bonded sheet of 2.4(b) formed in the solid state *via* NH...OC hydrogen bonds. Side chain ethyl, methyl and phenyl groups and non-acidic hydrogen atoms have been omitted for clarity.

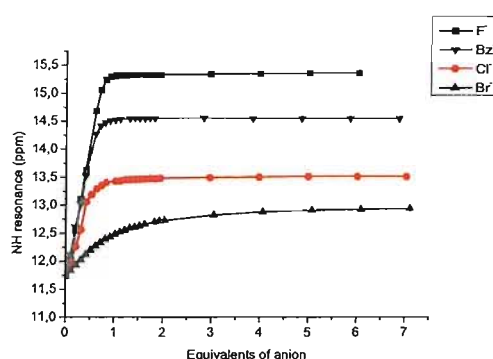
NH and amide NH convergent hydrogen bonding array, as in the butylamide analog (Figure 2.6(a)). The crystal structure again revealed a 3D network of hydrogen bonds between the NHs from the amidopyrrole moieties and the oxygens from the carboxylate groups. It is remarkable in this case the formation of hydrogen bonded dimers, which

are linked as well by hydrogen bonds with four neighboring molecules in similar way as it does **2.4(a)** (Figure 2.6).

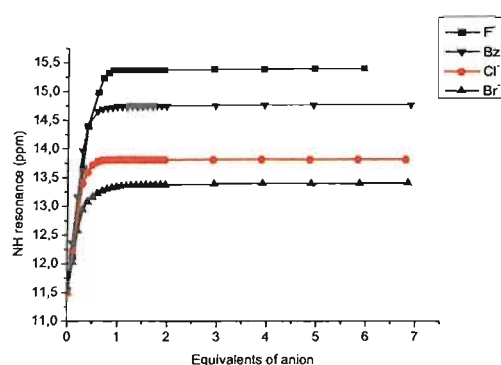
2.1.2 Binding studies results. Selectivity for dihydrogenphosphate

Proton NMR titration techniques have been used in order to investigate the anion binding properties of receptors **2.4(a)** and **2.4(b)**. Anions were added as their tetrabutylammonium salts, since this cation does not compete significantly with the anion binding site and therefore is considered a relatively 'innocent' counterion. Elaboration of the titration curves has been achieved by using *WinEQNMR*.⁶⁹

The anion complexation properties of receptors **2.4(a)** and **2.4(b)** have been initially investigated in dichloromethane- d_2 solution; however, the strong anion binding capability of these compounds in this solvent media (Figure 2.7) prevented us from obtaining any anion complexation constant.



(a) Compound **2.4(a)**



(b) Compound **2.4(b)**

FIGURE 2.7: ^1H NMR titration curves with fluoride, chloride, bromide, and benzoate in dichloromethane- d_2 at 298 K. Anions added as their tetrabutylammonium salts. NH downfield shift is observed to occur up to one equivalent of anion added, appearing afterwards a plateau that indicates saturation of the receptor.

Proton NMR titrations in DMSO- d_6 /5% water were used to determine the association constants of **2.4(a)** and **2.4(b)** with a variety of anionic guests (Figure 2.8).⁶⁹ The results, shown in Table 2.1, indicate that receptors **2.4(a)** and **2.4(b)** bind fluoride and benzoate with significant affinities in this solvent mixture with a 1:1 receptor:anion stoichiometry. The titration with dihydrogenphosphate and compound **2.4(a)** could not be fitted to a 1:1 receptor:anion binding model (Figure 2.8(a)). This behavior has been observed before in related systems.^{48,57,60,61,67} In the case of compound **2.4(b)**, the addition of aliquots of H_2PO_4^- gave a very sharp titration curve in DMSO- d_6 /5% water (Figure 2.8(b)) and hence the titrations with dihydrogenphosphate were performed in DMSO- d_6 /25% water with both compounds in order to obtain reliable stability constant values. These were found to be 19 M^{-1} and 234 M^{-1} for compounds **2.4(a)** and **2.4(b)** respectively (Figure 2.9).

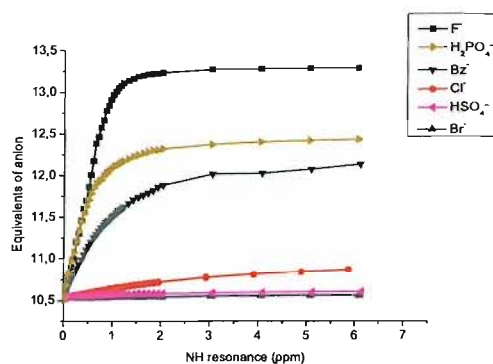
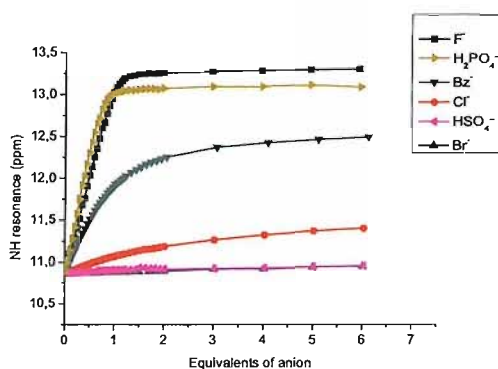
(a) Compound **2.4(a)**(b) Compound **2.4(b)**

FIGURE 2.8: ^1H NMR titration curves with fluoride, chloride, bromide, benzoate, hydrogensulfate and dihydrogenphosphate in DMSO- d_6 /5% water at 298 K. Anions added as their tetrabutylammonium salts.

In order to compare these compounds with the previous generation of pyrroleamide cleft systems (e.g. **2.10(a)** and **2.10(b)**) titrations were repeated with benzoate with these receptors in DMSO- d_6 /5% water. In these cases it was observed that the affinity of

Anion ^a	Compound 2.4(a) ^b	Compound 2.4(b) ^b
F ⁻	7560	8990
Cl ⁻	23	43
Br ⁻	13	10
H ₂ PO ₄ ⁻	^c	^c
HSO ₄ ⁻	44	128
Benzoate	354	424
F ^{-d}	11	114
H ₂ PO ₄ ^{-d}	20	234

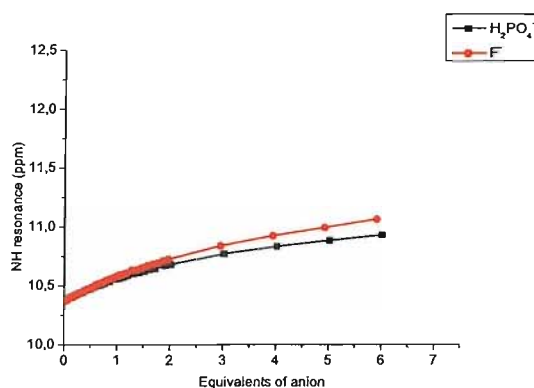
^aAdded as tetrabutylammonium salt.

^bErrors estimated to be no more than 15%.

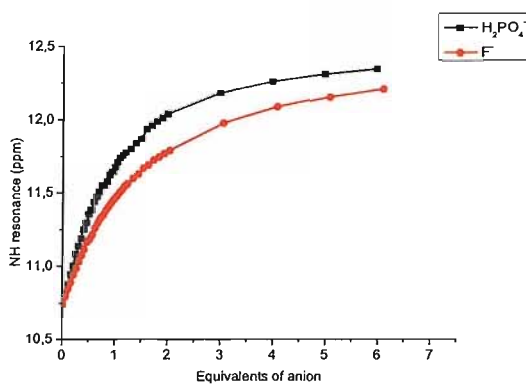
^cAn adequate fit could not be obtained.

^dMeasured in DMSO-*d*₆/25% water.

TABLE 2.1: Stability constants K_a (M^{-1}) of compounds 2.4(a) and 2.4(b) with a variety of putative anionic guests (added as tetrabutylammonium salts) at 298K in DMSO-*d*₆/5% water (except where noted).



(a) Compound 2.4(a)



(b) Compound 2.4(b)

FIGURE 2.9: ¹H NMR titration curves with fluoride, and dihydrogenphosphate in DMSO-*d*₆/25% water at 298 K. Anions added as their tetrabutylammonium salts.

compound **2.10(b)** was lower for benzoate (103 M^{-1}) whilst with compound **2.10(a)** broadening of the amide NH resonance prevented a stability constant determination by this method under these conditions.

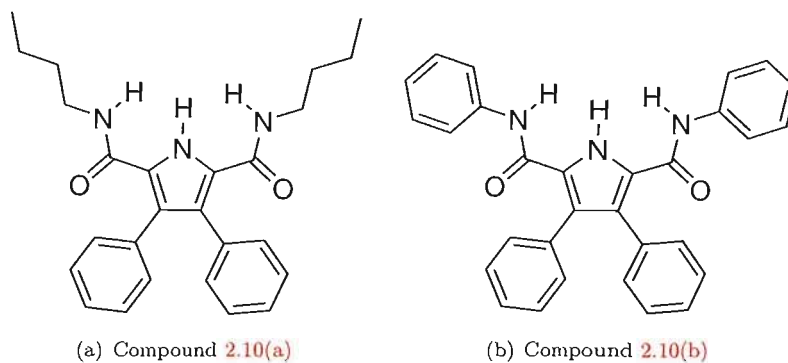
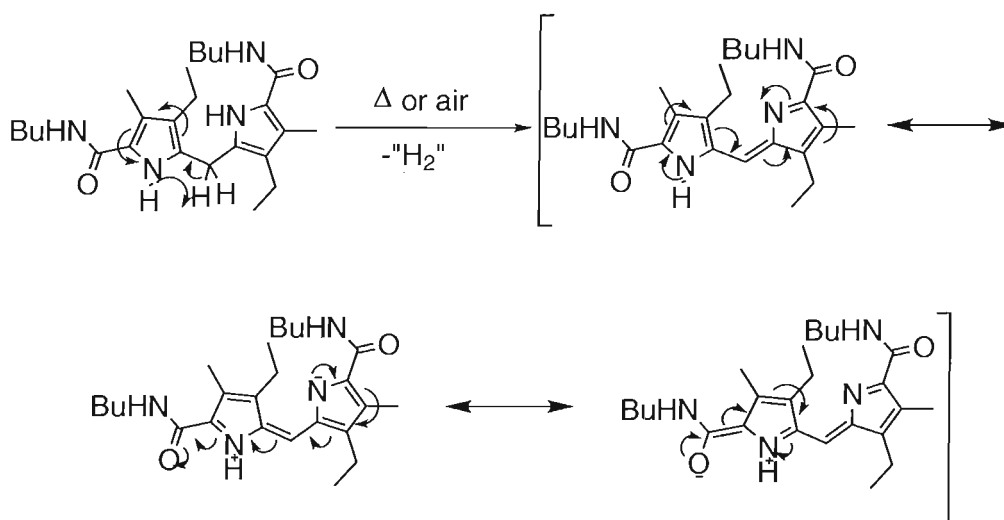


FIGURE 2.10: Previous generation of pyrrole-amide clefts used to compare the anion binding properties of the novel dypyrrolylamides **2.4(a)** and **2.4(b)**.

Compounds **2.4(a)** and **2.4(b)** both bind fluoride strongly in $\text{DMSO-}d_6/5\%$ water, but perhaps the most notable result from these studies is the fact that compound **2.4(b)**, a neutral hydrogen bond donor, was found to complex dihydrogenphosphate very strongly in this solvent mixture and even forms a complex with this anion in $\text{DMSO-}d_6/25\%$ water (an extremely competitive solvent mixture) with a stability constant of 234 M^{-1} . However, this anion is bound only weakly by compound **2.4(a)** (20 M^{-1}) under these



SCHEME 2.1: Suggested product from the oxidation of compound **2.4(a)**.

conditions. In order to provide a benchmark to which we could compare these results we redetermined the stability constants of **2.4(a)** and **2.4(b)** with fluoride in this more polar solvent mixture. We found that fluoride is bound by receptors **2.4(a)** and **2.4(b)** with stability constants of 11 and 114 M^{-1} respectively in $\text{DMSO-}d_6/25\%$ water (Figure 2.9).

These results have shown that bis-amido dipyrrolylmethanes are effective anion receptors even in partially aqueous solutions. Compounds **2.4(a)** and **2.4(b)** therefore expand the lexicon of acyclic pyrrolic anion receptors (the crystal structure of a fluoride complex of a simple dipyrrolylmethane has recently been reported by Sessler and co-workers)⁷⁰ and provide a new approach to anion complexation in competitive media.

We produced some new analogous receptors with two alkyl groups attached to each of the 'meso-carbons' for improved stability⁷¹ (these compounds discolour in solution over a few days due to oxidation (Scheme 2.1)).^{vii} Whilst being more stable, Lightner and co-workers have predicted, using molecular mechanics calculations on dipyrrolylmethanes, that the *gem*-dimethyl effect present due to the substitution on the meso carbon may destabilize conformations favourable for the formation of a convergent binding site by the four hydrogen bond donors.⁷² Hence, whilst the new compounds may be more stable than **2.4(a)** or **2.4(b)**, they may also have lower affinities for anions. The question remained whether this effect would preclude these receptors from functioning in partially aqueous DMSO solution. The results of these studies are reported in the next section.

2.2 5,5'-Dicarboxamido-dipyrrolylmethanes

A series of 5,5'-dicarboxamido-dipyrrolylmethanes (Figure 2.11) have been synthesized and in some cases crystallographically characterized. Proton NMR titrations have revealed that these compounds, that contain only four neutral hydrogen bond donors and are acyclic, selectively bind anions in very competitive solvent media such as DMSO-*d*₆/water mixtures.^{viii}

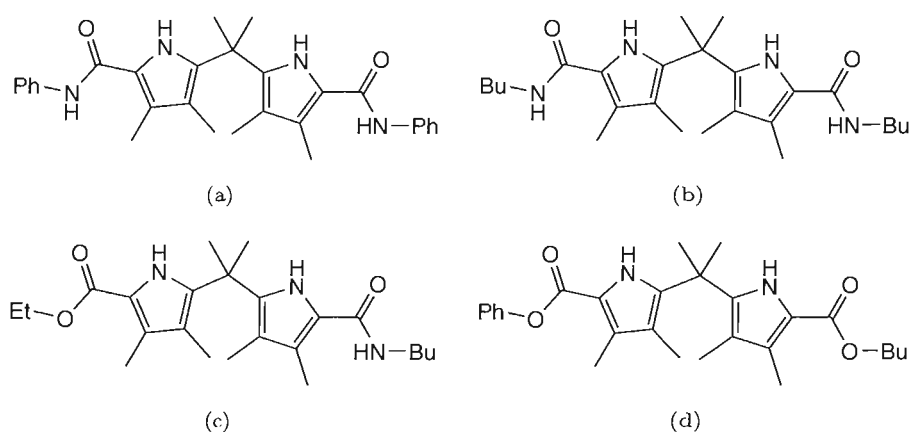


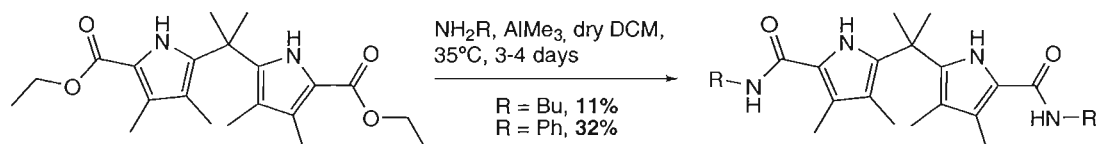
FIGURE 2.11: Compounds containing two alkyl groups attached to the sp^3 hybridized meso carbon which would not be as susceptible to oxidation.

^{vii}Oxidized analog from **2.4(a)** was observed through both ES⁺ mass spectrum ($m/z = 427.51$) and LRES⁺ mass spectrum ($m/z = 427.3071$).

^{viii}Porphyrinogens as calix[4]pyrroles are stabilized by attaching methyl groups to sp^3 carbons.⁷³

2.2.1 Synthesis and characterization

Compounds **2.11(a)** and **2.11(b)** were synthesized by reaction of ethyl 5-(2-(5-(ethoxycarbonyl)-3,4-dimethyl-1*H*-pyrrol-2-yl)propan-2-yl)-3,4-dimethyl-1*H*-pyrrole-2-carboxylate (prepared according Lightner and co-workers' method)⁷² with aniline or *n*-butylamine in the presence of trimethylaluminium in dry dichloromethane at 35°C. After quenching with HCl and purification by column chromatography, compounds **2.11(b)** and **2.11(a)** were isolated with 32 and 11% respective yields (Scheme 2.2).



SCHEME 2.2: Synthesis of the symmetric receptors **2.11(a)** and **2.11(b)**.

Compound **2.11(c)** was also isolated during chromatography on the reaction mixture of compound **2.11(b)** in 20% yield when the reaction time was four days. However **2.11(c)** was isolated in 22% yield as a single reaction product when the reaction time was reduced to two days. Compound **2.11(d)** was synthesized by reaction of **2.11(c)** with aniline in the presence of trimethylaluminium in dry dichloromethane at 35°C. After quenching and purification by column chromatography the compound was isolated in 39% yield.

Crystals of compounds **2.11(a)**, **2.11(b)** and **2.11(c)** were obtained by slow evaporation of solutions of the receptors in dichloromethane methanol mixtures (**2.11(a)** and **2.11(c)**) and nitromethane (**2.11(b)**). The crystal structures presented, especially that of **2.11(c)**, were obtained from poor quality crystals and as a result the standard R-factors are slightly higher than those found from more amenable samples. It was not possible to obtain better quality crystals and, in each case, the structures are unambiguous.

The crystal structure of **2.11(a)** (Figure 2.12) shows that the amide NH groups are *syn* to the pyrrole NH forming a convergent hydrogen bond donor array. One amidopyrrole unit binds to a carbonyl oxygen in an adjacent molecule whilst the other hydrogen bonds to a methanol solvent molecule which in turn is hydrogen bonded to a carbonyl oxygen. Hence a continuous zig-zag tape is formed in the crystal (Figure 2.12(c)).

Compound **2.11(b)** crystallized from nitromethane forming an extended three dimensional hydrogen bonding array containing three crystallographically distinct units (A-green, B-red, C-blue, Figure 2.13(c)) with the third differing from the other two in that one of its pyrrolic amide units is *trans* (i.e. the pyrrole and amide NH groups are oriented in opposite directions at one end of the molecule) whilst all the others are *cis*. This allows for a greater structural freedom in the building of the hydrogen bonded network, with the majority of the contacts being convergent double $\text{NH}\cdots\text{O}$ but also involving

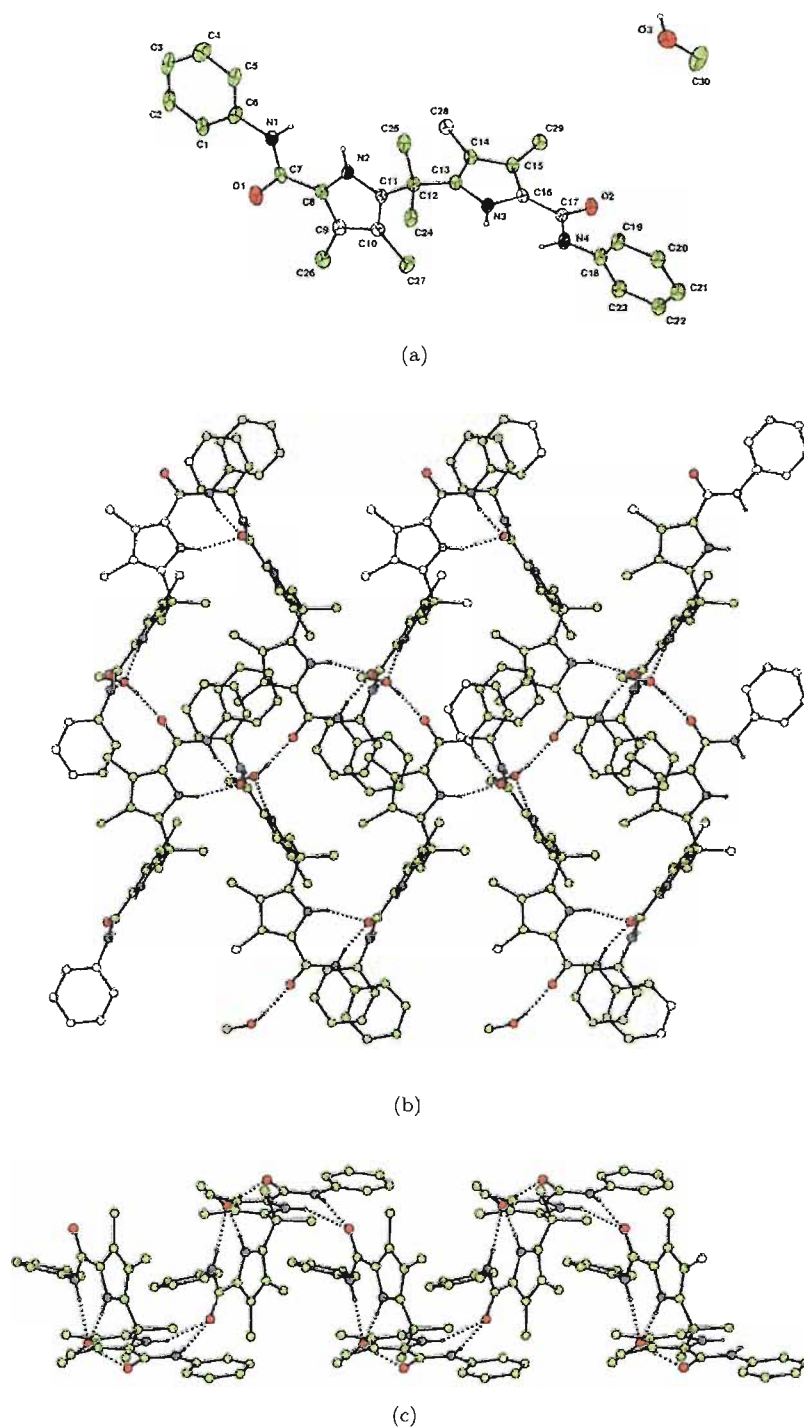


FIGURE 2.12: The X-ray crystal structure of **2.11(a)**·MeOH. Non-acidic hydrogen atoms have been omitted for clarity. The pyrrole and amide groups are involved in a three dimensional network of hydrogen bonds.

one single $\text{NH} \cdots \text{O}$. The extended structure is built up from chains of alternating A donors and B acceptors forming slabs two chains thick in the *ab* plane *via* bridging C molecules.

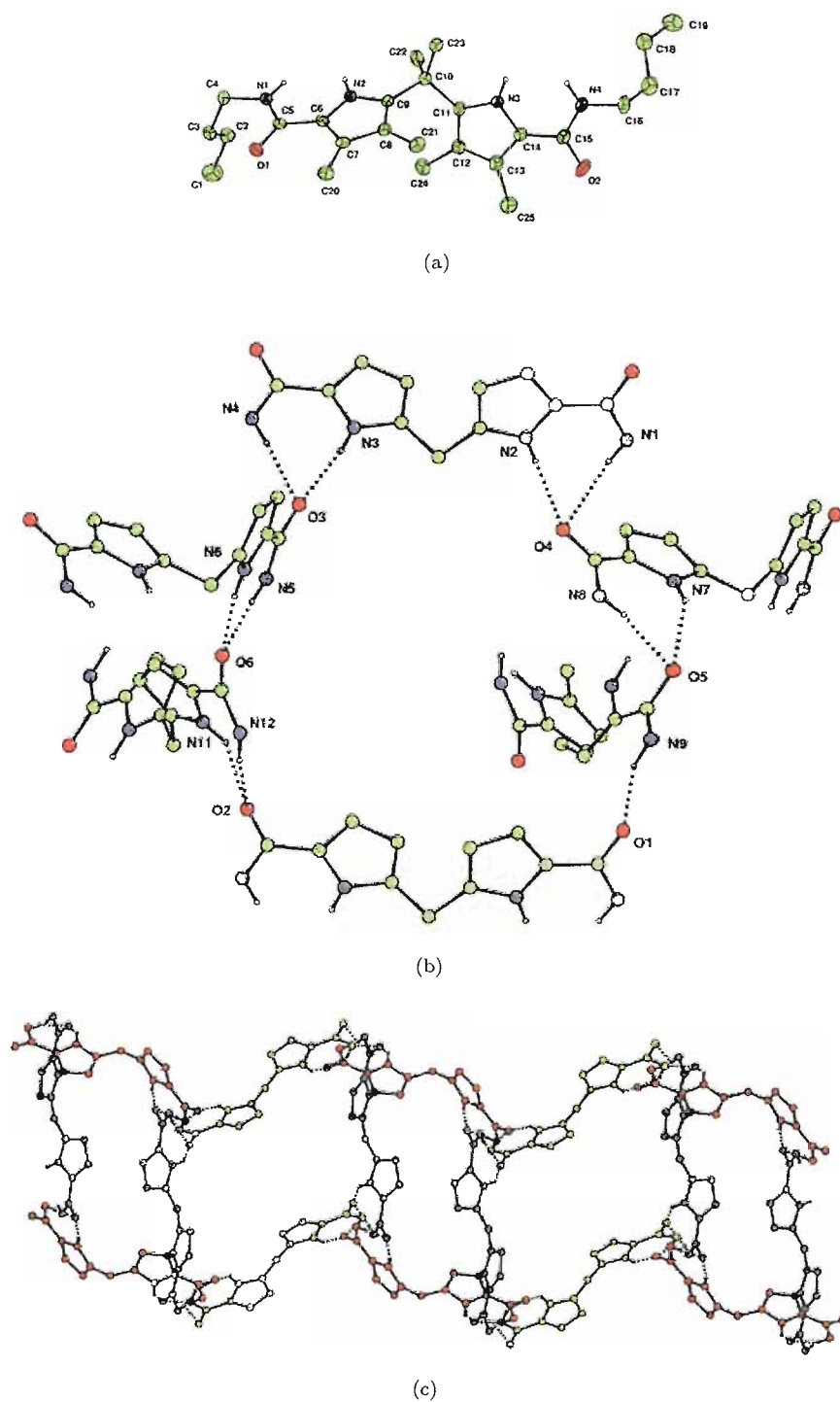


FIGURE 2.13: The X-ray crystal structure of **2.11(b)**. Non-acidic hydrogen atoms have been omitted for clarity. The pyrrole and amide groups are involved in a three dimensional network of hydrogen bonds.

In the solid state, the amidopyrrole unit of compound **2.11(c)** adopts a similar conformation to compound **2.11(a)** and binds to an amide oxygen in an adjacent molecule. The ester functionalized pyrrole dimerizes *via* $\text{NH} \cdots \text{OC}$ interactions with another pyr-

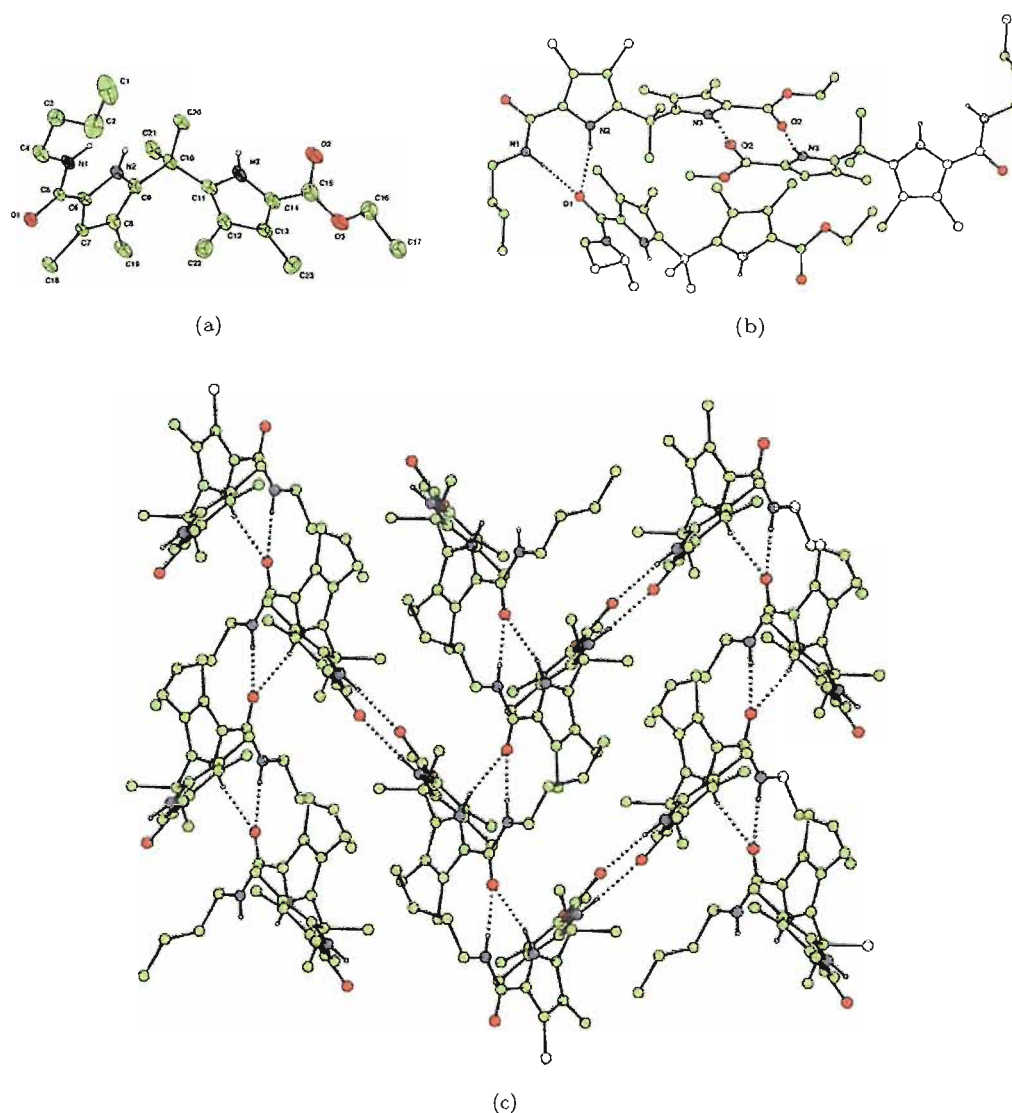


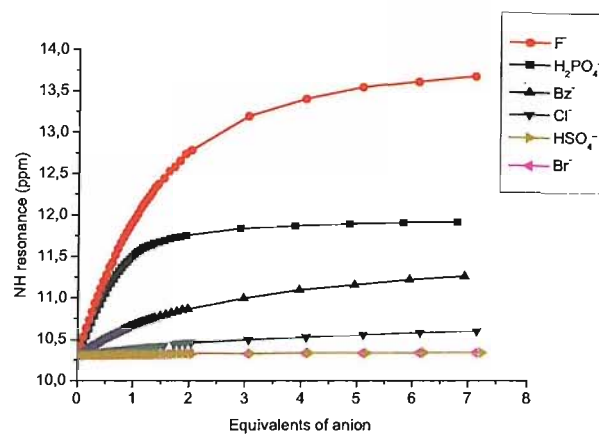
FIGURE 2.14: The X-ray crystal structure of **2.11(c)**. Non-acidic hydrogen atoms have been omitted for clarity. The pyrrole and amide groups are involved in a three dimensional network of hydrogen bonds. (a) Molecular structure, only one orientation of the disordered ethyl acetate is shown. (b) Detail of the hydrogen bonded slabs in the *bc* plane showing the two types of interaction. (c) View down the *a* axis.

role ester group in another adjacent molecule forming a network of dipyrrolylmethanes (Figure 2.14).

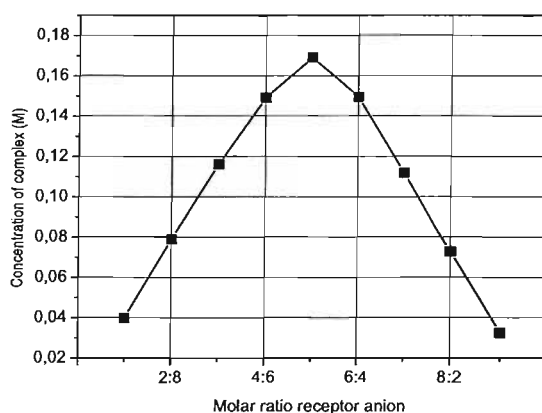
2.2.2 Binding studies results

The stability constants of compound **2.11(a)** (bis-phenylamide) were determined by ^1H NMR titration techniques in $\text{DMSO-}d_6/5\%$ water solution (the titration curves for compound **2.11(a)** and the various anionic guests are shown in Figure 2.15(a) with a Job plot⁷⁴ for compound **2.11(a)** and dihydrogen phosphate shown in Figure 2.15(b) indicat-

ing 1:1 receptor:anion stoichiometry). Compound **2.11(a)** was found to be selective for



(a)



(b)

FIGURE 2.15: (a) ^1H NMR titration curves for compound **2.11(c)** with fluoride, chloride, bromide, benzoate, dihydrogen phosphate and hydrogen sulfate in $\text{DMSO-}d_6/5\%$ water at 298 K. Anions added as their tetrabutylammonium salts and (b) Job plot of compound **2.11(c)** and tetrabutylammonium dihydrogen phosphate in $\text{DMSO-}d_6$ indicating 1:1 receptor:anion stoichiometry.

dihydrogen phosphate in this solvent mixture binding this anion with a stability constant of 1092 M^{-1} in $\text{DMSO-}d_6/5\%$ water (in $\text{DMSO-}d_6/25\%$ water the stability constant was dramatically reduced to approximately 10 M^{-1} , see Table 2.2). This is a weaker interaction than that observed between compound **2.4(b)** and dihydrogen phosphate, but is significant as the receptor is neutral and acyclic and yet binds this anion strongly in $\text{DMSO-}d_6/5\%$ water. Similar anion selectivity trends are observed with compounds **2.11(a)** and **2.4(b)**.

Anion ^a	Compound 2.11(a) ^b
H ₂ PO ₄ ⁻	1092
F ⁻	124
Benzoate	41
Cl ⁻	14
Br ⁻	^c
HSO ₄ ⁻	^c
H ₂ PO ₄ ^{-d}	9

^aAdded as tetrabutylammonium salt.

^bErrors estimated to be no more than 15%.

^cNo interaction observed.

^dMeasured in DMSO-*d*₆/25% water.

TABLE 2.2: Stability constants K_a (M^{-1}) of compound **2.11(a)** with a variety of putative anionic guests (added as tetrabutylammonium salts) at 298K in DMSO-*d*₆/5% water (except where noted).

Compounds **2.11(b)** (bis-butylamide) and **2.11(d)** (mono-phenyl-mono-butylamide) show decreasing affinities for dihydrogen phosphate, presumably due to the difference in basicity between the phenylamide and butylamide groups (Table 2.3). The same trend is

Anion ^a	Compound 2.11(b) ^b	Compound 2.11(d) ^b
H ₂ PO ₄ ⁻	81	307
F ⁻	89	429
Benzoate	20	33
Cl ⁻	^c	^c
Br ⁻	^c	^c
HSO ₄ ⁻	^c	^c

^aAdded as tetrabutylammonium salt.

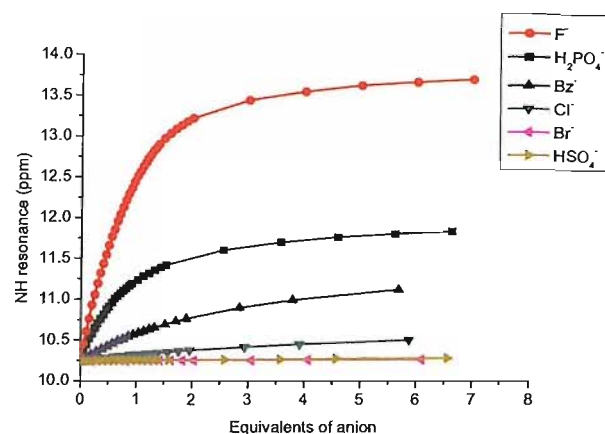
^bErrors estimated to be no more than 15%.

^cNo interaction observed.

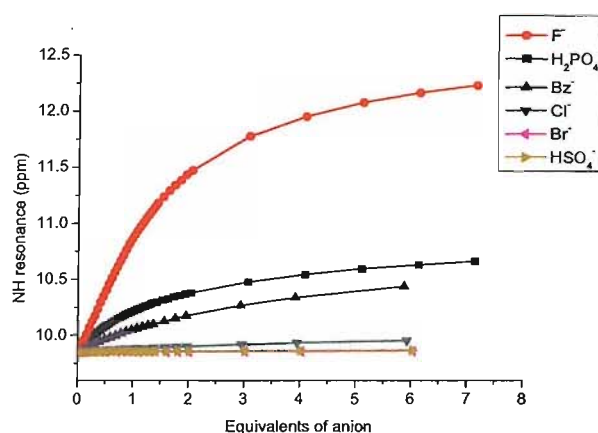
TABLE 2.3: Stability constants K_a (M^{-1}) of compounds **2.11(b)** and **2.11(d)** with a variety of putative anionic guests (added as tetrabutylammonium salts) at 298K in DMSO-*d*₆/5% water.

observed for benzoate, although this anion binds more weakly than dihydrogen phosphate (see Figure 2.16). The trend with fluoride is more difficult to rationalize and it is not yet clear why the highest affinity is observed with this anion and compound **2.11(d)**. Comparison of the dihydrogen phosphate binding properties of dipyrrolylmethane **2.11(a)** with an equivalent mono-pyrrole bis-amide^{48,57,59,61,67,75} namely 3,4-diphenyl-1*H*-pyrrole-2,5-diphenylcarboxamide showed that the dipyrrolylmethane binds dihydrogen phosphate approximately three times more strongly than the bis-amidopyrrole ($K_a = 350 \pm 10 M^{-1}$ for the monopyrrole binding dihydrogen phosphate in DMSO-*d*₆/5% water).

Titration with compound **2.11(c)** were conducted in the less competitive DMSO-*d*₆/0.5%



(a)



(b)

FIGURE 2.16: ^1H NMR titration curves for compounds **2.11(d)** (a) and **2.11(b)** (b) with fluoride, chloride, bromide, benzoate, dihydrogen phosphate and hydrogen sulfate in DMSO- d_6 /5% water at 298 K. Anions added as their tetrabutylammonium salts.

water solution as this receptor was found to form considerably weaker complexes with anions than the bis-amides (Figure 2.17). The results, summarized in Table 2.4 show that this receptor is selective for fluoride, with dihydrogen phosphate and benzoate forming complexes that are over an order of magnitude less stable.

However interestingly, examination of the ^1H NMR spectra during the titrations with anions showed that one of the pyrrole NH groups only shifts slightly upfield during the titration whilst the other pyrrole and the amide NH shift downfield (see Figure 2.18 for the stack plot titrations with both dihydrogen phosphate and fluoride). This finding is consistent with the ester functionalized pyrrole ring not interacting with the anionic guest (the anion is binding only to the amido-pyrrole group) - a binding mode supported

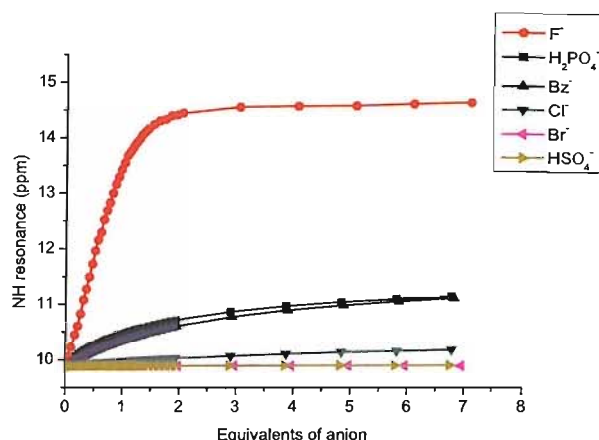


FIGURE 2.17: ^1H NMR titration curves for compound **2.11(c)** with fluoride, chloride, bromide, benzoate, dihydrogen phosphate and hydrogen sulfate in DMSO- d_6 /0.5% water at 298 K. Anions added as their tetrabutylammonium salts.

Anion ^a	Compound 2.11(c) ^b
H_2PO_4^-	83
F^-	1450
Benzoate	41
Cl^-	< 15
Br^-	^c
HSO_4^-	^c

^aAdded as tetrabutylammonium salt.

^bErrors estimated to be no more than 15%.

^cNo interaction observed.

TABLE 2.4: Stability constants K_a (M^{-1}) of compound **2.11(c)** with a variety of putative anionic guests (added as tetrabutylammonium salts) at 298K in DMSO- d_6 /0.5% water.

by DFT calculations albeit in the gas phase (Figure 2.19).^{ix} The possibility exists for the dihydrogen phosphate group to donate a hydrogen bond to the ester and accept one from the adjacent pyrrole. The fact that this does not appear to happen in solution may be due to the poor hydrogen bonding ability of ester carbonyl groups.⁷⁶

Attempts to obtain X-ray quality crystals of anion complexes with these species have, up to this point, been unsuccessful. We therefore decided to study the solution conformation of the receptors using NOESY spectroscopy. Compound **2.11(d)** proved ideal for these studies due its lack of symmetry.

NOESY experiments were carried out in DMSO- d_6 solutions of compound **2.11(d)** in the absence and presence of five equivalents of dihydrogen phosphate (added as the tetrabutylammonium salt) in order to obtain information about the structure of the free

^{ix}DFT structure calculated using Spartan 02: Spartan 02, Wavefunction Inc., Irvine CA, USA.

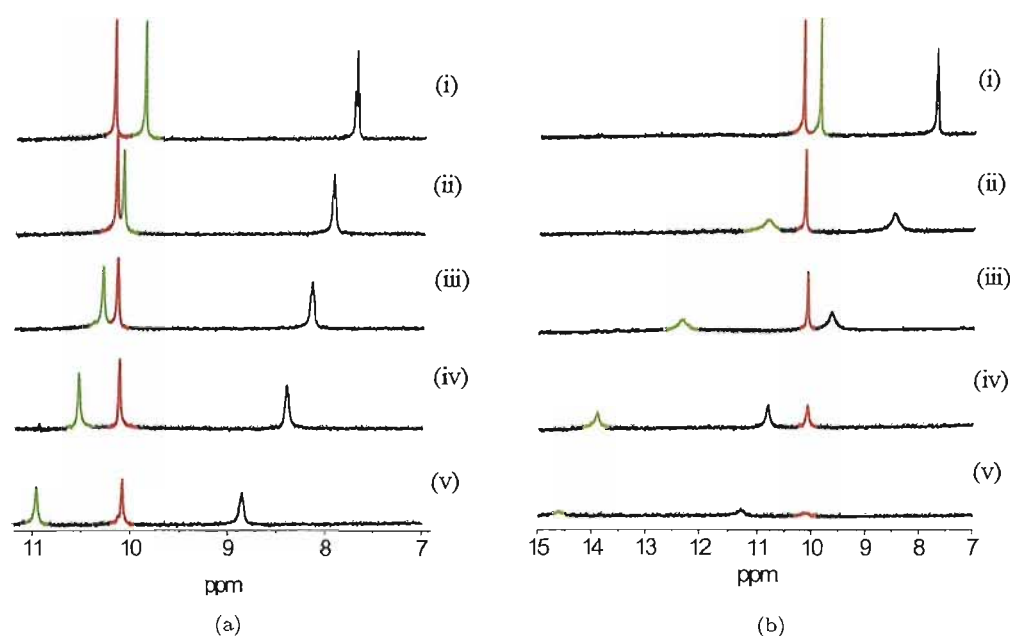


FIGURE 2.18: ^1H NMR stack plot titration of compound **2.11(c)** with (a) dihydrogen phosphate (i) 0, (ii) 0.24, (iii) 0.58, (iv) 1.20, (v) 3.90 equivalents, and (b) fluoride (i) 0, (ii) 0.25, (iii) 0.61, (iv) 1.21, (v) 3.00 equivalents in $\text{DMSO-}d_6/0.5\%$ water (amide proton resonance in blue, the adjacent pyrrole NH resonance is in green and the pyrrole-ester NH resonance is in red).

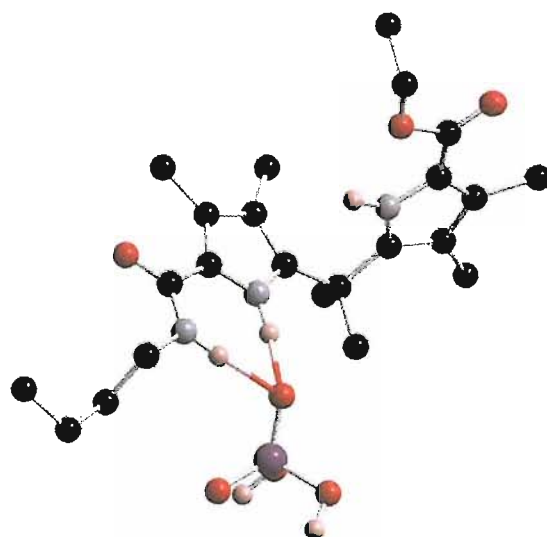
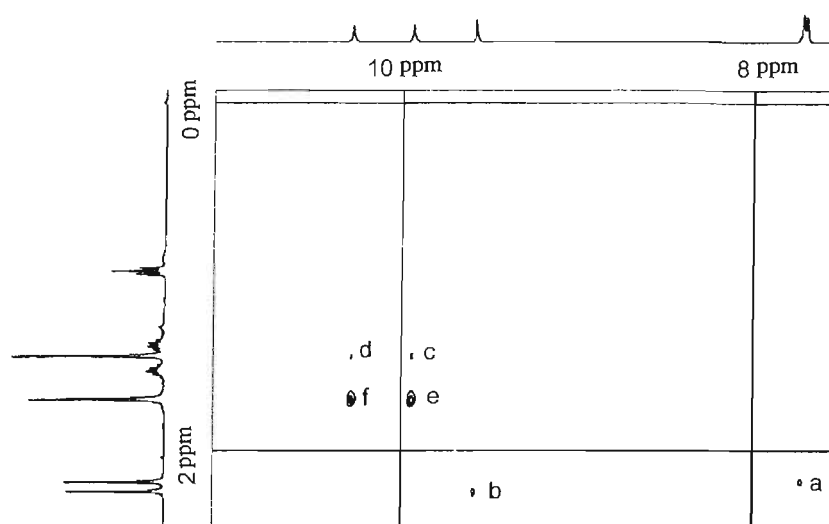
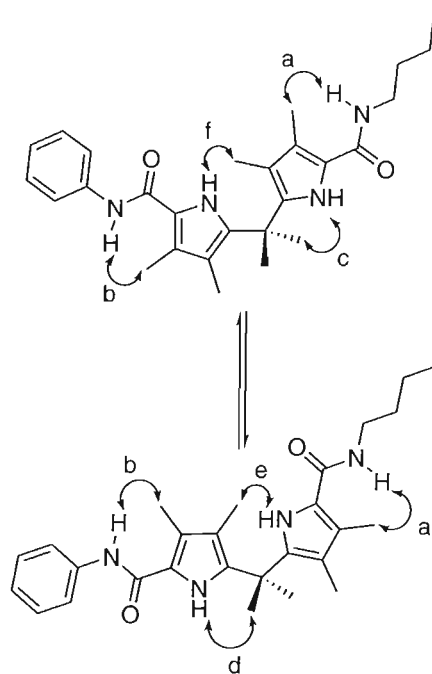


FIGURE 2.19: Structure of the dihydrogen phosphate complex of **2.11(c)** generated by DFT calculation using Spartan 02.

receptor and complex in solution. In the absence of the anion, a variety of negative cross peaks between methyl groups and pyrrole or amide NH groups were observed (Figure 2.20). These couplings suggest that the receptor is adopting a linear conformation in solution. No coupling was observed between NH groups. However, upon addition of



(a)

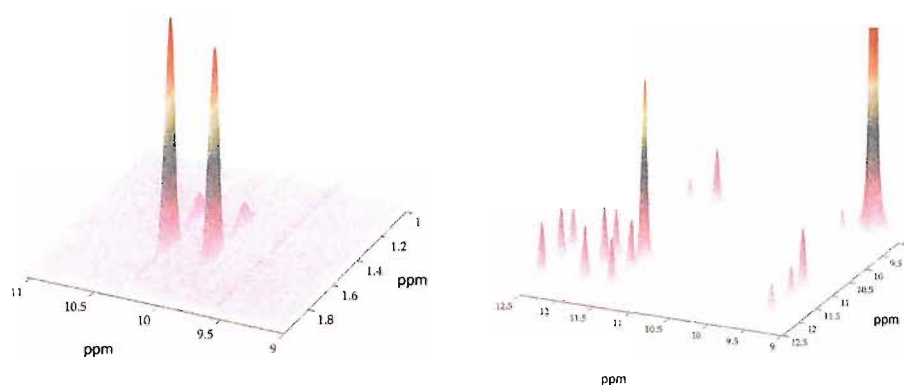


(b)

FIGURE 2.20: (a) A portion of the NOESY spectrum of compound **2.11(d)** in $\text{DMSO-}d_6$ and (b) a schematic showing the through space couplings present in this compound.

dihydrogen phosphate, the cross peaks between the methyl and the NH resonances disappeared and instead, positive cross peaks were observed between the amide NH to adjacent pyrrole NH resonance and between the two pyrrole NH resonances (Figure **2.21(b)**). Additionally, positive cross peaks were observed between the phenylamide NH and the pyrrole NH adjacent to the butylamide group. Weaker coupling was observed between

the butylamide NH and the pyrrole NH adjacent to the phenylamide group. These cross



(a) Three dimensional zoom in into the NOESY spectra of compound **2.11(d)** that shows the NOE negative cross-peaks c, d, e, and f (Figure 2.20(b)). (b) Three dimensional zoom in into the NOESY spectra of compound **2.11(d)** with five equivalents of tetrabutylammonium dihydrogen phosphate that shows positive crosspeaks among all the NH's. These crosspeaks are due to proton exchange processes.

FIGURE 2.21: Three dimensional views of the NOESY spectra of compound **2.11(d)** in DMSO- d_6 solutions.

peaks are presumably due proton exchange processes. When one hundred equivalents of D₂O were added to receptor **2.11(d)** in the presence of five equivalents of dihydrogen phosphate the NH resonances decreased in intensity due to proton-deuterium exchange (Figure 2.22).

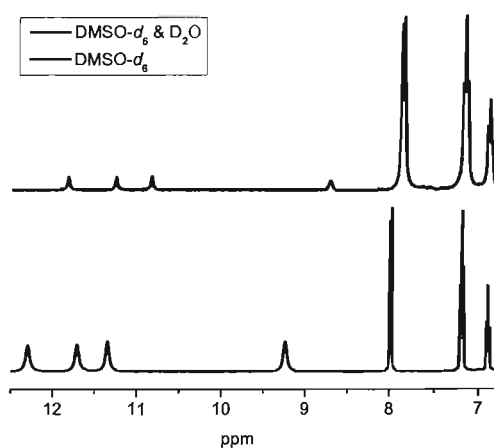


FIGURE 2.22: ¹H NMR stack plot of compound **2.11(d)** in the presence of five equivalents of dihydrogen phosphate (black) and ten minutes after the addition of one hundred equivalents of D₂O (blue).

A gas phase DFT geometry optimization calculation was performed on receptor **2.11(d)** and dihydrogen phosphate using the Spartan 02 computer program. The resultant structure (Figure 2.23) shows the receptor adopting a cleft conformation wherein the receptor binds to two oxygen atoms in the oxoanion, each by a pyrrole and amide hydrogen bond.

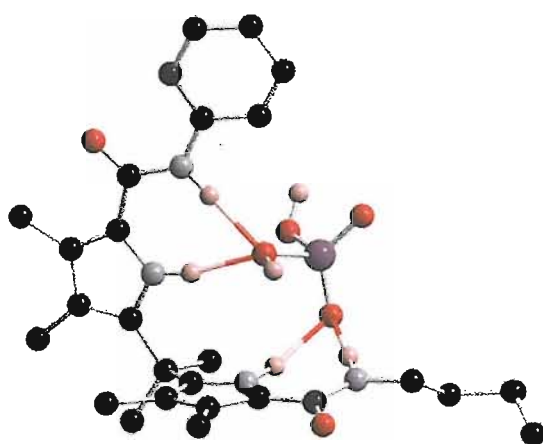


FIGURE 2.23: Structure of the dihydrogen phosphate complex of **2.11(d)** generated by DFT calculation using Spartan 02.

5,5'-Dicarboxamido-dipyrrolylmethanes have been synthesized and shown to have unusually high affinities for dihydrogen phosphate in partially aqueous DMSO- d_6 solutions. Both compounds **2.4(a)** and **2.4(b)** were found to be unstable in solution over short periods of time (days). Therefore the bis-amides **2.11(a)**, **2.11(b)**, and **2.11(d)** were synthesized which contained methyl groups attached to the *meso* carbon atom. These compounds were found to be stable under comparable conditions. Compound **2.11(a)** displayed a high affinity and selectivity for dihydrogen phosphate in competitive solvent media (e.g. DMSO- d_6 /5% water solution.) Unsymmetrically substituted receptor **2.11(d)** was used to study the conformation adopted by these species in solution. NOESY spectroscopy studies suggest that the receptor adopts a linear conformation in solution in the absence of an anion. Presumably the presence of dihydrogen phosphate induces a 'cleft-like' conformation in the receptor resulting in 1:1 receptor:anion stoichiometry for the complex in solution. A gas phase DFT calculation on compound **2.11(d)** with dihydrogen phosphate, also results in a 1:1 complex wherein the dihydrogen phosphate is bound by four hydrogen bonds from the receptor. Compound **2.11(c)**, a mono-amide, was found to have lower affinities for anions than the bis-amide receptors. Interestingly, only one of the pyrrole rings was involved in hydrogen bond donation to the anion in this case. The 5,5'-dicarboxamido-dipyrrolylmethane skeleton shows great promise as a new binding motif for phosphates under competitive conditions. We are currently working to incorporate this unit into a variety of selective anion and ion-pair receptors. The results of these studies will be reported in due course.

2.3 (Dipyrrol-2-yl)alkane receptors

Herein, we describe the syntheses of NH-hydrogendonor-elaborated *meso*-disubstituted dipyrromethanes. These molecules are 5,5' diformyl substituted, generating poor electron density pyrrole rings with enhanced anion binding capabilities. While dipyrrolides are proving to be versatile dianionic ligands for the electropositive metals,⁷⁷⁻⁸⁰ we describe in this section their anion binding capabilities.

2.3.1 Synthesis and characterization

Two dipyrrolyl bisformyl clefts **2.24(a)** and **2.24(b)** have been prepared in according to Scheme 2.3.^x

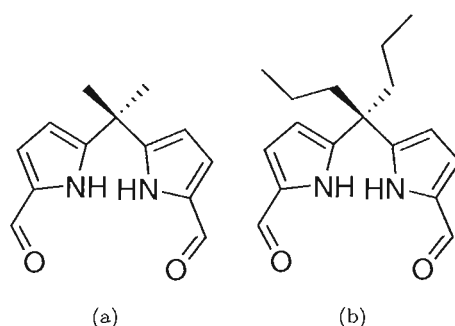
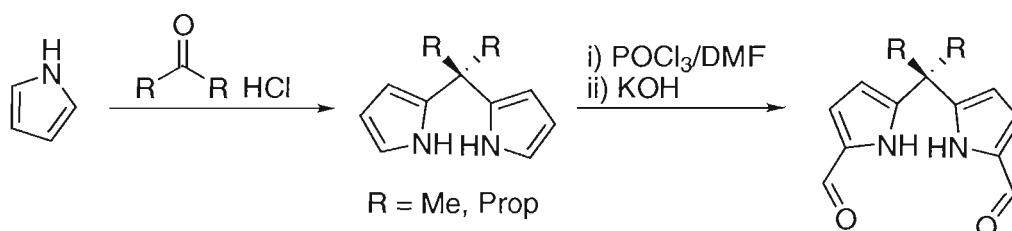


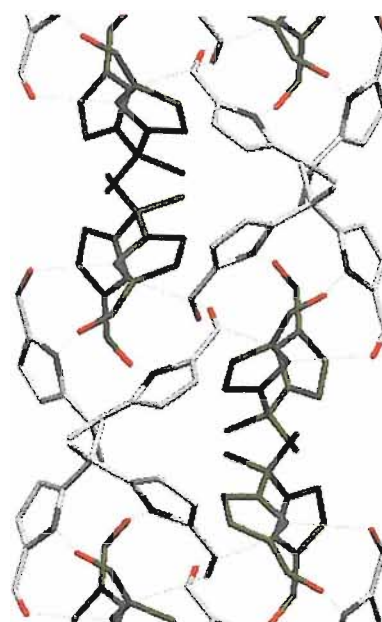
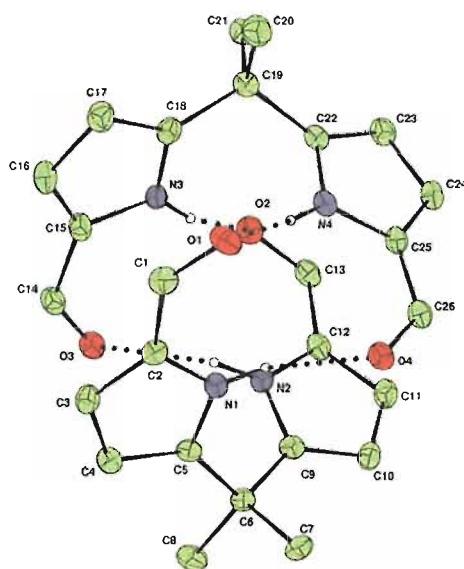
FIGURE 2.24: Dialdehyde dipyrrolyl anion based receptors.



SCHEME 2.3: General synthesis of the dialdehydes.

The Vilsmeier-Hack reactions between (dipyrrol-2-yl)alkane and POCl_3/DMF result in the carbonylation of the dipyrromethanes in the 5,5'-positions, so forming **2.24(a)** and **2.24(b)** (Scheme 2.3). Dialdehyde **2.24(a)** was crystallographically characterized, and adopts a dimeric structure formed by hydrogen bonding between the pyrrole protons and carbonyl oxygens of discrete monomers (Figure 2.27). Love and co-workers have reported the crystal structure of 5,5'-(diphenylmethylene)bis(1*H*-pyrrole-2-carbaldehyde).⁸¹ This compound shares with compound **2.24(a)** the skeleton and differs only on the groups attached to the *meso* carbon. The crystallization pattern chosen for both compounds is identical.

^xCompound **2.24(b)** was prepared by Sessler and co-workers at the University of Texas.



(a) Dimer that generates the asymmetric unit in the (b) View of the dimer's packing that generates the crystal. Hydrogen bonds are represented with dotted tal. Hydrogen bonds are represented in cyan lines.

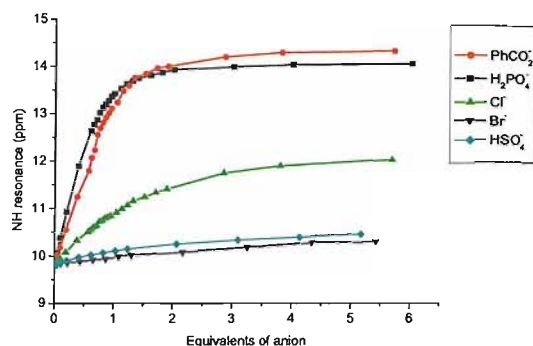
FIGURE 2.25: X-ray crystal structure of compound **2.24(a)**. Hydrogen atoms have been omitted for clarity. In the solid state each molecule^c interacts with another molecule^c through four hydrogen bonds between $\text{NH}^{\text{c}} \cdots \text{CO}^{\text{c}}$ and $\text{NH}^{\text{c}} \cdots \text{CO}^{\text{c}}$.

2.3.2 Binding studies results

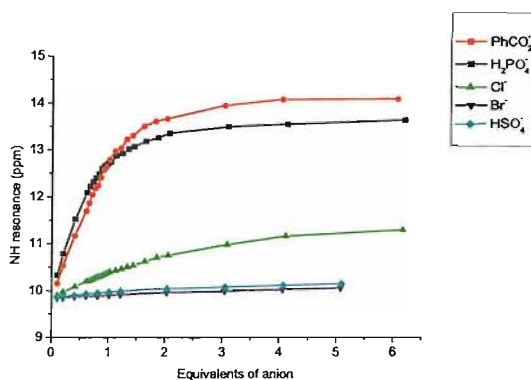
Anion binding studies were conducted with **2.24(a)** and **2.24(b)** in CD_3CN using ^1H NMR techniques.⁶⁹ The results obtained (Figure 2.26) show that a strong interaction takes place between receptors **2.24(a)** and **2.24(b)** with dihydrogen phosphate, although no suitable fit was obtained. The interaction with benzoate although smaller was fitted successfully being 1119 M^{-1} for compound **2.24(a)** and 553 M^{-1} in the case of compound **2.24(b)**. In all the cases the binding constants were higher when the receptor was compound **2.24(a)**. This results are according with the higher steric effects present in compound **2.24(b)**.

When both **2.24(a)** and **2.24(b)** were titrated with tetrabutylammonium fluoride the profiles of the titration curves (Figure 2.26(c)) were completely different from those obtained with the other anions (Figure 2.26(a) and Figure 2.26(b)).

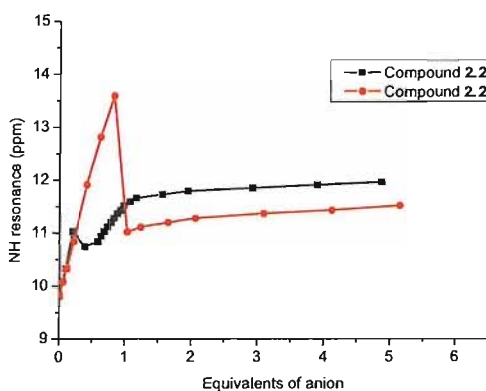
Upon addition of tetrabutylammonium fluoride to acetonitrile solutions of **2.24(a)** and **2.24(b)**, an initial downfield shift of the pyrrole NH protons was observed at low fluoride concentrations followed by a sharp upfield shift between 0.25 eq to 0.5 eq for compound **2.24(a)** and 0.8 eq to 1.1 eq for compound **2.24(b)**. Then, the NH shift inverts again to downfield, plateauing **2.24(a)** around 1.1 equivalents of fluoride added, and **2.24(b)** around 2 equivalents.



(a) Titration curves of compound **2.24(a)** with a variety of anionic putative guests.



(b) Titration curves of compound **2.24(b)** with a variety of anionic putative guests.



(c) Fluoride titration curves of compounds **2.24(a)** and **2.24(b)**.

FIGURE 2.26: Titrations performed in CD₃CN. Anions added as tetrabutylammonium salts.

Similar behavior was previously observed when fluoride was used as guest with compound **2.27(a)**. An explanation given to justify the profile of the titration curve was

the strong basicity of the fluoride anion that can withdraw the proton from the NH pyrrole.⁶⁰

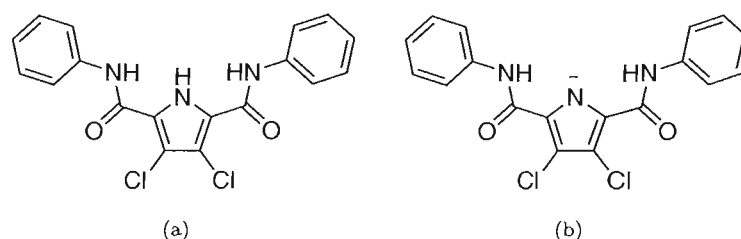


FIGURE 2.27: When tetrabutylammonium fluoride is added to dichloromethane- d_2 solutions of compound 2.27(a), pyrrolate anion 2.27(b) is formed.

An initial interpretation of the profile showed in Figure 2.26(c) was to assume that the first equivalents of the anion are interacting with the receptor through hydrogen bonds until the NH shift changes upfield, when pyrrolate anion starts to form. When the equilibrium is reached between pyrrole and pyrrolate, fluoride continues interacting through hydrogen bonds with the receptor shifting the NH pyrrole downfield again.

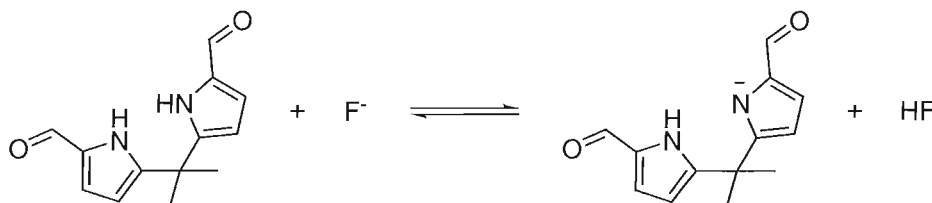


FIGURE 2.28: Formation of pyrrolate is the process that justifies the sharp upfield NH shift inversion. Once the equilibrium in this process is reached, the concentration of pyrrolate remains constant and we start seeing again a downfield NH pyrrole shift upon addition of more tetrabutylammonium fluoride.

Although hydrofluoric acid is the weakest acid in the family of halides, the pK_a value of this acid is lower than the pK_a of pyrrole. On the other hand, pyrrolate is a strong base even more basic than methoxide.

Acid	Base	pK_a (relative to water)
HF	F^-	3.2 ⁸²
MeOH	MeO^-	15.2 ⁸³
Pyrrole	Pyrrolate	23.0 ⁸⁴
NH_3	H_2N^-	38.0 ⁸⁵

TABLE 2.5: pK_a values.

The formyl group in position 5 on the dipyrrolyl receptors will make the NH pyrrole more acidic because of the trend of this group to withdraw charge from the ring (Figure 2.29).

Based on the pK_a values shown in Table 2.5, we can say that pyrrolate is stronger base than fluoride. On the other hand, hydrofluoric acid is stronger acid than pyrrole. Thus,

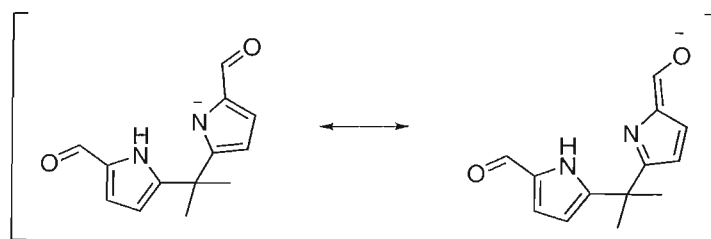


FIGURE 2.29: Delocalization of the negative charge in this molecule, leaving it over another electronegative atom will make this anion more stable being the pK_a lower than that reported for pyrrole.

the equilibrium in Figure 2.28 will be displaced to the reactants. The concentration of pyrrolate will be low, because the products will be stronger base and stronger acid than the reactants.

2.4 Conclusion

A series of dipyrrolic bis-amide (e.g. 2.4(a), 2.11(b)), mono-amide (e.g. 2.11(c)) and bisformyl (e.g. 2.24(a)) receptors have been synthesized and their anion coordination properties investigated by the use of ^1H NMR titration techniques. These receptors proved to be efficient anion receptors and showed selectivity toward oxoanions such as benzoate and dihydrogen phosphate. The first example of dipyrrolic diphenylamide cleft reported, bound dihydrogen phosphate in an extremely competitive solvent media. This sort of interaction is quite unusual for organic non-charged anion receptors. However, oxidation processes were observed to occur on the first generation of dipyrrolic anion receptors after periods of several weeks. Upon functionalization of the *meso* carbon of the dipyrrolic skeleton with methyl groups we achieve stable compounds *vs.* oxidation processes. Unexpectedly, these receptors abandon the U shape conformation and adopt a linear conformation geometry, much less efficient for anion binding. Despite the efforts invested to obtain crystals of the anion-receptor clefts, no crystals were obtained and hence we studied the behaviour of these clefts in solution by the means of NOESY experiments. We observed a change in the geometry of the receptors from linear to a U shape after adding some equivalents of anion. Binding studies of the dipyrrolic monoamide receptor certify that only the amidopyrrole moiety show activity as anion receptor. Surprisingly, the other pyrrole unit seems to play no role on binding anions. The formyl 5,5'-disubstituted dipyrroles show anion binding activity through the pyrroles. These results are consistent with the dipyrrole as an effective binding motif from which to construct a new armory of anion binding agents. In conclusion the synthesis of dipyrrole amide clefts proved to be successful in that:

- The high selectivity for oxoanions such as dihydrogenphosphate was achieved.

- An unusual high binding constant for dihydrogen phosphate into an extremely competitive solvent mixture.
- New receptors with enhanced stability and selectivity toward dihydrogen phosphate.

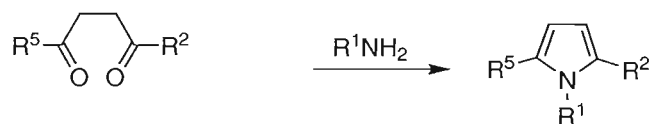
Chapter 3

NH *vs.* CH hydrogen bond formation in metal-organic anion receptors containing pyrrolylpyridine ligands and pyridine metal complexes with locked rotation around the metal

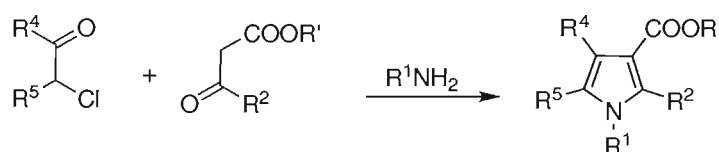
The coordination of anionic guest species by hydrogen bond donating receptors is an area of supramolecular chemistry that continues to attract attention.^{19,20,45,86–88} A high proportion of the anion receptors reported thus far are ‘built’ upon organic scaffolds such as the calix[4]arenes.^{89–92} However, the preparation of this type of receptor can often be synthetically challenging, a fact that prompted us to look for alternative means of arranging hydrogen bond donating groups in space. It occurred to us that some easy to prepare metal ligand complexes could be exploited as simple pieces of inorganic molecular scaffolding.³⁵ We initially chose to study square planar platinum(II) complexes due to their relative inertness towards ligand substitution and pyridine or iso-quinoline ligands due to their ease of synthesis and possibility of the hydrogen in the 2-position of the pyridine involving itself in potential CH...anion hydrogen bonding.^{36–38} Brammer and co-workers have studied the application of related PtL_4^{2+} (L = nicotinamide) complexes in the construction of crystal-engineered networks,⁹³ whilst Steed and co-workers have investigated the role anions can play in stabilising discrete complexes using similar organic ligands and kinetically labile templating metal centres.⁴³



(a) Knorr pyrrole synthesis



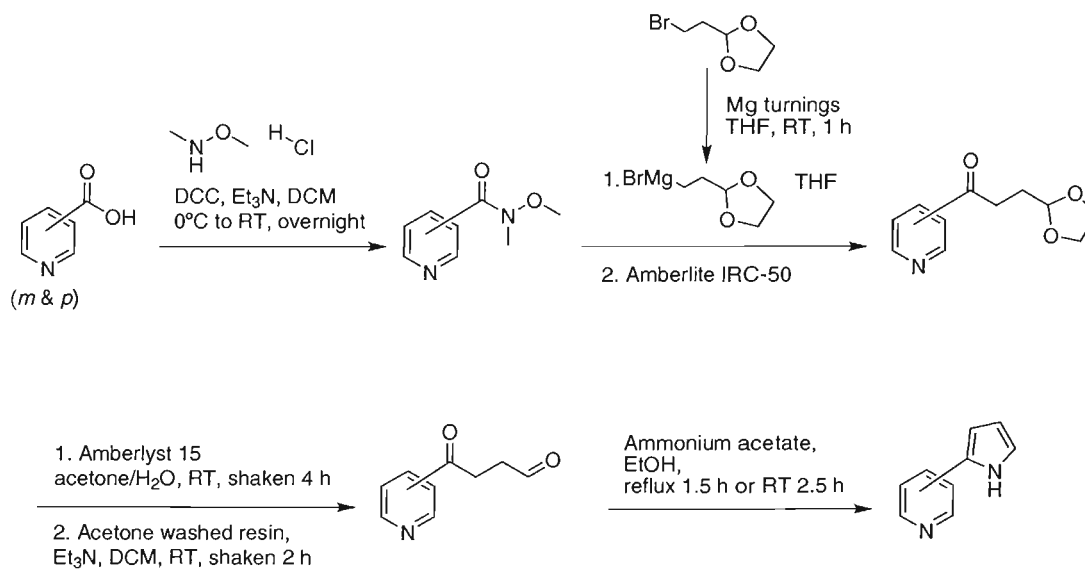
(b) Paal-Knorr pyrrole synthesis



(c) Hantzsch pyrrole synthesis

FIGURE 3.2: Classical syntheses of C-substituted pyrroles.

respectively, to afford substituted pyridines in up to 95 and 60% yields (Scheme 3.2).^{xii} The platinum complexes of these pyridines, **3.1(b)**·(BF₄)₂ and **3.1(c)**·(BF₄)₂, were prepared in an analogous fashion to **3.1(a)**·(BF₄)₂ (Scheme 3.1).

SCHEME 3.2: Synthesis of the *meta* and *para* pyrrolepyridine ligands.

Crystals of **3.1(b)**·(BF₄)₂ were obtained by slow evaporation of a nitromethane solution of the complex. The structure (see Figure 3.3) shows that the complex adopts

^{xii}Three main routes established for the synthesis of C-substituted pyrroles shown in Figure 3.2.⁹⁸⁻¹⁰⁰

the 1,2-alternate conformation in the solid state binding the BF_4^- anions *via* $\text{NH}\cdots\text{F}$ and $\text{CH}\cdots\text{F}$ hydrogen bonds (including $\text{N2}\cdots\text{F1}$ 2.882(3); $\text{N4}\cdots\text{F2}$ 2.884(3); $\text{C1}\cdots\text{F3}$ 3.322(3); $\text{C5}\cdots\text{F1}$ 3.447(3); $\text{C10}\cdots\text{F3}$ 3.442(4) Å).

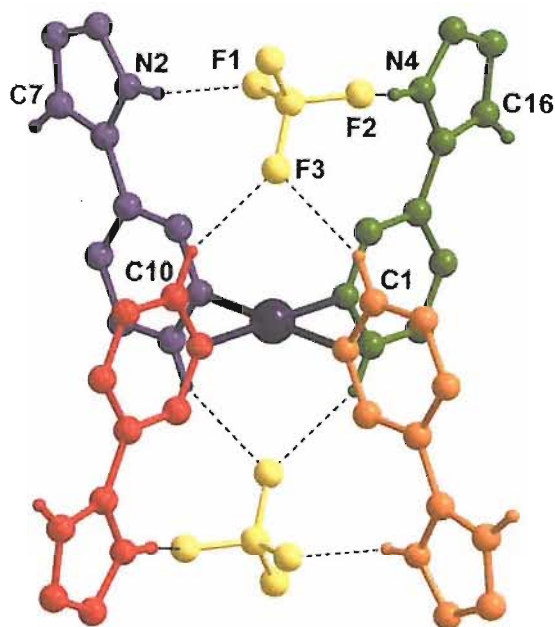
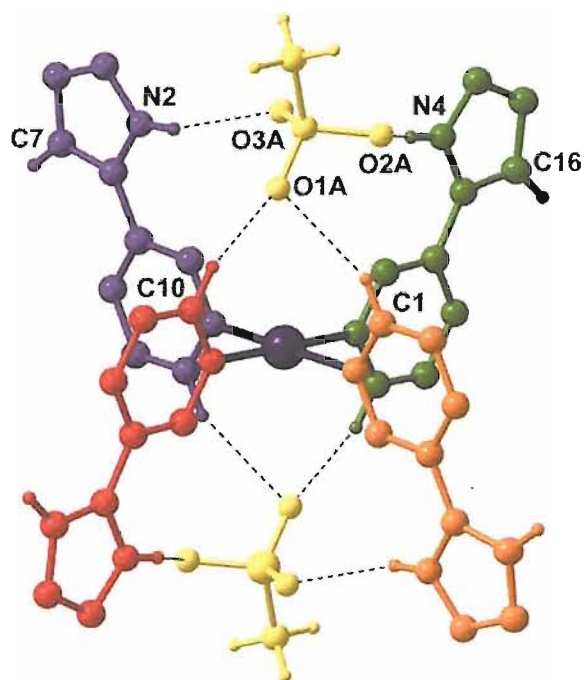


FIGURE 3.3: A ball-and-stick representation of the X-ray crystal structure of **3.1(b)**· $(\text{BF}_4)_2$ crystallized from nitromethane. The hydrogen bonding network is shown with BF_4^- anions bound above and below the plane of the complex by $\text{CH}\cdots\text{F}$ and $\text{NH}\cdots\text{F}$ hydrogen bonds.

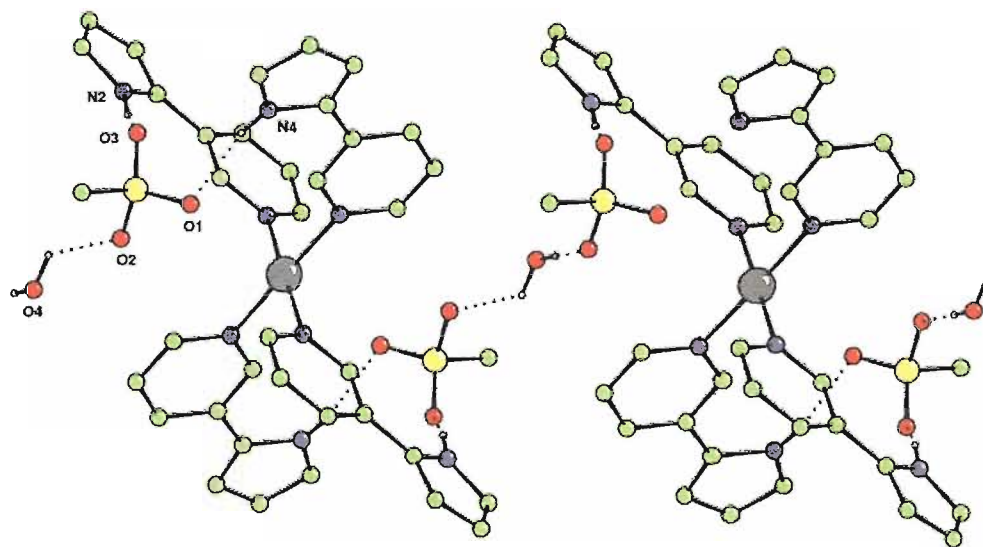
Crystals of **3.1(b)**· $(\text{MeSO}_3)_2\cdot\text{H}_2\text{O}$ were obtained by slow evaporation of a nitromethane solution of the salt (prepared by an analogous method using AgMeSO_3). Once again the complex adopts the 1,2-alternate conformation (see Figure 3.4), binding the methanesulfonate anions *via* both pyrrole $\text{NH}\cdots\text{O}$ and pyridine $\text{CH}\cdots\text{O}$ hydrogen bonds in the solid state (including $\text{N2}\cdots\text{O3A}$ 2.926(8)Å; $\text{N4}\cdots\text{O2A}$ 2.850(8) Å; $\text{C1}\cdots\text{O1A}$ 3.542(7) Å; $\text{C10}\cdots\text{O1A}$ 3.100(6) Å).

Unexpected crystals of **3.1(b)**· $(\text{PF}_2\text{O}_2)_2$ were obtained by slow evaporation of a nitromethane solution of the salt, prepared by an analogous method using an old batch of AgPF_6 .^{xiii} The complex follows the same crystallization pattern and adopts the 1,2-alternate conformation (see Figure 3.6), binding the difluorophosphate anions *via* both pyrrole $\text{NH}\cdots\text{O}$ and pyridine $\text{CH}\cdots\text{O}$ hydrogen bonds in the solid state (including $\text{N2}\cdots\text{O2}$ 2.896(8)Å; $\text{N4}\cdots\text{O2}$ 2.839(8) Å; $\text{C14}\cdots\text{O2}$ 3.441(7) Å; $\text{C5}\cdots\text{O2}$ 3.391(6) Å;

^{xiii}³¹P{¹H} NMR of this old batch of silver hexafluorophosphate from Aldrich shows high levels of difluorophosphate anions (see Figure 3.5). The same experiment revealed the presence of difluorophosphate as a contaminant even on a brand new sample from Aldrich.¹⁰¹



(a)



(b) The water links the complex into chains along the b axis.

FIGURE 3.4: A ball-and-stick representation of the X-ray crystal structure of the methanesulfonate salt of cation **3.1(b)**²⁺. The hydrogen bonding network is shown with MeSO₃⁻ anions bound above and below the plane of the complex by CH...O and NH...O hydrogen bonds.

C1...O3 3.203(6) Å).

³¹P{¹H} NMR of **3.1(b)**·(PF₂O₂)₂ confirmed the presence of PF₂O₂⁻ as the single counteranion.

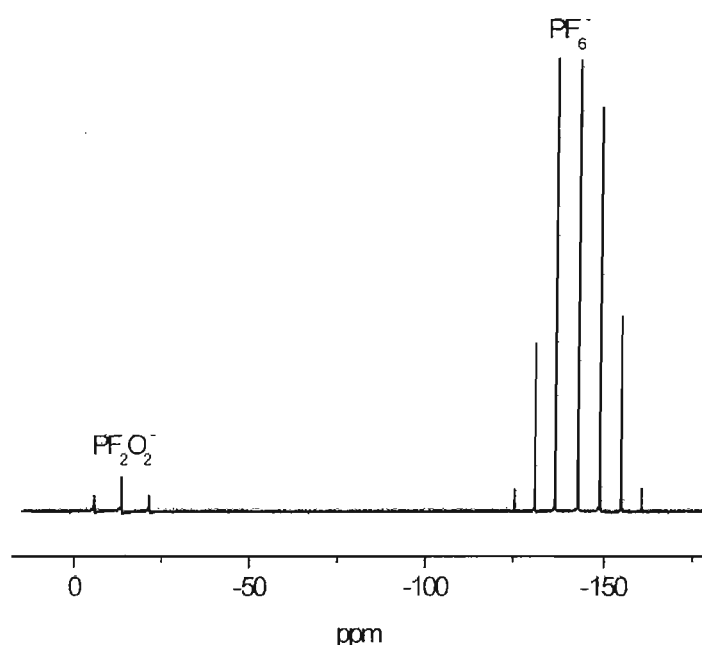


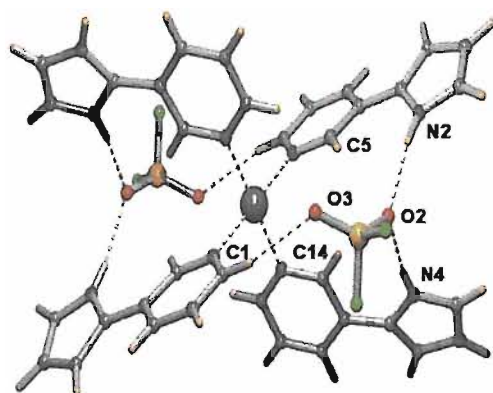
FIGURE 3.5: $^{31}\text{P}\{^1\text{H}\}$ NMR of the silver hexafluorophosphate used to prepare compound **3.1(b)**· $(\text{PF}_2\text{O}_2)_2$. The triplet is attributed to the presence of difluorophosphate anions.

3.1.2 Binding studies results

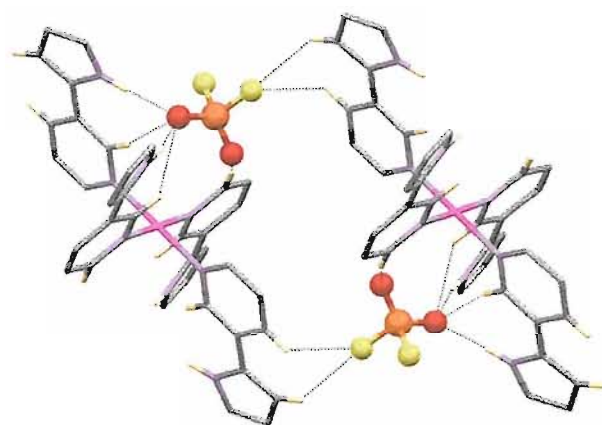
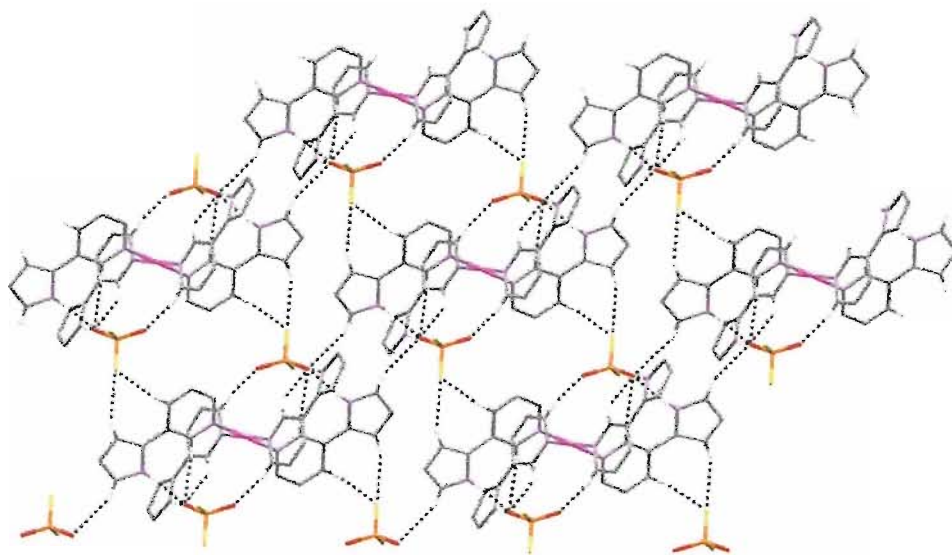
The anion binding properties of complexes **3.1(a)**, **3.1(b)** and **3.1(c)**· $(\text{BF}_4)_2$ were explored using ^1H NMR titration techniques in $\text{DMSO-}d_6$. Complex **3.1(a)**· $(\text{BF}_4)_2$ was titrated *vs.* a set of putative anions (Figure 3.7), and despite containing no NH hydrogen bond donor groups, was observed to interact with them with downfield shifts of up to 0.50 ppm for the hydrogen in the 2-position of the pyridine ring in the presence of three equivalents of chloride ion (see Figure 3.8 and Table 3.1). In most cases, this data could be fitted to a 1:1 receptor:anion binding model with the results shown in Table 3.2. However, the possibility exists that a second anion may associate with the 1:1 complex with a low K_2 that has not been detected in this experiment. This is true of all the ^1H NMR titration experiments reported in this section.

Complex **3.1(b)**· $(\text{BF}_4)_2$ shows the highest affinity for anions of the three receptors reported (Figure 3.9). Shifts of up to 1.15 ppm for the pyridine CH proton were observed with three equivalents of chloride (Table 3.1 and Figure 3.10(a)).

Most surprisingly however, the pyrrole NH proton does not shift significantly upon addition of Cl^- , Br^- , I^- , HSO_4^- , NO_3^- or MeSO_3^- (Figure 3.10). In the cases of the most basic anions studied, acetate (see Figure 3.11) and benzoate, the NH resonance does shift downfield by 1.36 and 1.03 ppm, respectively, in the presence of three equivalents of the anions, although precipitation occurs in the case of benzoate and the ratio of the receptor to anion in solution is uncertain. Acetate binds in a 1:2 receptor:anion



(a) View of the X-ray complex structure.

(b) Environment around the PF₂O₂⁻.

(c) Forms sheets in the 01-1 plane via CH and NH hydrogen bonds.

FIGURE 3.6: X-ray crystal structure of the unexpected PF₂O₂⁻ complex.

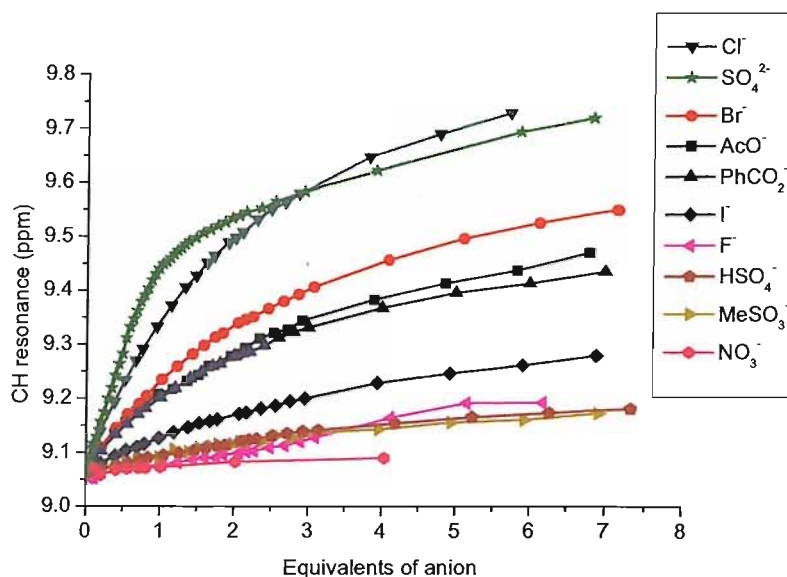


FIGURE 3.7: ^1H NMR titration curves for compound **3.1(a)** with fluoride, chloride, bromide, iodide, methanesulfonate, nitrate, acetate, benzoate, sulfate and hydrogen sulfate in $\text{DMSO-}d_6$ at 298 K. Anions added as their tetrabutylammonium salts.

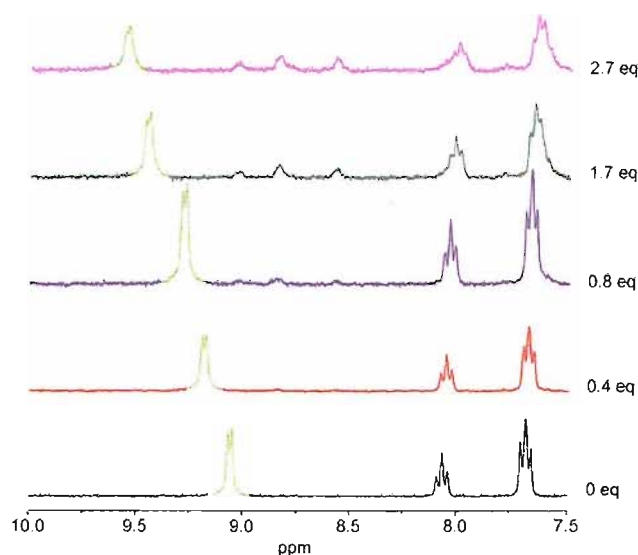


FIGURE 3.8: Proton NMR stack plot titration of compound **3.1(a)** in $\text{DMSO-}d_6$ with tetrabutylammonium chloride at 298 K showing a downfield shift of the pyridine CH proton in the 2-position (green).

stoichiometry (planar anions were found to bind in a 1:2 fashion to the previous generation of nicotinamide based platinum complexes)^{36–38} with $K_2 > K_1$. This suggests that an allosteric effect is operating which preorganises the second binding site upon complexation of the first equivalent of acetate. The same effect was also observed in the first generation nicotinamide systems.^{36–38} In the case of the other anions, downfield

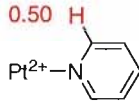
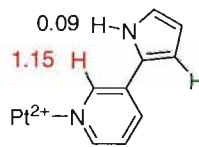
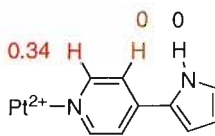
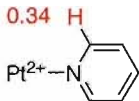

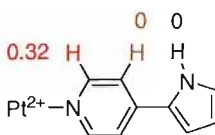
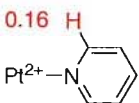

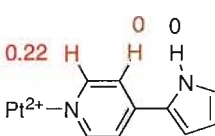
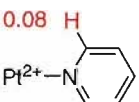
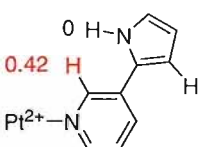
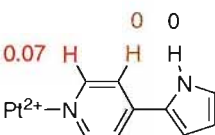
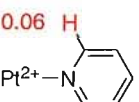
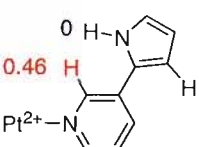
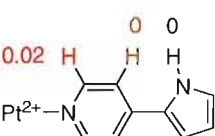
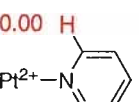
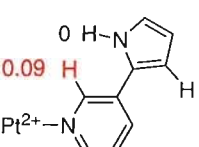
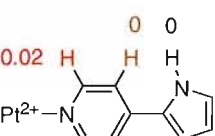
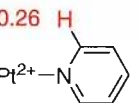
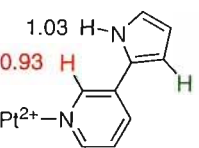

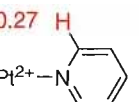
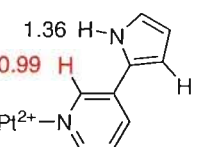
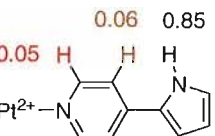
Anion	Compound 3.1(a)	Compound 3.1(b)	Compound 3.1(c)
Cl ⁻	 0.50 H Pt ²⁺ -N-pyridine	 0.09 H 1.15 H Pt ²⁺ -N-pyridine	 0.34 H 0 H 0 H Pt ²⁺ -N-pyridine
Br ⁻	 0.34 H Pt ²⁺ -N-pyridine	 -0.06 H 0.99 H Pt ²⁺ -N-pyridine	 0.32 H 0 H 0 H Pt ²⁺ -N-pyridine
I ⁻	 0.16 H Pt ²⁺ -N-pyridine	 -0.06 H 0.69 H Pt ²⁺ -N-pyridine	 0.22 H 0 H 0 H Pt ²⁺ -N-pyridine
HSO ₄ ⁻	 0.08 H Pt ²⁺ -N-pyridine	 0 H 0.42 H Pt ²⁺ -N-pyridine	 0.07 H 0 H 0 H Pt ²⁺ -N-pyridine
MeSO ₃ ⁻	 0.06 H Pt ²⁺ -N-pyridine	 0 H 0.46 H Pt ²⁺ -N-pyridine	 0.02 H 0 H 0 H Pt ²⁺ -N-pyridine
NO ₃ ⁻	 0.00 H Pt ²⁺ -N-pyridine	 0 H 0.09 H Pt ²⁺ -N-pyridine	 0.02 H 0 H 0 H Pt ²⁺ -N-pyridine
PhCO ₂ ⁻	 0.26 H Pt ²⁺ -N-pyridine	 1.03 H 0.93 H Pt ²⁺ -N-pyridine	 0.11 H 0.07 H 0.61 H Pt ²⁺ -N-pyridine
MeCO ₂ ⁻	 0.27 H Pt ²⁺ -N-pyridine	 1.36 H 0.99 H Pt ²⁺ -N-pyridine	 0.05 H 0.06 H 0.85 H Pt ²⁺ -N-pyridine

TABLE 3.1: ¹H NMR chemical shifts upon addition of three equivalents of tetrabutylammonium anion salt to solutions of [**3.1(a)**, **3.1(b)** and **3.1(c)**] \cdot (BF₄)₂ in DMSO-*d*₆.

shifts of a pyrrole CH proton were observed (Table 3.1). Amongst the non-carboxylate anions, the highest affinity was found with methanesulfonate (1115 M⁻¹) whilst HSO₄⁻ was bound considerably more strongly (837 M⁻¹) than was the case with complex **3.1(a)** (<10 M⁻¹).

Complex **3.1(c)** \cdot (BF₄)₂ does not contain a potential convergent anion-binding site that could involve all four of the pyrrole NH groups. Indeed similar, although not identi-

Anion ^a	Compound 3.1(a) ^b	Compound 3.1(b) ^b	Compound 3.1(c) ^b
Cl ⁻	195	960	216
Br ⁻	121	796	211
I ⁻	50	462	113
AcO ⁻	84	K ₁ = 216 ^c K ₂ = 2400 ^c ^d	117 ^c
PhCO ₂ ⁻	132		111 ^c
MeSO ₃ ⁻	45	1115	<10
NO ₃ ⁻		29	<10
HSO ₄ ⁻	<10	837	<10

^aAdded as tetrabutylammonium salt.

^bErrors estimated to be no more than 15%.

^cCalculated following the shift in the pyrrole NH proton.

^dPrecipitation during the titration, however shifts of protons suggest a strong interaction of **3.1(b)** with benzoate.

TABLE 3.2: Stability constants of the tetrafluoroborate salts of **3.1(a)**, **3.1(b)** and **3.1(c)** with anionic guests in DMSO-*d*₆ at 298 K calculated from the shift of the resonance of the pyridine hydrogen in the 2-position except where noted assuming 1:1 stoichiometry in all cases except where noted.

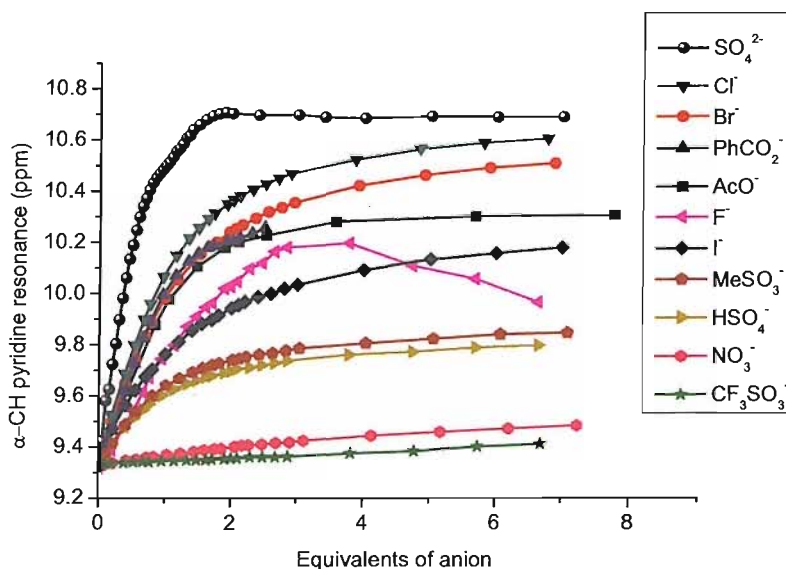
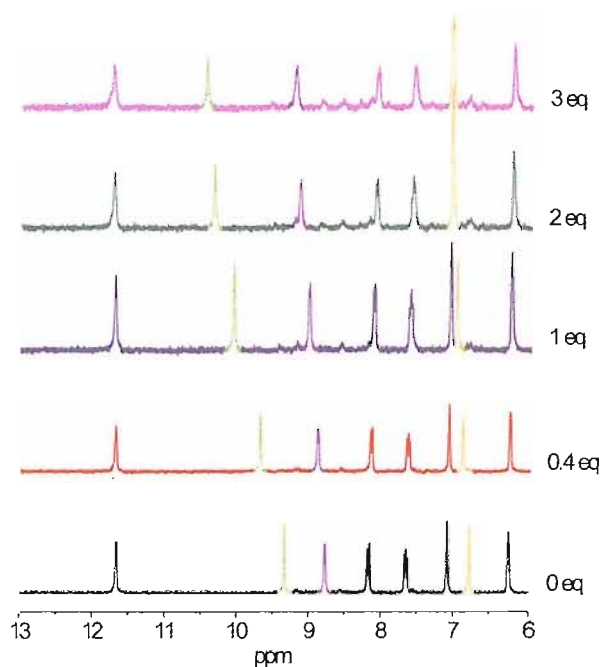
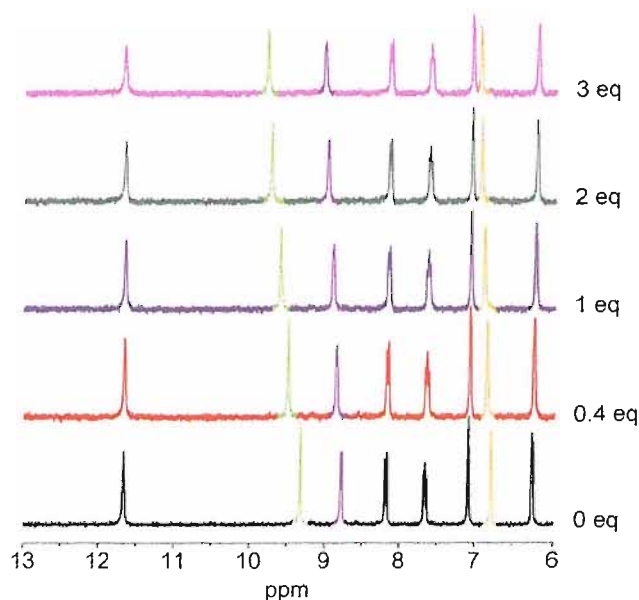


FIGURE 3.9: ¹H NMR titration curves for compound **3.1(a)** with fluoride, chloride, bromide, iodide, methanesulfonate, nitrate, acetate, benzoate, sulfate and hydrogen sulfate in DMSO-*d*₆ at 298 K. Anions added as their tetrabutylammonium salts. CH shift at 2-position of the pyridines.

cal, shifts of the pyridine CH resonance in the 2-position were observed with complexes **3.1(a)**·(BF₄)₂ and **3.1(c)**·(BF₄)₂ (see Figure 3.12). The exception to this are the interactions observed with the carboxylate anions Figure 3.13(a). Here, as with complex **3.1(b)**·(BF₄)₂, the pyrrole NH group was observed to shift downfield by between 0.61



(a) **3.1(b)** vs. Cl^- ^1H NMR stack plot.



(b) **3.1(b)** vs. MeSO_3^- ^1H NMR stack plot.

FIGURE 3.10: ^1H NMR stack plots titrations of compound **3.1(b)** in $\text{DMSO}-d_6$ with tetrabutylammonium chloride and methanesulfonate at 298 K showing a downfield shift of the pyridine CH proton in both the 2-position (green) and the 6-position (violet), the pyrrole proton in the 3-position (orange) does shifts downfield too.

and 0.85 ppm whilst only small shifts of the pyridine α -CH resonance were observed (Figure 3.13(b)). These results are evidence that a different mode of binding occurs

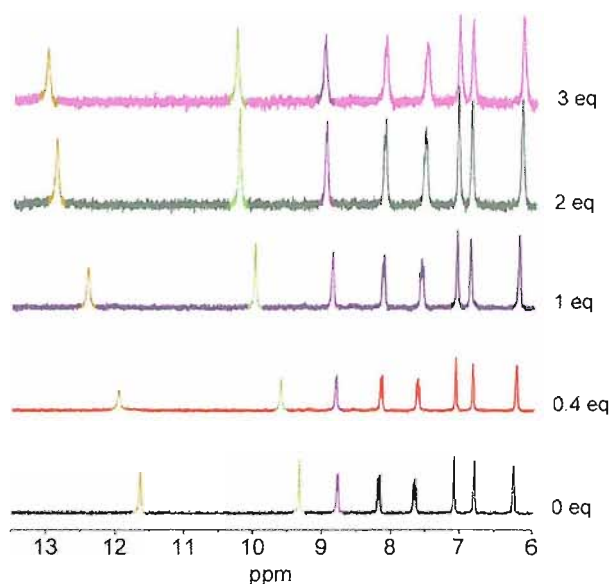
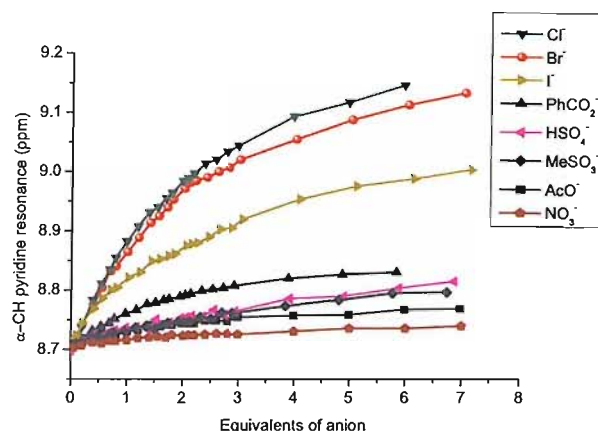


FIGURE 3.11: ^1H NMR stack plot titration of compound **3.1(b)** in $\text{DMSO-}d_6$ with tetrabutylammonium acetate at 298 K showing a downfield shift of the pyridine CH proton in the 2-position (green), the pyrrole NH proton does shifts downfield (dark yellow).

between complexes **3.1(b)** $\cdot(\text{BF}_4)_2$ and **3.1(c)** $\cdot(\text{BF}_4)_2$ and carboxylate anions than that which occurs between the complexes and the other less basic anions.

Crystals of **3.1(b)** $\cdot(\text{MeSO}_3)_2\cdot\text{H}_2\text{O}$ were obtained by slow evaporation of a nitromethane solution of the salt (prepared by an analogous method using AgMeSO_3). Once again the complex adopts the 1,2- alternate conformation (see Figure 3.14), binding the methanesulfonate anions *via* both pyrrole $\text{NH}\cdots\text{O}$ and pyridine $\text{CH}\cdots\text{O}$ hydrogen bonds in the solid state (including $\text{N2}\cdots\text{O3A}$ 2.926(8) Å; $\text{N4}\cdots\text{O2A}$ 2.850(8) Å; $\text{C1}\cdots\text{O1A}$ 3.542(7) Å; $\text{C10}\cdots\text{O1A}$ 3.100(6) Å). The solution binding experiments and the crystal structure of the methanesulfonate complex of **3.1(b)** serve to reiterate the important point that crystal structure data cannot be relied upon to predict the structure of complexes in solution. There is no evidence that the pyrrole NH groups interact with the methanesulfonate anion in $\text{DMSO-}d_6$ solution, but rather that the pyrrole CH group is involved in a $\text{CH}\cdots\text{O}$ hydrogen bond with the anion (Figure 3.10(b)). A comparison of the shifts observed in compound **3.1(c)** with acetate and chloride shows the halide binding presumably to the centre of the complex so taking advantage of the electrostatic interaction, whilst the more basic carboxylate induces a larger shift in the pyrrole NH group. In nitromethane, more typical behaviour is observed with compound **3.1(b)** upon addition of anions. For example, addition of aliquots of tetramethylammonium methanesulfonate to a nitromethane- d_3 solution of **3.1(b)** $\cdot(\text{BF}_4)_2$ causes the pyrrole NH resonance to shift downfield from 9.79 ppm to 11.56 ppm ($\Delta\delta = 1.77$ ppm at 2.0 equiv MeSO_3^-). Unfortunately, upon further additions of this anion, the complex precipitates. These



(a)

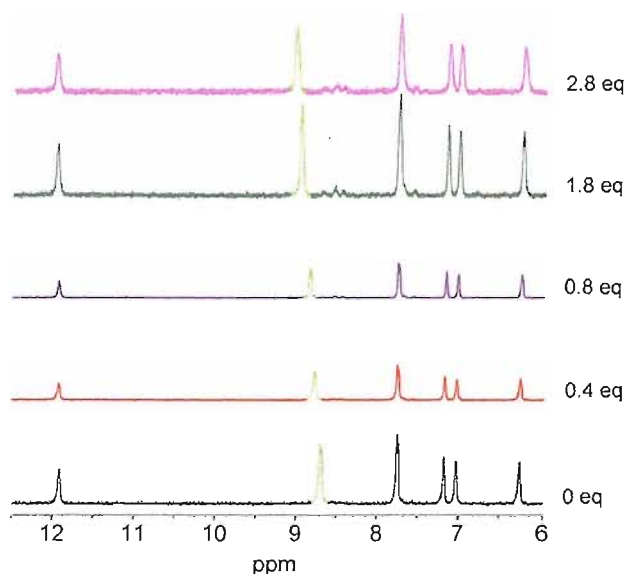
(b) **3.1(c)** vs. Cl^- ^1H NMR stack plot.

FIGURE 3.12: (a) ^1H NMR titration curves of the pyridine CH proton in the 2-position for compound **3.1(c)** with chloride, bromide, iodide, benzoate, acetate, methanesulfonate, nitrate and hydrogen sulfate in $\text{DMSO-}d_6$ at 298 K and (b) ^1H NMR stack plot titration of compound **3.1(c)** in $\text{DMSO-}d_6$ with chloride at 298 K showing a downfield shift of the pyridine CH proton in the 2-position (green). Anions added as their tetrabutylammonium salts.

results led us to conclude that a solvent competition mechanism, such as that shown in Figure 3.15, may be operating in DMSO solution. Nitromethane is a notoriously poor hydrogen-bond acceptor¹⁰² and hence when an anion is added to the receptor in this solvent it will bind to the most acidic hydrogen bond donor (the NH). However in DMSO (a good hydrogen bond acceptor), the anionic guest will either bind to the pyrrole NH if it is a basic anion, or if it is less basic, the pyrrole NH groups may orientate themselves

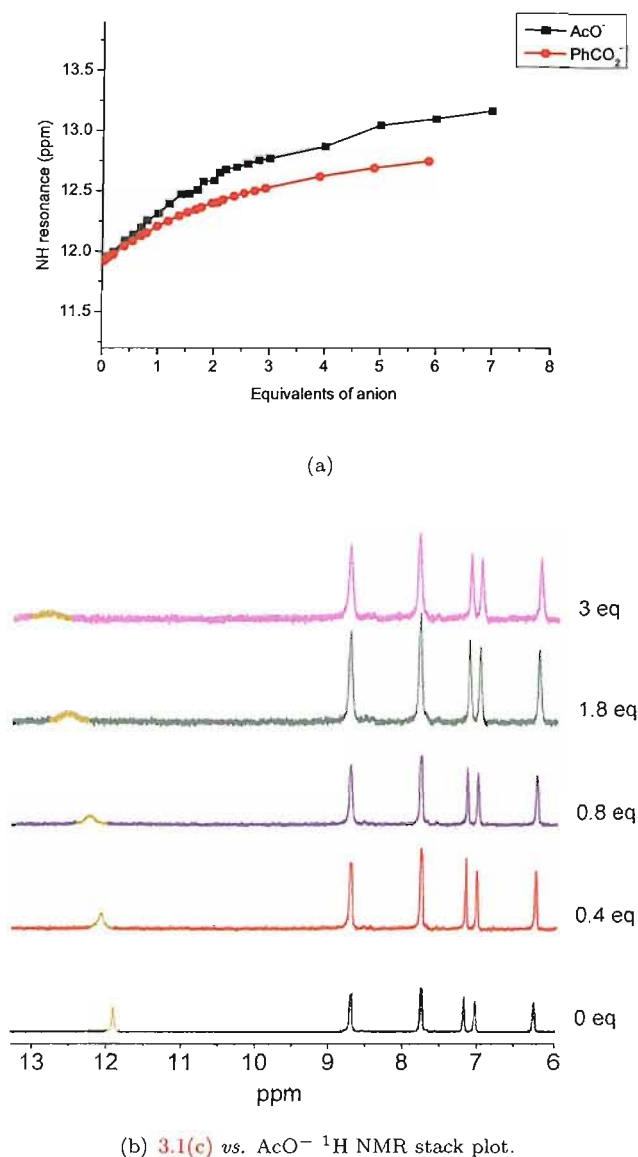


FIGURE 3.13: (a) ¹H NMR titration curves of the pyrrole NH proton for compound **3.1(c)** with benzoate and acetate in DMSO-*d*₆ at 298 K and (b) ¹H NMR stack plot titration of compound **3.1(c)** in DMSO-*d*₆ with acetate at 298 K showing a downfield shift of the pyrrole NH proton (dark yellow). Anions added as their tetrabutylammonium salts.

into the solvent allowing the formation of hydrogen bonds to the DMSO whilst the anion accepts CH hydrogen bonds from the platinum complex. This presumably leads to a greater overall stability of the complex than if the NH groups were oriented inwards and the solvent presented with the CH groups of the pyrrole. The profound effect of solvent on the binding mode of this receptor is an important phenomenon and should probably be looked at more closely as a design feature for future anion receptors containing NH hydrogen bond donor groups.¹⁰³

temperatures above ca. 60°C, consistent with the compound adopting a 1,3-alternate conformation. This conformational fluxionality proved to be more evident in more polar solvents such as acetonitrile. These results are consistent with the formation of a hydrogen bond network between the hydroxy groups at the lower rim of the calix[4]arene (Figure 3.16).¹⁰⁴ Evidence for the formation of intramolecular hydrogen bond comes from the unusually low frequency of the stretching vibration of the OH groups in the IR spectrum of the *p-tert*-butylcalix[4]arene.

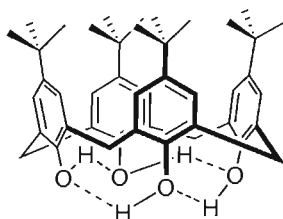


FIGURE 3.16: Hydrogen bond network within the calix[4]arene lower rim..

A new set of hydroxy and methoxy platinum (II) pyridines (Figure 3.17) were synthesized, characterized and in some cases their anion binding properties investigated by ¹H NMR titration experiments. The hydrogen bond functional group at the 2-position of the pyridine is involved in intramolecular hydrogen bond interactions that would lead to a more rigid structure and favor stronger and more selective anion interactions.

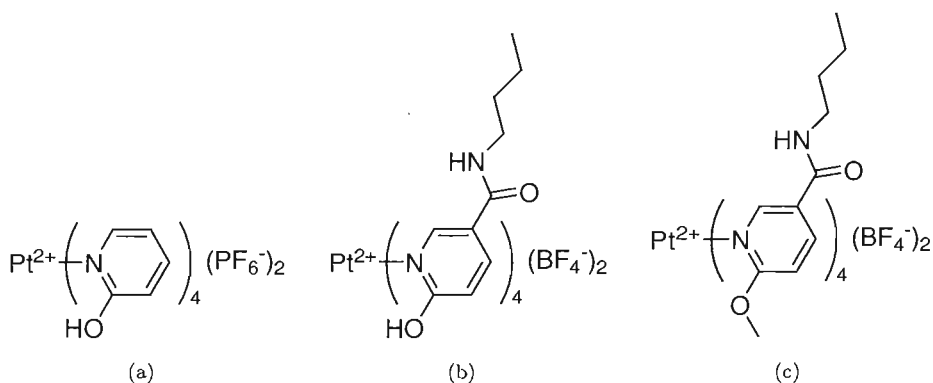
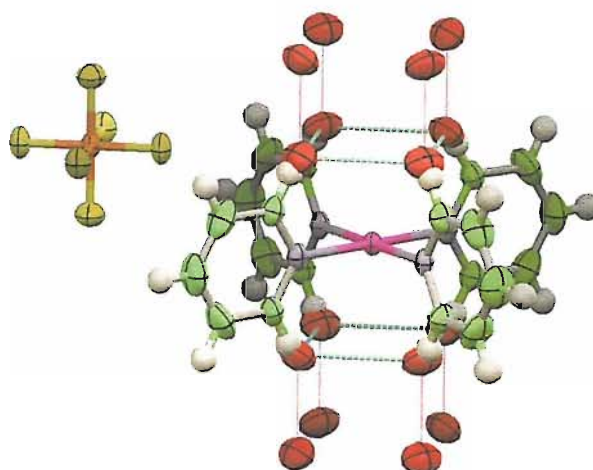


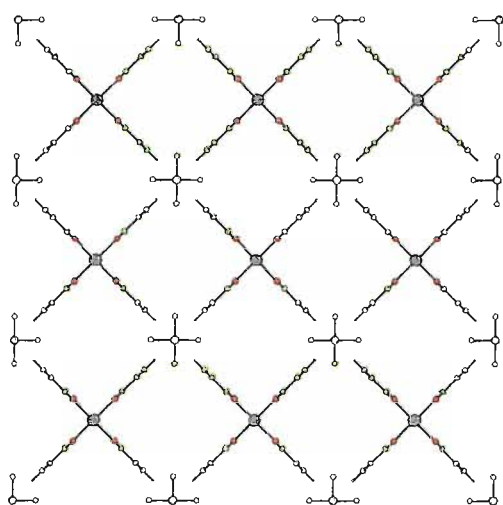
FIGURE 3.17: Platinum (II) complexes prepared to lock the free rotation of the ligands.

3.2.1 Synthesis and characterization

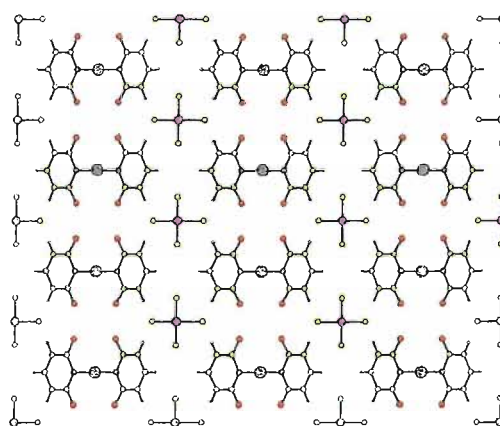
Compound 3.17(a) was prepared by refluxing 2-hydroxypyridine, $\text{PtCl}_2(\text{EtCN})_2$ and AgPF_6 in acetonitrile. Crystals of compound 3.17(a) were obtained by slow evaporation of acetonitrile solutions of the complex. In the solid state 3.17(a) was found to form intramolecular hydrogen bonds among the hydroxyl groups. Interestingly, the counter anion crystallizes in a parallel array to that formed by the complex.



(a) Crystal structure of **3.17(a)**. Ellipsoids drawn at the 35% probability level.



(b) View down the *c* axis.

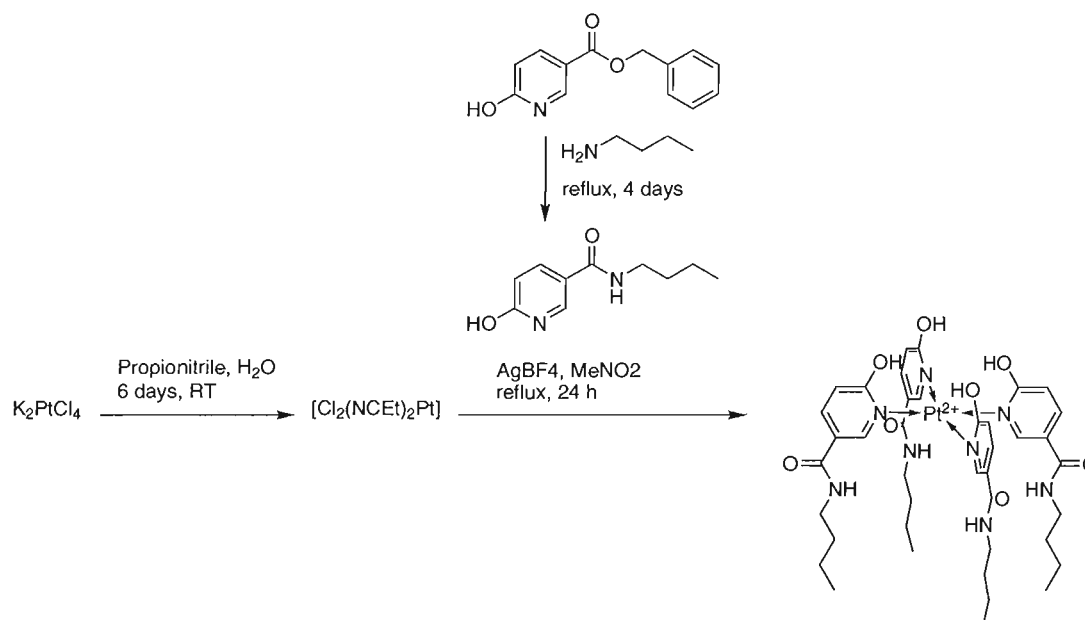


(c) View along the *a* axis.

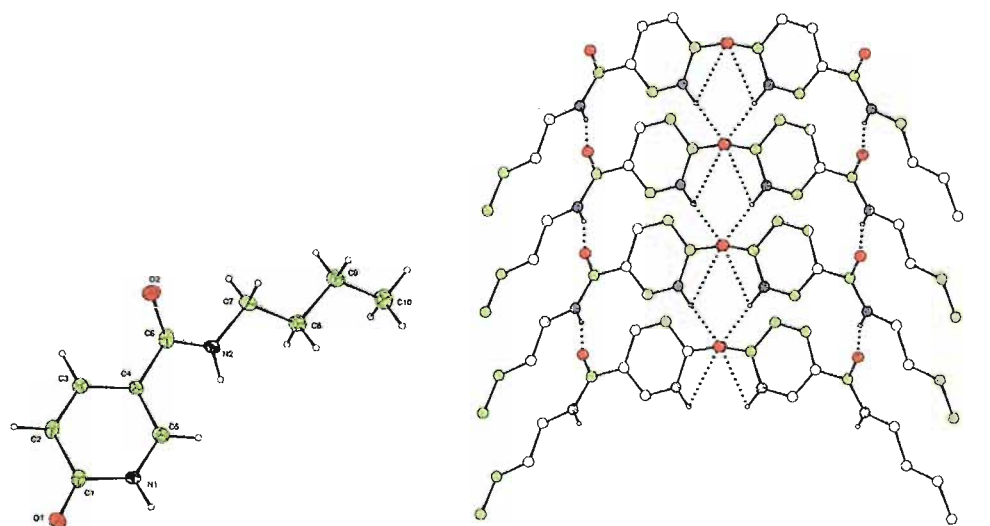
FIGURE 3.18: Platinum (II) complex of 2-hydroxypyridine. Intramolecular hydrogen bonds among the hydroxyl groups in the complex are observed in the solid state.

Compound **3.17(a)** is the basic skeleton from which to construct receptors with locked rotation, and taking inspiration from the work of Loeb and co-workers on platinum (II) nicotinamide complexes as anion receptors³⁶ we synthesized compound **3.17(b)** according to Scheme **3.3** in 17% yield. Unfortunately, attempts to crystallize this complex from many different solvent mixtures were not successful.

The ligand used in the synthesis of complex **3.17(b)** was prepared in a single step reaction by refluxing in butylamine the commercially available benzyl 6-hydroxynicotinate during four days, to afford the product as a white powder in 87% yield. Crystals were obtained by slow evaporation of the ligand in dichloromethane/methanol solutions (Figure **3.19**). Remarkably, this compound crystallizes in the resonant form of *N*-butyl-6-oxo-1,6-dihydropyridine-3-carboxamide. We believe that this resonant form is predominant

SCHEME 3.3: Path followed in the synthesis of **3.17(b)**.

in solution and is one reason of the low yield obtained in the synthesis of compound **3.17(b)**.

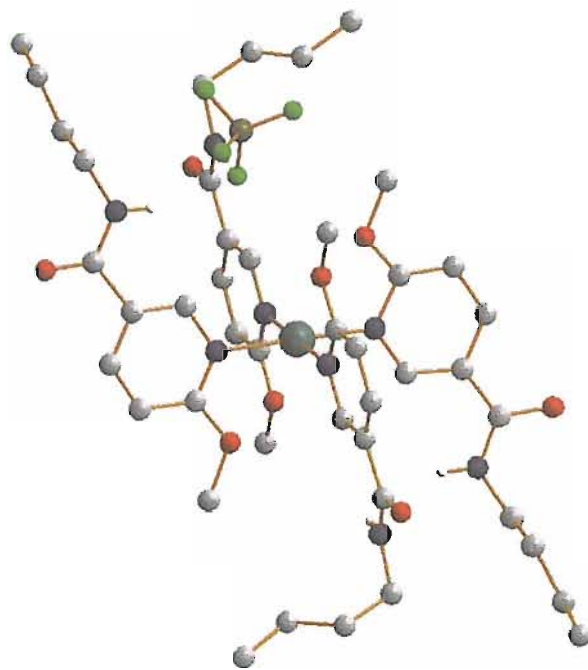


(a) Crystal structure of 2-hydroxypyridine. El- (b) View of the hydrogen bonded ladder sheet viewed down the *a* axis.

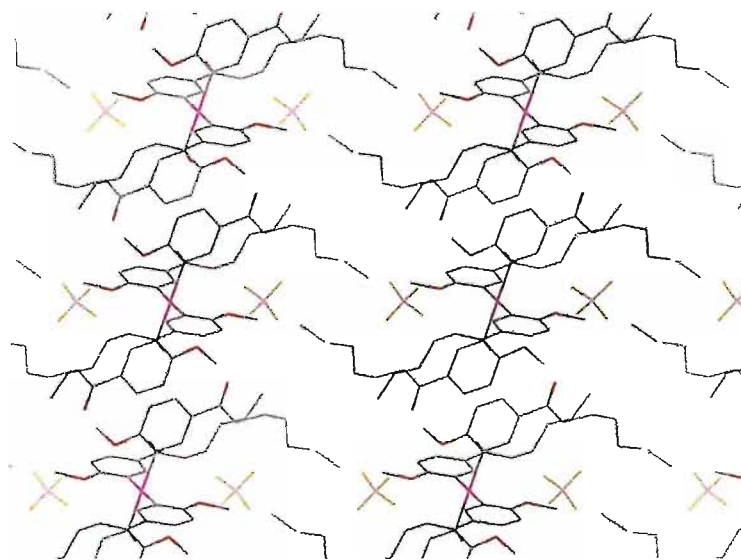
FIGURE 3.19: X-ray crystal structure of 2-hydroxypyridine.

N-butyl-6-methoxynicotinamide was synthesized by reacting 2-hydroxypyridine and iodomethane in the presence of Ag_2CO_3 with chloroform as reaction solvent, to afford methoxypyridine in up to 75% yield. The tetrafluoroborate platinum complex of these pyridine **3.17(c)** was prepared in analogous fashion to Scheme 3.3 in up to 20% yield.

Crystals of the platinum complex **3.17(c)** were obtained by slow evaporation of the complex from acetonitrile solutions (Figure 3.20). The X-ray crystal structure of **3.17(c)** shows that BF_4^- lies above and below the metal center of the 1,2-alternate conformation complex, and is hydrogen bonded by two of the amide groups from the pyridine ligands.



(a) Complex adopts 1,2-alternate conformation in the solid state.



(b) View down the *b* axis.

FIGURE 3.20: A ball-and-stick representation of the X-ray crystal structure of **3.17(c)** crystallized from acetonitrile.

3.2.2 Binding studies results

Proton NMR titration techniques have been used in order to investigate the anion binding properties of receptors **3.17(b)** and **3.17(c)**. Anions were added as their tetrabutylammonium salts, since this cation does not compete significantly with the anion binding site and therefore is considered a relatively ‘innocent’ counterion. Elaboration of the titration curves has been achieved by using WinEQNMR software.⁶⁹

The anion complexation properties of receptors **3.17(b)** and **3.17(c)** have been investigated in DMSO-*d*₆ solution.

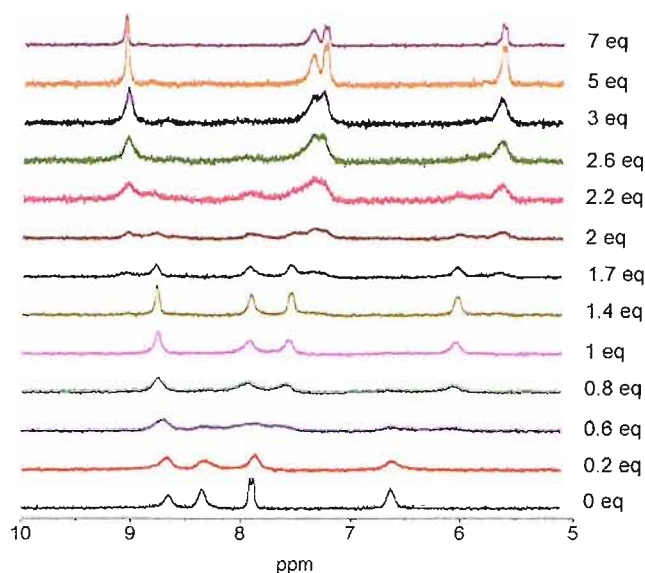


FIGURE 3.21: ¹H NMR stack plot titration curves of compound **3.17(b)** and tetrabutylammonium acetate.

¹H NMR titration experiments revealed the interesting anion complexation properties of **3.17(b)**. A strong selectivity for benzoate and acetate over other anions such as chloride, bromide and iodide was observed. Unfortunately precipitation and crystallization processes during the titration experiments with dihydrogen phosphate and compound **3.17(b)** in DMSO solution did not allow any quantitative anion binding investigation for this receptor, although interaction was detected. Other oxo-anions such as hydrogen-sulfate and methanesulfonate show no interaction with **3.17(b)**. Tetrabutylammonium sulfate^{xiv} was the only dinegative anion studied, and a strong interaction was observed.

Analysis of the ¹H NMR stack plot titration curves of compound **3.17(b)** and tetrabutylammonium acetate shows an unexpected binding behavior (see Figure 3.21). The NH amide signal is the only peak that shifts downfield during the titration experiment ($\Delta\delta = 0.42$ ppm). Upon addition of 1.4 equivalents of acetate, NH amide signal fades

^{xiv}A commercially available water solution of tetrabutylammonium sulfate taken to dryness was the source of anion for the ¹H NMR titration.

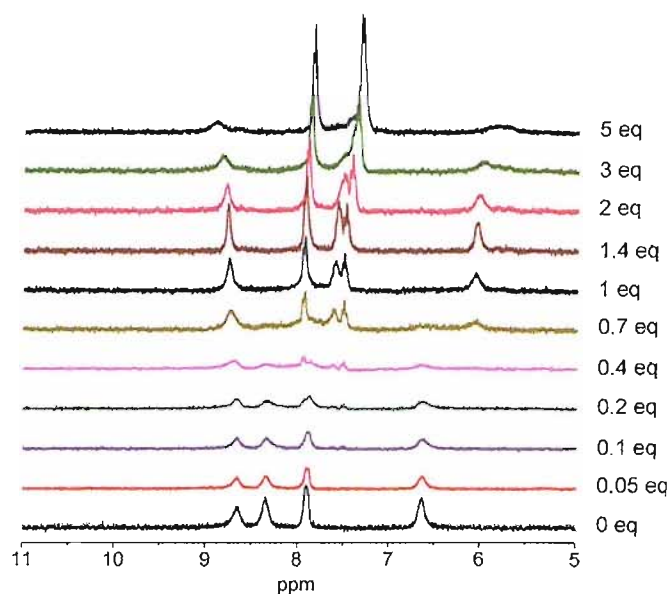


FIGURE 3.22: ^1H NMR stack plot titration curves of compound **3.17(b)** and tetrabutylammonium benzoate.

out and simultaneously a new NH amide signal emerges further downfield. On the other hand all the pyridine signals undergo an upfield shift, suggesting no hydrogen bond interaction. Noteworthy points of the titration are those at 0.6, 1.7, and 2 equivalents where peak signals fading and emerging co-exist. The lack of a signal shifting downfield during all the titration, prevented us from getting any binding constant. Furthermore, the upfield shift of the CH at 2-position of the pyridine suggest no hydrogen bond interaction with this part of the molecule, and probably an absence of relevance in this case of the metal-anion interaction.

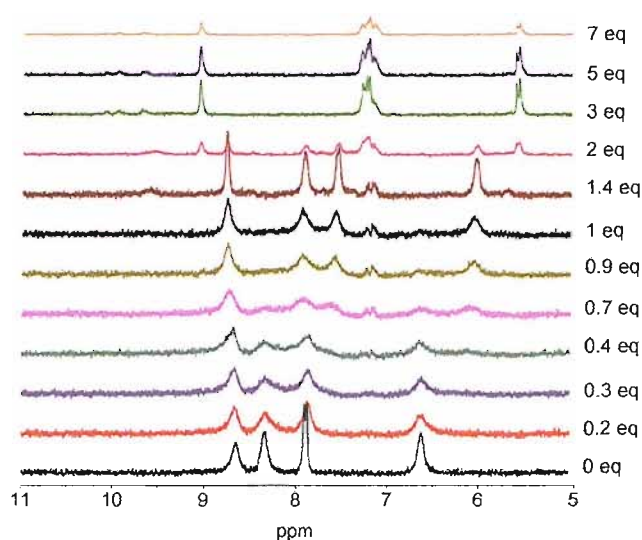
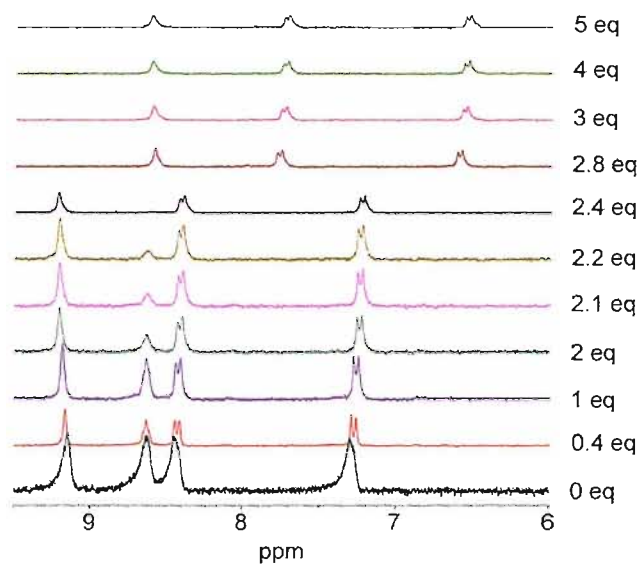
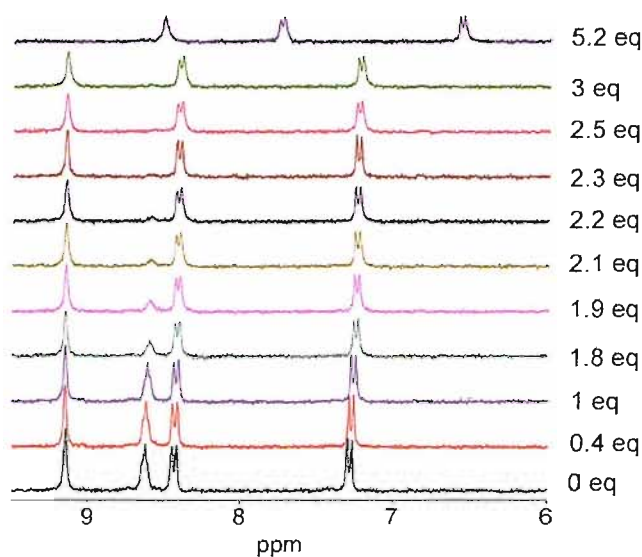


FIGURE 3.23: ^1H NMR stack plot titration curves of compound **3.17(b)** and tetrabutylammonium sulfate.

Similar behavior to that exhibited during the titration of compound **3.17(b)** and acetate was observed with benzoate (see Figure 3.22). In this case NH amide downfield shift was $\Delta\delta = 0.28$ ppm. As before it was not possible to obtain a valid binding constant for this anion.



(a) **3.17(c)** vs. Br⁻



(b) **3.17(c)** vs. I⁻

FIGURE 3.24: ¹H NMR stack plot titrations of compound **3.17(c)**.

¹H NMR titration of compound **3.17(b)** and sulfate exhibit the same interaction pattern than that obtained for acetate, and shows a downfield shift of the proton NH amide of $\Delta\delta = 0.43$ ppm (see Figure 3.23). During this titration all the pyridine proton signals shift upfield and a progressive fading of the peaks is observed. After 0.7 equivalents of

anion added it can be clearly observed some peaks almost disappearing and some new peaks replacing them further upfield. The same behavior occurs after two equivalent of anion added. The last part of this titration is not affected by the addition of further aliquots of anion, and no shift is observed for any peak.

More interesting results came from NMR experiments carried out on compound **3.17(c)** in DMSO- d_6 solution. Upon addition of aliquots of both bromide and iodide anions to solutions of this receptor, broadening of the signal of the CH pyridine at 2-position, and at some point disappearance of this signal is observed (see Figure **3.24**). Upon addition of more equivalents of anion it takes place an overall upfield shift of the remaining peaks that did not shift during the first stages of the titration.

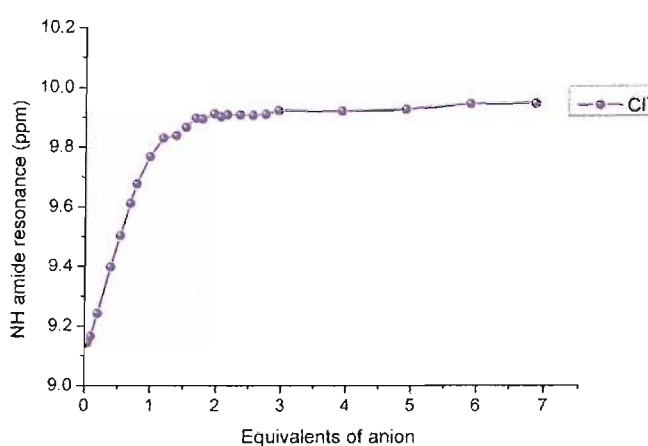
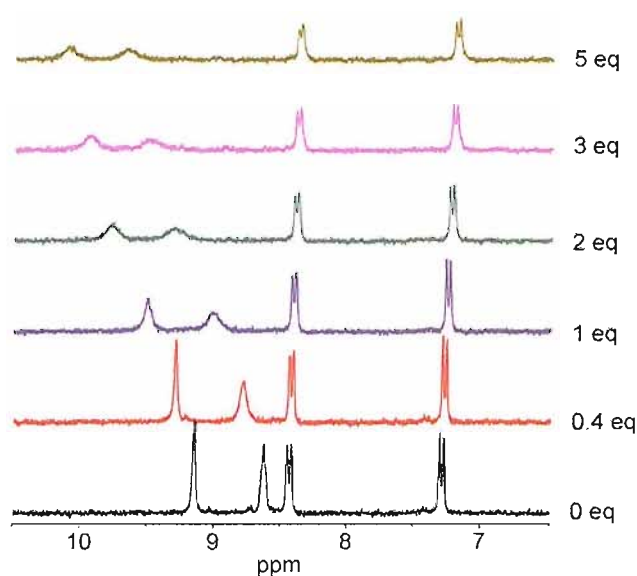


FIGURE 3.25: ^1H NMR stack plot titrations of compound **3.17(c)**.

Addition of either chloride, acetate or benzoate to a DMSO- d_6 solution of **3.17(c)** did

cause shift of the amide NH resonance and the CH pyridine at 2-position. Titration with chloride was fitted to a 1:1 receptor:anion model with a $K_a = 1680 \text{ M}^{-1}$ (Figure 3.25(b)), but broadening of the NH and CH peaks prevented us from getting any binding constant for acetate and benzoate.^{xv}

3.3 Conclusions

Anion complexation studies have been carried out on the platinum II complexes 3.1(a), 3.1(b), 3.1(c), 3.17(b), and 3.17(c) in order to investigate whether these compounds could behave as efficient receptors toward oxo and halide anions. ¹H NMR titration techniques have been used to obtain the stability constant and to determine the stoichiometry of the host/guest complex. Although determination of the stability constants could not be achieved in all cases, the NMR experiments proved to be useful in elucidating the processes occurring in solution. The influence of the solvent on the anion binding properties of these complexes was pointed out by the change of behavior of complex 3.1(b) in DMSO-*d*₆ and nitromethane-*d*₃. Another important fact in these complexes, is the role the CH protons play in binding anions. Some very simple complex such as 3.1(a), which can hydrogen bond only with CH protons, showed shifts up to 0.5 ppm at the CH proton at 2-position. Unusual titration behavior have been obtained with compounds 3.17(b) and 3.17(c). These complexes showed selectivity towards oxo-anions, although no binding constant was measured due to peak broadening. Moreover X-ray crystallographic analysis always revealed the presence of the counteranion hydrogen bonded by the ligands and electrostatically interacting with the metal center.

^{xv}Titration of acetate and benzoate with 3.17(c) generate the same kind of titration stack plot than chloride (Figure 3.25(a)), although the NH and CH at 2-position signals became wider and disappeared in the case of acetate.

Chapter 4

Hydrogen bond formation in metal-organic anion receptors containing quinolineamidopyrrole and pyridineamidopyrrole ligands

Selective synthetic receptors for the sulfate anion are relatively rare.¹⁷ Pflugrath and Quioco's crystal structure of sulfate bound within the sulfate binding protein revealed that nature uses seven hydrogen bonds from neutral donor groups to selectively complex the anion within the protein (see Figure 1.11 in Section 1.2).¹³ Synthetic receptors for anions frequently incorporate a combination of:

- i) hydrogen bond donor groups,
- ii) a positively charged component for effective electrostatic interactions,
- iii) a suitable framework onto which these structural components can be assembled.

Strategies to bind sulfate have followed these general principles and have involved the formation of multiple hydrogen bonds between the anion and receptor, resulting in strong complexation either by neutral receptors or by receptors that employ hydrogen bonds in combination with electrostatic interactions.^{105–109} Other approaches have included binding sulfate as a component of a transition metal sulfate ion pair.¹¹⁰ Loeb and co-workers reported the anion binding properties of platinum(II) tetranicotinamide receptors and introduced a loose analogy between these receptors and the calix[4]arenes in that both classes of receptor are capable of adopting similar “cone”, “partial cone”, “1,2-alternate”, or “1,3-alternate” conformations.³⁶ Unfortunately, in these first-generation systems, rotation around the platinum-pyridine bond was fast on the NMR time scale, even

in the presence of an anionic guest, and therefore the conformation adopted in solution could not be determined unambiguously. Loeb and co-workers reported a new metal-organic anion receptor containing urea functionalized isoquinoline ligands that exhibits remarkably strong binding of sulfate by completely encapsulating the anion in a “cone” conformation in both solution and the solid state (see Figure 1.16 in Section 1.3.1.1).³⁸

4.1 (isoquinoline & pyridinylmethyl) pyrrole carboxamide platinum II receptors

The results reported by Loeb and co-workers on pyridine platinum (II) complexes,^{36,37} and particularly on isoquinoline platinum (II) receptor,³⁸ as well as the well known anion binding properties of the amidopyrrole moiety (see Chapter 2), inspired us to synthesize and investigate the anion receptor properties of some novel isoquinolinepyrrole carboxamide platinum II receptors.

Compound 4.1(a) offers the putative anionic guest a choice of hydrogen bond donor (NH amide, NH pyrrole, or CH) as the amidopyrrole is free to rotate around the pyrrolepyridine bond *without significantly changing the shape of the binding site* due to the rigidity of the isoquinoline frame. On the other hand, complex 4.1(b) offers the anionic guest an electrostatic interaction and the same hydrogen bond donors at the center of the complex arranged on a more flexible frame.

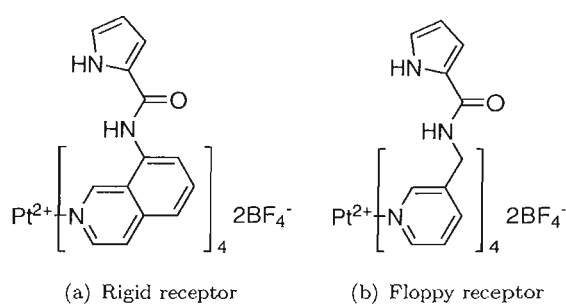


FIGURE 4.1: Series of platinum(II) pyrrole carboxamides salts prepared for anion complexation studies.

4.1.1 Synthesis and characterization

N-(isoquinolin-8-yl)-1*H*-pyrrole-2-carboxamide was synthesized in four reaction steps from isoquinolin-5-amine in an overall 8% yield (see Scheme 4.1).^{111,112} Unexpectedly, and as consequence of the condensation of two pyrrole carboxylic acid molecules with the isoquinoline-8-amine substrate, we isolated in 6% yield a fused racemic seven member

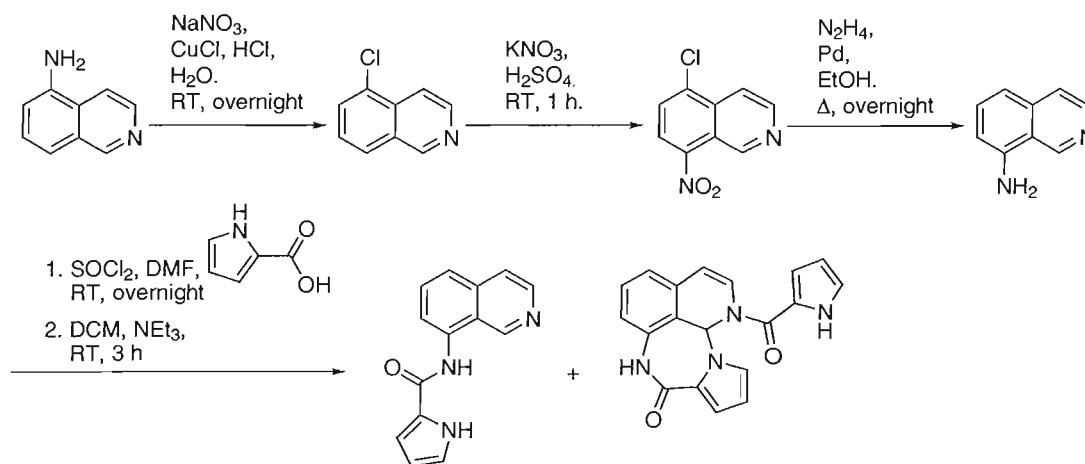
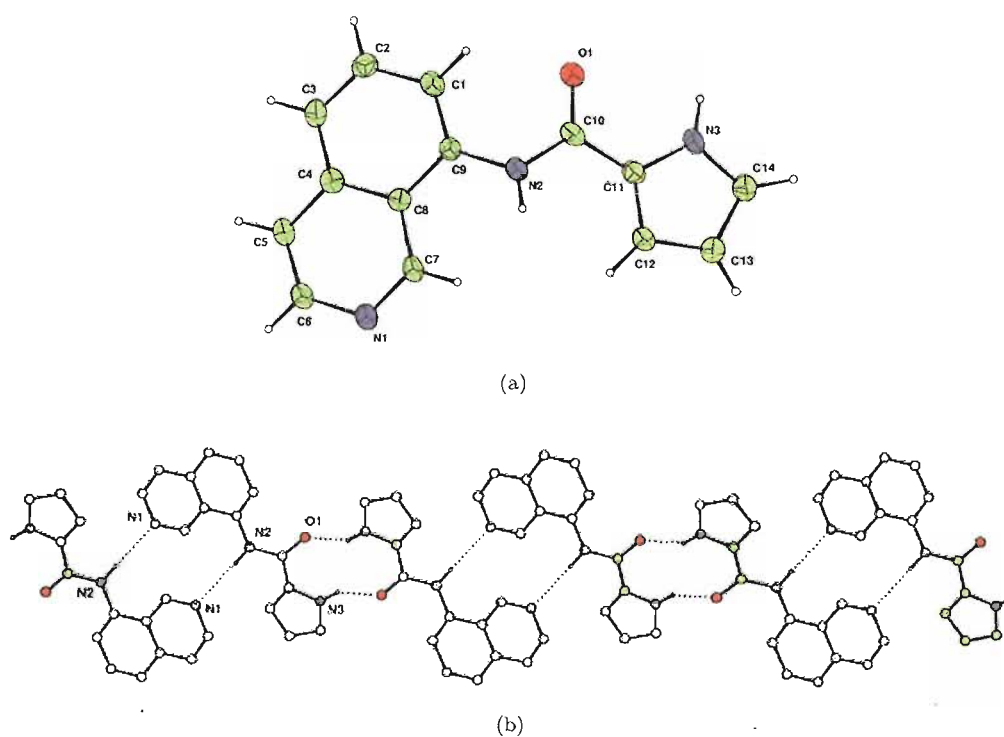
ring subproduct.^{xvi}SCHEME 4.1: Synthesis of the ligand *N*-(isoquinolin-8-yl)-1*H*-pyrrole-2-carboxamide.

FIGURE 4.2: (a) Thermal ellipsoids drawn at the 35% probability level, solvent omitted for clarity. (b) Part of a hydrogen bonded slab.

X-ray quality single crystals of *N*-(isoquinolin-8-yl)-1*H*-pyrrole-2-carboxamide have been obtained by slow evaporation of a dichloromethane/ethanol solution of this receptor (see Figure 4.2). The crystal structure reveals the formation of polymers bridged by intermolecular hydrogen bonds. Molecules link each other *via* NH...N amide...isoquinoline,

^{xvi}7,11a-diaza-1-(1*H*-pyrrole-2-carbonyl)-1*H*-azuleno[6,5,4-*ij*]isoquinolin-8(7*H*,11*aH*,11*bH*)-one

and $\text{NH}\cdots\text{OC}$ pyrrole \cdots carbonyl hydrogen bonds (including $\text{N1}\cdots\text{N2}$ 3.212(6); $\text{N3}\cdots\text{O1}$ 2.822(5) Å).

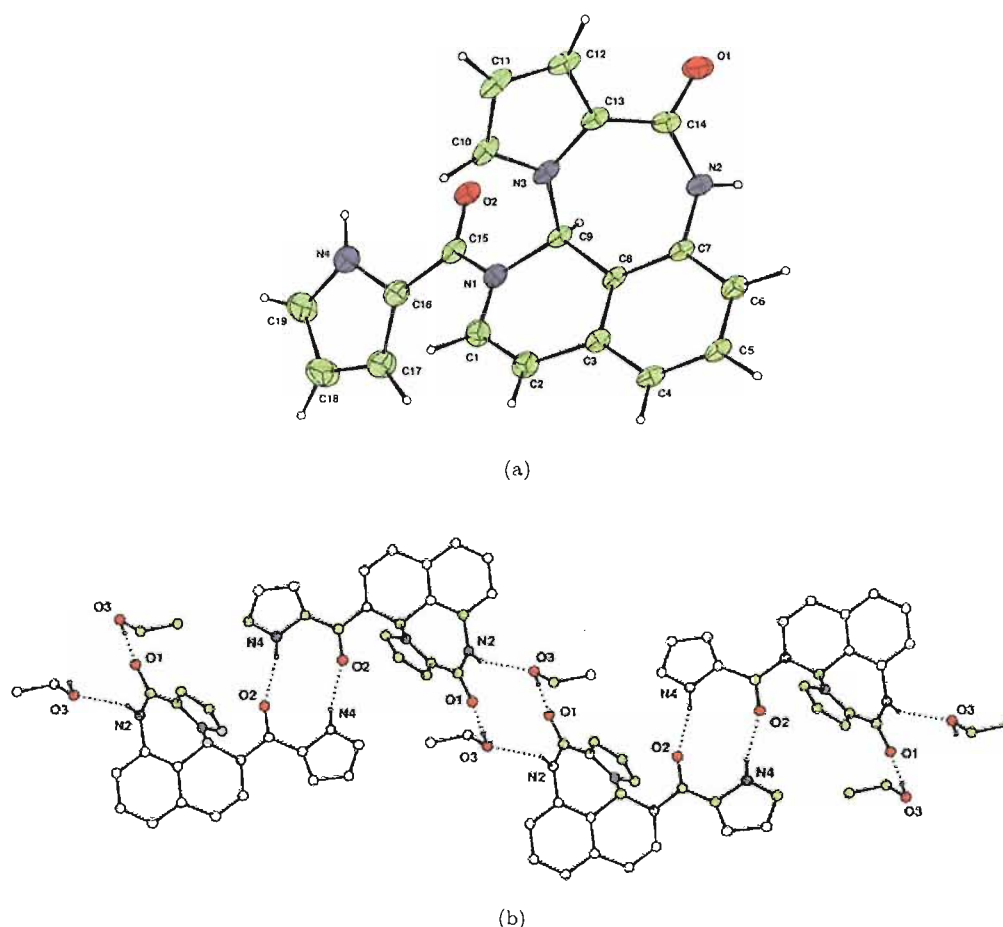
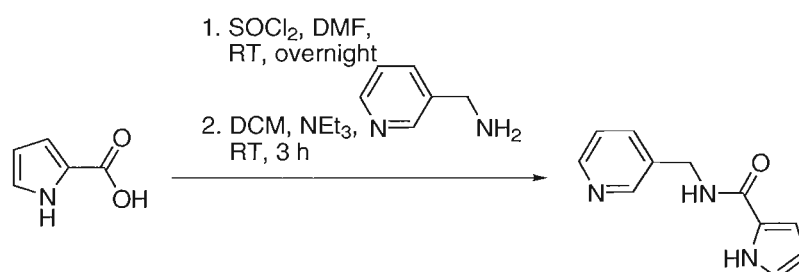
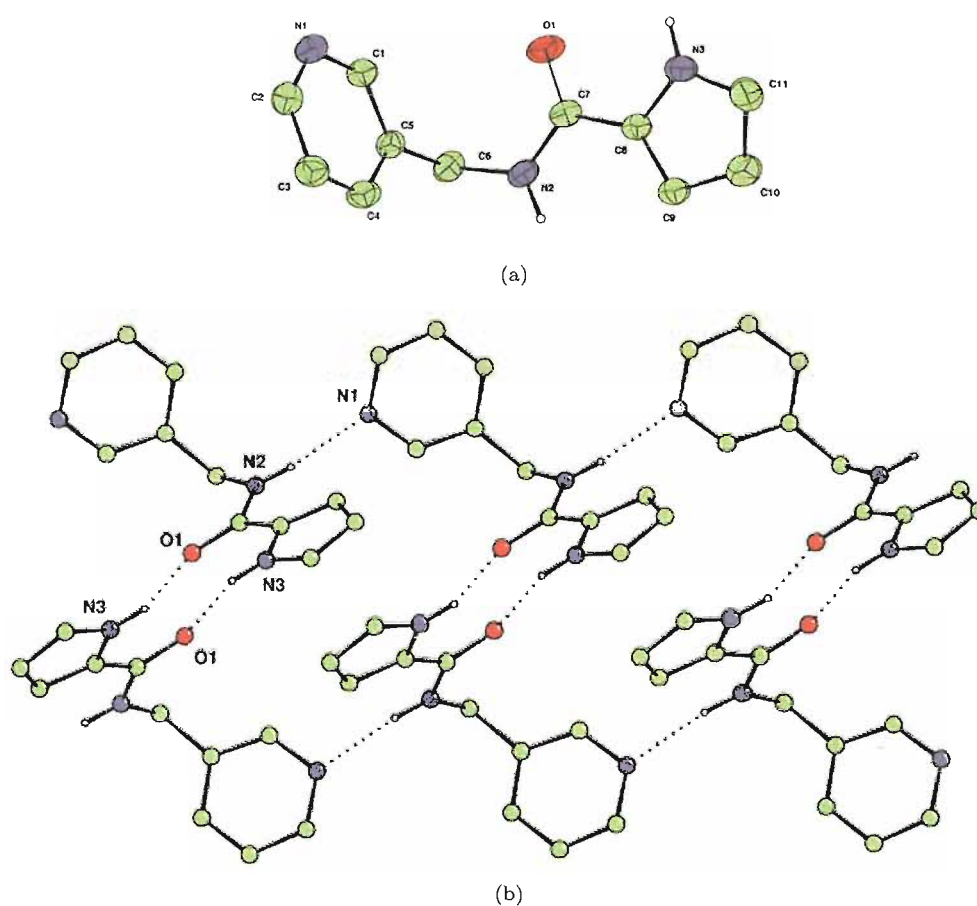


FIGURE 4.3: (a) Thermal ellipsoids drawn at the 35% probability level, solvent omitted for clarity. (b) Part of one of the chains of hydrogen bonded dimers linked *via* one of the solvent ethanols.

Crystals from the subproduct isolated from the double pyrrole carboxylic acid condensation were obtained by slow evaporation of an ethanol solution of this compound (see Figure 4.3). The structure shows that a dimer is formed *via* intermolecular $\text{NH}\cdots\text{OC}$ hydrogen bonds from two amidopyrrole moieties, and each dimer links to each other *via* $\text{NH}\cdots\text{OH}$ and $\text{OH}\cdots\text{OC}$ hydrogen bonds from the amide group at the seven membered ring and a couple of ethanol molecules.

N-((pyridin-3-yl)methyl)-1*H*-pyrrole-2-carboxamide was synthesized in single reaction step from pyridin-3-ylmethanamine in 23% yield (see Scheme 4.2). Single crystals of this ligand have been obtained by slow evaporation from a dichloromethane/methanol solution of this receptor. The crystal structure again revealed the formation of intermolecular hydrogen bonds linking each molecule *via* $\text{NH}\cdots\text{OC}$ pyrrole \cdots amide, and $\text{NH}\cdots\text{N}$ amide \cdots pyridine, hydrogen bonds (including $\text{N2}\cdots\text{N1}$ 2.986(2); $\text{N3}\cdots\text{O1}$ 2.834(2) Å).

SCHEME 4.2: Synthesis of the ligand *N*-(isoquinolin-8-yl)-1*H*-pyrrole-2-carboxamide.FIGURE 4.4: (a) Thermal ellipsoids drawn at the 35% probability level. (b) Slabs lie in the *ab* plane.

Receptors **4.1(a)** and **4.1(b)** were synthesized *via* literature procedures (Scheme **3.1**, Section **3.1.1**) in 64 and 67% yield respectively.^{36–38,95}

Unfortunately, no suitable crystals of **4.1(a)** nor of **4.1(b)** for X-ray characterization were obtained.^{xvii}

^{xvii}Receptors **4.1(a)** and **4.1(b)** were fully characterized by ^1H NMR, ^{13}C NMR, DEPT, H-H, and C-C correlation, and high resolution mass spectrum.

4.1.2 Binding studies results

The anion binding properties of complexes **4.1(a)** and **4.1(b)** were explored using ^1H NMR titration techniques in $\text{DMSO-}d_6$. Complex **4.1(a)** was titrated *vs.* a set

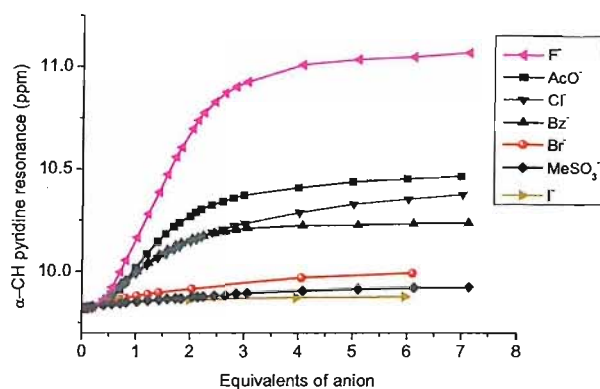


FIGURE 4.5: ^1H NMR titration curves for compound **4.1(a)** with fluoride, chloride, bromide, iodide, methanesulfonate, acetate, and benzoate in $\text{DMSO-}d_6$ at 298 K. Anions added as their tetrabutylammonium salts.

of putative anions (Figure 4.5), and despite containing two NH hydrogen bond donor groups, broadening of the NH ^1H NMR signals during the titration process,^{xviii} forced us to study the anion complexation properties of this receptor at the hydrogen on the 1-position of the isoquinoline ring (see Figure 4.6 and Table 4.1). In some cases, this

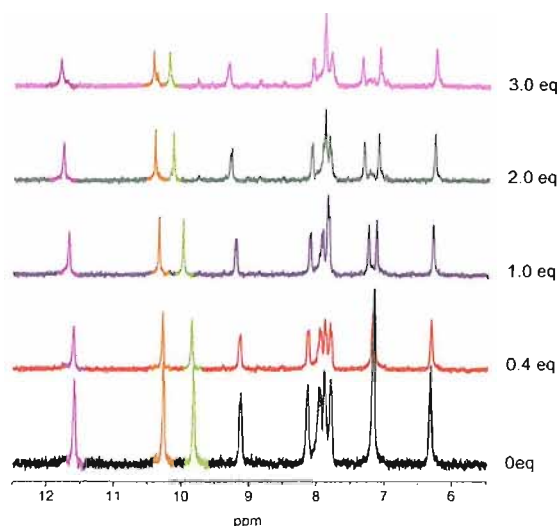


FIGURE 4.6: Proton NMR stack plot titration of compound **4.1(a)** in $\text{DMSO-}d_6$ with tetrabutylammonium chloride at 298 K showing a downfield shift of the isoquinoline CH proton in the 1-position (green), NH amide (brown), and NH pyrrole (violet).

^{xviii}Only Cl^- and Bz^- anions showed no broadening of the NH pyrrole and amide signals.

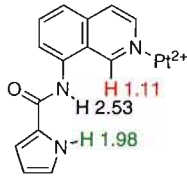
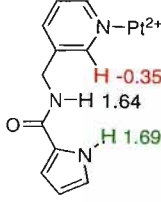
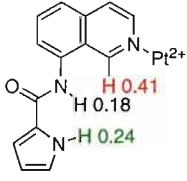
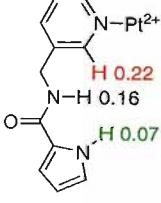
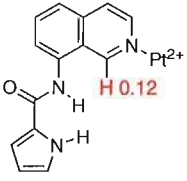
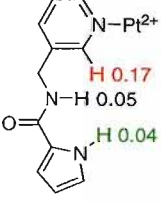
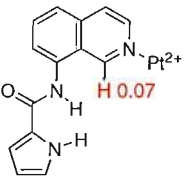
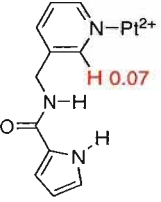
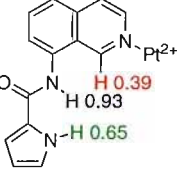
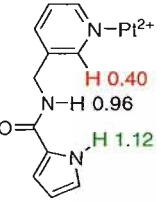
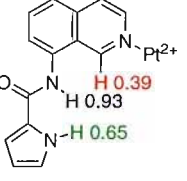
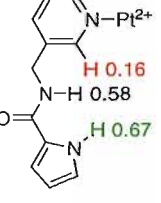
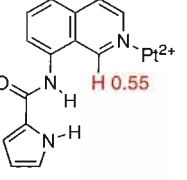
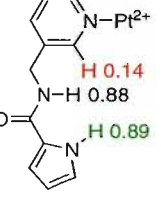
Anion	Compound 4.1(a)	Compound 4.1(b)
F ⁻		
Cl ⁻		
Br ⁻		
MeSO ₃ ⁻		
H ₂ PO ₄ ⁻		
PhCO ₂ ⁻		
MeCO ₂ ⁻		

TABLE 4.1: ¹H NMR chemical shifts upon addition of three equivalents of tetrabutylammonium anion salt to solutions of [4.1(a) and 4.1(b)]·(BF₄)₂ in DMSO-*d*₆.

data could be fitted to a 1:1 receptor:anion binding model with the results shown in Table 4.2. However, the possibility exists that a second anion may associate with the 1:1 complex with a low K_2 that has not been detected in this experiment. This is true of all the ^1H NMR titration experiments reported in this section.

Anion ^a	Compound 4.1(a) ^b	Compound 4.1(b) ^b
F ⁻	<i>c</i>	<i>c</i>
Cl ⁻	225	140
Br ⁻	178	35
I ⁻	-	18
AcO ⁻	<i>c</i>	118
PhCO ₂ ⁻	793	245
MeSO ₃ ⁻	77	32
HSO ₄ ⁻	-	31
H ₂ PO ₄ ⁻	<i>d</i>	118

^aAdded as tetrabutylammonium salt.

^bErrors estimated to be no more than 15%.

^cInteraction observed but no fit.

^dBroadening of ^1H NMR peaks.

TABLE 4.2: Stability constants of the salts 4.1(a) and 4.1(b) with anionic guests in DMSO-*d*₆ at 298 K calculated from the shift of the resonance of the isoquinoline and pyridine hydrogen in the 2-position assuming 1:1 stoichiometry in all cases.

The overall largest shifts appear during the titration of 4.1(a) and fluoride, where NH amide shifts of up to 2.53 ppm, NH pyrrole 1.98 ppm, and CH isoquinoline at 1-position 1.11 ppm. The same behavior is observed when titrated with benzoate, although lower shifts are observed. The chloride titration shows an inverted trend on the proton shift, and the larger shift is on the CH isoquinoline, while the NH amide undergo the lower shift change. Other less basic anions such as methanesulfonate, and bromide hydrogen bond weakly only with the CH isoquinoline at 1-position.

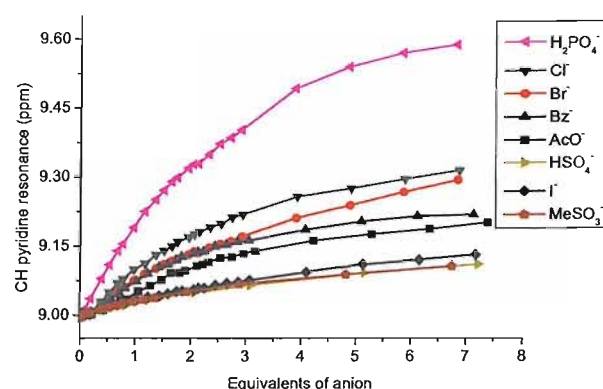


FIGURE 4.7: ^1H NMR titration curves for compound 4.1(b) with fluoride, chloride, bromide, iodide, methanesulfonate, acetate, benzoate, and dihydrogenphosphate in DMSO-*d*₆ at 298 K. Anions added as their tetrabutylammonium salts.

Compound **4.1(b)** offers the same array of hydrogen bond donors than complex **4.1(a)**, but arranged on a floppy scaffold. We expect therefore a less selective anion receptor (see Table **4.2**). However, this complex interacts with all the anions titrated (see Figure **4.7**, and Table **4.1**), and the reason is, its flexibility to adopt the required shape that fits with each anion. The strongest intereaction of this complex was observed with

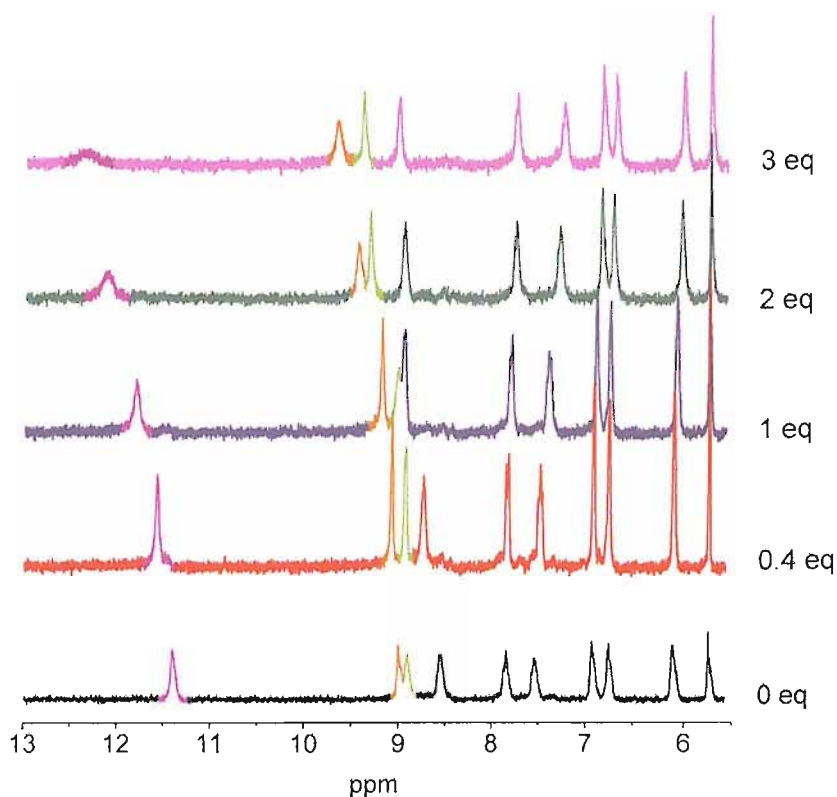


FIGURE 4.8: Proton NMR stack plot titration of compound **4.1(b)** in DMSO- d_6 with tetrabutylammonium dihydrogenphosphate at 298 K showing a downfield shift of the pyridine CH proton in the 2-position (green), NH amide (brown), and NH pyrrole (violet).

oxo-anions. Specially relevant is the interaction with dihydrogen phosphate, were in most of the occasions precipitation processes takes place with platinum complexes (see Figure **4.8**).^{36,37,113}

4.2 Conclusions

Two new platinum complexes were synthesized and their anion complexation properties elucidated by ^1H NMR titration techniques. We found that the rigid version of this receptor binds more selectively anions and with higher binding constants. This is the first attempt of combining a platinum (II) complex with an amidopyrrole moiety to prepare an anion receptor and the binding properties detected are in the range expected. There

are still many aspects to investigate into this new family of receptors and we believe that this research line will be of interest for many other researchers in this field of the *anion recognition*.

Chapter 5

Experimental

5.1 Solvent and reagent pre-treatment

Where necessary solvents were purified prior to use. Dichloromethane was distilled over calcium hydride. Toulene was distilled from sodium. Tetrahydrofuran and diethyl ether were distilled from sodium using benzophenone as an indicator. Anhydrous acetonitrile (water < 0.003%) was acquired from Fluka. Triethylamine was distilled from KOH and stored under nitrogen in the presence of an excess of KOH pellets. Thionyl chloride was distilled from 10% (*w/w*) triphenyl phosphite and stored under nitrogen. Unless otherwise stated on the text, commercial grade chemicals were used without further purification. Reagents prepared in accordance with literature are so referenced. All the synthesis have been performed under nitrogen.

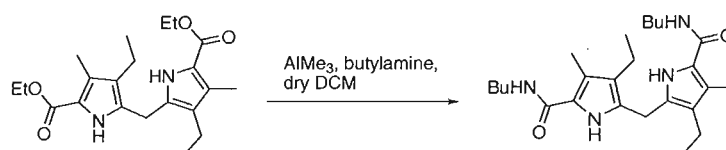
5.2 Instrumental methods

NMR spectra were recorded on Bruker AM300, AC300 and DPX400 spectrometers. Operating frequency have been used of 300 MHz for proton analyses, 75 MHz for ^{13}C analyses, 161 MHz for ^{31}P (referenced to H_3PO_4). Low resolution mass spectra were recorded on Micromass Platform single quadrupole mass spectrometer (in acetonitrile), whereas high resolution mass spectra were performed on VG 70-SE Normal geometry double focusing mass spectrometer (in acetonitrile) by the Mass Spectrometry service at the University of Southampton. Elemental analyses were carried out by Medac Ltd. Melting points were recorded in open capillaries on a Gallenkamp melting point apparatus and are uncorrected. Proton NMR titrations have been carried out by addition of discrete aliquots of a 0.1 M solution of the anion (as the tetrabutylammonium salt)

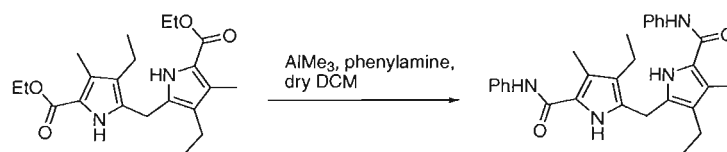
to a 0.01 M solution of the considered receptor in deuterated solvent. Elaboration of the observed data by using an appropriate software (e.g. WinEQNMR)⁶⁹ allowed the calculation of the stability constant.

5.3 Synthesis

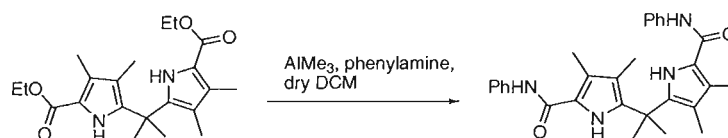
5.3.1 Syntheses included in chapter 2



Bis-*N*-butylamide-5,5'-methylenebis(4-ethyl-3-methyl-2-pyrrolecarboxylate) 2.4(a). Butylamine (1.14 g, 15.54 mmol, 6.0 eq) was dissolved in freshly distilled dichloromethane (26 ml), and a 2 M solution of AlMe₃ in hexanes (7.78 ml, 15.54 mmol, 6.0 eq) was added dropwise. After stirring for 30 min, a solution of diethyl-5,5'-methylenebis(4-ethyl-3-methyl-2-pyrrole carboxylate) (1 g, 2.67 mmol, 1.0 eq) in freshly distilled dichloromethane (10 ml) was added and the reaction mixture was stirred at 35°C during 3 days. The reaction was carefully quenched with dilute 0.7 M HCl (100 ml), and extracted with dichloromethane (2 × 40 ml). The organic phases were combined and dried together over MgSO₄ and filtered. The volatiles were removed in vacuo and the solid obtained was purified by gradient column chromatography on silica gel with dichloromethane-dichloromethane/2% methanol affording the desired compound (0.48 g, 43%). Suitable crystals for X-ray studies were obtained by slow evaporation of a solution of this product from dichloromethane/methanol solutions. Mp 189–190°C. R_f [DCM:MeOH 96.5:3.5] = 0.1. ¹H NMR 300 MHz in DMSO-*d*₆ δ (ppm): 0.86 (m, 12H, CH₃), 1.30 (tq, *J* (7.3, 6.7), 4H, CH₂), 1.46 (tt, *J* (7.2, 7.3), 4H, CH₂), 2.13 (s, 6H, CH₃), 2.27 (q, *J* 7.2, 4H, CH₂), 3.19 (dt, *J* (5.4, 7.2), 4H, CH₂), 3.72 (s, 2H, CH₂), 7.11 (t, *J* 5.4, 2H, NH), 10.56 (s, 2H, NH). ¹³C NMR 75.4 MHz in DMSO-*d*₆ δ (ppm): 10.4 (CH₃), 13.8 (CH₂), 15.7 (CH₃), 16.8 (CH₂), 19.7 (CH₃), 22.2 (CH₂), 31.7 (CH₂), 38.2 (CH₂), 120.1 (C), 120.9 (C), 121.5 (C), 127.5 (C), 161.6 (C). ES⁺ mass spectrum, *m/z*, 451.3 (M + Na)⁺. HRES⁺ mass spectrum, *m/z* calculated: 429.3224 (M + Na)⁺, *m/z* found: 429.3234 (Δ 1.8 ppm). Anal. Found for C₂₅H₄₀N₄O₂ + $\frac{1}{2}$ MeOH (Calc.): C, 68.75 (68.88); H, 9.53 (9.52); N, 12.72 (12.60). Crystal data: C_{25.17}H_{40.50}N_{4.17}O_{2.33}, M = 438.78, T = 120(2) K, Triclinic, Space group *P* 1, a = 13.0112(9) Å, b = 17.310(3) Å, c = 17.729(4) Å, α = 88.460(14)°, β = 81.647(10)°, γ = 88.021(10)°, V = 3947.3(11) Å³, Z = 6 (3 molecules in the asymmetric unit), Reflections collected; 66535, Independent reflections; 11332 [*R*_{int} = 0.0701], Final R indices [*F*² > 2 σ *F*²]: *R*1 = 0.0904, *wR*2 = 0.2491, R indices (all data): *R*1 = 0.1121, *wR*2 = 0.2694.

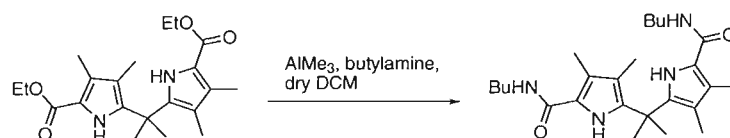


Bis-*N*-phenylamide-5,5'-methylene bis(4-ethyl-3-methyl-2-pyrrolecarboxylate) 2.4(b). Aniline (1.45 g, 15.54 mmol, 6.0 eq) was dissolved in freshly distilled dichloromethane (26 ml), and a 2 M solution of AlMe₃ in hexanes (7.78 ml, 15.54 mmol, 6.0 eq) was added dropwise. After stirring for 30 min, a solution of diethyl-5,5'-methylenebis(4-ethyl-3-methyl-2-pyrrole carboxylate) (1.0 g, 2.67 mmol, 1.0 eq) in freshly distilled dichloromethane (10 ml) was added and the reaction mixture was stirred at 35°C during 3 days. The reaction was carefully quenched with dilute 0.7 M HCl (100 ml), and extracted with dichloromethane (2 × 40 ml). The organic phases were combined and dried together over MgSO₄ and filtered. The volatiles were removed in vacuo and the solid obtained was purified by gradient column chromatography on silica gel with dichloromethane-dichloromethane/2% methanol affording the desired compound (0.48 g, 40%). Suitable crystals for X-ray studies were obtained by slow evaporation of a solution of this product from dichloromethane/methanol mixtures. Mp 257–259°C. R_f _[DCM:MeOH, 98:2] = 0.06. ¹H NMR 300 MHz in DMSO-*d*₆ δ (ppm): 0.89 (t, *J* 7.3, 6H, CH₃), 2.23 (s, 6H, CH₃), 2.33 (q, *J* 7.3, 4H, CH₂), 3.86 (s, 2H, CH₂), 7.02 (t, *J* 7.4, 2H, ArH), 7.30 (t, *J* 7.7, 4H, ArH), 7.64 (d, *J* 8.2, 4H, ArH), 9.26 (s, 2H, NH), 10.90 (s, 2H, NH). ¹³C NMR 75.4 MHz in DMSO-*d*₆ δ (ppm): 10.4 (CH₃), 15.5 (CH₂), 16.7 (CH₃), 22.6 (CH₂), 119.7 (C), 120.6 (CH), 122.4 (C), 122.8 (CH), 123.0 (C), 128.4 (CH), 128.6 (C), 139.5 (C), 159.9 (C). ES⁺ mass spectrum, *m/z*, 491.4 (M + Na)⁺. HRES⁺ mass spectrum, *m/z* calculated: 491.2417 (M + Na)⁺, *m/z* found: 491.2412 (Δ 1.0 ppm). Anal. Found for C₂₉H₃₂N₄O₂ + MeOH (Calc.): C, 72.14 (71.97); H, 6.93 (7.25); N, 10.92 (11.19). Crystal data: C₃₀H₃₆N₄O₃, M = 500.63, T = 120(2) K, Orthorhombic, Space group P212121, a = 11.1668(3) Å, b = 11.7777(3) Å, c = 20.3200(6) Å, V = 2672.47(13) Å³, Z = 4, Reflections collected: 32775, Independent reflections: 4702 [R_{int} = 0.1689], Final R indices [$F^2 > 2\sigma(F^2)$]: *R*1 = 0.0765, *wR*2 = 0.1793, R indices (all data): *R*1 = 0.1061, *wR*2 = 0.1945.



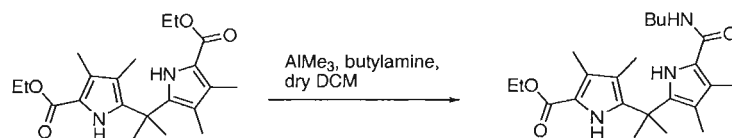
5-(2-(5-(phenylcarbamoyl)-3,4-dimethyl-1H-pyrrol-2-yl)propan-2-yl)-3,4-dimethyl-1H-pyrrole-2-carboxamide 2.11(a). Aniline (2.80 g, 30.10 mmol, 7.0 eq) was dissolved in freshly distilled dichloromethane (50 ml), and a 2 M solution of AlMe₃ in hexanes (15.05 ml, 30.10 mmol, 7.0 eq) was added dropwise. After stirring for 30 min, a solution of ethyl 5-(2-(5-(ethoxycarbonyl)-3,4-dimethyl-1H-pyrrol-2-

yl)propan-2-yl)-3,4-di-methyl-1*H*-pyrrole-2-carboxylate (1.61 g, 4.30 mmol, 1.0 eq) in freshly distilled dichloromethane (20 ml) was added and the reaction mixture was stirred at 35°C during 3 days. The reaction was carefully quenched with dilute 0.7 M HCl (100 ml), and extracted with dichloromethane (2 × 70 ml). The organic phases were combined and dried together over MgSO₄ and filtered. The volatiles were removed in vacuo and the solid obtained was purified by gradient column chromatography on silica gel with dichloromethane-dichloromethane/2% methanol affording the desired compound (0.64 g, 32%). Suitable crystals for X-ray studies were obtained by slow evaporation of a solution of this product from dichloromethane/methanol mixtures. Mp 145–146°C. R_f _[DCM:MeOH 96:4] = 0.34. ¹H NMR 300 MHz in DMSO-*d*₆ δ (ppm): 1.43 (s, 6H, CH₃), 1.70 (s, 6H, CH₃), 2.19 (s, 6H, CH₃), 7.04 (t, *J* 7.3, 2H, ArH), 7.33 (dd, *J* (7.3, 8.2), 4H, ArH), 7.66(d, *J* 8.2, 4H, ArH), 9.58 (s, 2H, NH), 10.31 (s, 2H, NH). ¹³C NMR 75.4 MHz in DMSO-*d*₆ δ (ppm): 8.7 (CH₃), 10.6 (CH₃), 27.8 (CH₃), 35.8 (C), 115.3 (C), 118.6 (C), 120.0 (CH), 122.8 (CH), 126.3 (C), 128.6 (CH), 136.9 (C), 139.4 (C), 159.5 (CO). ES⁺ mass spectrum, *m/z*, 469.3 (M + H)⁺. HRES⁺ mass spectrum, *m/z* calculated: 469.2598 (M + H)⁺, *m/z* found: 469.2590 (Δ 1.7 ppm). Anal. Found for C₂₉H₃₂N₄O₂ + $\frac{1}{2}$ MeOH (Calc.): C, 72.85 (73.11); H, 6.91 (7.07); N, 11.24 (11.56). Crystal data: C₃₀H₃₆N₄O₃, M = 500.63, T = 120(2) K, Orthorhombic, Space group *P*212121, a = 11.1668(3) Å, b = 11.7777(3) Å, c = 20.3200(6) Å, V = 2672.47(13) Å³, Z = 4, Reflections collected: 32775, Independent reflections: 4702 [*R*_{int} = 0.1689], Final R indices [*F*² > 2 σ (*F*²): *R*1 = 0.0765, *wR*2 = 0.1793, R indices (all data): *R*1 = 0.1061, *wR*2 = 0.1945.



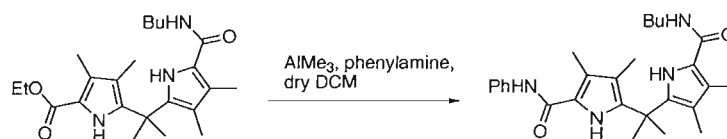
5-(2-(5-(butylcarbamoyl)-3,4-dimethyl-1*H*-pyrrol-2-yl)propan-2-yl)-3,4-dimethyl-*N*-butyl-1*H*-pyrrole-2-carboxamide **2.11(b)**. Butylamine (1.37 g, 18.69 mmol, 7.0 eq) was dissolved in freshly distilled dichloromethane (35 ml), and a 2 M solution of AlMe₃ in hexanes (9.35 ml, 18.69 mmol, 7.0 eq) was added dropwise. After stirring for 30 min, a solution of ethyl 5-(2-(5-(ethoxycarbonyl)-3,4-dimethyl-1*H*-pyrrol-2-yl)propan-2-yl)-3,4-dimethyl-1*H*-pyrrole-2-carboxylate (1.00 g, 2.67 mmol, 7.0 eq) in freshly distilled dichloromethane (13 ml) was added and the reaction mixture was stirred at 35°C during 4 days. The reaction was carefully quenched with dilute 0.7 M HCl (100 ml), and extracted with dichloromethane (2 times 50 ml). The organic phases were combined and dried together over MgSO₄ and filtered. The volatiles were removed in vacuo and the solid obtained was purified by gradient column chromatography on silica gel with petroleum ether/10% ethyl acetate, petroleum ether/20% ethyl acetate, and petroleum ether/40% ethyl acetate affording the desired compound (0.13 g, 11%). Compound **2.11(c)** was isolated as secondary product (214.4 mg, 20%). Suitable crystals

for X-ray studies were obtained by slow evaporation of a solution of this product in a mixture of acetonitrile/methanol. Mp 137–138°C. R_f _[AcOEt:petroleum ether 80:20] = 0.33. ¹H NMR 300 MHz in CDCl₃ δ (ppm): 0.96 (t, *J* 5.5, 6H, CH₃), 1.40 (tq, *J* (5.5, 3.4), 4H, CH₂), 1.55 (s, 6H, CH₃), 1.57 (tt, *J* (5.3, 3.4), 4H, CH₂), 1.63 (s, 6H, CH₃), 2.16 (s, 6H, CH₃), 3.43 (dt, *J* (5.3, 3.0), 4H, CH₂), 5.67 (s, 2H, NH amide), 8.89 (s, 2H, NH pyrrol). ¹³C NMR 75.4 MHz in CDCl₃ δ (ppm): 9.7 (CH₃), 11.4 (CH₃), 14.3 (CH₃), 20.7 (CH₂), 27.4 (CH₂), 32.5 (CH₂), 36.1 (C), 39.7 (CH₂), 116.5 (C), 119.9 (C), 120.4 (C), 136.1 (C), 162.6 (CO). ES⁺ mass spectrum, *m/z*, 429.3 (M + H)⁺, 451.2 (M + Na)⁺, 857.5 (2M + H)⁺, 879.4 (2M + Na)⁺. HRES⁺ mass spectrum, *m/z* calculated: 429.3224 (M + H)⁺, *m/z* found: 429.3218 (Δ 1.4 ppm). Anal. Found for C₂₅H₄₀N₄O₂ + $\frac{2}{3}$ MeOH (Calc.): C, 68.28 (68.51); H, 9.62 (9.56); N, 12.38 (12.45). Crystal data: C_{25.17}H_{40.50}N_{4.17}O_{2.33}, *M* = 438.78, *T* = 120(2) K, Triclinic, Space group *P* 1, *a* = 13.0112(9) Å, *b* = 17.310(3) Å, *c* = 17.729(4) Å, α = 88.460(14)°, β = 81.647(10)°, γ = 88.021(10)°, *V* = 3947.3(11) Å³, *Z* = 6 (3 molecules in the asymmetric unit), Reflections collected; 66535, Independent reflections; 11332 [*R*_{int} = 0.0701], Final R indices [*F*² > 2σ(*F*²)]: *R*1 = 0.0904, *wR*2 = 0.2491, R indices (all data): *R*1 = 0.1121, *wR*2 = 0.2694.

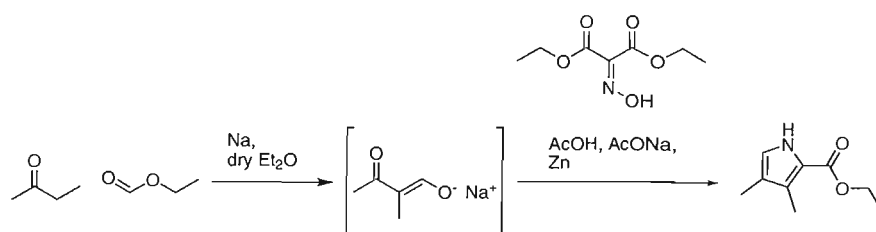


Ethyl 5-(2-(5-(butylcarbamoyl)-3,4-dimethyl-1H-pyrrol-2-yl)propan-2-yl)-3,4-dimethyl-1H-pyrrole-2-carboxylate 2.11(c). Butylamine (2.38 g, 32.30 mmol, 7.0 eq) was dissolved in freshly distilled dichloromethane (50 ml), and a 2 M solution of AlMe₃ in hexanes (15.05 ml, 32.30 mmol, 7.0 eq) was added dropwise. After stirring for 30 min, a solution of ethyl 5-(2-(5-(ethoxycarbonyl)-3,4-dimethyl-1H-pyrrol-2-yl)propan-2-yl)-3,4-dimethyl-1H-pyrrole-2-carboxylate (1.73 g, 4.62 mmol, 1.0 eq) in freshly distilled dichloromethane (20 ml) was added and the reaction mixture was stirred at 35 °C during 2 days. The reaction was carefully quenched with dilute 0.7 M HCl (100 ml), and extracted with dichloromethane (2 × 50 ml). The organic phases were combined and dried together over MgSO₄ and filtered. The volatiles were removed in vacuo and the solid obtained was purified by gradient column chromatography on silica gel with dichloromethane-dichloromethane/0.4% methanol affording the desired compound (0.41 g, 22%). Suitable crystals for X-ray studies were obtained by slow evaporation of a solution of this product in a mixture of dichloromethane/methanol. Mp 90–91°C. R_f _[DCM:MeOH 96:4] = 0.58. ¹H NMR 300 MHz in DMSO-*d*₆ δ (ppm): 0.91 (t, *J* 7.3, 3H, CH₃), 1.28 (t, *J* 7.3, 3H, CH₃), 1.34 (s, 6H, CH₃), 1.37 (m, 2H, CH₂), 1.48 (m, 2H, CH₂), 1.61 (s, 6H, CH₃), 3.20 (dt, *J* (5.5, 6.4), 2H, CH₂), 4.23 (q, *J* 7.3, 2H, CH₂), 7.70 (t, *J* 5.5, 1H, NH), 9.89 (s, 1H, NH), 10.19 (s, 1H, NH). ¹³C NMR 75.4 MHz in DMSO-*d*₆ δ (ppm): 8.8 (CH₃), 8.8 (CH₃), 10.4 (CH₃), 10.5 (CH₃), 13.8 (CH₃), 14.5 (CH₃), 19.8 (CH₃), 27.6 (CH₃), 31.7 (CH₂), 35.8 (CH₂), 38.1 (CH₂), 58.9 (CH₂), 114.5 (C), 115.5

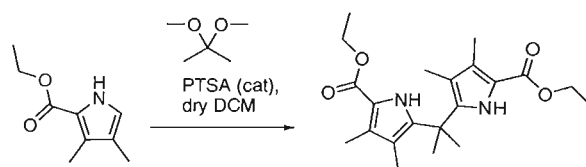
(C), 115.6 (C), 118.9 (C), 124.1 (C), 126.9 (C), 135.4 (C), 139.5 (C), 161.0 (CO), 161.2 (CO). ES⁺ mass spectrum, *m/z*, 402.4 (M + H)⁺, 424.4 (M + Na)⁺, 803.5 (2M + H)⁺. HRES⁺ mass spectrum, *m/z* calculated: 424.2570 (M + Na)⁺, *m/z* found: 424.2568 (Δ 0.5 ppm). Anal. Found for C₂₃H₃₅N₃O₃ (Calc.): C, 68.60 (68.80); H, 8.82 (8.79); N, 10.28 (10.46). Crystal data: C₂₃H₃₅N₃O₃, M = 401.54, T = 120(2) K, Monoclinic, Space group *P*21/*c*, *a* = 13.788(2) Å, *b* = 17.251(3) Å, *c* = 9.9242(10) Å, V = 2247.8(6) Å³, Z = 4, Reflections collected; 16670, Independent reflections; 3195 [Rint = 0.2070], Final R indices [*F*² > 2σ(*F*²)]: *R*1 = 0.1281, *wR*2 = 0.2857, R indices (all data): *R*1 = 0.1753, *wR*2 = 0.3148.



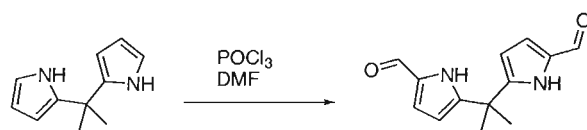
5-(2-(5-(butylcarbamoyl)-3,4-dimethyl-1*H*-pyrrol-2-yl)propan-2-yl)-3,4-dimethyl-*N*-phenyl-1*H*-pyrrole-2-carboxamide **2.11(d)**. Aniline (0.36 g, 3.84 mmol, 7.0 eq) was dissolved in freshly distilled dichloromethane (13 ml), and a 2 M solution of AlMe₃ in hexanes (1.92 ml, 3.84 mmol, 7.0 eq) was added dropwise. After stirring for 30 min, a solution of compound **2.11(c)** (0.22 g, 0.55 mmol, 1.0 eq) in freshly distilled dichloromethane (7 ml) was added and the reaction mixture was stirred at 35°C during 3 days. The reaction was carefully quenched with dilute 0.7 M HCl (50 ml), and extracted with dichloromethane (2 × 30 ml). The organic phases were combined and dried together over MgSO₄ and filtered. The volatiles were removed in vacuo and the solid obtained was purified by gradient column chromatography on silica gel with dichloromethane-dichloromethane/0.5% methanol affording the desired compound (95.4 mg, 39%). Mp 170–171°C. Rf_[DCM:MeOH 96:4] = 0.17. ¹H NMR 300 MHz in CDCl₃ δ (ppm): 0.96 (t, *J* 5.5, 6H, CH₃), 1.41 (tq, *J* (5.5, 3.4), 2H, CH₂), 1.56 (s, 6H, CH₃), 1.57 (tt, *J* (5.3, 3.4), 2H, CH₂), 1.59 (s, 3H, CH₃), 1.66 (s, 3H, CH₃), 2.17 (s, 3H, CH₃), 2.32 (s, 3H, CH₃), 3.45 (t, *J* 5.3, 2H, CH₂), 5.75 (s, 1H, NH amide), 7.10 (dd, *J* (5.6, 0.8), 1H, CH Ar), 7.34 (dd, *J* (5.7, 5.6), 2H, CH Ar), 7.52 (s, 1H, NH), 7.58 (dd, *J* (5.7, 0.8), 2H, CH Ar), 8.99 (s, 1H, NH), 9.06 (s, 1H, NH). ¹³C NMR 75.4 MHz in CDCl₃ δ (ppm): 9.3 (CH₃), 11.1 (CH₃), 13.9 (CH₃), 20.3 (CH₂), 26.9 (CH₃), 32.1 (CH₂), 35.9 (C), 39.5 (CH₂), 116.4 (C), 116.8 (C), 119.4 (C), 119.7 (C), 120.1 (CH), 120.7 (C), 121.3 (C), 124.1 (CH), 129.2 (CH), 136.1 (C), 137.1 (C), 138.4 (C), 160.2 (CO), 162.4 (CO). ES⁺ mass spectrum, *m/z*, 897.8 (2M + H)⁺. HRES⁺ mass spectrum, *m/z* calculated: 471.2730 (M + Na)⁺, *m/z* found: 471.2733 (Δ 0.5 ppm). Anal. Found for C₂₅H₄₀N₄O₂ + MeOH (Calc.): C, 69.67 (69.97); H, 8.23 (8.39); N, 11.43 (11.66).



Ethyl 3,4-dimethyl-1*H*-pyrrole-2-carboxylate. This compound was prepared following the literature procedure.^{114,115} Yield 4% of yellow crystalline needles. Mp 90–93°C (lit. 90–93°C). ¹H NMR 300 MHz in CDCl₃ δ (ppm): 1.35 (t, *J* 7.3, 3H, CH₃), 2.01 (s, 3H, CH₃), 2.27 (s, 3H, CH₃), 4.30 (q, *J* 7.3, 2H, CH₂), 6.66 (d, *J* 0.9, 1H, CH), 8.75 (br s, 1H, NH). ¹³C NMR 75.4 MHz in CDCl₃ δ (ppm): 10.29 (CH₃), 10.63 (CH₃), 14.93 (CH₃), 60.18 (CH₂), 119.68 (C), 120.48 (CH), 120.93 (C), 126.96 (C), 162.19 (CO).

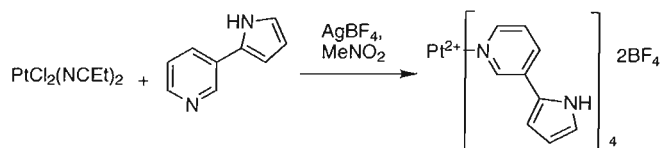


Ethyl 5-(2-(5-(ethoxycarbonyl)-3,4-dimethyl-1*H*-pyrrol-2-yl)propan-2-yl)-3,4-di-methyl-1*H*-pyrrole-2-carboxylate. This compound was prepared following the literature procedure.⁷² Yield 92% of white needles. Mp 122–125°C (lit. 122–125°C). ¹H NMR 300 MHz in CDCl₃ δ (ppm): 1.37 (t, *J* 7.2, 6H, CH₃), 1.54 (s, 6H, CH₃), 1.66 (s, 6H, CH₃), 2.21 (s, 6H, CH₃), 4.31 (q, *J* 7.2, 4H, CH₂), 8.59 (br s, 2H, NH). ¹³C NMR 75.4 MHz in CDCl₃ δ (ppm): 9.54 (CH₃), 10.85 (CH₃), 14.99 (CH₃), 27.14 (CH₃), 36.19 (C), 60.19 (CH₂), 116.48 (C), 117.30 (C), 128.79 (C), 137.54 (C), 162.36 (C). ES⁺ mass spectrum, *m/z*, 375.5 (M + H)⁺.



2,2-(di-5-formyl-1*H*-pyrrol-2-yl)propane 2.24(a). This compound was prepared following the literature procedure.⁸¹ Yield 88% (5.8 g) of a brown powder. ¹H NMR 300 MHz in DMSO-*d*₆ δ (ppm): 1.8 (s, 6H, CH₃), 6.2 (d, 2H, *J* 3.9, CH), 6.9 (d, 2H, *J* 3.9, CH), 9.3 (s, 2H, CHO), 10.6 (br s, 2H, NH). ¹³C NMR 75.4 MHz in DMSO-*d*₆ δ (ppm): 27.6 (CH₃), 36.0 (C), 107.8 (CH), 120.9 (CH), 133.4 (C), 148.6 (C), 178.8 (CO). Crystal data: C₁₃H₁₄N₂O₂, M = 230.26, T = 120(2) K, Orthorhombic, Space group Pca21, a = 16.6484(5) Å, b = 11.4329(4) Å, c = 12.4763(5) Å, V = 2374.73(15) Å³, Z = 8, Reflections collected: 13479, Independent reflections: 3946 [*R*_{int} = 0.0848], Final R indices [*F*² > 2σ(*F*²): *R*1 = 0.0468, *wR*2 = 0.1068, R indices (all data): *R*1 = 0.0555, *wR*2 = 0.1125.

5.3.2 Syntheses included in chapter 3

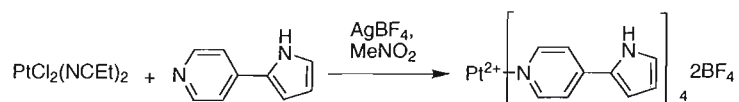
**Tetrakis(3-(1*H*-pyrrol-2-yl)pyridine)platinum(II) tetrafluoroborate 3.1(b).**

We placed into a 100 ml one necked flask $\text{PtCl}_2(\text{NCET})_2$ (100.0 mg, 0.27 mmol, 1.0 eq) and we added 16 ml of MeNO_2 . The flask containing this solution was wrapped with foil and AgBF_4 was added (113.9 mg, 0.58 mmol, 2.2 eq) and the mixture refluxed for three hours. The foil covering the reaction was removed and the mixture was filtered through a millipore filter paper when still hot. The filtrate was collected into another 100 ml one necked flask and 3-(1*H*-pyrrol-2-yl)pyridine (153.3 mg, 1.06 mmol, 4.0 eq) was added and the solution refluxed for further two hours. The reaction mixture was filtered again through a millipore filter paper and the yellow filtrate was allowed to cool down to ambient temperature. Addition of ether causes the complex to precipitate. We saturated the filtrate with ether and then we allowed the mixture stand overnight in the freezer to get a white precipitate that was collected by filtration, washed with DCM, and dried under vacuo. Yield 200 mg, 80%. Crystals suitable for X-ray diffraction were obtained from slow evaporation of this solid in MeNO_2 solutions. ^1H NMR 400 MHz in $\text{DMSO}-d_6$ δ (ppm): 11.66 (s, NH, 1H), 9.32 (d, J 1.5, 1H), 8.77 (d, J 5.5, 1H), 8.17 (d, J 8.5, 1H), 7.65 (dd, J (8.5, 5.5), 1H), 7.08 (m, 1H), 6.78 (m, 1H), 6.25 (dd, J (5.5, 2.5), 1H). ^{13}C NMR 100.6 MHz in $\text{DMSO}-d_6$ δ (ppm): 147.4 (CH), 146.4 (CH), 133.7 (CH), 132.3 (C), 127.6 (C), 125.1 (CH), 122.6 (CH), 110.2 (CH), 108.8 (CH). ES^+ mass spectrum, m/z , 857.0 ($\text{M} - \text{BF}_4$) $^+$, 386.0 ($\text{M} - 2\text{BF}_4$) $^{2+}$. ES^- mass spectrum, m/z , 1031.2 ($\text{M} + 3\text{BF}_4$) $^-$. HRES^+ mass spectrum, m/z calculated: 385.6193 (M^{2+}), m/z found: 385.6191 (Δ 0.6 ppm). Anal. Found for $\text{C}_{36}\text{H}_{32}\text{B}_2\text{F}_8\text{N}_8\text{Pt} + \frac{1}{2}\text{DCM}$ (Calc.): C, 44.29 (44.38); H, 3.39 (3.37); N, 11.17 (11.34). Crystal data: $M = 1067.49$, $T = 120(2)$ K, Triclinic, Space group P-1, $a = 9.4410 \text{ \AA}$, $b = 10.4860 \text{ \AA}$, $c = 11.2470 \text{ \AA}$, $\alpha = 77.57^\circ$, $\beta = 89.27^\circ$, $\gamma = 68.61^\circ$, $V = 1009.8(6) \text{ \AA}^3$, $Z = 1$, Reflections collected: 15299, Independent reflections: 4626 [$R_{\text{int}} = 0.0362$], Final R indices [$F^2 > 2\sigma(F^2)$]: $R1 = 0.0211$, $wR2 = 0.10466$, R indices (all data): $R1 = 0.0212$, $wR2 = 0.0467$. Crystal data for methanesulfonate salt:^{xi} $M = 979.99$, $T = 120(2)$ K, Triclinic, Space group P-1, $a = 9.059 \text{ \AA}$, $b = 10.489 \text{ \AA}$, $c = 11.080 \text{ \AA}$, $\alpha = 81.79^\circ$, $\beta = 73.74^\circ$, $\gamma = 69.24^\circ$, $V = 944.0 \text{ \AA}^3$, $Z = 1$, Reflections collected: 16456, Independent reflections: 4313 [$R_{\text{int}} = 0.0423$], Final R indices [$F^2 > 2\sigma(F^2)$]: $R1 = 0.0343$, $wR2 = 0.0777$, R indices (all data): $R1 = 0.0357$, $wR2 = 0.0785$. Crystal data for phosphorodifluoridate salt:^{xx} M

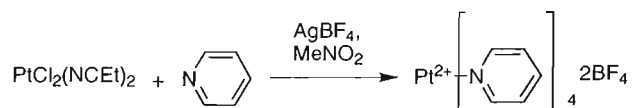
^{xi}Methanesulfonate complex prepared following the same procedure and using silver methane sulfonate as counteranion's complex source.

^{xx}Phosphorodifluoridate complex prepared following the same procedure and using an old batch of silver hexafluorophosphate as counteranion's complex source.

= 973.73, T = 120(2) K, Triclinic, Space group $P-1$, a = 9.7100(2) Å, b = 9.9440(3) Å, c = 10.8920(2) Å, $\alpha = 79.1790(17)^\circ$, $\beta = 70.8470(17)^\circ$, $\gamma = 64.6300(13)^\circ$, V = 896.29 Å³, Z = 1, Reflections collected: 18322, Independent reflections: 4108 [$R_{int} = 0.0382$], Final R indices [$F^2 > 2\sigma(F^2)$]: $R1 = 0.0224$, $wR2 = 0.0495$, R indices (all data): $R1 = 0.0227$, $wR2 = 0.0497$.

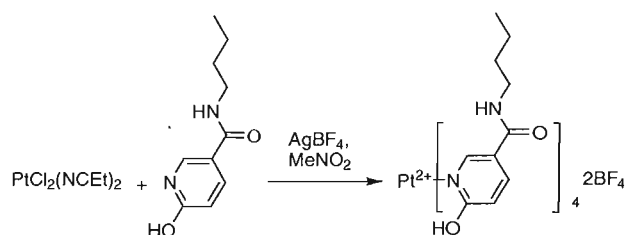


Tetrakis(4-(1*H*-pyrrol-2-yl)pyridine)platinum(II) tetrafluoroborate 3.1(c). $\text{PtCl}_2(\text{NCEt})_2$ (100.0 mg, 0.27 mmol, 1.0 eq) was dissolved in 16 ml of MeNO_2 . The flask containing this solution was wrapped with foil and AgBF_4 was added (113.9 mg, 0.58 mmol, 2.2 eq) and the mixture was refluxed for three hours. The foil was removed and the mixture was filtered through a millipore filter paper when still hot. The filtrate was collected into another 100 ml one necked flask and 4-(1*H*-pyrrol-2-yl)pyridine (153.3mg, 1.06 mmol, 4.0 eq) was added and the solution refluxed for further three hours. The reaction mixture was filtered again through a millipore filter paper and the yellow filtrate was allowed to cool down to ambient temperature. Addition of ether causes the complex to precipitate. We saturated the filtrate with ether and then we allowed the mixture stand overnight in the freezer to get a white precipitate that was collected by filtration, washed with DCM and dried under vacuo. Yield 180 mg, 72%. ¹H NMR 400 MHz in $\text{DMSO}-d_6$ δ (ppm): 11.89 (s, NH, 1H), 8.69 (d, J 7.0, 1H), 7.74 (d, J 7.0, 1H), 7.18 (s, 1H), 7.03 (s, 1H), 6.26 (s, 1H). ¹³C NMR 100.6 MHz in $\text{DMSO}-d_6$ δ (ppm): 151.0 (2 \times CH), 142.5 (C), 126.3 (CH), 125.3 (CH), 119.6 (2 \times CH), 113.0 (CH), 111.2 (C). ES^+ mass spectrum, m/z , 386.0 ($\text{M} - 2\text{BF}_4$)²⁺. HRES^+ mass spectrum, m/z calculated: 385.6193 (M)²⁺, m/z found: 385.6196 (Δ 0.6 ppm). Anal. Found for $\text{C}_{36}\text{H}_{32}\text{B}_2\text{F}_8\text{N}_8\text{Pt} + \frac{2}{3}\text{DCM}$ (Calc.): C, 43.90 (43.95); H, 3.24 (3.35); N, 11.18 (11.19).

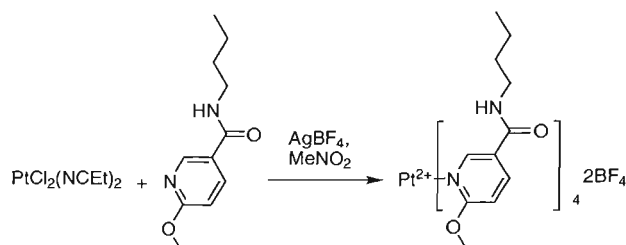


Tetrakis(pyridine)platinum(II) tetrafluoroborate 3.1(a). $\text{PtCl}_2(\text{NCEt})_2$ (200.0 mg, 0.53 mmol, 1.0 eq) was dissolved in 20 ml of MeNO_2 . The flask containing this solution was wrapped with foil and AgBF_4 was added (230.0 mg, 1.20 mmol, 2.2 eq) and the mixture was refluxed for three hours. The foil was removed and the mixture was filtered through a millipore filter paper when still hot. The filtrate was collected into another 100 ml one necked flask and pyridine (168.2 mg, 2.13 mmol, 4.0 eq) was added and the solution refluxed for further three hours. The reaction mixture was filtered through a millipore filter paper and the yellow filtrate was allowed to cool down

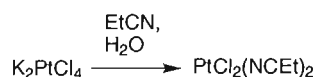
to ambient temperature. Addition of ether causes the complex to precipitate. We saturated the filtrate with ether and then we allowed the mixture stand overnight in the freezer to get a white precipitate that was collected by filtration, washed with DCM and dried under vacuo. Yield 300 mg, 82%. ^1H NMR 400 MHz in $\text{DMSO-}d_6$ δ (ppm): 9.07 (d, J 5.28, 2H), 8.06 (t, J 7.5, 1H), 7.68 (t, J 6.8, 2H). ^{13}C NMR 100.6 MHz in $\text{DMSO-}d_6$ δ (ppm): 151.7 ($2 \times \text{CH}$), 141.2 (CH), 127.7 ($2 \times \text{CH}$). ES^+ mass spectrum, m/z , 255.9 ($\text{M} - 2\text{BF}_4$) $^{2+}$. Anal. Found for $\text{C}_{20}\text{H}_{20}\text{B}_2\text{F}_8\text{N}_4\text{Pt}$ (Calc.): C, 35.06 (34.68); H, 2.94 (2.86); N, 8.17 (7.98).



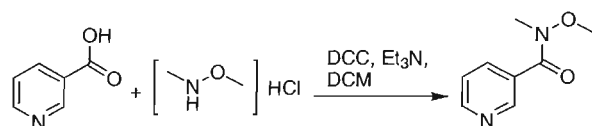
Tetrakis(*N*-butyl-6-hydroxynicotinamide)platinum(II) tetrafluoroborate 3.17(b). $\text{PtCl}_2(\text{NCEt})_2$ (126.0 mg, 0.33 mmol, 1.0 eq) was dissolved in 20 ml of MeNO_2 . The flask containing this solution was wrapped with foil and AgBF_4 was added (143.0 mg, 0.74 mmol, 2.2 eq) and the mixture was refluxed for three hours. The foil was removed and the mixture was filtered through a millipore filter paper when still hot. The filtrate was collected into another 100 ml one necked flask and *N*-butyl-6-hydroxynicotinamide (260.0 mg, 1.34 mmol, 4.0 eq) was added and the solution refluxed for further three hours. The reaction mixture was filtered through a millipore filter paper and the yellow filtrate was allowed to cool down to ambient temperature. Addition of ether causes the complex to precipitate. We saturated the filtrate with ether and then we allowed the mixture stand overnight in the freezer to get a white precipitate that was collected by filtration, washed with DCM and dried under vacuo. Yield 65 mg, 17%. ^1H NMR 300 MHz in $\text{DMSO-}d_6$ δ (ppm): 8.66 (ws, 1H, NH amide), 8.34 (ws, 1H, CH), 7.89 (d, J 8.3, 1H, CH), 6.63 (ws, 1H, CH), 3.49 (ws, 1H, OH), 3.18 (m, 2H, CH_2), 1.45 (m, 2H, CH_2), 1.30 (m, 2H, CH_2), 0.88 (t, J 7.2, 3H). ^{13}C NMR 75.4 MHz in $\text{DMSO-}d_6$ δ (ppm): 167.9 (CO), 162.8 (C), 149.4 (CH), 138.9 (CH), 120.9 (C), 114.1 (CH), 38.7 (CH_2), 31.1 (CH_2), 19.6 (CH_2), 13.6 (CH_3).



Tetrakis(*N*-butyl-6-methoxynicotinamide)platinum(II) tetrafluoroborate 3.17(c). PtCl₂(NCEt)₂ (126.0 mg, 0.33 mmol, 1.0 eq) was dissolved in 20 ml of MeCN. The flask containing this solution was wrapped with foil and AgBF₄ was added (143.0 mg, 0.74 mmol, 2.2 eq) and the mixture was refluxed for three hours. The foil was removed and the mixture was filtered through a millipore filter paper when still hot. The filtrate was collected into another 100 ml one necked flask and *N*-butyl-6-methoxynicotinamide (279.0 mg, 1.34 mmol, 4.0 eq) was added and the solution refluxed for further three hours. The reaction mixture was filtered through a millipore filter paper and the yellow filtrate was allowed to cool down to ambient temperature. Addition of ether causes the complex to precipitate. We saturated the filtrate with ether and then we allowed the mixture stand overnight in the freezer to get a white precipitate that was collected by filtration, washed with DCM and dried under vacuo. Yield 80 mg, 20%. ¹H NMR 300 MHz in DMSO-*d*₆ δ (ppm): 9.14 (ws, 1H, NH amide), 8.62 (ws, 1H, CH), 8.43 (d, *J* 9.4, 1H, CH), 7.29 (d, *J* 9.4, 1H, CH), 4.14 (s, 3H, CH₃), 3.26 (m, 2H, CH₂), 1.49 (m, 2H, CH₂), 1.30 (m, 2H, CH₂), 0.89 (t, *J* 7.2, 3H). ¹³C NMR 75.4 MHz in DMSO-*d*₆ δ (ppm): 165.8 (C), 161.7 (CO), 151.0 (CH), 141.3 (CH), 125.4 (C), 108.5 (CH), 58.3 (CH₃), 38.9 (CH₂), 30.9 (CH₂), 19.6 (CH₂), 13.6 (CH₃). ES⁺ mass spectrum, *m/z*, 513.7 (M - 2BF₄)²⁺, 1114.5 (M - BF₄)⁺. Crystal data, M = 1283.85, T = 173(2) K, Triclinic, Space group *P*-1, a = 9.193(5), b = 10.222(5), c = 15.574(8) Å, α = 94.230(6), β = 97.314(6), γ = 97.086(6)°, V = 1434.5(13) Å³, Z = 1, Reflections collected: 13743, Independent reflections: 5032 [R_{int} = 0.0286], Final R indices [F² > 2σ(F²)]: R1 = 0.0245, wR2 = 0.0624, R indices (all data): R1 = 0.0245, wR2 = 0.0624.

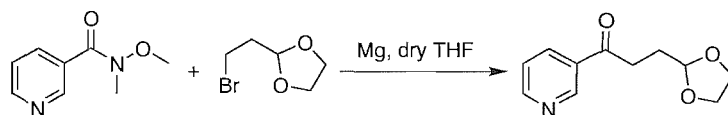


Bischlorodipropionitrileplatinum(II).¹¹⁶ K₂PtCl₄ (2.55 g, 6.14 mmol, 1.0 eq) was dissolved in water (24 ml). We added propionitrile (1.97 g, 34.74 mmol, 5.8 eq) and we allowed the solution to stand for 6 days. The product precipitated as yellow crystalline solid and was collected by filtration and dried by suction. Yield 1.94 g, 84%. ¹H NMR 400 MHz in DMSO-*d*₆ δ (ppm): 2.45 (q, *J* 7.6, 4H), 1.15 (t, *J* 7.6, 6H). ¹³C NMR 75.4 MHz in DMSO-*d*₆ δ (ppm): 121.6 (C), 10.1 (CH₂), 9.9 (CH₃). EI mass spectrum, *m/z*, 376 (M), 321 (M - propionitrile), 286 (M - propionitrile - chloride), 195 (Pt).

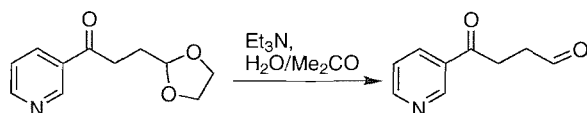


***N*-methoxy-*N*-methylnicotinamide.** This compound was prepared following the literature procedure.⁹⁷ Yield, 8.5 g, or 54%. ¹H NMR 300 MHz in CDCl₃ δ (ppm): 8.83

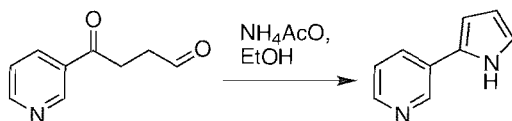
(dd, J 2.3, J 0.8, 1H), 8.56 (dd, J 4.9, J 1.9, 1H), 7.90 (dd, J 7.9, J 2.3, 1H), 7.24 (ddd, J 7.9, J 4.9, J 0.8, 1H), 1.30 (s, 3H), 1.30 (s, 3H). ^{13}C NMR 75.4 MHz in CDCl_3 δ (ppm): 166.6 (CO), 150.6 (CH), 148.5 (CH), 135.3 (CH), 129.1 (C), 122.6 (CH), 60.5 (CH_3), 32.4 (CH_3).



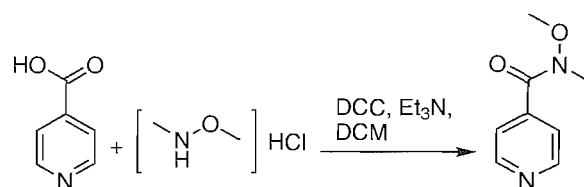
3-(1,3-dioxolan-2-yl)-1-(pyridin-3-yl)propan-1-one. This compound was prepared following the literature procedure.⁹⁷ Yield 2.7 g of yellow oil, or 74%. ^1H NMR 300 MHz in CDCl_3 δ (ppm): 9.12 (dd, J 1.5, J 0.8, 1H), 8.71 (dd, J 4.9, J 1.9, 1H), 8.18 (ddd, J 7.9, J 1.9, J 1.5, 1H), 7.36 (ddd, J 7.9, J 4.9, J 0.8, 1H), 4.95 (t, J 4.1, 1H), 3.90 (m, 2H), 3.80 (m, 2H), 3.07 (t, J 7.1, 2H), 2.15 (td, J 7.1, J 4.1, 2H). ^{13}C NMR 75.4 MHz in CDCl_3 δ (ppm): 198.2 (CO), 153.4 (CH), 149.6 (CH), 135.4 (CH), 132.2 (C), 123.6 (CH), 103.1 (CH), 65.0 ($2 \times \text{CH}_2$), 32.7 (CH_2), 27.7 (CH_2).



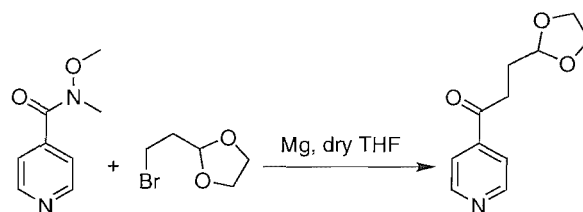
4-oxo-4-(pyridin-3-yl)butanal. This compound was prepared following the literature procedure.⁹⁷ Yield 0.6 g of yellow oil, or 73%. ^1H NMR 300 MHz in CDCl_3 δ (ppm): 9.89 (s, 1H), 9.19 (d, J 0.8, 1H), 8.78 (dd, J 0.8, J 3.6, 1H), 8.24 (dd, J 5.5, J 1.3, 1H), 7.42 (dd, J 3.6, J 5.5, 1H), 3.31 (t, J 4.5, 2H), 2.96 (t, J 4.7, 2H). ^{13}C NMR 75.4 MHz in CDCl_3 δ (ppm): 200.1 (CO), 196.8 (CO), 153.8 (CH), 149.7 (CH), 135.5 (CH), 131.9 (C), 123.8 (CH), 37.5 (CH_2), 31.3 (CH_2).



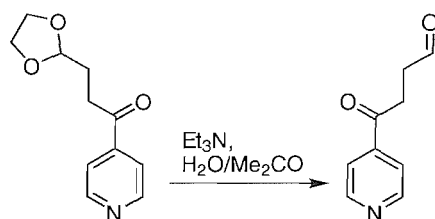
3-(1H-pyrrol-2-yl)pyridine. This compound was prepared following the literature procedure.^{96,117} Yield 1.2 g of white solid, or 84%. ^1H NMR 300 MHz in $\text{DMSO}-d_6$ δ (ppm): 11.43 (s, 1H), 8.87 (d, J 2.3, 1H), 8.33 (dd, J 1.5, J 4.9, 1H), 7.96 (ddd, J 7.9, J 1.5, J 2.25, 1H), 7.35 (dd, J 7.9, J 4.9, 1H), 6.92 (s, 1H), 6.63 (s, 1H), 6.15 (dd, J 3.4, J 6.0, 1H). ^{13}C NMR 75.4 MHz in CDCl_3 δ (ppm): 146.5 (CH), 144.9 (CH), 131.6 (CH), 129.3 (C), 128.6 (C), 124.0 (CH), 120.5 (CH), 110.6 (CH), 107.6 (CH).



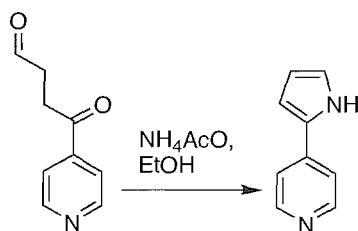
***N*-methoxy-*N*-methylisonicotinamide.** This compound was prepared following the literature procedure.⁹⁷ Yield 8.53 g of yellow oil, or 55%. ¹H NMR 300 MHz in CDCl₃ δ (ppm): 8.64 (dd, *J* 4.5, *J* 1.5, 2H), 7.45 (dd, *J* 4.5, *J* 1.5, 2H), 3.48 (s, 3H), 3.31 (s, 3H). ¹³C NMR 75.4 MHz in CDCl₃ δ (ppm): 167.5 (CO), 1149.9 (CH), 141.7 (C), 121.9 (CH), 61.3 (2 \times CH₃).



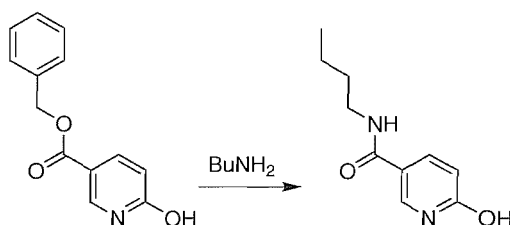
3-(1,3-dioxolan-2-yl)-1-(pyridin-4-yl)propan-1-one. This compound was prepared following the literature procedure.⁹⁷ Yield 4.1 g of yellow oil, or 54%. ¹H NMR 300 MHz in CDCl₃ δ (ppm): 8.76 (dd, *J* 3.1, *J* 1.5, 2H), 7.70 (dd, *J* 3.1, *J* 1.5, 2H), 4.96 (t, *J* 3.4, 1H), 3.91 (m, 2H), 3.82 (m, 2H), 3.07 (t, *J* 5.3, 2H), 2.12 (m, 2H). ¹³C NMR 75.4 MHz in CDCl₃ δ (ppm): 198.9 (CO), 150.9 (CH), 142.9 (C), 121.1 (CH), 103.1 (CH), 65.1 (CH₂), 32.7 (CH₂), 27.7 (CH₂).



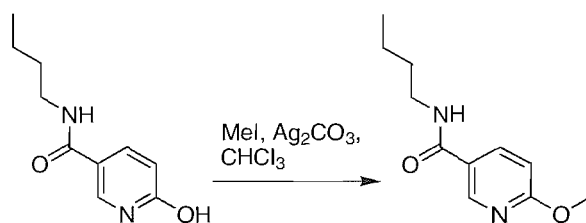
4-oxo-4-(pyridin-4-yl)butanal. This compound was prepared following the literature procedure.⁹⁷ Yield 1.32 g of yellow oil, or 42%. ¹H NMR 300 MHz in CDCl₃ δ (ppm): 9.84 (s, 1H), 8.78 (d, *J* 4.5, 2H), 7.72 (dd, *J* 3.4, *J* 1.1, 2H), 3.26 (t, *J* 4.5, 2H), 2.93 (t, *J* 4.9, 2H). ¹³C NMR 75.4 MHz in CDCl₃ δ (ppm): 206.8 (CO), 199.9 (CO), 150.9 (CH), 142.4 (C), 121.1 (CH), 37.4 (CH₂), 31.3 (CH₂).



4-(1*H*-pyrrol-2-yl)pyridine. This compound was prepared following the literature procedure.^{96,117} Yield 0.67 g of white solid, or 56%. ¹H NMR 300 MHz in DMSO-*d*₆ δ (ppm): 11.59 (s, 1H), 8.45 (d, *J* 4.5, 2H), 7.56 (d, *J* 4.5, 2H), 6.98 (s, 1H), 6.79 (s, 1H), 6.19 (s, 1H). ¹³C NMR 75.4 MHz in DMSO-*d*₆ δ (ppm): 149.9 (CH), 139.3 (C), 128.3 (C), 121.6 (CH), 117.3 (CH), 109.7 (CH), 108.7 (CH).



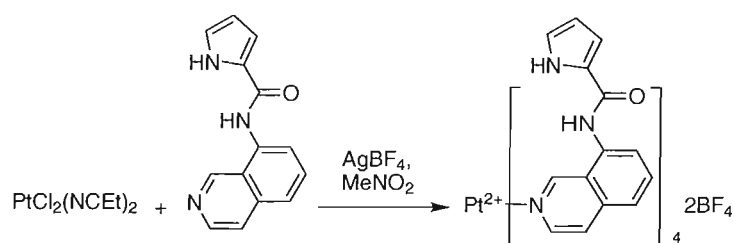
***N*-butyl-6-hydroxynicotinamide.** Benzyl 6-hydroxypyridine-3-carboxylate (2.0 g, 99%, 8.7 mmol, 1.0 eq) was refluxed in butylamine (30 ml) during four days. The solvent was removed under reduced pressure and the white solid collected was triturated with acetone (6 ml), filtered off, and the solid washed with further 12 ml of acetone. The solid was dried under reduced pressure to yield the title compound (88%, 1.5 g). ¹H NMR 300 MHz in DMSO-*d*₆ δ (ppm): 11.87 (s, 1H, NH pyridine), 8.14 (s, 1H, NH amide), 7.95 (d, *J* 1.9, 1H), 7.85 (dd, *J* 1.9, *J* 7.2, 1H), 6.33 (d, *J* 7.2, 1H), 3.19 (m, 2H), 1.45 (m, 2H), 1.30 (m, 2H), 0.89 (t, *J* 5.6, 3H). ¹³C NMR 75.4 MHz in DMSO-*d*₆ δ (ppm): 163.3 (CO), 162.2 (CO), 138.9 (CH), 136.9 (CH), 118.9 (CH), 112.5 (C), 38.6 (CH₂), 31.2 (CH₂), 19.6 (CH₂), 13.6 (CH₃).



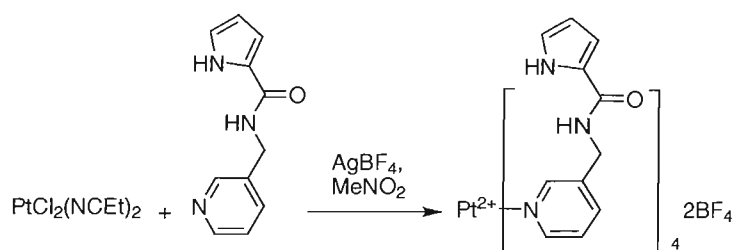
***N*-butyl-6-methoxynicotinamide.** Butyl 6-hydroxynicotinamide (2 g, 10 mmol, 1.0 eq) was dissolved in freshly distilled chloroform (70 ml) at room temperature under N₂ atmosphere. Ag₂CO₃ (5.7 g, 21 mmol, 2.0 eq) was added to the former solution

followed by MeI (1.46 g, 10.3 mmol, 1.0 eq) and the mixture stirred for three days. Further MeI (2.93 g, 20.6 mmol, 2.0 eq) was dissolved in CHCl₃ (8 ml) and added in small portions during two days. The reaction mixture was filtered, reduced in *vacuo*, and column chromatographed to afford the product as a white solid in 75% yield. $R_{f[\text{AcOEt:Hex } 4:6]} = 0.17$. ¹H NMR 300 MHz in CDCl₃ δ (ppm): 8.55 (d, *J* 2.5, 1H, ArH), 7.97 (dd, *J* (8.5, 2.5), 1H, ArH), 6.75 (d, *J* 8.7, 1H, ArH), 6.05 (ws, 1H, NH), 3.97 (s, 3H, CH₃), 3.44 (m, 2H, CH₂), 1.59 (m, 2H, CH₂), 1.40 (m, 2H, CH₂), 0.95 (t, *J* 7.3, 3H, CH₃). ¹³C NMR 75.4 MHz in CDCl₃ δ (ppm): 166.1 (CO), 165.8 (C), 146.2 (CH), 137.9 (CH), 124.1 (C), 110.9 (CH), 54.0 (CH₃), 39.9 (CH₂), 31.9 (CH₂), 20.3 (CH₂), 13.9 (CH₃).

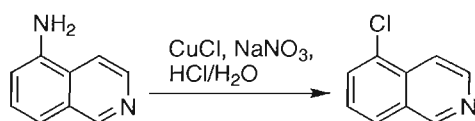
5.3.3 Syntheses included in chapter 4



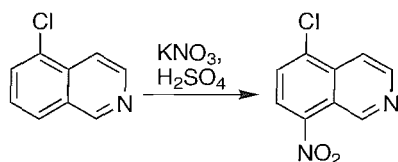
Tetrakis(*N*-(isoquinolin-8-yl)-1*H*-pyrrole-2-carboxamide)platinum(II) tetr-afluoroborate 4.1(a). $\text{PtCl}_2(\text{NCEt})_2$ (100.0 mg, 0.27 mmol, 1.0 eq) was dissolved in 16 ml of MeNO_2 . The flask containing this solution was wrapped with foil and AgBF_4 was added (113.9 mg, 0.58 mmol, 2.2 eq) and the mixture was refluxed for three hours. The foil was removed and the mixture was filtered through a millipore filter paper when still hot. The filtrate was collected into another 100 ml one necked flask and *N*-(isoquinolin-8-yl)-1*H*-pyrrole-2-carboxamide (258.0 mg, 1.08 mmol, 4.1 eq) was added and the solution refluxed for further three hours. The reaction mixture was filtered again through millipore filter paper and the yellow filtrate was allowed to cool down to ambient temperature. We saturated the filtrate with diethylether and then we allowed the mixture stand overnight in the freezer to get a white precipitate that was collected by filtration, washed with DCM and dried under vacuum. Yield 226 mg, 64%. ¹H NMR 400 MHz in $\text{DMSO-}d_6$ δ (ppm): 11.57 (s, NH, 1H), 10.26 (s, NH, 1H), 9.82 (s, 1H), 9.12 (d, *J* 6.5, 1H), 8.13 (d, *J* 6.5, 1H), 7.95 (dd, *J* (8.0, 7.3), 1H), 7.88 (d, *J* 8.0, 1H), 7.79 (d, *J* 7.3, 1H), 7.16 (m, 2H), 6.32 (m, 1H). ¹³C NMR 100.6 MHz in $\text{DMSO-}d_6$ δ (ppm): 165.5 (CO), 159.8 (CH), 153.4 (CH), 142.5 (C), 136.2 (C), 135.7 (CH), 134.2 (C), 125.4 (C), 125.1 (CH), 124.5 (CH), 123.9 (CH), 123.3 (CH), 112.7 (CH), 109.4 (CH). ES^+ mass spectrum, m/z , 237.8 ($\text{M} + \text{H}^+$), 474.52 ($2\text{M} + \text{H}^+$). ES^+ mass spectrum, m/z , 571.3 (PtL_4)²⁺, 1230.3 ($\text{PtL}_4 + \text{BF}_4^+$)⁺. HRES^+ mass spectrum, m/z calculated: 571.6622 (PtL_4)²⁺, m/z found: 571.6633 (Δ 1.9 ppm).



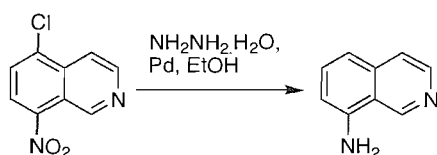
Tetrakis(*N*-(pyridin-3-ylmethyl)-1*H*-pyrrole-2-carboxamide)platinum(II) tetrafluoroborate 4.1(b). $\text{PtCl}_2(\text{NCET})_2$ (100.0 mg, 0.27 mmol, 1.0 eq) was dissolved in 16 ml of MeNO_2 . The flask containing this solution was wrapped with foil and AgBF_4 was added (113.9 mg, 0.58 mmol, 2.2 eq) and the mixture was refluxed for three hours. The foil was removed and the mixture was filtered through a millipore filter paper when still hot. The filtrate was collected into another 100 ml one necked flask and *N*-(pyridin-3-ylmethyl)-1*H*-pyrrole-2-carboxamide (214.0 mg, 1.06 mmol, 4.0 eq) was added and the solution refluxed for further three hours. The reaction mixture was filtered again through millipore filter paper and the yellow filtrate was allowed to cool down to ambient temperature. We saturated the filtrate with diethylether and then we allowed the mixture stand overnight in the freezer to get a white precipitate that was collected by filtration, washed with DCM and dried under vacuum. Yield 210 mg, 67%. ^1H NMR 400 MHz in $\text{DMSO}-d_6$ δ (ppm): 11.39 (s, NH, 1H), 8.99 (s, 1H), 8.91 (d, J 5.5, 1H), 8.55 (t, J 5.8, NH, 1H), 7.86 (d, J 8.3, 1H), 7.54 (dd, J (5.5, 8.3), 1H), 6.94 (m, 1H), 6.76 (m, 1H), 6.12 (m, 1H), 4.41 (d, J 5.8, 2H). ^{13}C NMR 100.6 MHz in $\text{DMSO}-d_6$ δ (ppm): 180.6 (CO), 160.9 (CH), 160.4 (CH), 149.9 (C), 139.6 (CH), 126.9 (CH), 125.3 (CH), 122.0 (CH), 110.5 (CH), 108.8 (C), 63.3(CH₂). ES^+ mass spectrum, m/z , 499.5 (PtL_4)²⁺. HRES^+ mass spectrum, m/z calculated: 499.66226 (PtL_4)²⁺, m/z found: 499.66231 (Δ 1.9 ppm).



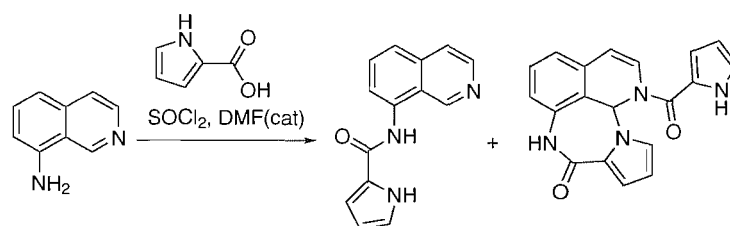
5-chloroisoquinoline. This compound was prepared following the literature procedure.¹¹¹ Yield, 3.1 g, or 60%; crystallized from petroleum ether, white needles, mp 73 to 74 °C (73 to 74 °C). ^1H NMR 300 MHz in CDCl_3 δ (ppm): 9.29 (s, 1H), 8.65 (d, J 2.6, 1H), 8.03 (d, J 4.4, 1H), 7.91 (d, J 6.0, 1H), 7.78 (dd, J 0.8, J 5.6, 1H), 7.54 (dd, J 6.0, J 5.6, 1H). ^{13}C NMR 75.4 MHz in CDCl_3 δ (ppm): 151.9 (CH), 143.4 (CH), 133.2 (C), 130.5 (C), 129.8 (CH), 126.8 (CH), 126.2 (CH), 116.4 (C).



5-chloro-8-nitroisoquinoline. This compound was prepared following the literature procedure.¹¹¹ Yield, 2.9 g, or 76%; crystallized from MeOH, brown-yellow needles, mp 134 to 135 °C (134 to 135 °C). ¹H NMR 300 MHz in CDCl₃ δ (ppm): 9.97 (s, 1H), 8.75 (d, *J* 5.7, 1H), 8.19 (d, *J* 8.3, 1H), 8.08 (d, *J* 6.0, 1H), 7.79 (d, *J* 8.3, 1H). ¹³C NMR 75.4 MHz in CDCl₃ δ (ppm): 148.7 (CH), 144.6 (CH), 145.2 (C), 138.2 (C), 134.5 (C), 128.9 (CH), 125.1 (CH), 121.1 (C), 116.9 (CH).

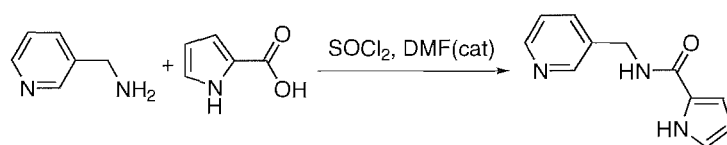


Isoquinolin-8-amine. This compound was prepared following the literature procedure.¹¹² Yield, 1.6 g, or 77%; crystallized from chloroform with light petroleum, yellow needles, mp 173 to 174 °C (173 to 174 °C). ¹H NMR 300 MHz in CDCl₃ δ (ppm): 9.37 (s, 1H), 8.46 (d, *J* 4.3, 1H), 7.57 (d, *J* 4.3, 1H), 7.45 (dd, *J* 6.0 *J* 5.6, 1H), 7.21 (d, *J* 6.0, 1H), 6.81 (d, *J* 5.6, 1H). ¹³C NMR 75.4 MHz in CDCl₃ δ (ppm): 146.4 (CH), 143.8 (C), 142.7 (CH), 137.1 (C), 131.7 (CH), 121.1 (CH), 118.9 (C), 116.7 (CH), 110.9 (CH).



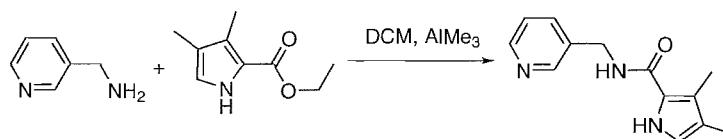
***N*-(isoquinolin-8-yl)-1*H*-pyrrole-2-carboxamide.** 1*H*-pyrrole-2-carboxylic acid (1.46 g, 13.10 mmol, 1.0 eq) was dissolved in thionyl chloride under N₂ atmosphere and the solution was stirred overnight at room temperature. The thionyl chloride was removed under vacuo and the residue was redissolved with dry DCM (15 ml) and added dropwise at room temperature over a solution of 8-aminoisoquinoline (1.25 g, 8.68 mmol, 0.67 eq), and NEt₃ (3.99 g, 39.0 mmol, 3.0 eq) in dry DCM (40 ml). The reaction mixture was stirred during 5 h and washed with 5% NaHCO₃/water solution (100 ml). The organic layer was extracted with 5% HCl/water (2 × 150 ml). The acid aqueous layer was washed with DCM (100 ml), basified with NaHCO₃, extracted with DCM (2 × 150 ml) and dried with MgSO₄. Evaporation of the solvent yielded a solid, mixture

of starting material and product. This solid was washed with AcOEt to get the desired product that can be recrystallized from warm AcOEt (0.03 g, 7%). ^1H NMR 400 MHz in $\text{DMSO-}d_6$ δ (ppm): 11.72 (s, 1H), 10.18 (s, 1H), 9.38 (s, 1H), 8.52 (d, J 6.0, 1H), 7.8 (m, 4H), 7.21 (m, 1H), 7.01 (m, 1H), 6.22 (m, 1H). ^{13}C NMR 100.6 MHz in $\text{DMSO-}d_6$ δ (ppm): 159.9 (CO), 148.5 (CH), 142.7 (CH), 135.9 (C), 134.6 (C), 130.4 (CH), 125.6 (C), 123.9 (CH, C), 123.5 (C), 122.7 (CH), 120.2 (CH), 111.9 (CH), 109.0 (CH). ES^+ mass spectrum, m/z , 237.8 ($\text{M} + \text{H}^+$), 474.52 ($2\text{M} + \text{H}^+$). HREI^+ mass spectrum, m/z calculated: 238.0975 ($\text{M} + \text{H}^+$), m/z found: 238.0978 (Δ 1.2 ppm). Anal. Found for $\text{C}_{14}\text{H}_{11}\text{N}_3\text{O}$ (Calc.): C, 70.87 (70.72); H, 4.67 (4.67); N, 17.70 (17.40). Crystal data, $M = 237.26$, $T = 120(2)$ K, monoclinic, space group $\text{P}21/\text{n}$, $a = 11.673(8)$ Å, $b = 4.0749(14)$ Å, $c = 23.609(19)$ Å, $\beta = 93.85(6)^\circ$, $V = 1120.5(12)$ Å³, $Z = 4$, Reflections collected: 10485, Independent reflections: 2202 [$R_{\text{int}} = 0.1701$], Final R indices [$F^2 > 2\sigma(F^2)$]: $R1 = 0.0824$, $wR2 = 0.1493$, R indices (all data): $R1 = 0.2154$, $wR2 = 0.1931$. The subproduct was isolated after recrystallization from the AcOEt fraction in 17% yield. $\text{Rf}_{[\text{AcOEt}:\text{petroleum ether } 7:3]} = 0.36$. ^1H NMR 300 MHz in $\text{DMSO-}d_6$ δ (ppm): 11.98 (s, 1H), 10.22 (s, 1H), 7.56 (d, J 7.8, 1H), 7.32 (m, 2H), 7.10 (m, 3H), 6.98 (s, 1H), 6.76 (d, J 2.0, 1H), 6.48 (ws, 1H), 6.23 (m, 2H), 6.08 (m, 1H). ^{13}C NMR 75.4 MHz in $\text{DMSO-}d_6$ δ (ppm): 146.39 (CO), 143.82 (CO), 136.3 (CH), 129.6 (CH), 128.4 (CH), 126.6 (C), 124.4 (CH), 122.7 (CH), 122.5 (C), 122.1 (CH), 120.9 (CH), 120.4 (CH), 120.1 (CH), 116.1 (C), 114.9 (C), 109.7 (CH), 108.1 (CH), 107.1 (CH), 62.9 (CH). Maldi-TOF mass spectrum, m/z , 331.0 ($\text{M} + \text{H}^+$), 353.0 ($\text{M} + \text{Na}^+$). Crystal data for $\text{C}_{19}\text{H}_{14}\text{N}_4\text{O}_2 + \frac{3}{2}\text{EtOH}$, $M = 399.44$, $T = 120(2)$ K, triclinic, space group $P-1$, $a = 7.3578(13)$ Å, $b = 10.822(2)$ Å, $c = 12.9449(13)$ Å, $\alpha = 93.912(12)^\circ$, $\beta = 100.365(12)^\circ$, $\gamma = 102.947(16)^\circ$, $V = 981.8(3)$ Å³, $Z = 2$, Reflections collected: 16705, Independent reflections: 4525 [$R_{\text{int}} = 0.0452$], Final R indices [$F^2 > 2\sigma(F^2)$]: $R1 = 0.0676$, $wR2 = 0.1826$, R indices (all data): $R1 = 0.1180$, $wR2 = 0.2108$.



***N*-((pyridin-3-yl)methyl)-1*H*-pyrrole-2-carboxamide.** 1*H*-pyrrole-2-carboxylic acid (1.7 g, 99%, 15.3 mmol, 1.0 eq) was stirred with SOCl_2 (25 ml) and DMF (2 drops) at room temperature overnight. The solution was reduced under vacuum and the residue redissolved in dry DCM (25 ml). The solution obtained was added dropwise with stirring over a solution of aminomethylpyridine (1.7 g, 99%, 15 mmol, 1.0 eq), and NEt_3 (2.3 g, 22.7 mmol, 1.5 eq) in DCM (20 ml) and stirred 3 h at room temperature. The reaction mixture was extracted with a 5% NaHCO_3 aqueous solution (50 ml). The organic layer was extracted with a 5% aqueous HCl solution (50 ml) and washed with DCM (2×100 ml). The aqueous acid layer was basified, and extracted with DCM (3×100 ml). The organic layer was dried with MgSO_4 and reduced under vacuum. The residue was flash

column chromatographed with AcOEt to yield pure title compound (0.7 g, 23%). R_f 0.07 (AcOEt). ^1H NMR 400 MHz in CDCl_3 δ (ppm): 9.65 (s, 1H), 8.58 (s, 1H), 8.53 (dd, J 1.5 J 4.8, 1H), 7.69 (d, J 8.0, 1H), 7.26 (dd, J 8.0 J 4.8, 1H), 6.93 (m, 1H), 6.59 (m, 1H), 6.39 (s, 1H), 6.23 (m, 1H), 4.35 (d, J 5.7, 2H). ^{13}C NMR 100.6 MHz in CDCl_3 δ (ppm): 161.3 (CO), 149.3 (CH), 148.9 (CH), 135.8 (CH), 134.4 (C), 125.6 (C), 123.8 (CH), 122.0 (CH), 110.1 (CH), 109.4 (CH), 40.9 (CH_2). ES^+ mass spectrum, m/z , 201.8 ($\text{M} + \text{H}^+$), 424.9 ($\text{M} + \text{Na}^+$). HREI^+ mass spectrum, m/z calculated: 202.0975 ($\text{M} + \text{H}^+$), m/z found: 202.0969 (Δ -2.85 ppm). Anal. Found for $\text{C}_{11}\text{H}_{11}\text{N}_3\text{O}$ (Calc.): C, 65.67 (65.66); H, 5.50 (5.51); N, 20.71 (20.87). Crystal data, $M = 201.23$, $T = 120(2)$ K, Monoclinic, Space group $\text{P2}_1/\text{n}$, $a = 6.8373(10)$, $b = 7.2747(14)$, $c = 20.329(3)$ Å, $V = 999.0(3)$ Å³, $Z = 4$, Reflections collected: 20925, Independent reflections: 2281 [$R_{\text{int}} = 0.0557$], Final R indices [$F^2 > 2\sigma(F^2)$]: $R1 = 0.0584$, $wR2 = 0.1545$, R indices (all data): $R1 = 0.0969$, $wR2 = 0.1841$.



3,4-dimethyl-N-((pyridin-3-yl)methyl)-1H-pyrrole-2-carboxamide. A solution of AlMe_3 in hexanes (3 ml, 2M, 5.98 mmol, 2.0 eq) was added dropwise with stirring over a solution of aminomethylpyridine (0.65, 99%, 5.98 mmol, 2.0 eq) in anhydrous DCM (12 ml). Evolution of gas was observed during the addition. We stirred the resulting solution during 30 min. Ethyl 3,4-dimethyl-1H-pyrrole-2-carboxylate¹¹⁴ (0.5 g, 2.99 mmol, 1.0 eq) was dissolved in anhydrous DCM (10 ml) and added dropwise over the aluminium solution. The temperature was fixed at 35 °C and the reaction was stirred 3 days. 1 M HCl aqueous solution (100 ml) was added dropwise at room temperature to the reaction mixture observing strong effervescence. The mixture obtained was extracted with DCM (2 × 100 ml). The aqueous layer was basified with a 5% NaHCO_3 aqueous solution up to pH 10, and extracted with DCM (3 × 50 ml). The combined organic layer were dried with MgSO_4 , filtered and volatiles removed under vacuo to yield pure product as a white solid (0.18 g, 26%). ^1H NMR 400 MHz in CDCl_3 δ (ppm): 9.16 (s, 1H), 8.58 (s, 1H), 8.52 (d, J 4.8, 1H), 7.68 (d, J 7.8, 1H), 7.26 (dd, J 7.8 J 4.8, 1H), 6.65 (d, J 2.5, 1H), 6.11 (t, J 5.9, 1H), 4.64 (d, J 5.9, 2H), 2.23 (s, 3H), 2.02 (s, 3H). ^{13}C NMR 100.6 MHz in CDCl_3 δ (ppm): 162.3 (CO), 149.2 (CH), 149.1 (CH), 135.6 (CH), 134.5 (C), 123.7 (CH), 122.5 (C), 120.4 (C), 119.3 (C), 119.2 (CH), 41.0 (CH_2), 11 (CH_3), 10.2 (CH_3). ES^+ mass spectrum, m/z , 229.8 ($\text{M} + \text{H}^+$), 481.0 ($\text{M} + \text{Na}^+$), 688.1 ($3\text{M} + \text{H}^+$). HREI^+ mass spectrum, m/z calculated: 230.1288 ($\text{M} + \text{H}^+$), m/z found: 230.1286 (Δ -0.76 ppm). Anal. Found for $\text{C}_{11}\text{H}_{11}\text{N}_3\text{O}$ (Calc.): C, 67.74 (68.10); H, 6.60 (6.59); N, 18.09 (18.32). Crystal data, $M = 229.28$, $T = 120(2)$ K, Monoclinic, Space group $\text{P2}_1/\text{c}$, $a = 8.6560(8)$, $b = 6.2887(11)$, $c = 21.576(3)$ Å, $V = 1174.0(3)$ Å³, $Z = 4$, Reflections collected: 12213, Independent reflections: 2682 [$R_{\text{int}} = 0.0608$],

Final R indices [$F^2 > 2\sigma(F^2)$]: $R1 = 0.0492$, $wR2 = 0.1079$, R indices (all data): $R1 = 0.0981$, $wR2 = 0.1298$.

5.4 General method used for NMR titration

All the ^1H NMR titration experiments were performed on a Bruker AM300 and AV300 NMR spectrometer. The anions were added as their tetrabutylammonium salts and would be dried under high vacuum pump overnight without heating. The receptor would be made up as a 0.01 M solution in a cooled yet previously oven dried NMR tube (5 mm), the top would be sealed using a suba-seal rubber septum which was secured using laboratory film. The anion would be made up as 0.1 M solution in a separate vial, the lid was made airtight so that the concentration would not change through the evaporation of the solvent. These solutions can be made quite simply; (1) for the receptor, molecule mass of the receptor divided by two hundred gives the required mass in milligram to be dissolved in 500 μl of the chosen solvent and accuracy percentage volume of water sometimes when it needed. (2) for the anion, molecule mass of the salt divided by ten gives the required mass in milligram to be dissolved in 1 ml of the same solvent. Small aliquots of the anionic guest would be introduced *via* syringe addition to the NMR tube after which a proton NMR spectrum of the receptor:anion solution would be recorded. The chemical shift of proton resonances believed to be involved in hydrogen bonding were recorded and the resulting data subsequently processed using WinEQNMR program⁶⁹ to calculate both the association constant and corresponding errors. A valid binding constant has an associated error below 15%.

Appendix A

X-ray Tables

Diffractometer: *Nonius KappaCCD* area detector (ϕ scans and scans to fill asymmetric unit). **Cell determination:** DirAx (Duisenberg, A.J.M.(1992). *J. Appl. Cryst.* 25, 92-96.) **Data collection:** Collect (Collect: Data collection software, R. Hooft, Nonius B.V., 1998). **Data reduction and cell refinement:** *Denzo* (Z. Otwinowski & W. Minor, *Methods in Enzymology* (1997) Vol. 276: *Macromolecular Crystallography*, part A, pp. 307-326; C. W. Carter, Jr. & R. M. Sweet, Eds., Academic Press). **Absorption correction:** Sheldrick, G. M. SADABS - Bruker Nonius area detector scaling and absorption correction - V2.10 **Structure solution:** *SHELXS97* (G. M. Sheldrick, *Acta Cryst.* (1990) A46 467-473). **Structure refinement:** *SHELXL97* (G. M. Sheldrick (1997), University of Göttingen, Germany). **Graphics:** Cameron - A Molecular Graphics Package. (D. M. Watkin, L. Pearce and C. K. Prout, *Chemical Crystallography Laboratory, University of Oxford*, 1993).

Special details: All hydrogen atoms were placed in idealised positions and refined using a riding model.

A.1 Bis-*N*-butylamide-5,5'-methylenebis(4-ethyl-3-methyl-2-pyrrolicarboxylate). 2.4(a)

TABLE A.1: Crystal data and structure refinement details.

Identification code	03ie001 (IE 23)
Empirical formula	C ₂₅ H ₄₀ N ₄ O ₂
Formula weight	428.61
Temperature	120(2) K
Wavelength	0.71073 Å

Continued on next page

Continued from previous page

Crystal system	Triclinic
Space group	<i>P</i> -1
Unit cell dimensions	$a = 12.7164(2) \text{ \AA}$ $\alpha = 77.2000(10)^\circ$ $b = 14.1868(2) \text{ \AA}$ $\beta = 75.5160(10)^\circ$ $c = 15.2266(2) \text{ \AA}$ $\gamma = 76.1900(10)^\circ$
Volume	2544.22(6) \AA^3
<i>Z</i>	4
Density (calculated)	1.119 Mg / m^3
Absorption coefficient	0.072 mm^{-1}
<i>F</i> (000)	936
Crystal	Colourless Block
Crystal size	0.2 × 0.1 × 0.1 mm^3
θ range for data collection	2.93 - 25.68°
Index ranges	-15 ≤ <i>h</i> ≤ 15, -17 ≤ <i>k</i> ≤ 17, -18 ≤ <i>l</i> ≤ 18
Reflections collected	50744
Independent reflections	9646 [<i>R</i> _{int} = 0.0565]
Completeness to $\theta = 25.68^\circ$	99.7 %
Absorption correction	None
Max. and min. transmission	0.9925 and 0.9851
Refinement method	Full-matrix least-squares on <i>F</i> ²
Data / restraints / parameters	9646 / 0 / 628
Goodness-of-fit on <i>F</i> ²	1.023
Final <i>R</i> indices [$\theta > 2\sigma(\theta)$]	<i>R</i> 1 = 0.0500, <i>wR</i> 2 = 0.1176
<i>R</i> indices (all data)	<i>R</i> 1 = 0.0617, <i>wR</i> 2 = 0.1243
Extinction coefficient	0.0179(14)
Largest diff. peak and hole	0.770 and -0.464 e \AA^3

TABLE A.2: Atomic coordinates ($\times 10^4$), equivalent isotropic displacement parameters ($\text{\AA}^2 \times 10^3$) and site occupancy factors. U_{eq} is defined as one third of the trace of the orthogonalized U^{ij} tensor.

Atom	<i>x</i>	<i>y</i>	<i>z</i>	<i>U</i> _{eq}	<i>S.o.f</i>
C23	12695(1)	2230(1)	6873(1)	25(1)	1
C19	3665(1)	5124(1)	4658(1)	20(1)	1
C24	11187(2)	1054(1)	11377(1)	33(1)	1
C25	7807(1)	444(1)	10509(1)	23(1)	1
C21	3384(2)	4043(1)	10204(1)	35(1)	1
C20	7209(1)	3288(1)	8172(1)	24(1)	1

Continued on next page

Continued from previous page

Atom	<i>x</i>	<i>y</i>	<i>z</i>	<i>U</i>_{eq}	<i>S.o.f</i>
C22	10975(2)	4266(1)	6415(1)	29(1)	1
C17	3224(1)	4471(1)	8071(1)	25(1)	1
C18	3788(2)	7150(1)	5198(1)	27(1)	1
O3	3853(1)	5778(1)	3965(1)	22(1)	1
O1	7575(1)	338(1)	11014(1)	29(1)	1
O2	7803(1)	2795(1)	8722(1)	32(1)	1
C26	10241(1)	2887(1)	9886(1)	26(1)	1
N5	3481(1)	4261(1)	4577(1)	24(1)	1
N6	7611(1)	3393(1)	7261(1)	26(1)	1
N7	7187(1)	931(1)	9888(1)	27(1)	1
O4	13114(1)	2692(1)	6117(1)	32(1)	1
N8	13025(1)	1254(1)	7115(1)	31(1)	1
C27	8676(1)	2821(1)	6870(1)	30(1)	1
C28	3398(2)	6752(1)	7403(1)	29(1)	1
C29	5702(1)	1193(1)	9026(1)	31(1)	1
C30	3508(2)	4027(1)	3685(1)	28(1)	1
C38	6191(1)	612(1)	9847(1)	31(1)	1
C32	3546(2)	2941(1)	3753(1)	29(1)	1
C36	9656(2)	500(1)	11765(1)	34(1)	1
C34	6409(2)	988(1)	8102(1)	35(1)	1
C31	5933(2)	3458(2)	10272(1)	32(1)	1
C37	8940(1)	3106(1)	5830(1)	32(1)	1
C35	9996(2)	2467(2)	5384(1)	42(1)	1
C33	10844(2)	1285(2)	12352(1)	46(1)	1
C39	3531(2)	2692(1)	2833(1)	34(1)	1
C40	2227(2)	7342(2)	7655(1)	43(1)	1
C41	9449(2)	4692(1)	8306(1)	34(1)	1
C42	3089(2)	3022(2)	10530(1)	45(1)	1
C43	13864(2)	650(1)	6516(1)	39(1)	1
C44	3742(2)	1594(2)	2843(2)	56(1)	1
C46	5881(2)	1559(2)	7294(2)	52(1)	1
C45	13387(2)	34(2)	6165(2)	54(1)	1
C48	9893(2)	5603(2)	8291(2)	55(1)	1
C47	10288(2)	2771(2)	4347(2)	64(1)	1
C49	12612(3)	511(2)	5561(2)	67(1)	1
C50	12061(3)	172(2)	5209(2)	74(1)	1
N2	3462(1)	4624(1)	6367(1)	20(1)	1

Continued on next page

Continued from previous page

Atom	<i>x</i>	<i>y</i>	<i>z</i>	<i>U</i>_{eq}	<i>S.o.f</i>
N3	11561(1)	2407(1)	8459(1)	24(1)	1
N4	8946(1)	1754(1)	10085(1)	23(1)	1
N1	5278(1)	4019(1)	7948(1)	22(1)	1
C4	3610(1)	5316(1)	5572(1)	20(1)	1
C9	8728(1)	849(1)	10581(1)	22(1)	1
C14	11811(1)	2750(1)	7519(1)	23(1)	1
C1	3379(1)	5045(1)	7109(1)	21(1)	1
C5	4245(1)	4205(1)	8475(1)	22(1)	1
C7	6053(1)	3715(1)	8506(1)	23(1)	1
C3	3632(1)	6194(1)	5824(1)	21(1)	1
C12	9844(1)	1940(1)	10296(1)	23(1)	1
C2	3484(1)	6019(1)	6798(1)	23(1)	1
C10	9519(1)	464(1)	11120(1)	24(1)	1
C8	4333(1)	4034(1)	9389(1)	25(1)	1
C15	11075(1)	3628(1)	7333(1)	23(1)	1
C11	10226(1)	1155(1)	10936(1)	25(1)	1
C6	5471(1)	3727(1)	9411(1)	25(1)	1
C13	10682(1)	3045(1)	8864(1)	23(1)	1
C16	10360(1)	3806(1)	8184(1)	24(1)	1

A.2 Bis-*N*-phenylamide-5,5'-methylene bis(4-ethyl-3-methyl-2-pyrrolicarboxylate). 2.4(b)

TABLE A.3: Crystal data and structure refinement details.

Identification code	02sot125 (IE 21)	
Empirical formula	C ₂₉ H ₃₂ N ₄ O ₂	
Formula weight	468.59	
Temperature	120(2) K	
Wavelength	0.71063 Å	
Crystal system	Monoclinic	
Space group	P21/c	
Unit cell dimensions	$a = 11.011(3)$ Å	$\alpha = 90^\circ$
	$b = 17.487(3)$ Å	$\beta = 95.628(16)^\circ$
	$c = 13.771(2)$ Å	$\gamma = 90^\circ$
Volume	2638.9(9) Å ³	
<i>Z</i>	4	
Density (calculated)	1.179 Mg / m ³	
Absorption coefficient	0.075 mm ⁻¹	
<i>F</i> (000)	1000	
Crystal	Colourless Block	
Crystal size	0.2 × 0.1 × 0.1 mm ³	
θ range for data collection	2.97 - 23.25°	
Index ranges	-11 ≤ <i>h</i> ≤ 12, -18 ≤ <i>k</i> ≤ 19, -15 ≤ <i>l</i> ≤ 15	
Reflections collected	12855	
Independent reflections	3783 [<i>R</i> _{int} = 0.0339]	
Completeness to $\theta = 23.25^\circ$	99.7 %	
Absorption correction	Semi empirical from equivalents	
Max. and min. transmission	0.9925 and 0.9851	
Refinement method	Full-matrix least-squares on <i>F</i> ²	
Data / restraints / parameters	3783 / 4 / 328	
Goodness-of-fit on <i>F</i> ²	1.043	
Final <i>R</i> indices [$\theta > 2\sigma(\theta)$]	<i>R</i> 1 = 0.0646, <i>wR</i> 2 = 0.1685	
<i>R</i> indices (all data)	<i>R</i> 1 = 0.0809, <i>wR</i> 2 = 0.1831	
Extinction coefficient	0.020(3)	
Largest diff. peak and hole	0.839 and 0.37 e Å ³	

TABLE A.4: Atomic coordinates ($\times 10^4$), equivalent isotropic displacement parameters ($\text{\AA}^2 \times 10^3$) and site occupancy factors. U_{eq} is defined as one third of the trace of the orthogonalized U^{ij} tensor.

Atom	x	y	z	U_{eq}	$S.o.f$
C25A	3836(8)	3083(6)	4333(7)	49(2)	0.50
C29A	5096(8)	3338(5)	4566(6)	78(2)	0.50
C25B	4384(8)	2999(6)	4570(7)	49(2)	0.50
C29B	3811(8)	3442(5)	3800(6)	78(2)	0.50
C1	226(3)	1837(2)	9500(2)	52(1)	1
C2	551(4)	1696(2)	10320(3)	72(1)	1
C3	1452(6)	1188(3)	10300(3)	130(3)	1
C4	1621(5)	804(3)	9445(3)	115(2)	1
C5	828(4)	920(2)	8620(3)	82(1)	1
C6	132(3)	1430(2)	8659(2)	49(1)	1
C7	1319(2)	2224(1)	7438(2)	32(1)	1
C8	2086(2)	2239(1)	6515(2)	32(1)	1
C9	2677(3)	2860(2)	6057(2)	44(1)	1
C10	3320(3)	2582(2)	5180(2)	51(1)	1
C11	3088(3)	1811(2)	5128(2)	36(1)	1
C12	3511(3)	1231(2)	4365(2)	39(1)	1
C13	2554(2)	649(2)	4187(2)	35(1)	1
C14	2529(3)	137(2)	4304(2)	35(1)	1
C15	1379(3)	393(2)	4053(2)	34(1)	1
C16	737(3)	250(1)	3788(2)	33(1)	1
C17	491(3)	314(1)	3496(2)	33(1)	1
C18	2014(3)	1249(2)	2972(2)	39(1)	1
C19	2191(3)	2028(2)	2893(3)	54(1)	1
C20	3236(3)	2306(2)	2552(3)	66(1)	1
C21	4127(3)	1820(2)	2295(2)	59(1)	1
C22	3971(3)	1045(2)	2394(2)	51(1)	1
C23	2927(3)	752(2)	2734(2)	45(1)	1
C24	2650(4)	3678(2)	6392(3)	71(1)	1
C26	3552(3)	628(2)	4581(2)	42(1)	1
C27	961(3)	1207(2)	4102(2)	41(1)	1
C28	4430(3)	849(2)	3701(2)	54(1)	1
N1	917(2)	1545(1)	7791(2)	40(1)	1
N2	2364(2)	1606(1)	5942(2)	32(1)	1

Continued on next page

Continued from previous page

Atom	<i>x</i>	<i>y</i>	<i>z</i>	<i>U_{eq}</i>	<i>S.o.f</i>
N3	1481(2)	875(1)	3889(2)	34(1)	1
N4	890(2)	1021(1)	3288(2)	39(1)	1
O1	1045(2)	2828(1)	7879(1)	43(1)	1
O2	1148(2)	257(1)	3435(1)	37(1)	1

A.3 5-(2-(5-(phenylcarbonyl)-3,4-dimethyl-1H-pyrrol-2-yl)propan-2-yl)-3,4-dimethyl-N-phenyl-1H-pyrrole-2-carboxamide. 2.11(a)

TABLE A.5: Crystal data and structure refinement details.

Identification code	03SOT0133 (IE 119)
Empirical formula	C ₃₀ H ₃₆ N ₄ O ₃
Formula weight	500.63
Temperature	120(2) K
Wavelength	0.71073 Å
Crystal system	Orthorhombic
Space group	<i>P</i> 2 ₁ 2 ₁ 2 ₁
Unit cell dimensions	<i>a</i> = 11.1668(3) Å <i>b</i> = 11.7777(3) Å <i>c</i> = 20.3200(6) Å
Volume	2672.47(13) Å ³
<i>Z</i>	4
Density (calculated)	1.244 Mg / m ³
Absorption coefficient	0.081 mm ⁻¹
<i>F</i> (000)	1072
Crystal	Colourless Block
Crystal size	0.22 × 0.2 × 0.1 mm ³
θ range for data collection	3.22 - 25.03°
Index ranges	-13 ≤ <i>h</i> ≤ 13, -14 ≤ <i>k</i> ≤ 14, -23 ≤ <i>l</i> ≤ 24
Reflections collected	32775
Independent reflections	4702 [<i>R</i> _{int} = 0.1689]
Completeness to $\theta = 23.03^\circ$	99.7 %
Absorption correction	Semi empirical from equivalents
Max. and min. transmission	0.9919 and 0.9819
Refinement method	Full-matrix least-squares on <i>F</i> ²
Data / restraints / parameters	4702 / 0 / 308
Goodness-of-fit on <i>F</i> ²	1.036
Final <i>R</i> indices [$\theta > 2\sigma(\theta)$]	<i>R</i> 1 = 0.0765, <i>wR</i> 2 = 0.1793
<i>R</i> indices (all data)	<i>R</i> 1 = 0.1061, <i>wR</i> 2 = 0.1945
Extinction coefficient	0.015(2)
Largest diff. peak and hole	0.518 and 0.380 e Å ³

TABLE A.6: Atomic coordinates ($\times 10^4$), equivalent isotropic displacement parameters ($\text{\AA}^2 \times 10^3$) and site occupancy factors. U_{eq} is defined as one third of the trace of the orthogonalized U^{ij} tensor.

Atom	x	y	z	U_{eq}	$S.o.f$
C1	6629(4)	6564(5)	4562(2)	42(1)	1
C2	7508(4)	7375(5)	4669(2)	49(1)	1
C3	7292(4)	8492(5)	4583(2)	50(1)	1
C4	6160(5)	8837(5)	4372(3)	54(1)	1
C5	5277(4)	8040(4)	4263(2)	40(1)	1
C6	5517(4)	6896(4)	4351(2)	37(1)	1
C7	4495(4)	5013(4)	4252(2)	32(1)	1
C8	3361(3)	4460(4)	4055(2)	33(1)	1
C9	3083(4)	3327(4)	4035(2)	35(1)	1
C10	1848(4)	3248(4)	3848(2)	35(1)	1
C11	1431(4)	4335(4)	3781(2)	32(1)	1
C12	154(4)	4756(4)	3655(2)	32(1)	1
C13	310(4)	4264(4)	3014(2)	32(1)	1
C14	105(3)	4411(4)	2377(2)	30(1)	1
C15	700(4)	3853(4)	1946(2)	33(1)	1
C16	1582(3)	3368(4)	2327(2)	28(1)	1
C17	2631(4)	2706(4)	2134(2)	32(1)	1
C18A	4533(4)	1889(5)	2501(3)	38(1)	0.495(6)
C19A	5473(6)	2511(5)	2235(3)	38(1)	0.495(6)
C20A	6615(5)	2044(5)	2208(3)	38(1)	0.495(6)
C21A	6817(4)	956(5)	2448(3)	38(1)	0.495(6)
C22A	5877(5)	333(4)	2714(3)	38(1)	0.495(6)
C23A	4735(4)	800(5)	2741(3)	38(1)	0.495(6)
C18B	4605(4)	1986(5)	2493(3)	38(1)	0.50
C19B	5631(6)	2651(4)	2531(3)	38(1)	0.50
C20B	6749(5)	2167(5)	2425(3)	38(1)	0.50
C21B	6842(4)	1017(5)	2280(3)	38(1)	0.50
C22B	5816(5)	351(4)	2241(3)	38(1)	0.50
C23B	4698(4)	836(5)	2347(3)	38(1)	0.50
C24	610(4)	4347(5)	4247(2)	42(1)	1
C25	91(4)	6037(4)	3629(3)	43(1)	1
C26	3876(4)	2331(4)	4181(3)	48(1)	1
C27	1183(5)	2147(4)	3766(3)	49(1)	1

Continued on next page

Continued from previous page

Atom	<i>x</i>	<i>y</i>	<i>z</i>	<i>U_{eq}</i>	<i>S.o.f</i>
C28	1222(4)	5037(4)	2170(2)	38(1)	1
C29	591(4)	3870(4)	1206(2)	38(1)	1
N1	4545(3)	6146(3)	4200(2)	33(1)	1
N2	2340(3)	5071(3)	3900(2)	31(1)	1
N3	1334(3)	3643(3)	2978(2)	29(1)	1
N4	3430(3)	2437(3)	2607(2)	38(1)	1
O1	5339(3)	4436(3)	4467(2)	44(1)	1
O2	2790(2)	2411(3)	1552(2)	36(1)	1
C30	7097(5)	7016(5)	647(3)	66(2)	1
O3	6902(3)	7967(3)	1052(2)	41(1)	1

A.4 5-(2-(5-(butylcarbamoyl)-3,4-dimethyl-1H-pyrrol-2-yl)propan-2-yl)-3,4-dimethyl-N-butyl-1H-pyrrole-2-carboxamide. 2.11(b)

TABLE A.7: Crystal data and structure refinement details.

Identification code	04sot0519 (IE 146)
Empirical formula	C _{25.17} H _{40.50} N _{4.17} O _{2.33}
Formula weight	438.78
Temperature	120(2) K
Wavelength	0.71073 Å
Crystal system	Triclinic
Space group	<i>P</i> -1
Unit cell dimensions	$a = 13.0112(9)$ Å $\alpha = 88.460(14)^\circ$ $b = 17.310(3)$ Å $\beta = 81.647(10)^\circ$ $c = 17.729(4)$ Å $\gamma = 88.021(10)^\circ$
Volume	3947.3(11) Å ³
<i>Z</i>	6 (3 Molecules in the asymmetric unit)
Density (calculated)	1.108 Mg / m ³
Absorption coefficient	0.072 mm ⁻¹
<i>F</i> (000)	1436
Crystal	Cut Prism; Colourless
Crystal size	0.22 × 0.2 × 0.15 mm ³
θ range for data collection	2.99 - 23.26°
Index ranges	-14 ≤ <i>h</i> ≤ 14, -19 ≤ <i>k</i> ≤ 19, -19 ≤ <i>l</i> ≤ 19
Reflections collected	66535
Independent reflections	11332 [<i>R</i> _{int} = 0.0701]
Completeness to $\theta = 23.26^\circ$	99.8 %
Absorption correction	Semi empirical from equivalents
Max. and min. transmission	0.9893 and 0.9844
Refinement method	Full-matrix least-squares on <i>F</i> ²
Data / restraints / parameters	11332 / 172 / 881
Goodness-of-fit on <i>F</i> ²	1.112
Final <i>R</i> indices [$\theta > 2\sigma(\theta)$]	<i>R</i> 1 = 0.0904, <i>wR</i> 2 = 0.2491
<i>R</i> indices (all data)	<i>R</i> 1 = 0.1121, <i>wR</i> 2 = 0.2694
Extinction coefficient	0.0069(16)
Largest diff. peak and hole	1.183 and -0.929 e Å ³

TABLE A.8: Atomic coordinates ($\times 10^4$), equivalent isotropic displacement parameters ($\text{\AA}^2 \times 10^3$) and site occupancy factors. U_{eq} is defined as one third of the trace of the orthogonalized U^{ij} tensor.

Atom	x	y	z	U_{eq}	$S.o.f$
O7	468(11)	1652(7)	628(7)	130(3)	0.50
N13	66(10)	1258(7)	327(7)	130(3)	0.50
C76	1160(11)	1296(13)	426(12)	130(3)	0.50
O8	553(11)	814(7)	88(7)	130(3)	0.50
N1	336(3)	7824(2)	5788(2)	32(1)	1
N2	117(2)	9321(2)	6466(2)	26(1)	1
N3	519(3)	11579(2)	8075(2)	30(1)	1
O1	955(2)	8162(2)	5107(2)	35(1)	1
O2	2514(3)	12704(2)	9257(2)	56(1)	1
C1	1348(5)	5681(3)	6755(4)	65(2)	1
C2	447(4)	6223(3)	6530(3)	45(1)	1
C3	342(3)	6486(3)	5701(3)	39(1)	1
C4	503(3)	7063(3)	5441(3)	37(1)	1
C5	363(3)	8347(2)	5561(2)	28(1)	1
C6	429(3)	9121(2)	5891(2)	26(1)	1
C7	1057(3)	9757(2)	5734(2)	29(1)	1
C8	865(3)	10356(2)	6227(2)	30(1)	1
C9	137(3)	10066(2)	6676(2)	26(1)	1
C10	320(3)	10451(2)	7306(3)	30(1)	1
C11	569(3)	10844(2)	7830(2)	30(1)	1
C12	1537(3)	10567(3)	8133(3)	35(1)	1
C13	2086(4)	11164(3)	8556(3)	42(1)	1
C14	1442(3)	11787(3)	8524(3)	33(1)	1
C15	1639(3)	12544(3)	8881(3)	39(1)	1
N4	888(3)	13055(2)	8798(2)	41(1)	1
C16	1027(4)	13827(2)	9146(3)	48(1)	1
C17	624(4)	13867(3)	9840(3)	62(2)	1
C18	523(3)	13733(3)	9849(3)	58(2)	1
C19	932(4)	13744(4)	10602(3)	61(2)	1
C20	1805(3)	9817(3)	5172(3)	39(1)	1
C21	1382(4)	11149(3)	6247(3)	40(1)	1
C22	874(4)	9850(3)	7787(3)	40(1)	1
C23	1131(3)	11035(3)	6939(3)	40(1)	1

Continued on next page

Continued from previous page

Atom	<i>x</i>	<i>y</i>	<i>z</i>	<i>U_{eq}</i>	<i>S.o.f</i>
C24	1930(4)	9773(3)	8029(3)	50(1)	1
C25	3196(4)	11115(4)	8961(4)	68(2)	1
N5	2682(3)	2905(3)	8496(2)	43(1)	1
N6	2845(3)	4048(2)	7296(2)	32(1)	1
N7	3225(3)	6617(2)	6313(2)	29(1)	1
N8	3696(3)	8204(2)	5921(2)	31(1)	1
O3	1169(2)	2534(2)	8160(2)	37(1)	1
O4	2096(2)	8548(2)	6521(2)	34(1)	1
C26	5575(5)	9555(3)	7269(4)	61(2)	1
C27	4661(4)	9270(3)	6912(3)	45(1)	1
C28	4880(3)	9268(3)	6042(3)	39(1)	1
C29	3980(3)	8992(2)	5673(3)	33(1)	1
C30	2790(3)	8039(2)	6353(2)	27(1)	1
C31	2623(3)	7239(2)	6616(2)	25(1)	1
C32	1882(3)	6952(2)	7195(2)	27(1)	1
C33	2055(3)	6134(2)	7234(2)	29(1)	1
C34	2881(3)	5941(2)	6680(3)	32(1)	1
C35	3452(3)	5182(3)	6446(3)	47(1)	1
C36	2730(3)	4520(2)	6683(3)	33(1)	1
C37	1838(3)	4320(2)	6405(3)	32(1)	1
C38	1392(3)	3704(2)	6876(3)	29(1)	1
C39	2028(3)	3541(2)	7433(2)	28(1)	1
C40	1935(3)	2965(2)	8047(2)	31(1)	1
C41	2670(5)	2350(4)	9125(3)	60(2)	1
C42	3264(6)	1612(5)	8884(5)	94(2)	1
C43	3322(8)	987(5)	9447(6)	115(3)	1
C44	3742(8)	252(6)	9076(6)	121(3)	1
C45	1104(3)	7411(3)	7726(3)	35(1)	1
C46	1460(3)	5616(3)	7830(3)	37(1)	1
C47	3793(5)	5172(3)	5576(4)	75(2)	1
C48	4441(4)	5098(3)	6834(4)	68(2)	1
C49	1386(4)	4698(3)	5747(3)	44(1)	1
C50	409(3)	3318(3)	6763(3)	38(1)	1
N9	3070(3)	2549(2)	4517(2)	30(1)	1
N10	4761(2)	2892(2)	2705(2)	30(1)	1
N11	5393(3)	3186(2)	69(2)	31(1)	1
C51	4553(5)	1521(3)	6801(3)	58(2)	1

Continued on next page

Continued from previous page

Atom	<i>x</i>	<i>y</i>	<i>z</i>	<i>U_{eq}</i>	<i>S.o.f</i>
C52	3832(4)	2128(3)	6499(3)	42(1)	1
C53	3724(4)	2003(3)	5669(3)	36(1)	1
C54	3054(3)	2619(3)	5339(2)	31(1)	1
C55	3888(3)	2773(2)	4014(3)	28(1)	1
C56	3893(3)	2671(2)	3203(2)	27(1)	1
C57	3207(3)	2365(2)	2760(2)	28(1)	1
C58	3693(3)	2403(2)	1991(2)	30(1)	1
C59	4647(3)	2738(2)	1973(2)	30(1)	1
C60	5492(3)	2897(3)	1303(3)	34(1)	1
C61	5038(3)	3333(2)	674(2)	26(1)	1
C62	4281(3)	3923(2)	693(2)	27(1)	1
C63	4174(3)	4125(3)	77(3)	34(1)	1
C64	4879(3)	3663(3)	543(3)	39(1)	1
C65	5087(3)	3631(3)	1361(3)	61(2)	1
N12A	6108(4)	3460(8)	1696(5)	53(2)	0.406(7)
C66A	6138(6)	3568(8)	2530(5)	48(1)	0.406(7)
C67A	7129(7)	3738(8)	2919(5)	48(1)	0.406(7)
C68A	7462(7)	3448(9)	3712(5)	48(1)	0.406(7)
C69A	6645(10)	3335(9)	4216(6)	48(1)	0.406(7)
N12B	5977(4)	3202(4)	1662(4)	53(2)	0.594(7)
C66B	6368(6)	2946(5)	2444(3)	48(1)	0.594(7)
C67B	7166(6)	3398(5)	2829(4)	48(1)	0.594(7)
C68B	7529(5)	3289(6)	3666(4)	48(1)	0.594(7)
C69B	6800(7)	2950(6)	4146(4)	48(1)	0.594(7)
C70	2166(3)	2027(3)	3036(3)	34(1)	1
C71	3229(4)	2133(3)	1314(3)	41(1)	1
C72	6349(4)	3386(4)	1535(3)	53(1)	1
C73	5992(4)	2104(3)	1032(3)	60(2)	1
C74	3696(3)	4312(3)	1383(3)	38(1)	1
C75	3458(4)	4761(3)	320(4)	62(2)	1
O5	4658(2)	3066(2)	4250(2)	32(1)	1
O6	4458(3)	3886(3)	1779(2)	89(2)	1

**A.5 Ethyl 5-(2-(5-(butylcarbamoyl)-3,4-dimethyl-1H-pyrrol
ol -2-yl)propan-2-yl)-3,4-dimethyl-1H-pyrrole-2-carbo-
xylate. 2.11(c)**

TABLE A.9: Crystal data and structure refinement details.

Identification code	03sot0144 (IE 120)
Empirical formula	C ₂₃ H ₃₅ N ₃ O ₃
Formula weight	401.54
Temperature	120(2) K
Wavelength	0.71073 Å
Crystal system	Monoclinic
Space group	<i>P</i> 2 ₁ <i>c</i>
Unit cell dimensions	$a = 13.788(2)$ Å $\alpha = 90^\circ$ $b = 17.251(3)$ Å $\beta = 107.786(9)^\circ$ $c = 9.9242(10)$ Å $\gamma = 90^\circ$
Volume	2247.8(6) Å ³
<i>Z</i>	4
Density (calculated)	1.187 Mg / m ³
Absorption coefficient	0.079 mm ⁻¹
<i>F</i> (000)	872
Crystal	Colourless needle
Crystal size	0.30 × 0.07 × 0.07 mm ³
θ range for data collection	3.10 - 23.26°
Index ranges	-15 ≤ <i>h</i> ≤ 15, -19 ≤ <i>k</i> ≤ 19, -11 ≤ <i>l</i> ≤ 10
Reflections collected	16670
Independent reflections	3195 [<i>R</i> _{int} = 0.2070]
Completeness to $\theta = 23.26^\circ$	99.1 %
Absorption correction	Semi empirical from equivalents
Max. and min. transmission	0.9945 and 0.9768
Refinement method	Full-matrix least-squares on <i>F</i> ²
Data / restraints / parameters	3195 / 72 / 265
Goodness-of-fit on <i>F</i> ²	1.065
Final <i>R</i> indices [$\theta > 2\sigma(\theta)$]	<i>R</i> 1 = 0.1281, <i>wR</i> 2 = 0.2857
<i>R</i> indices (all data)	<i>R</i> 1 = 0.1753, <i>wR</i> 2 = 0.3148
Extinction coefficient	0.0069(16)
Largest diff. peak and hole	0.651 and -0.607 e Å ³

TABLE A.10: Atomic coordinates ($\times 10^4$), equivalent isotropic displacement parameters ($\text{\AA}^2 \times 10^3$) and site occupancy factors. U_{eq} is defined as one third of the trace of the orthogonalized U^{ij} tensor.

Atom	x	y	z	U_{eq}	$S.o.f$
O1	4267(3)	2418(3)	4185(4)	35(1)	1
N1	4702(4)	2666(3)	6519(5)	35(2)	1
N2	3046(4)	1695(3)	6694(5)	32(1)	1
N3	188(5)	849(4)	8189(6)	45(2)	1
C1	6216(9)	4537(7)	9608(12)	99(4)	1
C2	5624(7)	4149(5)	8234(11)	73(3)	1
C3	6152(6)	3461(5)	7884(8)	53(2)	1
C4	5598(6)	3093(5)	6477(8)	50(2)	1
C5	4101(5)	2319(4)	5340(7)	32(2)	1
C6	3273(5)	1826(4)	5455(6)	32(2)	1
C7	2552(5)	1427(4)	4391(7)	32(2)	1
C8	1894(5)	1056(4)	5011(7)	38(2)	1
C9	2208(5)	1229(4)	6433(7)	37(2)	1
C10	1813(5)	948(4)	7620(7)	38(2)	1
C11	732(6)	1197(4)	7417(7)	40(2)	1
C12	123(6)	1787(5)	6647(7)	44(2)	1
C13	822(6)	1783(6)	6941(8)	52(2)	1
C14	724(5)	1218(5)	7882(7)	57(2)	1
C15A	1479(4)	897(3)	8610(5)	59(2)	0.50
O2A	1267(11)	219(4)	9317(9)	57(2)	0.50
O3A	2269(5)	1394(5)	8382(11)	57(2)	0.50
C16A	3000(10)	1313(10)	9090(16)	59(2)	0.50
C17A	3754(14)	649(10)	8486(18)	59(2)	0.50
C15B	1479(4)	897(3)	8610(5)	59(2)	0.50
O2B	1144(11)	414(6)	9724(8)	57(2)	0.50
O3B	2470(4)	1102(6)	8125(11)	57(2)	0.50
C16B	3059(10)	698(10)	8819(17)	59(2)	0.50
C17B	4095(10)	1083(11)	8094(18)	59(2)	0.50
C18	2514(6)	1355(4)	2859(7)	41(2)	1
C19	964(6)	589(5)	4212(8)	55(2)	1
C20	2466(6)	1229(5)	9070(7)	43(2)	1
C21	1883(6)	45(4)	7611(8)	51(2)	1
C22	355(7)	2371(5)	5651(9)	60(2)	1

Continued on next page

Continued from previous page

Atom	<i>x</i>	<i>y</i>	<i>z</i>	<i>U_{eq}</i>	<i>S.o.f</i>
C23	1680(6)	2345(7)	6340(10)	76(3)	1

A.6 Tetrakis(3-(1*H*-pyrrol-2-yl)pyridine)platinum(II) tetrafluoroborate. 3.1(b)

TABLE A.11: Crystal data and structure refinement details.

Identification code	05sot0165 (IE 243)	
Empirical formula	$C_{38}H_{38}B_2F_8N_{10}O_4Pt$ $C_{36}H_{32}N_8Pt \cdot 2BF_4 \cdot 2CH_3NO_2$	
Formula weight	1067.49	
Temperature	120(2) K	
Wavelength	0.71069 Å	
Crystal system	Triclinic	
Space group	<i>P</i> -1	
Unit cell dimensions	$a = 9.4410(3)$ Å	$\alpha = 77.568(2)^\circ$
	$b = 10.4860(3)$ Å	$\beta = 89.272(2)^\circ$
	$c = 11.2470(4)$ Å	$\gamma = 68.613(2)^\circ$
Volume	1009.80(6) Å ³	
<i>Z</i>	1	
Density (calculated)	1.755 Mg / m ³	
Absorption coefficient	3.566 mm ⁻¹	
<i>F</i> (000)	528	
Crystal	Prism; Pale Yellow	
Crystal size	0.1 × 0.07 × 0.04 mm ³	
θ range for data collection	2.93 - 27.48°	
Index ranges	-12 ≤ <i>h</i> ≤ 12, -13 ≤ <i>k</i> ≤ 13, -14 ≤ <i>l</i> ≤ 14	
Reflections collected	15299	
Independent reflections	4626 [<i>R</i> _{int} = 0.0362]	
Completeness to $\theta = 27.48^\circ$	99.6%	
Absorption correction	Semi empirical from equivalents	
Max. and min. transmission	0.8705 and 0.7169	
Refinement method	Full-matrix least-squares on <i>F</i> ²	
Data / restraints / parameters	4626 / 0 / 288	
Goodness-of-fit on <i>F</i> ²	1.075	
Final <i>R</i> indices [$\theta > 2\sigma(\theta)$]	<i>R</i> 1 = 0.0211, <i>wR</i> 2 = 0.0466	
<i>R</i> indices (all data)	<i>R</i> 1 = 0.0212, <i>wR</i> 2 = 0.0467	
Extinction coefficient	0.0038(5)	
Largest diff. peak and hole	0.511 and 0.887 e Å ³	

TABLE A.12: Atomic coordinates ($\times 10^4$), equivalent isotropic displacement parameters ($\text{\AA}^2 \times 10^3$) and site occupancy factors. U_{eq} is defined as one third of the trace of the orthogonalized U^{ij} tensor.

Atom	x	y	z	U_{eq}	$S.o.f$
C1	770(3)	-2814(2)	1568(2)	17(1)	1
C2	1674(3)	4160(3)	2160(2)	22(1)	1
C3	3221(3)	4656(2)	2021(2)	20(1)	1
C4	3863(3)	3798(2)	1277(2)	15(1)	1
C5	2880(2)	2451(2)	701(2)	13(1)	1
C6	5494(3)	4302(2)	1113(2)	16(1)	1
C7	6611(3)	5615(2)	1530(2)	19(1)	1
C8	8003(3)	5556(3)	1117(2)	20(1)	1
C9	7711(3)	4222(3)	464(3)	23(1)	1
C10	1526(3)	1030(2)	1606(2)	16(1)	1
C11	1749(3)	1530(3)	2604(2)	20(1)	1
C12	712(3)	1675(3)	3481(2)	19(1)	1
C13	558(3)	1314(2)	3368(2)	15(1)	1
C14	708(3)	811(2)	2349(2)	14(1)	1
C15	1668(3)	1482(2)	4291(2)	17(1)	1
C16	1758(3)	2079(3)	5281(2)	22(1)	1
C17	3049(3)	2013(3)	5882(2)	26(1)	1
C18	3723(3)	1386(3)	5255(2)	26(1)	1
C19	7169(4)	4179(3)	3756(3)	32(1)	1
B1	5907(3)	410(3)	1800(3)	18(1)	1
N1	1372(2)	1977(2)	846(2)	13(1)	1
N2	6196(2)	3471(2)	456(2)	22(1)	1
N3	308(2)	685(2)	1489(2)	13(1)	1
N4	2889(2)	1071(2)	4282(2)	20(1)	1
N5	7992(3)	3657(2)	4519(2)	25(1)	1
F1	5203(2)	1038(2)	1504(2)	36(1)	1
F2	6525(2)	817(2)	3009(1)	34(1)	1
F3	7083(2)	828(2)	1051(2)	36(1)	1
F4	4889(2)	1046(2)	1697(2)	32(1)	1
Pt1	0	0	0	11(1)	1
O1	7445(2)	3347(2)	5450(2)	33(1)	1
O2	9187(2)	3556(3)	4176(2)	45(1)	1

A.7 Tetrakis(3-(1*H*-pyrrol-2-yl)pyridine)platinum(II) methanesulfonate.

TABLE A.13: Crystal data and structure refinement details.

Identification code	2005sot0219 (IE 247)
Empirical formula	C ₃₈ H ₄₀ N ₈ O ₇ PtS ₂ C ₃₆ H ₃₂ N ₈ Pt.2SO ₃ CH ₃ .H ₂ O
Formula weight	979.99
Temperature	120(2) K
Wavelength	0.71073 Å
Crystal system	Triclinic
Space group	<i>P</i> -1
Unit cell dimensions	$a = 9.059$ Å $\alpha = 81.79^\circ$ $b = 10.489$ Å $\beta = 73.74^\circ$ $c = 11.080(4)$ Å $\gamma = 69.24^\circ$
Volume	944.0 Å ³
<i>Z</i>	1
Density (calculated)	1.724 Mg / m ³
Absorption coefficient	3.889 mm ⁻¹
<i>F</i> (000)	490
Crystal	Block; Orange
Crystal size	0.1 × 0.08 × 0.04 mm ³
θ range for data collection	3.49 - 27.48°
Index ranges	-11 ≤ <i>h</i> ≤ 11, -13 ≤ <i>k</i> ≤ 13, -14 ≤ <i>l</i> ≤ 14
Reflections collected	16456
Independent reflections	4313 [<i>R</i> _{int} = 0.0423]
Completeness to $\theta = 27.48^\circ$	99.6%
Absorption correction	Semi empirical from equivalents
Max. and min. transmission	0.8600 and 0.6971
Refinement method	Full-matrix least-squares on <i>F</i> ²
Data / restraints / parameters	4313 / 3 / 264
Goodness-of-fit on <i>F</i> ²	1.048
Final <i>R</i> indices [$\theta > 2\sigma(\theta)$]	<i>R</i> 1 = 0.0343, <i>wR</i> 2 = 0.0777
<i>R</i> indices (all data)	<i>R</i> 1 = 0.0357, <i>wR</i> 2 = 0.0785
Largest diff. peak and hole	0.693 and 0.812 e Å ³

TABLE A.14: Atomic coordinates ($\times 10^4$), equivalent isotropic displacement parameters ($\text{\AA}^2 \times 10^3$) and site occupancy factors. U_{eq} is defined as one third of the trace of the orthogonalized U^{ij} tensor.

Atom	x	y	z	U_{eq}	$S.o.f$
Pt1	5000	5000	0	34(1)	1
S1A	3230(2)	2060(1)	2812(1)	53(1)	0.60
O1A	2784(8)	3159(7)	1959(6)	70(1)	0.60
O2A	4645(8)	903(7)	2103(6)	70(1)	0.60
O3A	3911(8)	2344(7)	3779(6)	70(1)	0.60
C19A	1703(7)	1375(7)	3564(5)	70(2)	0.60
S1B	3230(2)	2060(1)	2812(1)	53(1)	0.40
O1B	2270(12)	3548(10)	3045(10)	70(1)	0.40
O2B	3531(12)	1813(10)	1538(9)	70(1)	0.40
O3B	4442(12)	1537(11)	3427(10)	70(1)	0.40
C19B	1703(7)	1375(7)	3564(5)	70(2)	0.40
N1	5154(4)	3999(3)	1480(3)	36(1)	1
N3	7248(4)	3754(3)	93(3)	34(1)	1
C14	7444(5)	2588(4)	812(3)	36(1)	1
N4	7831(5)	111(4)	2500(4)	52(1)	1
C6	6974(5)	4075(4)	4943(4)	40(1)	1
C4	6096(4)	3692(4)	3711(4)	37(1)	1
C10	8577(5)	4081(5)	547(4)	44(1)	1
C5	5901(4)	4357(4)	2638(3)	38(1)	1
C12	10318(5)	2049(5)	254(4)	48(1)	1
N2	7585(5)	5125(4)	5127(3)	52(1)	1
C13	8964(5)	1692(4)	928(4)	40(1)	1
C3	5455(5)	2643(4)	3534(4)	46(1)	1
C7	7384(6)	3516(5)	6080(4)	52(1)	1
C8	8269(6)	4245(5)	6969(4)	55(1)	1
C11	10116(5)	3244(5)	478(4)	49(1)	1
C15	9121(5)	452(4)	1752(4)	46(1)	1
C1	4564(5)	2967(4)	1319(4)	45(1)	1
C2	4706(6)	2266(5)	2334(4)	52(1)	1
C16	10506(6)	561(5)	1969(5)	60(1)	1
C9	8375(6)	5210(5)	6352(4)	56(1)	1
C18	8367(7)	1075(5)	3189(5)	62(1)	1
C17	10003(7)	1490(5)	2878(5)	65(1)	1

Continued on next page

Continued from previous page

Atom	<i>x</i>	<i>y</i>	<i>z</i>	<i>U_{eq}</i>	<i>S.o.f</i>
O4	6033(10)	0(9)	9899(8)	74(2)	0.50

A.8 Tetrakis(3-(1*H*-pyrrol-2-yl)pyridine)platinum(II) phosphorodifluoridate.

TABLE A.15: Crystal data and structure refinement details.

Identification code	2005sot0978 (IE 236)	
Empirical formula	C ₃₆ H ₃₂ F ₄ N ₈ O ₄ P ₂ Pt	
Formula weight	973.73	
Temperature	120(2) K	
Wavelength	0.71069 Å	
Crystal system	Triclinic	
Space group	<i>P</i> -1	
Unit cell dimensions	<i>a</i> = 9.7100(2) Å	α = 79.1790(17)°
	<i>b</i> = 9.9440(3) Å	β = 70.8470(17)°
	<i>c</i> = 10.8920(2) Å	γ = 64.6300(13)°
Volume	896.29(4) Å ³	
<i>Z</i>	1	
Density (calculated)	1.804 Mg / m ³	
Absorption coefficient	4.078 mm ⁻¹	
<i>F</i> (000)	480	
Crystal	Prism; Pale Orange	
Crystal size	0.3 × 0.08 × 0.05 mm ³	
θ range for data collection	2.93 - 27.48°	
Index ranges	-12 ≤ <i>h</i> ≤ 12, -12 ≤ <i>k</i> ≤ 12, -14 ≤ <i>l</i> ≤ 13	
Reflections collected	18322	
Independent reflections	4108 [<i>R</i> _{int} = 0.0382]	
Completeness to $\theta = 27.48^\circ$	99.8%	
Absorption correction	Semi empirical from equivalents	
Max. and min. transmission	0.8221 and 0.3743	
Refinement method	Full-matrix least-squares on <i>F</i> ²	
Data / restraints / parameters	4108 / 24 / 267	
Goodness-of-fit on <i>F</i> ²	1.025	
Final <i>R</i> indices [$\theta > 2\sigma(\theta)$]	<i>R</i> 1 = 0.0224, <i>wR</i> 2 = 0.0495	
<i>R</i> indices (all data)	<i>R</i> 1 = 0.0227, <i>wR</i> 2 = 0.0497	
Largest diff. peak and hole	0.490 and -0.660 e Å ³	

TABLE A.16: Atomic coordinates ($\times 10^4$), equivalent isotropic displacement parameters ($\text{\AA}^2 \times 10^3$) and site occupancy factors. U_{eq} is defined as one third of the trace of the orthogonalized U^{ij} tensor.

Atom	x	y	z	U_{eq}	$S.o.f$
Pt1	0	0	0	19(1)	1
N1	252(2)	867(2)	1782(2)	20(1)	1
N2	3600(3)	825(3)	5195(2)	30(1)	1
N3	688(2)	1577(2)	203(2)	19(1)	1
N4	2236(3)	4507(2)	3294(2)	25(1)	1
C1	1686(3)	1821(3)	1925(3)	25(1)	1
C2	1879(3)	2350(3)	3142(3)	28(1)	1
C3	620(3)	1890(3)	4230(3)	28(1)	1
C4	872(3)	891(3)	4097(2)	23(1)	1
C5	997(3)	420(3)	2839(2)	21(1)	1
C6	2227(3)	391(3)	5231(2)	25(1)	1
C7	2421(3)	1004(3)	6485(3)	31(1)	1
C8	3939(4)	135(3)	7222(3)	37(1)	1
C9	4644(4)	981(3)	6413(3)	35(1)	1
C10	2060(3)	1653(3)	537(3)	27(1)	1
C11	2535(3)	2701(3)	335(3)	30(1)	1
C12	1613(3)	3660(3)	637(3)	26(1)	1
C13	191(3)	3584(3)	1438(2)	22(1)	1
C14	223(3)	2523(3)	1170(2)	21(1)	1
C15	777(3)	4494(3)	2559(3)	23(1)	1
C16	435(4)	5366(3)	3154(3)	31(1)	1
C17	1701(4)	5911(3)	4261(3)	36(1)	1
C18	2794(3)	5370(3) 4327(3)	31(1)	1	
P1	4576(1)	3303(1)	1862(1)	29(1)	1
F1	6387(2)	4027(2)	2286(2)	55(1)	1
F2	4271(3)	4684(2)	1119(2)	61(1)	1
O2	4014(2)	2995(2)	3021(2)	31(1)	1
O3	4042(3)	2168(3)	964(2)	50(1)	1

A.9 Tetrakis(2-hydroxypyridine)platinum(II) hexafluorophosphate.

TABLE A.17: Crystal data and structure refinement details.

Identification code	02SOT155 (IE 20)
Empirical formula	$C_{20}H_{20}F_6N_4O_4PPt$
Formula weight	720.46
Temperature	120(2) K
Wavelength	0.71073 Å
Crystal system	Tetragonal
Space group	$P4/mmm$
Unit cell dimensions	$a = 10.85350(10)$ Å $b = 10.85350(10)$ Å $c = 6.7924(2)$ Å
Volume	800.13(3) Å ³
Z	1
Density (calculated)	1.495 Mg / m ³
Absorption coefficient	4.495 mm ⁻¹
$F(000)$	347
Crystal	Colourless Block
Crystal size	0.1 × 0.1 × 0.1 mm ³
θ range for data collection	3.00 - 25.00°
Index ranges	$-12 \leq h \leq 12, -12 \leq k \leq 12, -8 \leq l \leq 8$
Reflections collected	8088
Independent reflections	460 [$R_{int} = 0.0541$]
Completeness to $\theta = 25.00^\circ$	99.6%
Absorption correction	Semi empirical from equivalents
Max. and min. transmission	0.8221 and 0.3743
Refinement method	Full-matrix least-squares on F^2
Data / restraints / parameters	460 / 0 / 39
Goodness-of-fit on F^2	1.577
Final R indices [$\theta > 2\sigma(\theta)$]	$R1 = 0.0424, wR2 = 0.1422$
R indices (all data)	$R1 = 0.0424, wR2 = 0.1422$
Largest diff. peak and hole	1.945 and -0.911 e Å ⁻³

TABLE A.18: Atomic coordinates ($\times 10^4$), equivalent isotropic displacement parameters ($\text{Å}^2 \times 10^3$) and site occupancy factors. U_{eq} is defined as one third of the trace of the orthogonalized U^{ij} tensor.

Atom	<i>x</i>	<i>y</i>	<i>z</i>	<i>U_{eq}</i>	<i>S.o.f</i>
Pt1	0	0	0	32(1)	1
N1	1319(9)	1319(9)	0	39(3)	1
O1	1291(17)	1291(17)	3340(40)	98(8)	0.50
C1	1765(8)	1765(8)	1700(20)	57(3)	1
C2	2665(12)	2665(12)	1720(30)	89(5)	1
C3	3134(15)	3134(15)	0	92(8)	1
P1	5000	5000	5000	34(2)	1
F1	5000	5000	2660(20)	61(4)	1
F2	5000	3527(9)	5000	53(2)	1

A.10 Tetrakis(*N*-butyl-6-methoxynicotinamide)platinum(II) tetrafluoroborate. 3.17(c)

TABLE A.19: Crystal data and structure refinement details.

Identification code	crb54 (IE 188)	
Empirical formula	C ₄₈ H ₇₀ B ₂ F ₈ N ₁₀ O ₈ Pt	
Formula weight	1283.85	
Temperature	173(2) K	
Wavelength	0.71073 Å	
Crystal system	Triclinic	
Space group	<i>P</i> -1	
Unit cell dimensions	$a = 9.193(5)$ Å	$\alpha = 94.230(6)^\circ$
	$b = 10.222(5)$ Å	$\beta = 97.314(6)^\circ$
	$c = 15.574(8)$ Å	$\gamma = 97.086(6)^\circ$
Volume	1434.5(13) Å ³	
<i>Z</i>	1	
Density (calculated)	1.486 Mg / m ³	
Absorption coefficient	2.529 mm ⁻¹	
<i>F</i> (000)	652	
Crystal	Colourless Block	
Crystal size	0.1 × 0.1 × 0.1 mm ³	
θ range for data collection	2.25 - 25.00°	
Index ranges	-10 ≤ <i>h</i> ≤ 10, -12 ≤ <i>k</i> ≤ 12, -18 ≤ <i>l</i> ≤ 18	
Reflections collected	13743	
Independent reflections	5032 [<i>R</i> _{int} = 0.0286]	
Completeness to $\theta = 25.00^\circ$	99.6%	
Absorption correction	Semi empirical from equivalents	
Refinement method	Full-matrix least-squares on <i>F</i> ²	
Data / restraints / parameters	5032 / 0 / 361	
Goodness-of-fit on <i>F</i> ²	1.065	
Final <i>R</i> indices [$\theta > 2\sigma(\theta)$]	<i>R</i> 1 = 0.0245, <i>wR</i> 2 = 0.0624	
<i>R</i> indices (all data)	<i>R</i> 1 = 0.0245, <i>wR</i> 2 = 0.0624	
Largest diff. peak and hole	1.139 and -0.494 e Å ³	

TABLE A.20: Atomic coordinates ($\times 10^4$), equivalent isotropic displacement parameters ($\text{\AA}^2 \times 10^3$) and site occupancy factors. U_{eq} is defined as one third of the trace of the orthogonalized U^{ij} tensor.

Atom	<i>x</i>	<i>y</i>	<i>z</i>	U_{eq}	<i>S.o.f</i>
C19	1.4011(5)	-0.1317(4)	0.6614(2)	0.0521(10)	1
H19A	1.3405	-0.2177	0.6403	0.062	1
H19B	1.5063	-0.1463	0.6695	0.062	1
C20	1.3786(6)	-0.0349(6)	0.5936(3)	0.0827(16)	1
H20A	1.4520	0.0449	0.6113	0.099	1
H20B	1.4023	-0.0753	0.5382	0.099	1
C21	1.2355(7)	0.0078(7)	0.5765(4)	0.0961(19)	1
H21A	1.2131	0.0533	0.6306	0.115	1
H21B	1.1606	-0.0714	0.5608	0.115	1
C22	1.2201(8)	0.0992(7)	0.5053(4)	0.111(2)	1
H22A	1.1195	0.1232	0.4980	0.166	1
H22B	1.2390	0.0545	0.4508	0.166	1
H22C	1.2916	0.1794	0.5207	0.166	1
F1	1.0997(4)	0.2653(3)	0.33767(18)	0.0928(10)	1
F2	0.8968(4)	0.3702(3)	0.3337(2)	0.0872(9)	1
F3	1.0704(3)	0.4235(3)	0.24922(19)	0.0714(7)	1
F4	0.9233(3)	0.2313(3)	0.22017(16)	0.0704(7)	1
B1	0.9980(6)	0.3224(4)	0.2869(3)	0.0488(10)	1
N1S	1.1210(10)	-0.2992(6)	0.4065(4)	0.149(3)	1
C1S	1.1625(8)	-0.3802(6)	0.4433(4)	0.0853(17)	1
C2S	1.2137(8)	-0.4857(6)	0.4897(4)	0.0808(16)	1
H2SA	1.174(8)	-0.484(7)	0.550(5)	0.13(2)	1
H2SB	1.183(11)	-0.572(10)	0.448(7)	0.20(4)	1
H2SC	1.349(9)	-0.458(8)	0.506(5)	0.16(3)	1

A.11 N-butyl-6-hydroxynicotinamide.

TABLE A.21: Crystal data and structure refinement details.

Identification code	03SOT126 (IE 174)
Empirical formula	C ₁₀ H ₁₂ N ₂ O ₂
Formula weight	192.22
Temperature	120(2) K
Wavelength	0.71069 Å
Crystal system	Monoclinic
Space group	C2/c
Unit cell dimensions	$a = 7.232(5)$ Å $b = 7.136(5)$ Å $\beta = 90.733(5)^\circ$ $c = 37.510(5)$ Å
Volume	1935.6(19) Å ³
Z	8
Density (calculated)	1.319 Mg / m ³
Absorption coefficient	0.094 mm ⁻¹
$F(000)$	816
Crystal	Colourless Plate
Crystal size	0.2 × 0.1 × 0.02 mm ³
θ range for data collection	4.01 - 25.02°
Index ranges	-7 ≤ h ≤ 7, -7 ≤ k ≤ 7, -44 ≤ l ≤ 44
Reflections collected	2534
Independent reflections	719 [$R_{int} = 0.0568$]
Completeness to $\theta = 25.02^\circ$	42.4%
Absorption correction	Semi empirical from equivalents
Max. and min. transmission	0.9981 and 0.9815
Refinement method	Full-matrix least-squares on F^2
Data / restraints / parameters	719 / 0 / 129
Goodness-of-fit on F^2	1.048
Final R indices [$\theta > 2\sigma(\theta)$]	$R1 = 0.0430$, $wR2 = 0.0953$
R indices (all data)	$R1 = 0.0638$, $wR2 = 0.1032$
Largest diff. peak and hole	0.128 and -0.139 e Å ³

TABLE A.22: Atomic coordinates ($\times 10^4$), equivalent isotropic displacement parameters ($\text{Å}^2 \times 10^3$) and site occupancy factors. U_{eq} is defined as one third of the trace of the orthogonalized U^{ij} tensor.

Atom	x	y	z	U_{eq}	$S.o.f$
C1	6667(5)	2249(5)	7225(1)	23(1)	1

Continued on next page

Continued from previous page

Atom	<i>x</i>	<i>y</i>	<i>z</i>	<i>U</i>_{eq}	<i>S.o.f</i>
C2	5849(5)	806(5)	7009(1)	26(1)	1
C3	4767(5)	1248(6)	6723(1)	25(1)	1
C4	4444(5)	3121(6)	6623(1)	22(1)	1
C5	5204(5)	4472(6)	6832(1)	24(1)	1
C6	3183(5)	3569(6)	6320(1)	25(1)	1
C7	2231(5)	5889(5)	5870(1)	27(1)	1
C8	2784(5)	7814(5)	5749(1)	27(1)	1
C9	1554(5)	8568(5)	5452(1)	29(1)	1
C10	2225(5)	10445(5)	5311(1)	39(1)	1
N1	6249(4)	4047(4)	7119(1)	24(1)	1
N2	3457(4)	5201(5)	6151(1)	26(1)	1
O1	7683(4) 2028(3)	7492(1)	32(1)	1	
O2	1905(3)	2491(3)	6229(1)	31(1)	1

A.12 7,11a-diaza-1-(1H-pyrrole-2-carbonyl)-1H-azuleno[6,5,4-ij]isoquinolin-8(7H,11aH,11bH)-one.

TABLE A.23: Crystal data and structure refinement details.

Identification code	04sot0969 (IE 218)
Empirical formula	C ₂₂ H ₂₃ N ₄ O _{3.50} C ₁₉ H ₁₄ N ₄ O _{2.5} EtOH
Formula weight	399.44
Temperature	120(2) K
Wavelength	0.71073 Å
Crystal system	Triclinic
Space group	<i>P</i> -1
Unit cell dimensions	$a = 7.3578(13)$ Å $\alpha = 93.912(12)^\circ$ $b = 10.822(2)$ Å $\beta = 100.365(12)^\circ$ $c = 12.9449(13)$ Å $\gamma = 102.947(16)^\circ$
Volume	981.8(3) Å ³
<i>Z</i>	2
Density (calculated)	1.351 Mg / m ³
Absorption coefficient	0.094 mm ⁻¹
<i>F</i> (000)	422
Crystal	Slab; Colourless
Crystal size	0.37 × 0.15 × 0.05 mm ³
θ range for data collection	3.22 - 27.73°
Index ranges	-9 ≤ <i>h</i> ≤ 9, -14 ≤ <i>k</i> ≤ 14, -16 ≤ <i>l</i> ≤ 16
Reflections collected	16705
Independent reflections	4525 [<i>R</i> _{int} = 0.0452]
Completeness to $\theta = 27.50^\circ$	99.5%
Absorption correction	Semi empirical from equivalents
Max. and min. transmission	0.9953 and 0.9662
Refinement method	Full-matrix least-squares on <i>F</i> ²
Data / restraints / parameters	4525 / 0 / 274
Goodness-of-fit on <i>F</i> ²	1.057
Final <i>R</i> indices [$\theta > 2\sigma(\theta)$]	<i>R</i> 1 = 0.0676, <i>wR</i> 2 = 0.1826
<i>R</i> indices (all data)	<i>R</i> 1 = 0.1180, <i>wR</i> 2 = 0.2108
Largest diff. peak and hole	0.926 and -0.310 e Å ³

TABLE A.24: Atomic coordinates ($\times 10^4$), equivalent isotropic displacement parameters ($\text{\AA}^2 \times 10^3$) and site occupancy factors. U_{eq} is defined as one third of the trace of the orthogonalized U^{ij} tensor.

Atom	x	y	z	U_{eq}	$S.o.f$
C1	2570(4)	2712(3)	7794(2)	37(1)	1
C2	2104(4)	2627(3)	8742(2)	37(1)	1
C3	2303(3)	3761(2)	9463(2)	30(1)	1
C4	2053(3)	3717(3)	10506(2)	32(1)	1
C5	2230(3)	4832(3)	11144(2)	31(1)	1
C6	2616(3)	5994(3)	10759(2)	32(1)	1
C7	2853(3)	6056(2)	9713(2)	28(1)	1
C8	2751(3)	4947(2)	9083(2)	27(1)	1
C9	3043(3)	5055(2)	7967(2)	28(1)	1
C10	116(4)	4854(3)	6505(2)	37(1)	1
C11	965(4)	5678(3)	6137(2)	45(1)	1
C12	275(4)	6831(3)	6784(2)	42(1)	1
C13	1214(4)	6693(3)	7552(2)	33(1)	1
C14	2335(4)	7632(3)	8421(2)	36(1)	1
C15	4192(3)	4041(3)	6603(2)	31(1)	1
C16	4868(4)	3000(3)	6166(2)	38(1)	1
C17	5444(5)	1962(3)	6543(2)	50(1)	1
C18	6244(6)	1433(3)	5776(3)	64(1)	1
C19	6142(5)	2144(3)	4946(2)	59(1)	1
N1	3274(3)	3885(2)	7450(1)	31(1)	1
N2	3207(3)	7274(2)	9336(2)	33(1)	1
N3	1424(3)	5473(2)	7369(1)	32(1)	1
N4	5323(4)	3091(2)	5177(2)	42(1)	1
O1	2470(3)	8785(2)	8342(1)	47(1)	1
O2	4434(2)	5079(2)	6248(1)	33(1)	1
O3	5740(3)	10699(2)	8979(2)	42(1)	1
C20	7317(5)	10092(3)	9118(2)	53(1)	1
C21	7693(6)	9583(4)	8126(3)	75(1)	1
C22	39(8)	9503(4)	5373(4)	103(2)	1
O4	1269(11)	9925(5)	6501(4)	104(2)	0.50

A.13 N-(isoquinolin-8-yl)-1H-pyrrole-2-carboxamide.

TABLE A.25: Crystal data and structure refinement details.

Identification code	04sot0969 (IE 257)
Empirical formula	C ₁₄ H ₁₁ N ₃ O
Formula weight	237.26
Temperature	120(2) K
Wavelength	0.71073 Å
Crystal system	Monoclinic
Space group	<i>P</i> 2 ₁ / <i>n</i>
Unit cell dimensions	<i>a</i> = 11.673(8) Å <i>b</i> = 4.0749(14) Å <i>β</i> = 93.85(6)° <i>c</i> = 23.609(19) Å
Volume	1120.5(12) Å ³
<i>Z</i>	4
Density (calculated)	1.406 Mg / m ³
Absorption coefficient	0.093 mm ⁻¹
<i>F</i> (000)	496
Crystal	Blade; Colourless
Crystal size	0.12 × 0.03 × 0.02 mm ³
<i>θ</i> range for data collection	3.46 - 26.37°
Index ranges	-14 ≤ <i>h</i> ≤ 14, -5 ≤ <i>k</i> ≤ 4, -29 ≤ <i>l</i> ≤ 24
Reflections collected	10485
Independent reflections	2202 [<i>R</i> _{int} = 0.1701]
Completeness to <i>θ</i> = 26.37°	96.5%
Absorption correction	Semi empirical from equivalents
Max. and min. transmission	0.9982 and 0.9890
Refinement method	Full-matrix least-squares on <i>F</i> ²
Data / restraints / parameters	2202 / 0 / 164
Goodness-of-fit on <i>F</i> ²	1.008
Final <i>R</i> indices [<i>θ</i> > 2σ(<i>θ</i>)]	<i>R</i> 1 = 0.0824, <i>wR</i> 2 = 0.1493
<i>R</i> indices (all data)	<i>R</i> 1 = 0.2154, <i>wR</i> 2 = 0.1931
Largest diff. peak and hole	0.326 and -0.221 e Å ³

TABLE A.26: Atomic coordinates (× 10⁴), equivalent isotropic displacement parameters (Å² × 10³) and site occupancy factors. U_{eq} is defined as one third of the trace of the orthogonalized U^{*ij*} tensor.

Atom	<i>x</i>	<i>y</i>	<i>z</i>	<i>U_{eq}</i>	<i>S.o.f</i>
C1	1349(4)	5915(10)	740(2)	45(1)	1
C2	146(4)	6438(10)	690(2)	46(1)	1
C3	551(4)	5238(10)	1087(2)	47(1)	1
C4	62(4)	3439(9)	1552(2)	40(1)	1
C5	731(4)	2141(10)	1979(2)	44(1)	1
C6	232(4)	372(10)	2409(2)	43(1)	1
C7	1560(4)	980(9)	2079(2)	40(1)	1
C8	1136(3)	2869(9)	1606(2)	36(1)	1
C9	1846(4)	4161(10)	1182(2)	40(1)	1
C10	3788(4)	3449(10)	822(2)	44(1)	1
C11	4903(4)	1971(10)	980(2)	41(1)	1
C12	5270(4)	145(10)	1439(2)	43(1)	1
C13	6421(4)	810(10)	1366(2)	51(1)	1
C14	6701(4)	477(10)	852(2)	47(1)	1
N1	924(3)	250(7)	2476(2)	42(1)	1
N2	3037(3)	3567(8)	1246(1)	44(1)	1
N3	5776(3)	2145(8)	624(2)	47(1)	1
O1	3537(3)	4450(7)	338(1)	54(1)	1

A.14 3,4-dimethyl-*N*-((pyridin-3-yl)methyl)-1*H*-pyrrole-2-carboxamide.

TABLE A.27: Crystal data and structure refinement details.

Identification code	04sot0969 (IE 250)
Empirical formula	C ₁₃ H ₁₅ N ₃ O
Formula weight	229.28
Temperature	120(2) K
Wavelength	0.71073 Å
Crystal system	Monoclinic
Space group	<i>P</i> 2 ₁ / <i>n</i>
Unit cell dimensions	<i>a</i> = 8.6560(8) Å <i>b</i> = 6.2887(11) Å <i>β</i> = 91.601(10)° <i>c</i> = 21.576(2) Å
Volume	1174.0(3) Å ³
<i>Z</i>	4
Density (calculated)	1.297 Mg / m ³
Absorption coefficient	0.085 mm ⁻¹
<i>F</i> (000)	488
Crystal	Block; Colourless
Crystal size	0.2 × 0.1 × 0.08 mm ³
<i>θ</i> range for data collection	3.37 - 27.48°
Index ranges	-11 ≤ <i>h</i> ≤ 11, -8 ≤ <i>k</i> ≤ 8, -27 ≤ <i>l</i> ≤ 27
Reflections collected	12213
Independent reflections	2682 [<i>R</i> _{int} = 0.0608]
Completeness to <i>θ</i> = 27.48°	99.7%
Absorption correction	Semi empirical from equivalents
Max. and min. transmission	0.9932 and 0.9832
Refinement method	Full-matrix least-squares on <i>F</i> ²
Data / restraints / parameters	2682 / 0 / 165
Goodness-of-fit on <i>F</i> ²	1.031
Final <i>R</i> indices [<i>θ</i> > 2σ(<i>θ</i>)]	<i>R</i> 1 = 0.0492, <i>wR</i> 2 = 0.1079
<i>R</i> indices (all data)	<i>R</i> 1 = 0.0981, <i>wR</i> 2 = 0.1298
Extinction coefficient	0.015(3)
Largest diff. peak and hole	0.208 and -0.224 e Å ³

TABLE A.28: Atomic coordinates ($\times 10^4$), equivalent isotropic displacement parameters ($\text{\AA}^2 \times 10^3$) and site occupancy factors. U_{eq} is defined as one third of the trace of the orthogonalized U^{ij} tensor.

Atom	x	y	z	U_{eq}	$S.o.f$
C1	6606(2)	555(3)	4666(1)	25(1)	1
C2	7772(2)	1740(3)	5347(1)	34(1)	1
C3	7343(2)	3462(3)	4988(1)	36(1)	1
C4	6512(2)	3118(3)	4441(1)	29(1)	1
C5	6134(2)	1053(3)	4268(1)	22(1)	1
C6	5206(2)	560(3)	3682(1)	25(1)	1
C7	3926(2)	3652(3)	3197(1)	22(1)	1
C8	2561(2)	5028(3)	3162(1)	21(1)	1
C9	1058(2)	4899(3)	3371(1)	22(1)	1
C10	292(2)	6794(3)	3181(1)	22(1)	1
C11	1345(2)	7990(3)	2864(1)	24(1)	1
C12	299(2)	3111(3)	3712(1)	28(1)	1
C13	1333(2)	7430(3)	3313(1)	29(1)	1
N1	7412(2)	268(3)	5198(1)	31(1)	1
N2	3898(2)	1982(2)	3587(1)	23(1)	1
N3	2705(2)	6929(2)	2853(1)	22(1)	1
O1	5066(1)	4051(2)	2877(1)	28(1)	1

A.15 N-((pyridin-3-yl)methyl)-1H-pyrrole-2-carboxamide.

TABLE A.29: Crystal data and structure refinement details.

Identification code	04sot0969 (IE 253)
Empirical formula	C ₁₁ H ₁₁ N ₃ O
Formula weight	201.23
Temperature	120(2) K
Wavelength	0.71073 Å
Crystal system	Monoclinic
Space group	<i>P</i> 2 ₁ / <i>n</i>
Unit cell dimensions	<i>a</i> = 6.8373(10) Å <i>b</i> = 7.2747(14) Å <i>β</i> = 98.895(13)° <i>c</i> = 20.329(3) Å
Volume	999.0(3) Å ³
<i>Z</i>	4
Density (calculated)	1.338 Mg / m ³
Absorption coefficient	0.090 mm ⁻¹
<i>F</i> (000)	424
Crystal	Block; Colourless
Crystal size	0.13 × 0.1 × 0.05 mm ³
<i>θ</i> range for data collection	3.33 - 27.48°
Index ranges	-8 ≤ <i>h</i> ≤ 8, -9 ≤ <i>k</i> ≤ 9, -26 ≤ <i>l</i> ≤ 26
Reflections collected	20925
Independent reflections	2281 [<i>R</i> _{int} = 0.0557]
Completeness to <i>θ</i> = 27.48°	99.8%
Absorption correction	Semi empirical from equivalents
Max. and min. transmission	0.9955 and 0.9884
Refinement method	Full-matrix least-squares on <i>F</i> ²
Data / restraints / parameters	2281 / 0 / 136
Goodness-of-fit on <i>F</i> ²	0.953
Final <i>R</i> indices [<i>θ</i> > 2σ(<i>θ</i>)]	<i>R</i> 1 = 0.0584, <i>wR</i> 2 = 0.1545
<i>R</i> indices (all data)	<i>R</i> 1 = 0.0969, <i>wR</i> 2 = 0.1841
Largest diff. peak and hole	0.579 and -0.260 e Å ³

TABLE A.30: Atomic coordinates ($\times 10^4$), equivalent isotropic displacement parameters ($\text{\AA}^2 \times 10^3$) and site occupancy factors. U_{eq} is defined as one third of the trace of the orthogonalized U^{ij} tensor.

Atom	<i>x</i>	<i>y</i>	<i>z</i>	U_{eq}	<i>S.o.f</i>
C1	4193(3)	7651(3)	935(1)	53(1)	1
C2	2550(3)	7132(3)	101(1)	60(1)	1
C3	4259(4)	7315(3)	368(1)	63(1)	1
C4	5989(3)	7706(3)	47(1)	59(1)	1
C5	5979(3)	7878(3)	720(1)	47(1)	1
C6	7845(3)	8280(3)	1199(1)	56(1)	1
C7	8810(3)	5362(3)	1715(1)	48(1)	1
C8	10151(3)	3813(3)	1759(1)	45(1)	1
C9	11851(3)	3470(3)	1498(1)	54(1)	1
C10	12566(3)	1780(3)	1729(1)	63(1)	1
C11	11285(3)	1114(3)	2116(1)	60(1)	1
N1	2478(3)	7283(3)	540(1)	60(1)	1
N2	9152(2)	6720(3)	1313(1)	53(1)	1
N3	9843(3)	2343(3)	2133(1)	54(1)	1
O1	7422(2)	5402(2)	2039(1)	67(1)	1

Bibliography

- [1] Lehn, J. M. *Angew. Chem. Int. Ed.*, **1988**, *27*, 89–112.
- [2] Lehn, J. M. *J. Inclusion. Phenom.*, **1988**, *6*, 351–396.
- [3] Lehn, J. M. *Chem. Scripta*, **1988**, *28*, 237–262.
- [4] Lehn, J. M. *Prix Nobel*, **1988**, 129–176.
- [5] Fleischer, E. B.; Tasker, P. A. *J. Am. Chem. Soc.*, **1970**, *92*, 7072–7077.
- [6] Cabbiness, D. K.; Margerum, D. W. *J. Am. Chem. Soc.*, **1970**, *92*, 2151–2153.
- [7] Pedersen, C. J. *J. Am. Chem. Soc.*, **1970**, *92*, 391–394.
- [8] Pedersen, C. J. *J. Am. Chem. Soc.*, **1970**, *92*, 386–391.
- [9] Pedersen, C. J. *J. Am. Chem. Soc.*, **1967**, *89*, 7017–7036.
- [10] Gale, P. A.; Light, M. E.; Quesada, R. *Chem. Commun.*, **2005**, 5864–5866.
- [11] Desiraju, G. R. *Nature*, **2001**, *412*, 397–400.
- [12] Poerschke, D. *Biologie*, **1971**, *1*, 68–79.
- [13] Pflugrath, J. W.; Quioco, F. A. *Nature*, **1985**, *314*, 257–260.
- [14] Jacobson, B. L.; He, J. J.; Vermersch, P. S.; Lemon, D. D.; Quioco, F. A. *J. Biol. Chem.*, **1991**, *266*, 5220–5225.
- [15] Hunter, C. A.; Sanders, J. K. M. *J. Am. Chem. Soc.*, **1990**, *112*, 5525–5534.
- [16] Steed, J. W.; Atwood, J. L. *Supramolecular Chemistry*. John Wiley & Sons Inc, New York, 1st edition, **2000**.
- [17] Beer, P. D.; Gale, P. A. *Angew. Chem.-Int. Edit.*, **2001**, *40*, 486–516.
- [18] Bianchi, A.; Bowman-James, K.; García-España, E. *Supramolecular Chemistry of Anions*. Wiley-VCH, New York, **1997**.
- [19] Gale, P. A. *Coord. Chem. Rev.*, **2000**, *199*, 181–233.

- [20] Gale, P. A. *Coord. Chem. Rev.*, **2001**, *213*, 79–128.
- [21] Gale, P. A. *Coord. Chem. Rev.*, **2003**, *240*, 191–221.
- [22] Camargo, J. A.; Alonso, A.; de la Puente, V. M. *Water Research*, **2005**, *39*, 3376–3384.
- [23] Ozawa, M.; Ishida, M.; Sano, Y. *Radiochemistry*, **2003**, *45*, 225–232.
- [24] Copplestone, D.; Jackson, D.; Hartnoll, R. G.; Johnson, M. S.; McDonald, P.; Wood, N. *J. Environ. Radioact.*, **2004**, *73*, 29–48.
- [25] Holloway, J. M.; Dahlgren, R. A.; Hansen, B.; Casey, W. H. *Nature*, **1998**, *395*, 785–788.
- [26] Tejada, L.; Oster, J. R.; Singer, I.; Bourgoignie, J. J.; Fishman, L. M.; Roos, B. A. *Am. J. Med. Sci.*, **1995**, *310*, 167–74.
- [27] Littler, B. J.; Miller, M. A.; Hung, C. H.; Wagner, R. W.; OShea, D. F.; Boyle, P. D.; Lindsey, J. S. *J. Am. Soc. Nephrol.*, **2000**, *11*, 778–783.
- [28] Zager, R. A. *J. Lab. Clin. Med.*, **1982**, *100*, 230–239.
- [29] Sutters, M.; Gaboury, C. L.; Bennett, W. M. *J. Am. Soc. Nephrol.*, **1996**, *7*, 2056–2061.
- [30] Schucker, J. J.; Ward, K. E. *Am. J. Health Syst. Pharm.*, **2005**, *62*, 2355–2361.
- [31] Wang, Z.; Luecke, H.; Yao, N.; Quioco, F. A. *Nat. Struct. Biol.*, **1997**, *4*, 519–521.
- [32] Hosseini, M. W.; Lehn, J. M.; Maggiora, L.; Mertes, K. B.; Mertes, M. P. *J. Am. Chem. Soc.*, **1987**, *109*, 537–544.
- [33] Goodman, M. S.; Jubian, V.; Hamilton, A. D. *J. Am. Chem. Soc.*, **1995**, *117*, 11610–11611.
- [34] Goodman, M. S.; Jubian, V.; Hamilton, A. D. *Tetrahedron Lett.*, **1995**, *36*, 2551–2554.
- [35] Uppadine, L. H.; Drew, M. G. B.; Beer, P. D. *Chem. Commun.*, **2001**, 291–292.
- [36] Bondy, C. R.; Gale, P. A.; Loeb, S. J. *Chem. Commun.*, **2001**, 729–730.
- [37] Bondy, C. R.; Gale, P. A.; Loeb, S. J. *J. Supramol. Chem.*, **2002**, *2*, 93–96.
- [38] Bondy, C. R.; Gale, P. A.; Loeb, S. J. *J. Am. Chem. Soc.*, **2004**, *126*, 5030–5031.
- [39] Wallace, K. J.; Daari, R.; Belcher, W. J.; Abouderbala, L. O.; Boutelle, M. G.; Steed, J. W. *J. Organomet. Chem.*, **2003**, *666*, 63–74.

- [40] Nieto, S.; Perez, J.; Riera, V.; Miguel, D.; Alvarez, C. *Chem. Commun.*, **2005**, 546–548.
- [41] Renard, S. L.; Kilner, C. A.; Fisher, J.; Halcrow, M. A. *J. Chem. Soc., Dalton Trans.*, **2002**, *22*, 4206–4212.
- [42] Renard, S. L.; Franken, A.; Kilner, C. A.; Kennedy, J. D.; Halcrow, M. A. *New J. Chem.*, **2002**, *26*, 1634–1637.
- [43] Turner, D. R.; Spencer, E. C.; Howard, J. A. K.; Tocher, D. A.; Steed, J. W. *Chem. Commun.*, **2004**, 1352–1353.
- [44] Turner, D. R.; Smith, B.; Spencer, E. C.; Goeta, A. E.; Evans, I. R.; Tocher, D. A.; Howard, J. A. K.; Steed, J. W. *New J. Chem.*, **2005**, *29*, 90–98.
- [45] Harding, L. P.; Jeffery, J. C.; Riis-Johannessen, T.; Rice, C. R.; Zeng, Z. *Chem. Commun.*, **2004**, 654–655.
- [46] Harding, L. P.; Jeffery, J. C.; Riis-Johannessen, T.; Rice, C. R.; Zeng, Z. *Dalton Trans.*, **2004**, 2396–2397.
- [47] Coles, S. J.; Gale, P. A.; Hursthouse, M. B. *Cryst. Eng. Commun.*, **2001**, *53*, 1–3.
- [48] Gale, P. A.; Camiolo, S.; Tizzard, G. J.; Chapman, C. P.; Light, M. E.; Coles, S. J.; Hursthouse, M. B. *J. Org. Chem.*, **2001**, *66*, 7849–7853.
- [49] Schmuck, C.; Dudaczek, J. *Tetrahedron Lett.*, **2005**, *46*, 7101–7105.
- [50] Mahoney, J. M.; Marshall, R. A.; Beatty, A. M.; Smith, B. D.; Camiolo, S.; Gale, P. A. *J. Supramol. Chem.*, **2001**, *1*, 289–292.
- [51] Scherer, M.; Sessler, J. L.; Gebauer, A.; Lynch, V. *Chem. Commun.*, **1998**, 85–86.
- [52] Baeyer, A. *Ber. Dtsch. Chem. Ges.*, **1886**, *19*, 2184–2185.
- [53] Bates, G. W.; Gale, P. A.; Light, M. E. *Cryst. Eng. Comm.*, **2006**, *8*, 300–302.
- [54] Warriner, C. N.; Gale, P. A.; Light, M. E.; Hursthouse, M. B. *Chem. Commun.*, **2003**, *15*, 1810–1811.
- [55] Sessler, J. L.; Camiolo, S.; Gale, P. A. *Coord. Chem. Rev.*, **2003**, *240*, 17–55.
- [56] Gale, P. A.; Jr., P. A.; Sessler, J. L. *Coord. Chem. Rev.*, **2001**, *222*, 57–102.
- [57] Gale, P. A.; Camiolo, S.; Chapman, C. P.; Light, M. E.; Hursthouse, M. B. *Tetrahedron Lett.*, **2001**, *42*, 5095–5097.
- [58] Camiolo, S.; Gale, P. A.; Hursthouse, M. B.; Light, M. E. *Tetrahedron Lett.*, **2002**, *43*, 6995–6996.

- [59] Denuault, G.; Gale, P. A.; Hursthouse, M. B.; Light, M. E.; Warriner, C. N. *New J. Chem.*, **2002**, *26*, 811–813.
- [60] Camiolo, S.; Gale, P. A.; Hursthouse, M. B.; Light, M. E.; Shi, A. J. *Chem. Commun.*, **2002**, 758–759.
- [61] Gale, P. A.; Navakhun, K.; Camiolo, S.; Light, M. E.; Hursthouse, M. B. *J. Am. Chem. Soc.*, **2002**, *124*, 11228–11229.
- [62] Louie, G. V.; Brownlie, P. D.; Lambert, R.; Cooper, J. B.; Blundell, T. L.; Wood, S. P.; Warren, M. J.; Woodcock, S. C.; Jordan, P. M. *Nature*, **1992**, *359*, 33–39.
- [63] Boger, D. L.; Patel, M. *Tetrahedron Lett.*, **1987**, *28*, 2499–2502.
- [64] Ohkuma, S.; Sato, T.; Okamoto, M.; Matsuya, H.; Arai, K.; Kataoka, T.; Nagai, K.; Wasserman, H. H. *Biochem. J.*, **1998**, *334*, 731–741.
- [65] Tanigaki, K.; Sato, T.; Tanaka, Y.; Ochi, T.; Nishikawa, A.; Nagai, K.; Kawashima, H.; Ohkuma, S. *FEBS Lett.*, **2002**, *524*, 37–42.
- [66] Gerber, N. N. *Crit. Rev. Microbiol.*, **1975**, *3*, 469–485.
- [67] Camiolo, S.; Gale, P. A.; Hursthouse, M. B.; Light, M. E. *Org. Biomol. Chem.*, **2003**, *1*, 741–744.
- [68] Basha, A.; Lipton, M.; Weinreb, M. S. *Tetrahedron Lett.*, **1977**, *18*, 4144–4254.
- [69] Hynes, M. J. *J. Chem. Soc.-Dalton Trans.*, **1993**, 311–312.
- [70] Sessler, J. L.; Camiolo, S.; Gale, P. A. *Coord. Chem. Rev.*, **2003**, *240*, 17–55.
- [71] Gale, P. A.; Sessler, J. L.; Král, V. *Chem. Commun.*, **1998**, 1–8.
- [72] Lightner, D. A.; Tipton, A. K.; Lightner, D. A. *Monatsche. Chem.*, **2000**, *131*, 451–461.
- [73] Gale, P. A.; Sessler, J. L.; Král, V.; Lynch, V. *J. Am. Chem. Soc.*, **1996**, *118*, 5140–5141.
- [74] Job, P. *Ann. Chim.*, **1928**, *9*, 113–203.
- [75] Camiolo, S.; Gale, P. A.; Hursthouse, M. B.; Light, M. E.; Shi, A. J. *Chem. Commun.*, **2002**, 758–759.
- [76] Leigh, D. A.; Wong, J. K. Y.; Dehez, F.; Zerbetto, F. *Nature*, **2003**, *424*, 174–179.
- [77] Aharonian, G.; Gambarotta, S.; Yap, G. P. A. *Organometallics*, **2002**, *21*, 4257–4263.
- [78] Dubé, T.; Conoci, S.; Gambarotta, S.; Yap, G. P. A. *Organometallics*, **2000**, *19*, 1182–1185.

- [79] Shi, Y.; Hall, C.; Ciszewski, J. T.; Cao, C.; Odom, A. L. *Chem. Commun.*, **2003**, 584–585.
- [80] Novak, A.; Blake, A. J.; Wilson, C.; Love, J. B. *Chem. Commun.*, **2002**, 2796–2797.
- [81] Love, J. B.; Blake, A. J.; Wilson, C.; Reid, S. D.; Novak, A.; Hitchcock, P. B. *Chem. Commun.*, **2003**, 1682–1683.
- [82] Pearson, R. G.; Dillon, R. L. *J. Am. Chem. Soc.*, **1952**, *75*, 2439–2443.
- [83] Mackay, G. I.; Bohme, D. K. *J. Am. Chem. Soc.*, **1978**, *100*, 327–329.
- [84] Bordwell, F. G.; Drucker, G. E.; Fried, H. E. *J. Org. Chem.*, **1981**, *46*, 632–635.
- [85] Buncel, E.; Menon, B. *J. Organomet. Chem.*, **1977**, *141*, 1–7.
- [86] Gale, P. A. *Chem. Commun.*, **2005**, 3761–3772.
- [87] Beer, P. D.; Gale, P. A. *Angew. Chem. Int. Ed.*, **2001**, *40*, 486–516.
- [88] Schmidtchen, F. P.; Berger, M. *Chem. Rev.*, **1997**, *97*, 1609–1646.
- [89] Haino, T.; Nakamura, M.; Kato, N.; Hiraoka, M.; Fukazawa, Y. *Tetrahedron Lett.*, **2004**, *45*, 2281–2284.
- [90] Zlatušková, P.; I. Stibor, M. T.; Lhoták, P. *Tetrahedron*, **2004**, *60*, 11383–11390.
- [91] Pelizzi, N.; Casnati, A.; Friggeri, A.; Ungaro, R. *J. Chem. Soc. Perkin Trans.*, **1998**, *2*, 1307–1311.
- [92] Cameron, B. R.; Loeb, S. J. *Chem. Commun.*, **1997**, 573–574.
- [93] Rivas, J. C. M.; Brammer, L. *New J. Chem.*, **1998**, *22*, 1315–1318.
- [94] Bryantsev, V. S.; Hay, B. P. *J. Am. Chem. Soc.*, **2005**, *127*, 8282–8283.
- [95] Kukushkin, V. Y.; Oskarsson, A.; Elding, L. I. *Inorg. Synth.*, **1997**, *31*, 279–284.
- [96] Kruse, C. G.; Bouw, J. P.; van Hes, R.; van de Kuilen, A.; den Hartog, J. A. *Heterocycles*, **1987**, *26*, 3141–3151.
- [97] Baxendale, I. R.; Brusotti, G.; Matsuoka, M.; Ley, S. V. *J. Chem. Soc., Perkin Trans.*, **2002**, *1*, 143–154.
- [98] Patterson, J. M. *Synthesis*, **1976**, 281–304.
- [99] Sobenina, L. N.; Mikhaleva, A. I.; Trofimov, B. A. *Khim. Geterotsikl. Soedin.*, **1989**, 291–308.
- [100] Sobenina, L. N.; Mikhaleva, A. I.; Trofimov, B. A. *Russ. Chem. Rev. (Engl. Transl.)*, **1989**, *58*, 163–180.

- [101] Camiolo, S.; Gale, P. A.; Light, M. E.; Hursthouse, M. B. *Supramol. Chem.*, **2001**, *13*, 613–618.
- [102] Kamlet, M. J.; Abboud, J. L. M.; Abraham, M. H.; Taft, R. W. *J. Org. Chem.*, **1983**, *48*, 2877–2887.
- [103] Rossi, S.; Kyne, G. M.; Turner, D. L.; Wells, N. J.; Kilburn, J. D. *Angew. Chem. Int. Ed.*, **2002**, *41*, 4233–4236.
- [104] Gutsche, C. D.; Bauer, L. J. *J. Am. Chem. Soc.*, **1985**, *107*, 6052–6059.
- [105] Kubik, S.; Goddard, R. *Proc. Natl. Acad. Sci. U. S. A.*, **2002**, *99*, 5127–5132.
- [106] Kubik, S.; Kirchner, R.; Nolting, D.; Seidel, J. *J. Am. Chem. Soc.*, **2002**, *124*, 12752–12760.
- [107] Seidel, D.; Lynch, V.; Sessler, J. L. *Angew. Chem.-Int. Edit.*, **2002**, *41*, 1422–1425.
- [108] Hossain, M. A.; Llinares, J. M.; Powell, D.; Bowman-James, K. *Inorg. Chem.*, **2001**, *40*, 2936–2937.
- [109] Navakhun, K.; Gale, P. A.; Camiolo, S.; Light, M. E.; Hursthouse, M. B. *Chem. Commun.*, **2002**, 2084–2085.
- [110] Akkus, N.; Campbell, J. C.; Davidson, J.; Henderson, D. K.; Miller, H. A.; Parkin, A.; Parsons, S.; Plieger, P. G.; Swart, R. M.; Tasker, P. A.; West, L. C. *Dalton Trans.*, **2003**, 1932–1940.
- [111] Manske, R. H. F.; Kulka, M. *Can. J. Research*, **1949**, *27B*, 161–167.
- [112] Ahmad, Y.; Hey, D. H. *J. Chem. Soc.*, **1961**, 3882–3885.
- [113] Vega, I. E. D.; Gale, P. A.; Light, M. E.; Loeb, S. J. *Chem. Commun.*, **2005**, 4913–4915.
- [114] Xie, M.; Lightner, D. A. *Tetrahedron*, **1993**, *49*, 2185–2200.
- [115] Xie, M.; Holmes, D. L.; Lightner, D. A. *Tetrahedron*, **1993**, *49*, 9235–9250.
- [116] Fraccarollo, D.; Bertani, R.; Mozzon, M.; Belluco, U.; Michelin, R. A. *Inorg. Chim. Acta*, **1992**, *201*, 15–22.
- [117] Noland, W. E.; Cole, K. P.; Britton, D. *Acta Crystallogr. Sect. C-Cryst. Struct. Commun.*, **2003**, *59*, O263–O267.